Baryogenesis and Inflation from the Higgs sector

A thesis presented for the degree of
Doctor of Physics by

Yann Cado

supervised by
Dr. Mariano Quirós

UAB tutor
Prof. Dr. Àlex Pomarol

June 16, 2023

Universitat Autònoma de Barcelona

Abstract

Although the ΛCDM model is the most complete model of modern cosmology to date, it still lacks a compelling description of the baryonic matter origin and of the cosmological inflationary period. In this thesis, we study the implications of the inflaton coupling to the Chern-Simons density in various scenarios, focusing on the role played by the Higgs sector in the baryogenesis and preheating capabilities. At first, we focus on the Higgs inflation model, as it relates cosmological observables to properties of electroweak physics, which makes the Higgs a candidate of particular interest for the inflaton. Then we propose a modified model of the latter, where the Higgs is combined with a new scalar field. Both fields participate in the inflation process in a unitary theory that predicts values of the cosmological observables in agreement with the results from the Planck/BICEP/Keck Collaborations. From a phenomenological perspective, this model can solve the Standard Model instability problem and, under some specified conditions, lead to the prediction of a TeV scale inflaton that could be produced and detected at the LHC. This model thus combines Higgs inflation, baryogenesis via production of helical magnetic fields, and stabilization of the Higgs potential by modifying the renormalization group running, to provide a successful history of the Universe.

Contents

Conventions and abbreviations

- Unless otherwise specified, we set all the physical constants to unity

$$c = \hbar = \epsilon_0 = \mu_0 = k_B = 1.$$

- We use the Einstein summation convention between upper and lower Greek indices (running from 0 to 3) and between letters from any other alphabet without any particular instructions.

- Bold characters stand for 3-vectors.

- We use dots to represent cosmic time derivatives and primes to represent conformal time derivatives

$$\dot{a} \equiv \frac{da}{dt}, \qquad\qquad a' \equiv \frac{da}{d\tau}.$$

Primes are also used to denote the derivative of a function with respect to its prime variable. This is most often the case for the potential

$$V'(\phi) \equiv \frac{dV}{d\phi},$$

but it can be for any single variable function.

- The metric signature is $(-, +, +, +)$.

- The function log denotes the natural logarithm, i.e. in the base of the mathematical constant $e = 2.718\,281....$ This is the same for the exponential function exp.

- We use the convention of Peskin and Schroeder for SM, hence the Higgs VEV is downstair in the doublet and

$$Q = I_3 + Y.$$

Abbreviations used in this work

ALP	Axion-like particles		FRW	Friedmann-Robertson-Walker
ATLAS	A Toroidal LHC Apparatus		GUT	Grand unified theory
BAU	Baryon asymmetry of the Universe		HE-LHC	High-Energy Large hadron collider
BBN	Big Bang nucleosynthesis		HI	Higgs inflation
BD	Bunch-Davies		IMF	Intergalactic magnetic fields
BSM	Beyond the Standard Model		IR	Infrared
CERN	European Organization for Nuclear Research		LHC	Large hadron collider
CDM	Cold dark matter		LHS	Left hand side
CHI	Critical Higgs inflation		MHD	Magnetohydrodynamics
CKM	Cabibbo-Kobayashi-Maskawa		MOND	Modified Newton dynamics
CMB	Cosmic microwave background		MS	Minimal Subtraction
CMS	Compact Muon Solenoid		$\overline{\text{MS}}$	Bare Minimal Subtraction
COBE	Cosmic Background Explorer		PT	Phase transition
CPI	Chiral plasma instability		QCD	Quantum chromodynamics
CS	Chern-Simons		QFT	Quantum field theory
DM	Dark matter		RGE	Renormalization group equation
EFT	Effective field theory		RHS	Right hand side
EM	Electromagnetism		RK4	Fourth order Runge-Kutta
EoM	Equation(s) of motion		SM	Standard Model
EW	Electroweak		UV	Ultraviolet
EWPT	Electroweak phase transition		VEV	Vacuum expectation value
FN	Froggatt-Nielsen		WIMP	Weakly Interacting Massive Particle

Introduction

The ΛCDM model is, today, the most elegant and complete model of modern Cosmology. It adds a period of accelerated expansion prior to the Hot Big Bang model, called the *inflationary paradigm* (or *inflation*), and postulates the existence of Cold Dark Matter that accounts for the dynamics of large-scale structures. The theory of Big Bang Nucleosynthesis (BBN), accounting for the birth of the lightest elements, is embedded in this model as well as the description of the Cosmic Microwave Background (CMB) radiation. Moreover, associated with so-called *dark energy*, a tiny cosmological constant Λ is also accounting for the actual accelerated expansion.

From the point of view of particle physics, the Standard Model (SM) of the strong and electroweak interactions provides results and predictions that agree with all experiments, with tremendous accuracy. But the SM is somehow postulating the existence of its content without giving it an origin. Moreover, the SM is a quantum field theory based on a gauge symmetry group. An unavoidable requirement from Noether's theorem is then the existence of associated conserved quantities called charges. Therefore matter and antimatter must come by the same amount. They can annihilate each other leaving behind, if no dynamical process is present, either an exact equal amount of matter and antimatter, or only radiation. The obvious existence of matter, compared to the lack of evidence of antimatter, as well as the CMB analysis and the BBN constraints, drive physicists to think of a dynamical process that creates a matter/antimatter asymmetry during the early Universe, called *baryogenesis*.

For baryogenesis to happen, the Universe must contain a source of baryon number B, charge conjugation $\mathcal{C}$ and $\mathcal{CP}$ violations, and provide an out-of-thermal equilibrium period when these processes can generate an asymmetry in the baryon/lepton sector before freezing out. It appears that the SM contains all the necessary ingredients, as the weak interaction couples only to left-handed particles and breaks $\mathcal{CP}$ through the CKM phase. This chiral aspect of the model is, by the same token, anomalous and violates the baryon+lepton number. Lastly, the Higgs mechanism, which breaks the electroweak symmetry into electromagnetism, might provide the desired out-of-equilibrium condition. However, even if all the ingredients for a successful baryogenesis model exist in the SM, they are present in only very little amounts, as the electroweak phase transition (EWPT) is a crossover and the $\mathcal{CP}$ violation induced by the CKM phase (or the Jarlskog invariant) is too small. Therefore, most baryogenesis mechanisms rely on beyond the SM (BSM) extensions, for which the EWPT might be strong first order, and have an extra source of $\mathcal{CP}$ violation.

The reluctancy of experimental data to confirm deviations with respect to the SM predictions has motivated people to reanalyze many phenomena with SM tools as much as possible. This thesis fits into this movement as we aim to explain the baryon asymmetry of the Universe (BAU), and the inflationary period, by using as much of the Higgs sector as possible. Although this particle was discovered at CERN in 2012, many of its properties remain unknown today, such as its high-energy interactions. As we will demonstrate, some higher order interactions allow the Higgs boson to be at the origin of matter in the present Universe. Even if our false electroweak vacuum is metastable, with a lifetime much larger than the age of our Universe, should the Higgs participate in the inflationary period we may want to solve the *Higgs vacuum instability problem*, which states

that our current (low-energy) understanding of the Higgs interaction predicts a true vacuum of its potential at an energy scale of $\sim 10^{11}$ GeV that could lead the entire Universe to an unphysical phase. This is because when radiative corrections are considered in the SM effective potential, the value of the Higgs self- (quartic) coupling becomes a function of the Higgs background and turns negative at scale $\sim 10^{11}$ GeV, mainly through the contribution from the top quark. To prevent such a behavior, one must introduce new high-energy physics in the Higgs sector.

In doing so we will bring inflation into the picture, as besides solving the flatness and horizon problems of standard cosmology, the inflationary paradigm opens up a variety of possibilities for new scenarios, as it requires BSM physics. First, cosmological inflation requires the presence of a scalar field ϕ, the inflaton, with an appropriately flat potential. We will demonstrate that it can generate the BAU with the appropriate coupling to the hypercharge Chern-Simons (CS) density. When identified with the Higgs boson, it leads to models dubbed as Higgs inflation (HI) and we will also provide conditions for baryogenesis in this framework. Finally we will present a modified HI model where the SM potential is stabilized by an extra BSM field, inflation is realized and the BAU generated at the electroweak crossover.

This thesis hence lies at the intersection between inflation, baryogenesis and Higgs physics, which lines up in (p)reheating and low-energy particle phenomenology. While each component has been previously explored and extensively studied, we have integrated these ideas within a unified framework, the main goal being to establish specific constraints or predictions regarding the baryogenesis capability in different models of inflation, all involving the Higgs field.

This thesis is divided as follows. In Part I we will review some aspects of theoretical high energy physics, in order to set the framework for the subsequent chapters. In particular, Chap. 1 is devoted to the standard and inflationary models of Cosmology, as well as some insights into the actual open questions in the field, whereas Chap. 2 reviews the physics of elementary particles, the SM, the Higgs vacuum instability, gauge field theory and axion physics. Our aim here is to be as comprehensive as possible, without getting bogged down in detail, while focusing on the necessary aspects for a proper understanding of the thesis. Over and above the necessary theoretical background, the aim is to introduce the key topics, mainly the slow roll inflation paradigm, Higgs inflation, the Sakharov conditions for baryogenesis, the SM chiral anomaly and its link with helicity and the weak sphaleron.

In Part II we set the grounds for the baryogenesis mechanism used in this work. We will then go into more detail, and be more technical. In Chap. 3 we show how helical hypermagnetic fields can convert into baryon asymmetry during the EWPT, a crossover, and how these fields can be produced during inflation assuming the appropriate couplings. Chap. 4 is devoted to the detailed description of a major backreaction effect in the early Universe plasma thus produced, called the *Schwinger effect*. In addition to some analytical estimates, we will present the results of our own numerical simulations.

Finally, Part III brings everything together into the formulation of two models for baryogenesis and/or inflation. In Chap. 5 we show that the helical gauge fields produced at the end of HI from the dimension-six interaction between the Higgs and the CS density, lead to a window in the parameter space for baryogenesis, as least in the metric formulation. This model still faces the vacuum instability problem which, as said above, happens at a scale of $\sim 10^{11}$ GeV, much below the values at which HI takes place, i.e. $\sim 10^{-2} M_{\mathrm{pl}}$. Addressing this problem usually requires an UV completion of the model which can modify the relationship between the low-energy and high-energy SM parameters, and in particular the value of the quartic coupling at the inflationary scale.

With this aim in mind, we study in Chap. 6 a modification of the HI scenario where we introduce an extra scalar coupled to the Ricci scalar and mixed with the Higgs field. The new scalar field stabilizes the Higgs potential, provided that its mass is lower than the instability scale, triggers cosmological inflation and, if coupled to the CS density, generates enough helical hypermagnetic

fields to source the baryogenesis mechanism at EWPT. Finally, if the new scalar mass is at the TeV scale, the mixing with the Higgs field becomes sizable while the theory turns natural. The latter thus predicts modifications of the Higgs trilinear and quartic couplings, that could be explored at the HE-LHC, as well as at future colliders, and allows for direct production at the LHC followed by decay into di-Higgs. Present results from ATLAS and CMS already put (mild) bounds on the mass of the heavy scalar as $m \gtrsim 0.55$ TeV at 95% C.L.

Part I

Framework

Chapter 1

Cosmology

Although the human species has always looked to the stars seeking an explanation of the observed world, human thinking before the 19th century always led to cosmogony and mythology. Its desire for knowledge, and its imagination were strong, but it was lacking observational resources. It is possible to derive one of the fundamental equations of the Universe (the Friedmann equation) with newtonian mechanics, but at the time of Newton the Universe did not have the same definition as today, hence contemporary scientists had no clue about the framework, nor the observation, that could confirm or reject their theory. Before the 19th century, the observations of many astronomers, Galileo, Kepler, Copernicus, Halley, Messier, Herschel, etc., lead to the acceptance that the Universe was roughly the size of the Solar system and later of the Milky Way, as the distance between all visible objects in the sky was greatly underestimated.

It is at the beginning of the 20th century that modern cosmology was born thanks to two revolutionary discoveries: one observational, the other theoretical. The second one is the theory of general relativity published by Albert Einstein in 1915. It took many years for this theory to establish itself and become one of the most important tools of modern science. But without the other event, it would have remained confined to its use in the Milky Way, since it was always the broadest framework that physicists could think of. The first confirmations of general relativity actually occurred on the anomalous perihelion advance of Mercury.

On the other side, the astronomical community was faced for several decades with an important debate on the subject of nebulae. Defined as diffuse stars that the instruments could not resolve at that time, many scientist were claiming there were separate galaxies, an idea that dates back to Kant. In 1920, after the Great Debate between Shapley and Curtis, the scale of the Universe was revised upwards considerably thanks to Edwin Hubble who showed that the Andromeda nebulae was far outside the Milky Way by measuring Cepheid variable stars.

But Hubble's major contribution to modern cosmology, not to say its foundation, was his redshift law which shows that the escape velocity of extra-galactic objects increases with their distance. This is when the question of large scale dynamics arose in the scientific community. For the first time in History, the Universe was seen as a subject of study in itself and no more as the container of astrophysical objects. Modern cosmology was born.

1.1   A review of Standard Cosmology

In this chapter, we aim to provide a brief review of the fundamentals of modern cosmology. So in this section, we will first go over the basics in a more technical way and review the successes and issues of the standard cosmological model, before moving to inflation in Sec. 1.2 and some contemporary puzzles of cosmology in Sec. 1.3.

1.1.1   The Friedmann equations

The goal of this section is to relate the Einstein equations of general relativity [1]

$$G_{\mu\nu} = 8\pi G\, T_{\mu\nu} \tag{1.1}$$

to the large scale observation of the Universe. These relate the energy density to spacetime distortions within a covariant formulation. The right-hand side (RHS) involves the energy-momentum tensor $T_{\mu\nu}$ and the gravitational constant $G \simeq 6.67 \cdot 10^{-11}$ Nm^2/kg^2. On the left-hand side (LHS) we find the Einstein tensor

$$G_{\mu\nu} = R_{\mu\nu} - \frac{1}{2} R\, g_{\mu\nu}, \tag{1.2}$$

which contains non-linear combinations of up to second order derivatives of the metric tensor $g_{\mu\nu}$, defined below. The Ricci tensor $R_{\mu\nu}$ and the Ricci scalar R are contractions of the Riemann tensor $R_{\rho\sigma\mu\nu}$ with the metric

$$R_{\mu\nu} = g^{\rho\sigma} R_{\rho\mu\sigma\nu}, \tag{1.3a}$$

$$R = g^{\mu\nu} R_{\mu\nu}. \tag{1.3b}$$

The Riemann tensor indicates the evolution of the geodesics relative to each other and hence characterizes the geometry of the space. Its mathematical expression is given by

$$R^{\rho}{}_{\sigma\mu\nu} = \partial_\mu \Gamma^{\rho}{}_{\nu\sigma} - \partial_\nu \Gamma^{\rho}{}_{\mu\sigma} + \Gamma^{\rho}{}_{\mu\lambda} \Gamma^{\lambda}{}_{\nu\sigma} - \Gamma^{\rho}{}_{\nu\lambda} \Gamma^{\lambda}{}_{\mu\sigma}, \tag{1.4a}$$

$$\Gamma^{\mu}{}_{\nu\rho} = \frac{1}{2} g^{\mu\sigma} \left(\partial_\nu g_{\sigma\rho} + \partial_\rho g_{\nu\sigma} - \partial_\sigma g_{\rho\nu} \right). \tag{1.4b}$$

It involves the Christoffel symbols which describe how the basic vectors $\hat{\boldsymbol{e}}_\mu$ change when moving through spacetime. This provides a relation between them and the metric as

$$\partial_\mu \hat{\boldsymbol{e}}_\nu = \Gamma^{\rho}{}_{\mu\nu} \hat{\boldsymbol{e}}_\rho. \tag{1.5}$$

This non triviality has of course an impact on the derivative. Hence, the covariant derivative

$$\nabla_\mu v_\nu = \partial_\mu v_\nu - \Gamma^{\rho}{}_{\mu\nu} v_\rho \tag{1.6}$$

is hence defined in order to transform like the basis under a change of coordinates.

We recover a set of ten coupled differential equations for the metric; six hyperbolic and four elliptic. However, because both the energy-momentum and the Einstein tensor are symmetric (and real), only six equations are linearly independent.

The metric is the name given to the matrix representation of the bilinear form that defines the scalar product in a given vector space. The squared norm of the infinitesimal vector dx^μ is given by

$$ds^2 = g_{\mu\nu}\, dx^\mu dx^\nu. \tag{1.7}$$

The whole challenge of applying the Einstein equations to the Universe is reduced to choosing the metric accordingly. Hence, based on the paradigm of relativity, that is on the lack of absolute or preferential reference frames, Einstein formulated the cosmological principle which states that the Earth does not occupy a special position in the Universe. Besides, observations beyond the Milky Way suggest that our Universe is isotropic from our perceptive. These two considerations imply that each point of the Universe is isotropic and hence that the Universe is homogeneous, as confirmed by the observation of the cosmic microwave background (CMB) in 1965 by Penzias and

Wilson, see Sec. 1.1.5 and Fig. 1.1. Homogeneity and isotropy bring about strong constraints on Einstein equations, when these are applied to the Universe.

The cosmological principle implies the following form for the line element

$$ds^2 = -dt^2 + a^2(t) \left(\frac{dr^2}{1 - kr^2} + r^2 d\theta^2 + r^2 \sin^2\theta \, d\varphi^2 \right), \tag{1.8}$$

which defines the Friedmann-Robertson-Walker (FRW) metric. We choose the spherical coordinates (t, r, θ, φ) as they reflect the symmetry from our reference frame. Isotropy of space forces the metric to be diagonal and adding the homogeneity makes the spatial part of the metric proportional to a term that is at most time dependent. This term, denoted by $a(t)$, gives the scale of the spatial length and is therefore called the scale factor. Finally, k is a constant related to the curvature of space[1], and using the scale invariance of the line element, i.e. $a \to \lambda a$, $r \to r/\lambda$, $k \to \lambda^2 k$, we can rescale r to make k dimensionless. In this case k has three possible values: if $k = +1$ space is said to be closed and has the shape of a four dimensional sphere, if $k = -1$ it is open and its shape takes the form of a saddle, and if $k = 0$ space is said flat. In this thesis we will consider the last case and use the above representation of the line element by which $a(t)$ is dimensionless and r and $k^{-1/2}$ have length dimension.

The isotropy and homogeneity of the Universe also constrain the energy-momentum tensor defined as

$$T_{\mu\nu} = (\rho + p)u_\mu u_\nu + p g_{\mu\nu}, \tag{1.9}$$

where u_μ is the 4-velocity, ρ and p are the total energy density and pressure. For a comoving observer, $u_\mu = (-1, 0, 0, 0)$, the tensor has to be diagonal with equal elements associated to the three different spatial directions:

$$T_{\mu\nu} = \begin{pmatrix} \rho & 0 & 0 & 0 \\ 0 & p & 0 & 0 \\ 0 & 0 & p & 0 \\ 0 & 0 & 0 & p \end{pmatrix}, \tag{1.10}$$

hence we see that we are considering the Universe to be a perfect fluid.

The solution to the Einstein equations in this set-up yields two equations, one for the time component and another for the spatial one, which is a logical outcome of the choice of index for $T_{\mu\nu}$. The first Friedmann equation hence describes the time evolution of the Universe by relating the scale factor to energy and curvature. Indeed, it is sufficient to know the energy in order to describe an isotropic homogeneous system; spherical symmetry allows us to restrict ourselves to a one dimensional analysis of the scale factor. It writes

$$\frac{\dot{a}^2}{a^2} = \frac{8\pi G}{3}\rho - \frac{k}{a^2}, \tag{1.11}$$

and can be derived with newtonian mechanics for $k = 0$. The second Friedmann equation is

$$\frac{\ddot{a}}{a} = -\frac{4\pi G}{3}(\rho + 3p). \tag{1.12}$$

A third, redundant, equation can be casted, namely the energy-momentum conservation

$$\nabla_\mu T^{\mu\nu} = 0, \tag{1.13}$$

with the covariant derivative defined by (1.6). Out of this three last equations, only two are

---

[1]The curvature radius of space is given by $R_{\mathrm{curv}} \equiv a(t)/\sqrt{|K|}$

independent. For the time component, $\nu = 0$, the last one becomes

$$\nabla_\mu T^{\mu 0} = \dot{\rho} + 3\frac{\dot{a}}{a}(\rho + p) = 0. \tag{1.14}$$

and is helpful to describe the global dynamics of the Universe. The only thing we are now lacking in order to fully engage in cosmology is an equation of state

$$p = w\rho \tag{1.15}$$

in order to distinguish the different forms that energy can take.

A key success of the standard cosmological model is its ability to correctly link the rate of expansion of the Universe to its content. In order words, the energy characterization allows us to find the function $a(t)$. Plugging the equation of state into (1.14) we find

$$\frac{d\rho}{da}\frac{da}{dt} + 3\frac{\rho}{a}\frac{da}{dt}(1 + w) = 0 \quad \Rightarrow \quad \rho \propto \frac{1}{a(t)^{3(1+w)}}. \tag{1.16}$$

The value $w = 0$ corresponds to matter, which has an energy density but no pressure. Unsurprisingly, $\rho_m a^3$ is constant in this case, which is consistent with the definition of the volumetric mass density[2]. With the use of the first Friedmann equation it is now straightforward to compute the explicit time evolution of the scale factor for a flat Universe. In a matter dominated Universe we have

$$\frac{\dot{a}_m^2}{a_m^2} \propto \rho_m \propto a_m^{-3} \tag{1.17}$$

and we find

$$a_m(t) \propto t^{2/3}. \tag{1.18}$$

Similarly, the dynamics of a radiation dominated Universe, $w = 1/3$, is

$$\frac{\dot{a}_\gamma^2}{a_\gamma^2} \propto \rho_\gamma \propto a_\gamma^{-4} \quad \Rightarrow \quad a_\gamma(t) \propto t^{1/2}. \tag{1.19}$$

We can already conclude that for a mix of matter and radiation, i.e. what we observe from the sky, the Universe is expanding, in agreement with the Hubble law that will be discussed in the next section. Beforehand, let us point out that although the equation of state allows us to imagine any kind of exotic energy species, there is a non trivial one motivated from the Einstein equations themselves. Indeed, because the equations of motion (EoM) are obtained from derivatives, there is a redundancy such that we can always add a constant term proportional to the metric and obtain the same physics. This can be done in two ways: either redefining the Einstein tensor with an extra constant term or, more commonly, adding a $T_{\mu\nu}^\Lambda$ term to the energy-momentum tensor $T_{\mu\nu}$ with

$$T_{\mu\nu}^\Lambda = -\frac{\Lambda}{8\pi G}g_{\mu\nu}. \tag{1.20}$$

The parameter Λ is called the cosmological constant and the above contribution corresponds to a constant energy density despite the expansion, hence $w = -1$. This can be viewed as radiative energy with negative pressure.

As the Einstein equations do not exclude this term, it is good to study its consequences in the

---

[2]This is valid only in the absence of processes that create or annihilate massive particles.

dynamics of the Universe. Recasting (1.16) we get

$$\frac{\dot{a}_\Lambda^2}{a_\Lambda^2} \propto \rho_\Lambda, \tag{1.21}$$

which is constant. Thus $\dot{a}$ is proportional to a, which implies an exponential behavior for the scale factor:

$$a_\Lambda(t) \propto \exp\left(\frac{\Lambda t}{\sqrt{3}}\right). \tag{1.22}$$

This regime, named *de Sitter* after the Dutch physicist, is of peculiar interest because, unlike the two others, it provides $\ddot{a} > 0$, which fits to the accelerated expansion observed in 1998 [2, 3]. Today the most common explanation given to this fact is that the Universe is currently dominated by the $T_{\mu\nu}^\Lambda$ contribution called dark energy. The origin of this phenomenon is one of the biggest unsolved problems of modern physics, see Sec. 1.3.1.

1.1.2 The Hubble law and the abundances

Since the Universe is expanding, one expects to observe a redshift over the whole electromagnetic spectrum of distant[3] galaxies. However, although we can measure this redshift, the observed objects are not actually moving away from us in spacetime. In fact it is the dilation of spacetime itself which leads to our impression that these objects are moving away. Since this phenomenon has a different nature than the usual redshift, it is called cosmological redshift.

A photon travels at the speed of light, hence its line element is $ds_\gamma^2 = 0$. Consider now a radial ray of light emitted at time t_i from position R_e that we observe today t_0 in R_o. We do not expect either the emitter, the observer nor the scale factor to vary during the timescale of one wavelength λ. Hence we have, according to our line element

$$\int_{t_i}^{t_0} \frac{dt}{a(t)} = \int_{t_i + \frac{c}{\lambda_i}}^{t_0 + \frac{c}{\lambda_0}} \frac{dt}{a(t)} = \int_{R_e}^{R_o} \frac{dr}{\sqrt{1 - kr^2}}, \tag{1.23}$$

where we restored the units to be explicit. Thus, after rearranging the integrals, this yields

$$\int_{t_0}^{t_0 + \frac{c}{\lambda_0}} \frac{dt}{a_0} = \int_{t_i}^{t_i + \frac{c}{\lambda_i}} \frac{dt}{a_i} \Rightarrow \frac{\lambda_i}{\lambda_0} = \frac{a_i}{a_0}, \tag{1.24}$$

which means that the wavelength grows with the scale factor of the Universe. This result is in agreement with (1.16), which tells us that the relation between the energy density and the scale factor depends on the nature of the content of the Universe: the mass does not change with the expansion, unlike the radiation energy which is proportional to its wavelength. This leads to a factor a difference in the energy densities.

Using that property, Hubble could estimate the escaping velocity v of Cepheid-type stars while their distance relative to us d can be obtained from their luminosity magnitude. In 1929 he showed that there is the linear relation [4]

$$v = H_0 d \tag{1.25}$$

known as the Hubble law. Today there is some disagreement on the precise value of the Hubble constant, as differently measured, often referred to as the *Hubble tension*. Modern direct measurements

---

[3]The light of the Andromeda galaxy is blue-shifted because $\rho_{\text{loc}} > \rho_c$ (see Eq. (1.29) and below) within the local group. The above statement is valid at scales at which the Universe is homogeneous and the FRW metric can be applied.

on the same principle provide a high value of the Hubble parameter, the latest being [5]

$$H_0 = 73.04 \pm 1.04 \text{ km/s Mpc}. \tag{1.26}$$

On the other hand, indirect methods from the CMB observation (see Sec. 1.1.5) provide [6]

$$H_0 = 67.37 \pm 0.54 \text{ km/s Mpc}. \tag{1.27}$$

We can see that, besides the numbers, the tension lies between early and late time Universe measurement. Nowadays, many proposal have been made to solve that tension [7] but no consensus has been found. Since in this thesis we are studying early Universe phenomena, we will use today's Hubble value from the CMB measurement and we will not enter the tension problem.

On a cosmological timescale, the Hubble constant is no more a constant and is viewed as a parameter computed from the scale factor as

$$H = \frac{\dot{a}}{a}. \tag{1.28}$$

The above Hubble constant H_0 is therefore the value of the Hubble parameter today $H_0 = H(t_0)$. In the literature, the Friedman equation (1.11) is often written in terms of H. We can change its shape further by inserting the critical density defined as

$$\rho_c = \frac{3H_0^2}{8\pi G} \simeq 10^{-47} \text{ GeV}^4, \tag{1.29}$$

which yields

$$H^2 = H_0^2 \left(\frac{\rho}{\rho_c} - \frac{k}{a^2 H_0^2} \right). \tag{1.30}$$

We now define the abundances of the different types of energy (radiation, matter,...) as the energy to critical energy ratio

$$\Omega_i = \frac{\rho_i}{\rho_c}. \tag{1.31}$$

In these terms, the first Friedmann equation becomes today,

$$\Omega^0 - 1 = \frac{k}{a^2 H_0^2} \equiv \Omega_k^0, \qquad \Omega \equiv \sum_i \Omega_i. \tag{1.32}$$

where for coherence with the previously used notation we define the RHS as the curvature abundance. It is not an abundance, strictly speaking, but it measures the energy the Universe uses to curve spacetime. We will come back on this quantity when presenting the curvature problem of the standard model of cosmology in Sec. 1.1.7.

The total energy density is referred to as critical when $\Omega_k^0 = 0$, i.e. when it is flat today. Then the effects of gravitation and expansion compensate each other. The energy density value is hence related to the geometry of the Universe. Locally we have a contraction of spacetime when $\rho_{\text{loc}} > \rho_c$ and an expansion of spacetime when $\rho_{\text{loc}} < \rho_c$. Data from CMB and observations of type-Ia supernovae put the constraint $|\Omega_k^0| < 0.01$ [8]. Hence, assuming a flat Universe today, equation (1.32) simply becomes

$$\sum_i \Omega_i^0 = 1. \tag{1.33}$$

This allows cosmologists to draw the pie chart of the Universe energy as

$$\begin{aligned} \Omega_\Lambda^0 &= 0.691 & \Omega_m^0 &= 0.308 \\ \Omega_b^0 &= 0.0486 & \Omega_\gamma^0 &\sim 10^{-5}. \end{aligned} \tag{1.34}$$

These values are at the foundation of the Λ cold dark matter (ΛCDM) model of cosmology which is implemented in terms of the abundances of radiation (γ), dark energy (Λ), and total matter (m), which contains baryonic matter (b). According to these values, the majority of the Universe's content is dark energy, which confirms the link made with the accelerated expansion. Today we do not have any convincing explanation on why this share has such a value. Besides, a lack of matter is found when comparing Ω_m^0 and Ω_b^0. This indicates the presence of an exotic type of matter that accounts for roughly 26% of the Universe's content today called *dark matter*, see Sec. 1.3.2.

1.1.3 Comoving reference frame

The expansion of the Universe implies that all computations must be made in a curved spacetime, even if the spatial part is flat, $k = 0$, which introduces additional difficulties for e.g. computing vectorial geometry (curl, divergence, cross product, etc.). It is however possible to get around this complication by using comoving coordinates, i.e. coordinates that scale with the expansion. In that frame, we recover the usual flat spacetime metric $\eta_{\mu\nu} = \text{diag}(-1, 1, 1, 1)$ called Minkowski spacetime, and the geometry computations stay trivial.

We do so by introducing the so-called conformal time τ, defined by

$$d\tau = \frac{dt}{a(t)}. \tag{1.35}$$

Note that the RHS previously occurred in the derivation of the redshift. This change of variable simplifies the flat FRW metric

$$ds^2 = -dt^2 + a^2(t)d\boldsymbol{x}^2, \tag{1.36}$$

where $d\boldsymbol{x}$ denotes the spatial coordinates, to

$$ds^2 = a^2(\tau) \left[-d\tau^2 + d\boldsymbol{x}^2 \right]. \tag{1.37}$$

Up to a global factor much easier to deal with, we recover a reference frame where, for instance, computing vectorial analysis is trivial since it removes all terms related to spacetime curvature. In other words, using conformal time guarantees that spacetime is flat since $g_{\mu\nu} = a^2(\tau)\,\eta_{\mu\nu}$. We recall that in this thesis, we denote the derivative with respect to conformal time τ with a prime and the derivative with respect to the cosmic time t with a dot, e.g. $a' = da/d\tau$ and $\dot{a} = da/dt$.

For matter, radiation and a Λ dominated Universe we then have

$$a_m(\tau) \propto \tau^2, \qquad a_\gamma(\tau) \propto \tau, \qquad a_\Lambda(\tau) \propto -\frac{1}{H\tau}. \tag{1.38}$$

The Hubble parameter can be rewritten as

$$H(\tau) = \frac{a'}{a^2} \tag{1.39}$$

and therefore, for any function f depending on time, the following relation holds

$$a^{-2}f'' = \ddot{f} + H\dot{f}. \tag{1.40}$$

As in this work the scale factor is dimensionless, both cosmic and conformal times are quantities

that carry a dimension. Hence, it can be useful to use the scale factor a as the time variable to remove that problem. Using (1.28) and (1.35) we can write the following changes of variables:

$$\frac{d}{dt} = aH\frac{d}{da}, \qquad\qquad \frac{d^2}{dt^2} = aH^2\left[a\frac{d^2}{da^2} + (1-\mathcal{F})\frac{d}{da}\right], \qquad\qquad (1.41a)$$

$$\frac{d}{d\tau} = a^2H\frac{d}{da}, \qquad\qquad \frac{d^2}{d\tau^2} = a^3H^2\left[a\frac{d^2}{da^2} + (2-\mathcal{F})\frac{d}{da}\right], \qquad\qquad (1.41b)$$

where we have defined

$$\mathcal{F} = -\frac{a}{H}\frac{dH}{da} = -\frac{a}{2H^2}\frac{dH^2}{da} = -\frac{a}{2\rho}\frac{d\rho}{da}, \qquad\qquad (1.42)$$

and in the last equality we used the flat Friedmann equation (1.11). These relations will become handy in Chap. 4.

1.1.4 Thermal history of the early Universe

An expanding Universe implies the concept of an arrow of time, as the Universe is not static. Hence the Universe has a present, but also a future and, more importantly, a past. If we reverse the direction of time and let the Universe evolve back in the past we shall have, according to the laws of thermodynamics, a much more hot and dense Universe, and, eventually, a singularity when $a = 0$. Without a theory that unifies general relativity and quantum field theory it is difficult to come up with a description of what happens during that epoch (called the Planck era). At intermediate times, when the Universe was big enough to avoid quantum gravity effects, but also hot enough for its whole content to be a plasma of particles, the Universe was in thermal equilibrium and can hence be described by statistical thermodynamics. This is called the *Hot Big Bang* theory.

Statistical thermodynamics

In this section we will review in a nutshell the basics of early Universe thermodynamics. We first consider a plasma in thermal equilibrium with a constant total number of particles. A particle with g internal degrees of freedom has a density of states g/h^3 in the 6-dimensional phase space. In the natural units where $\hbar = 1$, the density writes as $g/(2\pi)^3$. The latter is a measurement of "the available space" in phase space, and is independent of the physical volume so we can apply it to arbitrarily large systems; the observable Universe for instance. Because of the laws of thermodynamics, this available space is not filled in randomly when in thermodynamic equilibrium, but satisfies the requirement that the physical state has maximum entropy S. The function which indicates how the particles populate the phase space under this contraint is called the *distribution function*

$$f(p) = \frac{1}{\exp\left(\frac{E-\mu}{T}\right) \pm 1}, \qquad\qquad (1.43)$$

where the plus sign holds for fermions and the minus sign for bosons (see Sec. 2.3.1 for details). Because of homogeneity and isotropy, this function depends only on the momentum modulus p implicit in the energy E. Its time dependence is implicit too and lies in the temperature T and the chemical potential μ. The temperature is related to the energy density in the system and the chemical potential is related to the number density $n = N/V$ of particles in the system, where V is the volume of the system. In other words, they are conjugate variable, one is extensive, the other intensive. The fundamental equation of thermodynamics associate them both by pairs

$$E = TS - pV + \sum \mu_i N_i \qquad\qquad (1.44)$$

where here p is the system's pressure.

If a system is in *thermal equilibrium* all species in interaction have the same temperature. If a system is in *chemical equilibrium*, the chemical potentials of different particle species are related according to

$$A + B \leftrightharpoons C + D \quad \Leftrightarrow \quad \mu_A + \mu_B = \mu_C + \mu_D. \tag{1.45}$$

This only makes sense if the quantities A, B, C, D represent conserved quantities like particle/baryon/lepton number, see Sec. 2.3.6 for a more in-depth description of this concept. Because of that, the photon has zero chemical potential, which implies that particle and antiparticle share the same chemical potential with the opposite sign. This can be seen from the annihilation equation or pair creation (depending on the reading direction of the equation)

$$\psi + \bar{\psi} \leftrightharpoons \gamma + \gamma \tag{1.46}$$

to which is subject any particle/anti-particle ψ, $\bar{\psi}$ pair. *Thermodynamic equilibrium* refers to having both these equilibria, but this criterion is most of the time simply denoted as *thermal equilibrium* in the literature and so will it be in this thesis.

The Hot Big Bang

The energy E, momentum p and mass m of each particle are related by

$$E^2 = p^2 + m^2. \tag{1.47}$$

Now it is straightforward to compute the number density, the energy density and the pressure for all species (labelled with i) in thermal equilibrium. By definition they compute

$$n_i = \frac{g_i}{(2\pi)^3} \int f_i(p) d^3 p, \tag{1.48a}$$

$$\rho_i = \frac{g_i}{(2\pi)^3} \int E(p) f_i(p) d^3 p, \tag{1.48b}$$

$$p_i = \frac{g_i}{(2\pi)^3} \int \frac{p^2}{3E(p)} f_i(p) d^3 p, \tag{1.48c}$$

where g_i is the number of internal degrees of freedom (spin, color,...) of each species and $d^3 p = 4\pi p^2 dp$ because of isotropy. In order to compute these integrals, we consider two limits for both bosons and fermions.

- The highly relativistic limit, where $T \gg |\mu|$, m and therefore $E \simeq p$, $m \simeq 0$: in the early Universe, all particles are eventually in the relativistic limit because of the temperature increase.

- The non-relativistic limit, where $T \ll |\mu|$, $T \ll m - \mu$ and therefore $E \simeq p^2/2m$: in this case, the fermion and boson statistics are replaced by the Maxwell-Boltzmann statistics since $\exp\left(\frac{E-\mu}{T}\right) \pm 1 \simeq \exp\left(\frac{E-\mu}{T}\right)$. As a matter of fact, there is no statical distinction between non-relativistic fermions and bosons.

The results are shown in Table 1.1. We see that the number density, and hence the energy density and the pressure, of non-relativistic particles are exponentially suppressed by temperature. Because of that, their contribution, if any, to the total quantities of the early Universe thermal bath can be neglected. With this at hand, total energy density reads

$$\rho = \sum_i \rho_i = \frac{\pi^2}{30} g_* T^4, \qquad g_* = \sum_i \left(g_i^{\text{bosons}} + \frac{7}{8} g_i^{\text{fermions}} \right), \tag{1.49}$$

	Relativistic fermions	Relativistic bosons	Non-relativistic particles
$n_i =$	$\dfrac{3\zeta(3)}{4\pi^2} g_i T^3$	$\dfrac{\zeta(3)}{\pi^2} g_i T^3$	$g_i \left(\dfrac{m_i T}{2\pi}\right)^{\frac{3}{2}} e^{-(m_i - \mu_i)/T}$
$\rho_i =$	$\dfrac{7\pi^2}{240} g_i T^4$	$\dfrac{\pi^2}{30} g_i T^4$	$m_i n_i$
$p_i =$	$\dfrac{\rho_i}{3}$	$\dfrac{\rho_i}{3}$	$n_i T$

Table 1.1. Number density, energy density and pressure for the particle species i in thermal equilibrium.

where g_* is the effective number of relativistic degrees of freedom. When all the Standard Model species are in thermal equilibrium, we have $g_* = 106.75$. Another useful quantity in the early Universe is the total entropy density defined as

$$s = \frac{\rho + p}{T} = \frac{2\pi^2}{45} g_* T^3. \tag{1.50}$$

A Universe in equilibrium

As the Universe expands, T and μ change, so that energy continuity and particle number conservation are satisfied. In principle, an expanding universe is not in equilibrium, which could be a problem since the Hot Big Bang results are only valid in that case. Therefore, the validity criterion is that the expansion is sufficiently slow compared to particle interaction rates Γ, so that the particle soup usually has time to settle close to local equilibrium. The thermal equilibrium is maintained as long as the particles exchange energy and momentum efficiently via their three main interactions which are scattering, annihilation and pair creation. At equilibrium each reaction is associated to a backreaction with the same rate Γ, implying that the number of particles for each species is conserved.

Mathematically this condition translates to $\Gamma \gg H$, as the Hubble parameter acts as the expansion rate of the Universe. Another way to see it is to inverse the relation as $\Gamma^{-1} \ll H^{-1}$ where Γ^{-1} now denotes the typical interaction time and H^{-1} the current age of the Universe. This means that local thermal equilibrium is reached before the effect of the expansion becomes relevant, as the latter tends to separate the particles that eventually no longer meet.

Although the expansion rate is faster for higher temperature, since combining Eqs. (1.11), (1.28) and (1.49) yields

$$H = \sqrt{\frac{4\pi^3 G}{45} g_*}\, T^2, \tag{1.51}$$

the interaction rates were also much higher because of the higher density and higher particle energies. There exists, therefore, a temperature above which all SM is in thermal equilibrium, which is found to be $T \sim 200$ GeV.

The departure from thermal equilibrium occurs when $H \sim \Gamma$, meaning that a given species ψ is frozen out when $\Gamma_\psi \ll H$. One is generally interested in the freeze out temperature that we can obtain from (1.51) if we know the temperature dependence of Γ. At lower temperatures, the species at issue does not contribute anymore to the thermal bath, which decreases g_* when the temperature drops down to its current value $g_*(t_0) \simeq 3.384$ [6].

Out-of-equilibrium particle decay and creation prevents us from using the distribution function (1.43) and all the results that follow. In such cases, we shall use the Boltzmann transport equa-

tion, which is a nonlinear integro-differential equation that involves convection and diffusion. We comment more about that in Sec. 3.1.3. Its simplest realization is

$$\frac{\partial n}{\partial t} + ... = -\Gamma n + ... \, , \tag{1.52}$$

where on the LHS the dots accounts for any possible background spacetime term[4], and on the RHS the dots account for all the sources, washout and/or background processes in the studied medium. Γ is the generic rate of all the processes in which the species may be involved.

The study of such out-of-equilibrium processes is crucial for baryogenesis, as we will see in Sec. 1.3.3, where it will be shown that it is a necessary requirement. We will use the Boltzmann transport equation in Chap. 3 to explain how we can convert helical fields to baryon asymmetry.

1.1.5   The cosmic microwave background

The Hot Big Bang received recognition through the observation of a primordial electromagnetic radiation called the *cosmic microwave background* (CMB). It was discovered by accident in 1965 by two radio astronomers that were installing a new telescope [9]. This relic radiative signal comes from the last scattering surface.

With the temperature drop from the expansion, the electrons eventually coupled with the primordial nuclei to form neutral atoms, an event known as the *recombination epoch*. This happened at $T \sim 0.3$ eV $\simeq 3\,000$ K or approximately $380\,000$ years after the initial singularity. Unlike the plasma, these atoms could not scatter thermal radiation by scattering, and the Universe became transparent since photons could then travel in spacetime without interacting with matter. Then, a little later, around $T \approx 0.256$ eV, the photon decoupling took place [10]. The CMB encapsulates all photons' last interaction with charged particles before their decoupling (the so-called last-scattering surface). After this, the Universe went from radiation to matter domination.

Most of the radiation energy in the Universe today is in the CMB, making up an abundance of roughly $\Omega^0_{\rm CMB} \simeq 6 \cdot 10^{-5}$. The CMB analysis is one of the biggest sources of information about the early Universe, with the most outstanding result being that its spectrum is the one of a perfect black body with temperature $T \simeq 2.725$ K, see Fig. 1.1. This high degree of uniformity throughout the observable universe and its faint but measured anisotropy, lend strong support for the Big Bang model in general and the ΛCDM model in particular, see Sec. 1.2.3.

1.1.6   The Big Bang nucleosynthesis

If we continue our journey back in time, we reach the MeV scale at which the lightest elements were formed. When $T \sim 10$ MeV, which corresponds to 10^{-2} seconds after the initial singularity, the plasma is cold enough for quarks and gluons to have gathered into baryons (QCD phase transition), but too hot for larger structures to remain in thermal equilibrium. At this stage, the Universe consists only of protons p, neutrons n, electrons and positrons $e^{\pm}$, photons γ, neutrinos ν and antineutrinos $\bar{\nu}$.

We can compute the ratio of protons versus neutrons number by studying the following interactions:

$$n + \nu_e \leftrightharpoons p + e^- \qquad\qquad n + e^+ \leftrightharpoons p + \bar{\nu}_e \tag{1.53}$$

and their antiparticles version, that are in thermal equilibrium for $T \gtrsim 0.73$ MeV. Past this temperature, which corresponds to 1 second after the initial singularity, the number of neutrons and protons ceases to be identical because, being heavier, the neutrons decouple from the plasma. Their

---

[4]In a homogeneous FRW expansion we should add the term $3Hn$.
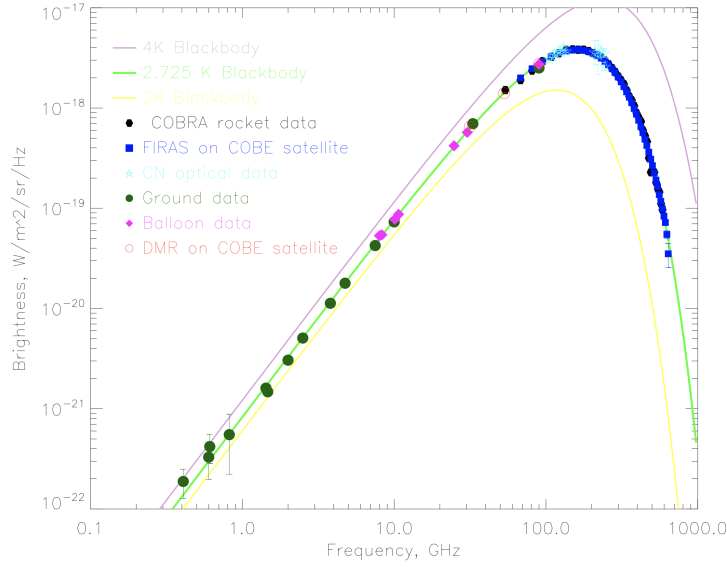
Figure 1.1. Measurements of the CMB flux vs. frequency together with a fit to the data. Superimposed are the expected black body curves for $T = 2K$ (yellow), $T = 2.725K$ (green) and $T = 4K$ (purple). Figure taken from [11].

relative concentration is then given by

$$\frac{n_n}{n_p + n_n} \simeq \left[1 + \exp\left(\frac{m_n - m_p}{T}\right)\right]^{-1}\Bigg|_{T \simeq 0.73\text{MeV}} \simeq \frac{1}{7}. \tag{1.54}$$

The neutrons, that do not have time to disintegrate (their half-life time is 15 min), then get captured by the nuclei and the lightest elements are formed by the following processes

$$\begin{aligned}
p + n &\rightarrow {}^2\text{H} + \gamma \\
{}^2\text{H} + {}^2\text{H} &\rightarrow {}^3\text{H} + p \\
{}^2\text{H} + {}^2\text{H} &\rightarrow {}^3\text{He} + n \\
{}^2\text{H} + {}^2\text{H} &\rightarrow {}^4\text{He} + \gamma \\
{}^2\text{H} + {}^3\text{He} &\rightarrow {}^4\text{He} + p \\
&\quad ...
\end{aligned} \tag{1.55}$$
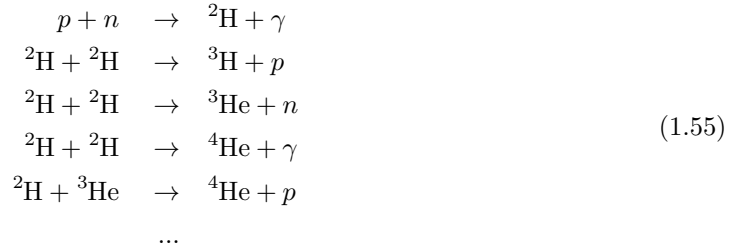
leaving the Universe at $T \lesssim 1$ MeV filled with H, ^{2}H, ^{3}H, ^{3}He, ^{4}He, ^{7}Li, $e^{\pm}$, γ, ν and $\bar{\nu}$. This transformation lasted for ~ 30 minutes. These reaction rates are very small and thus are not in thermal equilibrium.

In summary, Big Bang nucleosynthesis (BBN) is the production of nuclei during the early phases of the Universe. The heaviest one produced is lithium, at a very small fraction. The heavier elements are produced in star cores and supernovae explosions. The currently observed quantities of hydrogen (90%) and helium (10%) come almost exclusively from the BBN epoch. The cumulative activity of stars has barely changed these proportions.

As ^{4}He maximizes the binding energy per nucleon number (for light elements), we can make the approximation that all neutrons will end up in helium nuclei. As two neutrons are necessary

for the formation of a ^{4}He nucleus, we can estimate its fraction as

$$Y_p \simeq \frac{2n_n}{n_n + n_p} \approx 0.25 \tag{1.56}$$

consistent with contemporary observation [12]. Besides, since $n_n < n_p$, a majority of protons will remain alone and will become hydrogen at recombination. No other source of helium that produces such a quantity is currently known in the universe. This prediction is another big success of the the standard cosmological model.

1.1.7 Problems of the standard model of cosmology

The main puzzles of standard cosmology do not arise from the model itself but from the initial condition it requires. The question of whether the initial conditions of a theory should be contained in it is not the subject here. In all cases, the situation is the same: the model presented so far needs fine-tuning. The horizon problem is a direct consequence of the initial homogeneity and the flatness problem is related to the initial amount of potential versus kinetic energy. So to be rigorous, these first two problems are not strict inconsistencies in the standard cosmological model, but still need to be addressed. Finally, the standard model of cosmology is a homogeneous theory, hence it cannot account for the formation of structures.

Horizon problem

The most outstanding result about the CMB observation is that its spectrum is the one of a black body with temperature $T \simeq 2.725$ K, see Fig. 1.1. Today, more accurate measurements of the tiny deviations, $\Delta T/T \sim 10^{-4}$, provide plenty of information about the Universe structure and content (see Sec. 1.2.3). There is however major evidence that at the time of recombination, the Universe was in thermal equilibrium. The horizon problem is the following: today we receive the signal of a thermal equilibrium among regions of space that were not able to interact at the time there were supposed to, even if they do now. The distance at which a region can interact with another one is bounded by the (finite) age of the Universe. It can be computed by the null geodesic as

$$r = \int_0^t \frac{dt'}{a(t')} = \int_0^a r_H \, d\log a \tag{1.57}$$

where $c = 1$ and $r_H = (aH)^{-1}$ is the comoving Hubble radius. For a universe dominated by a fluid with equation of state (1.15) we get $r_H^2 \sim a^{1+3w}$, hence for matter and/or radiation, $w \geqslant 0$, r_H grows monotonically and regions that could never interact eventually enter into causal contact.

The question is to find how those regions exhibit a perfect black body thermal equilibrium, despite never having been in causal contact. This puzzle was first pointed out by Rindler in 1956 [13].

Flatness problem

As seen in Sec. 1.1.2, observations yield the constraint $|\Omega_k^0| < 0.01$ [8], implying that, since Ω_k redshifts as a^{-2}, a flat Universe today means that the Universe has always been flat. This is because the critical value $\Omega = 1$ is an unstable fixed point. In other words, the flatness observed today requires an extreme fine-tuning of Ω close to unity in the early Universe, as the first Friedmann equation tells us that any deviation of Ω from 1 would have been magnified. Indeed, we can write Eq. (1.32) as

$$\Omega - 1 = k \, r_H^2. \tag{1.58}$$

Recall that in standard cosmology, the Hubble comoving radius r_H grows with time, therefore any deviation from $k = 0$ would lead to $\Omega \neq 1$. For instance, if we assume a radiation dominated

Universe, Ω_k at the time of nucleosynthesis ($t = 1$ s) should be 23 orders of magnitude smaller than today's value! If we reject such fine tuning, we should look for some dynamical process to have made the Universe flat. This problem was first mentioned by Dicke in 1969 [14].

Formation of structures

The Friedmann equations successfully relate the Universe shape and content to its time evolution. However it is out of their scope to describe any inhomogeneous physics as they are grounded on the cosmological principle and consequently they assume a homogeneous universe. There is, nevertheless, structure in the Universe at lower scales, as we are living in it, whose origin should be taken into account by a more complete theory of cosmology.

1.2   Inflationary Cosmology

Inflation was developed in the late 1970s in order to solve the problems of the standard model of cosmology mentioned above by postulating a period before BBN where the Hubble horizon is shrinking [15–17] (for up-to-date references, see e.g. [18–20]). We stress that inflation is not a theory but a paradigm, a collection of different models that must conform to observations. For each one of them, the origin of all the concerned details must be specified by some appropriate ultraviolet (UV) completion of the inflationary model. As we shall see, once done, this paradigm nevertheless solves all the aforementioned problems.

First, the causally disconnected patches at the time of CMB are homogeneous because they were in thermal contact at an earlier time. In other words, there was a time, at the very beginning of inflation where all the universe we observe today was causally connected. During inflation, the Universe undergoes a period of exponential expansion, as we will see next, and causal contact is lost among regions. When inflation ends, r_H starts to grow again and allows bigger scales to re-enter the horizon.

Second, the flatness problem is immediately solved by a decreasing r_H as Eq. (1.58) for $k = \pm 1$ yields $|\Omega - 1| = r_H^2$. Hence during inflation, the solution $\Omega = 1$ becomes an attractor and the Universe is flattened out.

Third, inflation is such a tremendous expansion that quantum fluctuations become macroscopic and seed the primordial inhomogeneity. Gravity and time then allow these little deviations to become the large scale structure of the Universe we see today.

1.2.1   Conditions for inflation

Mathematically, a shrinking Hubble horizon translates into an accelerated expansion:

$$\frac{d\,r_H}{dt} < 0 \quad \Leftrightarrow \quad \ddot{a} > 0, \tag{1.59}$$

where we used the Hubble parameter definition (1.28). In the previous section we have seen that neither matter domination nor radiation domination in the energy content of the Universe could provide such a condition. Indeed, if we take the derivative of the first Friedmann equation (1.11) with respect to time and use (1.14) to cancel $\dot{\rho}$, we get

$$\ddot{a} = -\frac{\dot{a}}{2M_{\text{pl}}} \sqrt{\frac{\rho}{3}} \, (1 + 3w), \tag{1.60}$$

where we used the reduced Planck mass

$$M_{\text{pl}} \equiv \frac{1}{\sqrt{8\pi G}} \simeq 2.435 \cdot 10^{18} \text{ GeV}. \tag{1.61}$$

We immediately see that an accelerated expansion requires $w < -1/3$. Therefore, in a first approximation, a natural choice for the dominant type of energy is dark energy, to which an exponentially growing scale factor $a_{\Lambda D}(t) \propto e^{Ht}$ is associated. Note that in de Sitter space the Hubble parameter is constant in virtue of (1.21). However, a strict cosmological constant leads to exponential inflation forever (eternal inflation), which cannot be followed by a radiation era. Indeed, we are interested in a period of accelerated expansion that, in addition to being characterized by very different energy scales in the early Universe, ultimately ends up leaving room for the standard radiation dominated and BBN cosmological phases.

In order to have an arrow of time, the energy responsible for inflation cannot be exactly constant (or in equilibrium), but should be dynamical, just as a quasi-static process in thermodynamics, where a change occurs in a series of states at equilibrium. This is why in realistic models of inflation, the Hubble parameter is not exactly constant. We can illustrate this by taking the time derivative of Eq. (1.28) to write

$$\frac{\ddot{a}}{a} = H^2(1 - \epsilon_H), \qquad \epsilon_H \equiv -\frac{\dot{H}}{H^2}. \tag{1.62}$$

Two things can be deduced from this equation. First, if the Hubble parameter is constant, then $\epsilon_H = 0$ and the accelerated expansion lasts forever. This is a pure Λ-dominated Universe. Second, if $\epsilon_H = 1$, the acceleration is zero and inflation does not occur. Hence in order to have a finite inflationary period, we need a non-zero $\epsilon_H \ll 1$ at early times and provide conditions for this parameter to grow until it reaches unity while satisfying the observational constraints. In sum, we see that ϵ_H is a parameter that controls inflation and it will become handy when we discuss the slow roll inflation approximation.

Finally, to solve the horizon and flatness problems using inflation, the Universe must have expanded by a factor of $10^{21\text{-}26}$ in $\sim 10^{-36\text{-}32}$ seconds. We usually rewrite this condition with the e-folding number

$$N = \log \frac{a}{a_i}, \tag{1.63}$$

thus making use of the change of variable $dN = d\log a$ that appeared in (1.57). The fluctuations observed in the CMB are created $N_* \approx 50\text{-}60$ e-folds before the end of inflation. The precise value depends on the details of the post-inflationary history of the Universe.

1.2.2 Scalar field inflation

So far we have discussed the general conditions needed to solve the big problems of the standard cosmology, but have not addressed the question of its realization. The goal is to have a pre-BBN short period of almost Λ dominated Universe. In other words, at early times the Universe should be filled by some homogeneous exotic matter with negative pressure but in a dynamical way such that this energy eventually gets converted into radiation. From the point of view of particle physics, the simplest solution is a scalar field whose energy share is dominated by its potential.

The simplest inflaton model

Let's introduce a new real scalar field ϕ, the inflaton, in the theory with Lagrangian

$$\mathcal{L}_\phi = \frac{1}{2} g^{\mu\nu} \partial_\mu \phi \partial_\nu \phi - V(\phi). \tag{1.64}$$

Its energy-momentum tensor is computed from the standard definition

$$T_{\mu\nu} = 2 \frac{\delta \mathcal{L}_\phi}{\delta g^{\mu\nu}} - g_{\mu\nu} \mathcal{L}_\phi \tag{1.65}$$

and reads

$$T_{\mu\nu} = \partial_\mu\phi\partial_\nu\phi - g_{\mu\nu}\mathcal{L}_\phi, \tag{1.66}$$

which, combined with (1.10), gives

$$\rho_\phi = \frac{1}{2}\dot{\phi}^2 + V(\phi), \tag{1.67a}$$

$$p_\phi = \frac{1}{2}\dot{\phi}^2 - V(\phi). \tag{1.67b}$$

The criterion $w < -1/3$ is then fulfilled by imposing $V(\phi) \gg \frac{1}{2}\dot{\phi}^2$ as

$$w_\phi = \frac{\frac{1}{2}\dot{\phi}^2 - V(\phi)}{\frac{1}{2}\dot{\phi}^2 + V(\phi)}. \tag{1.68}$$

The slow roll inflation

Using the second Friedmann equation (1.12), Eqs. (1.67) and (1.62) we can write

$$\frac{\ddot{a}}{a} = H^2 - \frac{1}{2}\dot{\phi}^2 \quad \Rightarrow \quad \dot{H} = -\frac{1}{2}\dot{\phi}^2 \tag{1.69}$$

which leads to the fact that

$$\epsilon_H = \frac{3}{2}\left(w_\phi + 1\right). \tag{1.70}$$

We can still use the criterion $\epsilon_H < 1$ for accelerated expansion. As the kinetic energy is suppressed compared to the potential energy, the dynamics regime is denoted as *slow roll* inflation and inflation is controlled by the slow roll parameters, the first one being ϵ_H. There is however a second condition for a sucessfull inflation, which is that the slow rolling regime ensured by $\epsilon_H < 1$ lasts long enough for the N_* e-folds to happen before the end. Hence, even if $\dot{\phi}$ is negligible, we must ensure that it stays so for a sufficiently long period of time by asking that $\ddot{\phi}$ is small enough, i.e. $|\eta_H| < 1$ with

$$\eta_H = -\frac{\ddot{\phi}}{H\dot{\phi}}, \tag{1.71}$$

the second slow-roll parameter. Now, the only freedom left is in the choice of the potential $V(\phi)$.

Varying the action in the FRW flat metric (1.36) with respect to ϕ yields the dynamics of the field

$$\ddot{\phi} + 3H\dot{\phi} - \frac{\nabla^2\phi}{a^2} + V'(\phi) = 0. \tag{1.72}$$

Since the inflaton is homogeneous, we have $\nabla\phi = 0$ and the result is none other than the Klein-Gordon equation in an expanding Universe. Depending on the model, i.e. on the potential $V(\phi)$, it is usual, based on what we have just seen, to use the so-called slow roll approximation:

$$3H\dot{\phi} \simeq -V'(\phi), \tag{1.73a}$$

$$3M_{\rm pl}^2 H^2 \simeq V(\phi), \tag{1.73b}$$

and express the slow roll parameters as conditions on the shape of the inflationary potential. Assuming the slow roll approximation, we can use (1.62) and (1.69) to write the slow roll parameter in terms of the potential

$$\epsilon_H \simeq \epsilon_V \equiv \frac{M_{\rm pl}^2}{2}\left(\frac{V'(\phi)}{V(\phi)}\right)^2 \tag{1.74}$$

where the first equality is only valid deep inside the inflation regime, i.e. when $\epsilon_H, \epsilon_V \ll 1$. Similarly,

the second slow roll parameter writes

$$\eta_H \simeq \eta_V - \epsilon_V, \qquad \eta_V \equiv M_{\rm pl}^2 \frac{V''(\phi)}{V(\phi)}. \tag{1.75}$$

There is also a third slow roll parameter defined as

$$\xi_V^2 = M_{\rm pl}^4 \frac{V'(\phi)V'''(\phi)}{V^2(\phi)} \tag{1.76}$$

which measures the running of the scalar tilt $n_s' = dn_s/d\log k$, as we will see in Eq. (1.85). Inflation is then guaranteed by the conditions $\epsilon_V \ll 1$, $|\eta_V| \ll 1$, $\xi_V^2 \ll 1$.

When the slow roll approximation is made, the Hubble parameter is approximately constant $H \simeq H_{\rm inf}$ and the Universe metric is approximately de Sitter $a \propto e^{Ht}$. In this work, we will mainly use the potential slow roll parameters and from now on we will drop the associate index as it will be clear from the context. Also, if there is any difference between the Hubble and the potential version, it is small and only for values near the end of inflation.

1.2.3 Density perturbations

As already mentioned when the CMB was discussed, the Universe is homogeneous on large scales, its spectrum having a perfect black-body shape around $T \simeq 2.725$ K, but remains highly inhomogeneous on small scales. These tiny deviations,

$$\frac{\delta T}{T} \sim \frac{\delta \rho}{\rho} \sim 10^{-5} \tag{1.77}$$

called primordial fluctuations, were the seeds of the present structure, and inflation can provide an explanation for them. On Fig. 1.2 we show the CMB anisotropies map from Planck, obtained in 2013, and its power spectrum.

Inflation is modeled by the classical description of a (or many) field. At the quantum level, all fields fluctuate around their expectation value according to the Heisenberg principle

$$\phi(t, \boldsymbol{x}) = \bar{\phi}(t) + \delta\phi(t, \boldsymbol{x}). \tag{1.78}$$

These fluctuations lead to a local delay in the time at which inflation ends, which means that different parts of the universe will end inflation at slightly different times. Because the perturbations are small, expanding the Einstein equations (1.1) at linear order in perturbations approximates the full non-linear solution to very high accuracy

$$\delta G_{\mu\nu} = 8\pi G \, \delta T_{\mu\nu}. \tag{1.79}$$

During inflation we define perturbations around the homogeneous background solutions for the inflaton as (1.78) and the metric as

$$g_{\mu\nu}(t, \boldsymbol{x}) = \bar{g}_{\mu\nu}(t) + \delta g_{\mu\nu}(t, \boldsymbol{x}), \tag{1.80}$$

where, in the absence of anisotropic stresses, which is verified during inflation,

$$ds^2 = -(1 + 2\Phi)dt^2 + 2aB_i dx^i dt + a^2[(1 - 2\Phi)\delta_{ij} + E_{ij}]dx^i dx^j. \tag{1.81}$$

We can identify scalar (Φ), vector (B_i) and tensor (E_{ij}) perturbation modes, although this is not the canonical way of decomposition and there are issues with the gauge invariance (for more details,
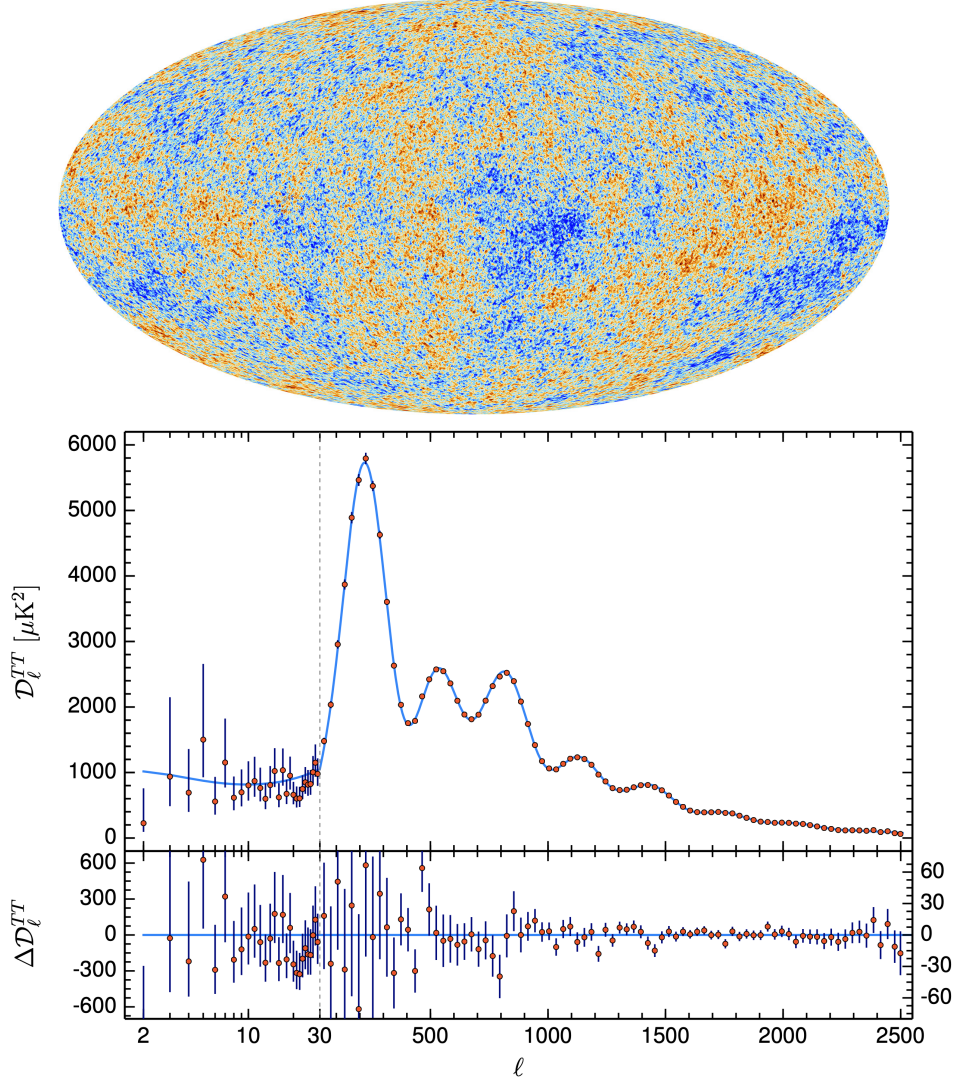
Figure 1.2. Top map: The anisotropies of the CMB as observed by Planck. The color scale displays deviation from the mean temperature from -300 μK (blue) to +300 μK (red). Bottom plots: CMB temperature power spectrum, also called multipole expansion, results from the Planck 2018 Collaboration [6]. The larger the multipole ℓ, the smaller the correlation angle α, and hence the distance, with $\ell \simeq 200 \Leftrightarrow \alpha \simeq 1°$. The lower panel shows the residuals with respect to the base-ΛCDM theoretical model whose fit is in blue. The error bars show $\pm 1\sigma$ diagonal uncertainties. Figures taken from the European Space Agency website (picture link) and Ref. [6].

see e.g. Ref. [20, 21]). Nevertheless, we recall that our aim in these sections is to motivate the main chapters and not to give a complete description of all the topics.

We can change variable and work out the perturbation study in Fourier space to reduce the observed inhomogeneity in the CMB to a few parameters. This detailed calculation also shows that there is no vector perturbation in the absence of sources with vorticity. Primordial fluctuations are typically quantified by a power spectrum which gives the power of the variations as a function of spatial scale. The power spectrum is computed from the average of all the 2-point correlation

function

$$\langle \delta_k \delta_{k'} \rangle = \frac{2\pi^2}{k^3} \delta(k - k') \, \mathcal{P}(k), \qquad\qquad \delta_k \equiv \frac{\delta\rho(k)}{\rho} \tag{1.82}$$

The scalar and tensor components of the fluctuations obey power laws

$$n_s = 1 + \frac{d\log \Delta_s^2}{d\log k}, \qquad\qquad n_t = \frac{d\log \Delta_t^2}{d\log k}, \tag{1.83}$$

where

$$\Delta^2(k) \equiv \frac{k^3}{2\pi^2} \, \mathcal{P}(k). \tag{1.84}$$

The value $n_s = 1$ corresponds to scale invariant fluctuations. We may also be interested in the indices running

$$n_s' = \frac{dn_s}{d\log k}, \qquad\qquad n_t' = \frac{dn_t}{d\log k} \tag{1.85}$$

while the amplitude of the scalar spectrum A_s is obtained from

$$\Delta_s^2(k) = A_s(k_\star) \left(\frac{k}{k_\star} \right)^{n_s(k_\star) - 1 + \frac{n_s'(k_\star)}{2} \log \frac{k}{k_\star}} \tag{1.86}$$

where $k_\star$ is an arbitrary reference or pivot scale.

Tensor fluctuations are often normalized relative to the (measured) amplitude of scalar fluctuations. The tensor-to-scalar ratio is

$$r(k) \equiv \frac{\mathcal{P}_t(k)}{\mathcal{P}_s(k)}. \tag{1.87}$$

Given a potential, the previous expressions allow us to construct the scalar amplitude and spectral index, as well as the tensor-to-scalar ratio, in terms of the inflaton field values at the pivot scale. At the leading order in the slow roll approximation, the amplitudes of the scalar and the tensor spectra are given

$$\mathcal{P}_s(k) \simeq \left(\frac{H^2}{2\pi\dot\phi} \right)^2_{k=aH} \qquad\qquad \mathcal{P}_t(k) \simeq \frac{8}{M_{\rm pl}^2} \left(\frac{H^2}{2\pi} \right)^2_{k=aH}, \tag{1.88}$$

both evaluated at Hubble-radius crossing $k = aH$. This yields for the amplitude of scalar fluctuations

$$A_s(\phi) = \frac{1}{24\pi^2 M_{\rm pl}^4} \frac{V(\phi)}{\epsilon(\phi)}. \tag{1.89}$$

Since Δ_s^2 is fixed and $\Delta_t^2 \simeq H^2 \simeq V$, the tensor-to-scalar ratio is a direct measure of the energy scale of inflation, as

$$V \sim \left(\frac{r}{0.01} \right) \left(10^{16} \text{ GeV} \right)^4. \tag{1.90}$$

Constraints on inflation

Observations of the CMB spectrum lead to constraints on the inflation model. There are two sets of (related) parameters to classify the inflation models:

- The slow roll parameters, whose current observational bounds are, from Ref. [22]:

$$
\begin{aligned}
\epsilon &< 0.0044 & \text{(95\% C.L.)}, \\
\eta &= -0.015 \pm 0.006 & \text{(68\% C.L.)}, \\
\xi^2 &= 0.0029^{+0.0073}_{-0.0069} & \text{(95\% C.L.)}.
\end{aligned}
\tag{1.91}
$$
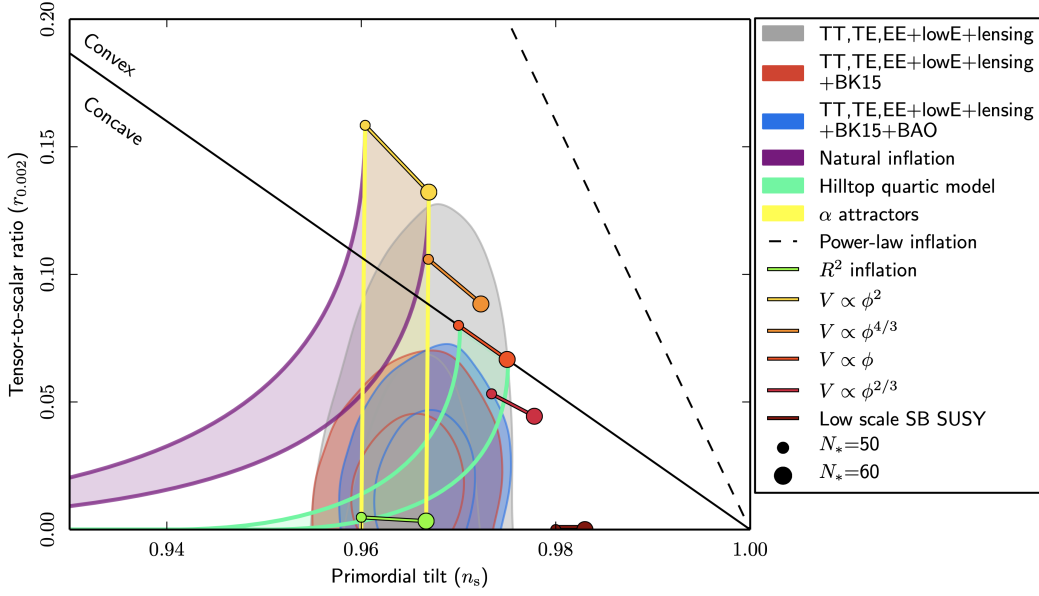
Figure 1.3. The marginalized joint 68 and 95% C.L. regions for the tilt in the scalar perturbation spectrum and the relative magnitude of the tensor perturbations, obtained from the Planck 2018 and lensing data alone, and their combinations with BICEP2/Keck Array (BK15) and (optionally) BAO data, confronted with the predictions of some of the most known inflationary models. Figure is taken from [22].

- The scalar spectral index n_s, the spectral index running n'_s, and the relative magnitude of the tensor perturbations r, with experimental values

$$n_s = 0.9649 \pm 0.0042, \qquad n'_s = -0.0045 \pm 0.0067, \qquad r = 0.014^{+0.010}_{-0.011} \qquad (1.92)$$

where we have included, in the last r determination, the most recent combined result from the BICEP/Keck collaboration [22, 23]. We show the allowed window in the parameter space of (n_s, r) on Fig. 1.3 in red and blue.

Both sets can be used for calculations and constraints and one can switch from one to the other with

$$n_s \simeq 1 - 6\epsilon + 2\eta, \qquad (1.93a)$$
$$n'_s \simeq 16\epsilon\eta - 24\epsilon^2 - 2\xi^2, \qquad (1.93b)$$
$$r = 16\,\epsilon. \qquad (1.93c)$$

To perform the exact change of basis, the correlation between the variables must be taken into account and the procedure is more complicated. Nevertheless the above relations are good approximation for most of the cases.

In this work, we find it more convenient to use the slow roll parameters as we will always specify the inflation model with its potential. To compare any model with the present bounds, we should evaluate all these parameters at the field value $\phi_* = \phi(N_*)$ with

$$N_* = \frac{1}{M_{\rm pl}^2} \int_{\phi_E}^{\phi_*} \frac{V(\phi)}{V'(\phi)}\, d\phi, \qquad (1.94)$$

being N_* the number of e-folds at which the reference scale exits the horizon. Here ϕ_E, the value of ϕ at the end of inflation, is defined by the condition $\epsilon(\phi_E) = 1$.

Observations indicate that the amplitude of the scalar perturbation associated with a mode that crossed the Hubble radius about $N_* \simeq 60$ e-folds before the end of inflation is about [22]

$$A_s^{\text{obs}} \simeq 2.2 \cdot 10^{-9}. \tag{1.95}$$

This value contrains the inflationary potential, as $A_s(\phi_*) = A_s^{\text{obs}}$ should hold, with $A_s(\phi)$ given by Eq. (1.89). We can combine all these results to also give a constraint on the Hubble parameter value at the onset of inflation [22]

$$H_*^{\text{obs}} \lesssim 6 \cdot 10^{13}\,\text{GeV}\ (95\%\,\text{CL}). \tag{1.96}$$

1.2.4 Reheating

By definition the Universe expands adiabatically, therefore a dazzling accelerated expansion, such as inflation, cools it down to absolute zero. To be able to fit in the historic timeline of the Universe, where inflation is followed by the Hot Big Bang, any inflation model shall come with an explanation on how the Universe reheats.

In the simplest picture the inflaton ϕ is rolling down its potential. At first slowly rolling, hence leading to successful inflation, the field starts accelerating when $\epsilon, |\eta| \sim 1$, and then rapidly oscillates around its potential minimum. This leads to the decay of the inflaton into radiation. The details of this mechanism are intricately related to the model so we cannot comment it further. In all cases, the inflaton model usually specifies the decay rate $\Gamma_{\phi \to \gamma\gamma}$ of the inflaton into photons, or at least the decay rate Γ_ϕ of the inflaton into species (of a given model) that eventually decay to photons.

The inflaton starts to decay when its lifetime becomes comparable to the age of the Universe, $\Gamma_\phi^{-1} \sim H^{-1}$, see Sec. 1.1.4. Thus we can compute the reheating temperature using (1.51) where we identify Γ_ϕ as H therein which provides

$$T_{\text{rh}} = \left(\frac{90}{\pi^2 g_*} \right)^{\frac{1}{4}} \sqrt{\Gamma_\phi M_{\text{pl}}}, \tag{1.97}$$

where we also used (1.61). Besides, in this thesis we define $T_{\text{rh}}^{\text{ins}}$ as a reference temperature given by the above equation with Γ_ϕ being the Hubble rate at the end inflation H_E. It would correspond to the reheating temperature for instant reheating, i.e. immediately after inflation ends.

When this last mechanism is not fulfilled, it has been shown that the temperature follows a non-trivial dynamics between the end of inflation and the reheating epoch. Indeed, the temperature first grows from zero to a maximum temperature T_0 given by [24, 25]

$$T_0 \simeq 0.61 \sqrt{T_{\text{rh}} T_{\text{rh}}^{\text{ins}}}. \tag{1.98}$$

The temperature T_0 is attained at a time t_0 when the scale factor a grows by an $\mathcal{O}(1)$ factor after the end of inflation, i.e. $a_0 \simeq 1.5\,a_E$, and, after that[5], the Universe evolves toward the reheating temperature following the law $T \sim a^{-3/8}$ [26], with a scale factor a_{rh} given by

$$a_{\text{rh}} \simeq 0.4\,a_E \left(\frac{T_{\text{rh}}^{\text{ins}}}{T_{\text{rh}}} \right)^{\frac{4}{3}}. \tag{1.99}$$

---

[5]The energy density is dominated, after the end of inflation, by the inflaton energy density $\rho_\phi(t)$, which decays as $e^{-\Gamma_\phi t}$, so that at the reheating temperature the energy density is dominated by the radiation energy density $\rho_\gamma(t)$.

At the reheating temperature, the inflaton energy density has completely decayed and the Universe is fully dominated by radiation, giving rise to a radiation dominated era where the temperature evolves as $T \sim 1/a$. Of course, the value of the inflaton decay width Γ_ϕ, and the reheating temperature T_{rh}, depend on the particular interactions between the inflaton and the Standard Model particles.

Note that, when studying the reheating process only, a good approximation is to use $V(\phi) \simeq \frac{1}{2}m^2\phi^2$ since the mass term is the leading one of the potential expansion in the vicinity of its minimum. This term however forbids describing the full inflationary period, see next section on monomial inflation.

For some models, it is also possible that the photon production happens non-perturbatively, i.e. through an energy transfer that happens at the classical level in the equation of motion. In those cases this phenomenon is ofter referred to as *preheating*, as after this energy transfer to radiation the inflaton will still decay and reheats the Universe through a perturbative process.

For the remainder of this section, we will briefly present some models of inflation, for later use in this thesis.

1.2.5   Inflation models

In this section we introduce several classes of models that all satisfy the cosmological constraints. They should be considered as a sample of possible models, and they are chosen for later use in this thesis. They do not exhaust by any means all the allowed inflationary models.

Monomial inflation

Monomial inflation was suggested because of its simplicity, as the inflaton potential is taken to be

$$V(\phi) = \lambda M_{\mathrm{pl}}^{n-4}\phi^n, \tag{1.100}$$

where λ is a dimensionless coupling. The case $n = 4$ (*chaotic inflation* [27]) corresponds to the self-coupling of the scalar field, an interaction that is natural from the point of view of effective theory.

Now using (1.74) and (1.94) we compute

$$\phi_E = \frac{nM_{\mathrm{pl}}}{\sqrt{2}}, \qquad \phi_* = M_{\mathrm{pl}}\sqrt{2n\left(N_* + \frac{n}{4}\right)}. \tag{1.101}$$

Then, the slow roll parameters evaluated N_* e-fold before the end of inflation write

$$\epsilon(\phi_*) = \frac{n}{4N_* + n}, \qquad \eta(\phi_*) = \frac{2(n-1)}{4N_* + n}. \tag{1.102}$$

The constraints (1.91) are not satisfied for $n \geqslant 2$, hence all monomial models are ruled out.

α-attractor models

The α-attractor potential is given by [28]

$$V_\alpha(\phi) = \Lambda_\alpha^4 \left[1 - \exp\left(-\sqrt{\frac{2}{3\alpha}}\frac{|\phi|}{M_{\mathrm{pl}}}\right)\right]^2. \tag{1.103}$$

Setting $\alpha = 1$ yields the R^2 model, or Starobinsky potential, see Sec. 1.2.6. In the slow roll approximation, the field value at the end of inflation is

$$\phi_E = \sqrt{\frac{3\alpha}{2}}\, M_{\text{pl}} \log\left(1 + \frac{2}{\sqrt{3\alpha}}\right). \tag{1.104}$$

We can readily compute ϕ_*, and evaluate the slow roll parameters $N_* = 60$ e-folds before the end of inflation. The slow roll parameters and the cosmic observables are in agreement with the cosmological contraints for the range

$$1 \leqslant \alpha \lesssim 100. \tag{1.105}$$

In particular, for $\alpha = 1\,(100)$ we get

$$\epsilon_* \simeq 0.00019\,(0.00387), \qquad \eta_* \simeq -0.0159\,(-0.00331)$$
$$n_s \simeq 0.967\,(0.97), \qquad r_* \simeq 0.003\,(0.062), \qquad H_E \simeq 0.82\,(1.13)\cdot 10^{13}\text{ GeV}. \tag{1.106}$$

in agreement with the observed values (1.91), (1.92) and (1.96). Using the observed value of A_s given by Eq. (1.95), we fix the vacuum energy. The result depends on α and is approximately given by $\Lambda_\alpha \simeq 3.4\cdot 10^{-3}\,\alpha^{1/5}\,M_{\text{pl}}$. We then obtain the values $\Lambda_1 = 3.152\cdot 10^{-3}\,M_{\text{pl}}$ and $\Lambda_{100} = 8.313\cdot 10^{-3}\,M_{\text{pl}}$.

Hilltop quartic models

The hilltop model potential is given by [29]

$$V_{\text{h}}(\phi) = \Lambda_{\text{h}}^4\left[1 - \left(\frac{\phi}{\mu}\right)^p\right]^2 \tag{1.107}$$

with $p \geqslant 2$. The case $p = 4$ can be compatible with the Planck measurements. There are two ways for the field to relax to the minimum at $\phi = \mu$, with different initial conditions:

1. $\phi_* > \phi_E$: In this case the field $\phi > \mu$ is relaxing in a potential region that can be approximated by $V_{\text{h}} \sim \phi^8$, and thus, the slow roll conditions are not met, as monomial inflation is ruled out.

2. $\phi_* < \phi_E$: In this case the field $\phi < \mu$ is relaxing in a flat potential region and the model predicts correct inflationary observables for a large range of the parameter space. In this thesis, this option will be retained.

The slow roll parameters and the cosmic observables are in agreement with the contraints for the range

$$10 M_{\text{pl}} \lesssim \mu \lesssim 50 M_{\text{pl}}. \tag{1.108}$$

We fix the vacuum energy from the constraint on the amplitude of scalar fluctuations. The result depends on μ and is approximately $\Lambda_{\text{h}} \simeq 6\cdot 10^{-4}\,\mu^{2/3}\,M_{\text{pl}}^{1/3}$. We then have the values $\Lambda_{\text{h}} = 3.243\cdot 10^{-3}\,M_{\text{pl}}$ for $\mu = 10\,M_{\text{pl}}$ and $\Lambda_{\text{h}} = 8.081\cdot 10^{-3}\,M_{\text{pl}}$ for $\mu = 50\,M_{\text{pl}}$.

In particular, for $\mu = 10\,(50)\,M_{\text{pl}}$ we get

$$\epsilon_* \simeq 0.00021\,(0.0041) \qquad \eta_* \simeq -0.0207\,(-0.00328)$$
$$n_s \simeq 0.957\,(0.97) \qquad r_* \simeq 0.00335\,(0.0654), \qquad H_E \simeq 0.64\,(1.1)\cdot 10^{13}\text{ GeV}. \tag{1.109}$$

D-brane models

The D-brane potential is given by [30–32]

$$V_{\mathrm{D}}(\phi) = \Lambda_{\mathrm{D}}^4 \left[1 - \left(\frac{\mu}{\phi} \right)^p \right]^2 \tag{1.110}$$

with $p > 0$. As in the last case, there are two ways for the field to relax to the minimum at $\phi = \mu$ and only the option $\phi_* > \phi_E$ is viable for inflation as the potential region $\phi < \mu$ is too steep. The slow roll parameters and the cosmic observables are in agreement with the constraints for the range

$$8M_{\mathrm{pl}} \lesssim \mu \lesssim 14 M_{\mathrm{pl}} \qquad (p = 1) \tag{1.111a}$$

$$9M_{\mathrm{pl}} \lesssim \mu \lesssim 26 M_{\mathrm{pl}} \qquad (p = 2) \tag{1.111b}$$

$$4M_{\mathrm{pl}} \lesssim \mu \lesssim 37 M_{\mathrm{pl}} \qquad (p = 3). \tag{1.111c}$$

For $p \geqslant 4$ there is no lower bound anymore and the upper bound keeps raising.

Because the results depend on the value of p we will not provide the values of the slow roll parameters at ϕ_* but they can easily be computed with the same methods as in the previous examples. Finally, unlike the others, we will not use this model in the following chapters, but we have introduced it anyway because we will have the opportunity to comment on it.

Non minimal couplings

In this class of models, a non minimal coupling is added to gravity in the so-called *Jordan frame* where this coupling appears explicitly in the Lagrangian [33–36]. The latter writes in M_{pl} units

$$S = \int d^4 x \sqrt{-g} \left(-\frac{1 + g\phi^p}{2} R + \frac{1}{2} \partial_\mu \phi \partial^\mu \phi - U(\phi) \right), \tag{1.112}$$

where $p \in \mathbb{N}^*$. To ensure a flat potential for $\phi \to \infty$, the dominant term in the Jordan frame potential needs to be

$$U(\phi) \simeq \lambda \phi^{2p}, \qquad (\phi \to \infty). \tag{1.113}$$

Hereafter we will see that this choice guarantees a slow roll regime.

In order to use the canonical tools at our disposal, one must go to the *Einstein frame* where the graviton has a canonical kinetic term. The interaction between the Higgs and Ricci then modifies the potential and the Higgs kinetic term, as we will see now.

For values of the ϕ field such that $g\phi^p > 1$, we must redefine the metric and go to the so-called Einstein frame to recover the Einstein-Hilbert action for the Ricci scalar. To do so, we perform a Weyl redefinition of the metric:

$$g_{\mu\nu} \to \Theta \, g_{\mu\nu}, \qquad\qquad \sqrt{-g} \to \Theta^2 \sqrt{-g}. \tag{1.114}$$

For the Ricci scalar this implies

$$R \to \frac{R}{\Theta} - \bar{R}, \qquad \bar{R} = \frac{6}{\Theta^{3/2}} \frac{\partial_\mu \left(g^{\mu\nu} \sqrt{-g} \, \partial_\nu \sqrt{\Theta} \right)}{\sqrt{-g}}. \tag{1.115}$$

Note that R is absent in the correction term $\bar{R}$, hence we will define Θ by demanding that the explicit coupling between ϕ and R disappears from the Lagrangian in the Einstein frame. The Ricci

part of the action transforms then as

$$S_R \to S_R^E = - \int d^4x \sqrt{-g} \, \frac{1+g\phi^p}{2} \left(R\Theta - \bar{R}\Theta^2 \right) \tag{1.116}$$

and so the definition

$$\Theta(\phi) = \frac{1}{1+g\phi^p} \tag{1.117}$$

leads to

$$S_R^E = \int d^4x \sqrt{-g} \left(-\frac{R}{2} + 3\Theta^2 g^2 \phi^p \, \partial_\mu \phi \partial^\mu \phi \right). \tag{1.118}$$

In the meantime the kinetic term gets transformed to $\frac{\Theta}{2} \partial_\mu \phi \partial^\mu \phi$ so that the remainder of the action becomes

$$S_E = \int d^4x \sqrt{-g} \left[-\frac{R}{2} + \frac{\Theta}{2} \left(1 + 6g^2 \phi^p \, \Theta \right) \partial_\mu \phi \partial^\mu \phi - V(\phi) \right] \tag{1.119}$$

where the Einstein frame potential $V(\phi)$ is given by

$$V(\phi) = \Theta^2 U(\phi) = \frac{\lambda}{g^2} \left(1 + \frac{1}{g\phi^p} \right)^{-2} \simeq \frac{\lambda}{g^2} \left(1 - \frac{1}{g\phi^p} \right)^2 \tag{1.120}$$

where the last approximation is valid in the regime $g\phi^p \gg 1$ where the Einstein frame departs from the Jordan frame.

The true inflaton field χ has a canonical kinetic term, unlike ϕ, hence we perform the following change of variable

$$\frac{d\chi}{d\phi} = \sqrt{\Theta(1 + 6g^2 \phi^p \, \Theta)}, \tag{1.121}$$

such that

$$S_E = \int d^4x \sqrt{-g} \left[-\frac{R}{2} + \frac{1}{2} \partial_\mu \chi \partial^\mu \chi - V[\phi(\chi)] \right]. \tag{1.122}$$

Solving the differential equation (1.121) is possible analytically and the result depends on the value of p. In the limit $g\phi^p \gg 1$ we obtain

$$\phi(\chi) \simeq \frac{g}{1+6g} \frac{\chi^2}{4} \qquad\qquad (p=1) \tag{1.123a}$$

$$\phi(\chi) \simeq \frac{1}{2\sqrt{g(1+6g)}} \exp\left(\sqrt{\frac{g}{1+6g}} \chi \right) \qquad\qquad (p=2) \tag{1.123b}$$

$$\phi(\chi) \simeq A_p \left(c_p - \chi \right)^{\frac{2}{2-p}} \qquad\qquad (p \geqslant 3) \tag{1.123c}$$

where, for the last case, the constants A_p and c_p are such that

$$A_p = \left(\frac{p-2}{2} \right)^{\frac{2}{2-p}} \left(\frac{g}{1+6g} \right)^{\frac{1}{2-p}}, \qquad \lim_{\phi \to \infty} \chi(\phi) = c_p, \qquad \chi \in [0, c_p]. \tag{1.124}$$

Their particular values are not important for the discussion.

The potential written as a function of the canonically normalized field χ in the same limit is then

$$V(\chi) \simeq \frac{\lambda}{g^2} \left(1 - \frac{v_1^2}{\chi^2} \right)^2, \qquad\qquad v_1 = \frac{2\sqrt{1+6g}}{g} \qquad (p=1) \tag{1.125a}$$

$$V(\chi) \simeq \frac{\lambda}{g^2} \left[1 - 4(1+6g)\exp\left(-\sqrt{\frac{4g}{1+6g}}\,\chi\right) \right]^2 \qquad\qquad (p=2) \qquad (1.125\mathrm{b})$$

$$V(\chi) \simeq \frac{\lambda}{g^2} \left[1 - \left(\frac{c_p - \chi}{v_p}\right)^{\frac{2p}{p-2}} \right]^2, \qquad v_p = \frac{2g^{-1/p}}{p-2}\sqrt{1+6g}. \qquad (p \geqslant 3) \qquad (1.125\mathrm{c})$$

For the case $p=1$, we get a potential in the class obtained from D-brane models, shown above. For the case $p=2$, we get an α-attractor potential with $\alpha = 1 + \frac{1}{6g}$. For the cases $p \geqslant 3$, we can see that $\frac{2p}{p-2} > 0$ in the limit where $\phi \gg 1$, i.e. when $(c_p - \chi) \ll 1$. Also, the potential for $p \geqslant 3$ is flat and can provide a good inflationary model. This kind of potential for $p \geqslant 3$ coincides with the *hilltop models* considered above. In particular for $p=4$, the field dependence of the potential is $(c_4 - \chi)^4$, as in the hilltop model.

To conclude, we can see that we recover some of the previous potentials, though with a major difference, which is that we changed variables $\phi \to \chi$. So in one case we have the potential from the start, without any coupling to the Ricci, and in the other case the potential arises from the Weyl rotation to the Einstein frame. In the meantime, we have redefined the inflaton field, as ϕ has no canonical kinetic term. Thus it is important to distinguish between the two cases and not just stop at their potentials because they really represent two different models.

1.2.6   Higgs inflation

Identifying the Higgs Φ as the inflaton went without saying since it is the only scalar field in the Standard Model of particle physics (SM). These theories, dubbed as Higgs inflation (HI) [37–39], first proposed monomial potentials because the Higgs self-interaction $V(\Phi) = \lambda_h |\Phi|^4$ comes naturally in the theory and is the dominant term at the energy scale where inflation takes place. However, we have seen in the last section that this option is ruled out by cosmological observations.

Today, *Higgs inflation* refers to another class of models where the inflaton is still identified with the SM physical Higgs field, but with an added non minimal coupling to gravity according to the model we have just seen in last section (for a review see [40]). Adapting the action (1.112) to Higgs physics leads to the starting point

$$S = \int d^4x\,\sqrt{-g}\left(-\frac{M_{\mathrm{pl}}^2}{2}R - \xi_h|\Phi|^2 R + (D_\mu\Phi)^\dagger D^\mu\Phi - U(\Phi)\right), \qquad (1.126)$$

where U the Higgs potential in the Jordan frame. The Higgs doublet writes

$$\Phi = e^{i\zeta^a\tau^a}\begin{pmatrix} 0 \\ \frac{h}{\sqrt{2}} \end{pmatrix}, \qquad (1.127)$$

where ζ^a are the three Goldstone bosons, τ^a are the $SU(2)$ generators (see Sec. 2.2.2) and h is the physical Higgs. The covariant derivative D_μ given by (2.80) couples the four Higgs degrees of freedom to the weak and hypercharge interactions, see Sec. 2.3.1 for more details.

As we study inflation, the physical Higgs VEV is then large (except for the brief moments when it crosses zero in case it oscillates in the reheating period) and EW symmetry is broken, see Sec. 2.3.3. Furthermore, for the Higgs sector, the Goldstone bosons χ^a are eaten up in the unitary gauge $\omega(\alpha^a) = \exp(i\alpha^a\tau^a)$, with $\alpha^a = -\zeta^a$, while the Higgs field h is chargeless under electromagnetism, $Q = 0$, hence its covariant derivative reduces to ∂_μ, leading to the action

$$S = \int d^4x\sqrt{-g}\left(-\frac{M_{\mathrm{pl}}^2 + \xi_h h^2}{2}R + \frac{1}{2}\partial_\mu h\partial^\mu h - U(h)\right). \qquad (1.128)$$

For the scale involved in inflation, we can use

$$U(h) \simeq \frac{\lambda_h}{4} h^4, \tag{1.129}$$

where λ_h is taken as a positive free parameter. We hence implicitly assume that the Higgs potential is stabilized by some mechanism that leads to non-negative self-coupling at the energy scale at which inflation takes place (see Sec. 2.3.5).

Using the results from the last section with $\phi = h$, $p = 2$ and $g = \xi_h$, we obtain in the limit $\xi_h h^2 \gg 1$ that the Higgs field is given as a function of χ, i.e. $h(\chi)$ by Eq. (1.123b). The potential written as a function of the canonically normalized field χ in the same limit is then given by (1.125b). Assuming $\xi_h \gg 1$, which will be proven in the next section, we can write

$$h(\chi) \simeq \frac{M_{\mathrm{pl}} e^{\frac{\chi}{\sqrt{6} M_{\mathrm{pl}}}}}{\sqrt{24}\, \xi_h} \tag{1.130}$$

and

$$V(\chi) \simeq \frac{\lambda M_{\mathrm{pl}}^4}{4\xi_h^2} \left[1 - 24\xi_h\, e^{-\sqrt{\frac{2}{3}}\, \frac{\chi}{M_{\mathrm{pl}}}} \right]^2. \tag{1.131}$$

Slow roll Higgs inflation

Using the latter approximations, which is justified provided that $\sqrt{\xi_h} h \gtrsim M_{\mathrm{pl}}$ and $\xi_h \gg 1$, we solve $\epsilon(\chi_E) = 1$ to obtain

$$\chi_E = \sqrt{\frac{3}{2}}\, M_{\mathrm{pl}} \log\left(24\xi_h\beta\right), \qquad \beta \equiv 1 + \frac{2}{\sqrt{3}}, \tag{1.132}$$

and from Eq. (1.94) we get

$$\chi_* = \sqrt{\frac{3}{2}}\, M_{\mathrm{pl}} \left(\log\left(24\xi_h\beta\right) - \frac{4N_*}{3} - \beta - W_* \right), \tag{1.133}$$

where $\mathcal{W}_*$ is the Lambert function evaluated at

$$W_* \equiv \mathcal{W}_{-1}\left[-\beta \exp\left(-\beta - \frac{4N_*}{3} \right) \right]. \tag{1.134}$$

The slow roll parameters and the cosmic observables are in agreement with the cosmological contraints as

$$\epsilon_* = \frac{4}{3\left(1 + W_*\right)^2}, \qquad \eta_* = \frac{4\left(2 + W_*\right)}{3\left(1 + W_*\right)^2} \tag{1.135}$$

In particular, for $N_* = 60$ (50) one has

$$
\begin{aligned}
\epsilon_* &\simeq 0.00019\ (0.00026) & \eta_* &\simeq -0.0155\ (-0.0184) \\
n_s &\simeq 0.968\ (0.962) & r_* &\simeq 0.003\ (0.004).
\end{aligned}
\tag{1.136}
$$

We now use the constraint on the amplitude of scalar fluctuations Eq. (1.89) to find an analytical relation between the Higgs self-coupling λ and ξ_h as

$$\xi_h \simeq 5.0\ (4.2) \cdot 10^4\, \sqrt{\lambda_h} \tag{1.137}$$

for $N_* = 60$ (50). This validates our approximation $\xi_h \gg 1$ for $\lambda_h \gtrsim 10^{-8}$.

Lastly, using these results we can estimate the typical values for the Higgs field, given by (1.130)

$$h_E \simeq 1.16 \cdot 10^{-2} \, M_{\mathrm{pl}}, \qquad\qquad h_* \simeq 7.34 \, (7.36) \cdot 10^{-2} \, M_{\mathrm{pl}}, \qquad (1.138)$$

for $N_* = 60 \ (50)$ and where we used $\lambda_h = 0.1$.

Some related issues

The last result is often seen as a fundamental problem of HI as such a big value for a coupling parameter can be at odds with the validity of the effective field theory, with a naive value of the cutoff equal to M_{pl}/ξ_h. Indeed, perturbative theory favors couplings smaller than one to allow the expansion in the effective point of view. Such value of the Higgs self-coupling questions the unitarity constraint of the theory. In fact, we can already see from the second (dimension-six effective operator) term in Eq. (1.118) that the cutoff of the theory Λ_h is identified as $\Lambda_h \equiv M_{\mathrm{pl}}/\xi_h$. This (dynamical) value is nevertheless defined for values of the Higgs at the electroweak scale, i.e. $h \sim v$ [41–46], while at values of the Higgs where inflation happens, i.e. $h \sim M_{\mathrm{pl}}/\sqrt{\xi_h}$, the cutoff has been proven to be $\sim M_{\mathrm{pl}}/\sqrt{\xi_h}$, at least for two-by-two tree level scattering amplitudes, thus avoiding unitarity violation [47–49]. Anyway, in this thesis we aim to also present a model in which HI is realized, although modified, with values of the coupling $\sim \mathcal{O}(1)$. This is done with the introduction of another scalar field which mixes itself with the Higgs, see Chap. 6.

Another issue is that all SM couplings are running because of radiative corrections (see Sec. 2.3.5), which means their value changes with the energy scale at which they are considered. Therefore, the value $\lambda_h \simeq 0.12$, valid at the electroweak scale, i.e. $\sim \mathcal{O}(100)$ GeV, is not valid at the inflation scale $\sim \mathcal{O}(10^{15\text{-}18})$ GeV anymore . Hence, every model involving the Higgs scalar at such scale must justify a credible value of the Higgs quartic coupling, i.e. $0 < \lambda_h < 1$. We will come back to this topic when addressing the subject of β functions in Sec. 2.3.5 and discussing the different models in Chaps. 5 and 6.

Palatini formalism

Until now we have used the metric formulation of gravity, where the connection giving rise to the Ricci scalar is identified with the connection $\Gamma^{\mu}_{\ \nu\rho}$, see definitions (1.3) and (1.4). In the Palatini formulation of HI however (for a review see e.g. Ref. [50]), the connection from which the Ricci tensor is calculated does not depend on the metric. Hence the Weyl rescaling (1.114) leaves R invariant and, in the Einstein frame, the action writes

$$S_E = \int \mathrm{d}^4 x \, \sqrt{-g} \left(-\frac{R}{2} + \frac{\Theta^2}{2} \, \partial_\mu h \partial^\mu h - V(h) \right). \qquad (1.139)$$

The canonical inflaton χ is obtained by

$$\frac{d\chi}{dh} = \Theta = \frac{1}{\sqrt{1 + \xi_h h^2}}. \qquad (1.140)$$

This simplifies considerably the equations in terms of χ as we can now write exact analytical relations such as

$$h(\chi) = \frac{\sinh\left(\sqrt{\xi_h}\,\chi\right)}{\sqrt{\xi_h}}, \qquad (1.141\text{a})$$

$$V(\chi) = \frac{\lambda}{4\xi_h^2} \tanh^4\left(\sqrt{\xi_h}\,\chi\right). \qquad (1.141\text{b})$$

The slow roll analysis from inflation is then modified as we now have

$$\sinh(2\sqrt{\xi_h}\chi_E) = 4\sqrt{2\xi_h} \tag{1.142a}$$

$$\cosh(2\sqrt{\xi_h}\chi_*) \simeq 16\xi_h N_*, \tag{1.142b}$$

in the limit $\xi_h \gg 1$. This approximation is largely satisfied as we will see hereafter. The amplitude of fluctuations at N_* is given by Eq. (1.89)

$$A_s = \frac{\lambda_h}{768\pi^2} \frac{\sinh^4(\sqrt{\xi_h}\chi_*)\tanh^2(\sqrt{\xi_h}\chi_*)}{\xi_h^3}. \tag{1.143}$$

Using now Eq. (1.142b) and the observed scalar amplitude (1.95) this leads to

$$\frac{\lambda_h}{12\pi^2}\frac{N_*^2}{\xi_h} \simeq A_s^{\mathrm{obs}} \qquad \Rightarrow \qquad \xi_h \simeq 1.4\times 10^9\,\frac{\lambda_h}{0.1}\left(\frac{N_*}{60}\right)^2. \tag{1.144}$$

We see that the two formalisms of gravity, the metric and the Palatini formulations, lead to different inflationary predictions.

The Palatini formulation provides exact results, especially for the potential in the Einstein frame and the true inflaton expression $h(\chi)$.

1.3 Open questions in modern Cosmology

In addition to the true nature of inflation, there are other open questions in modern cosmology. In the following section, we will restrict our description to the essence of these problems for completeness.

Nowadays, the energy content of the Universe has been observationally constrained to (1.34). These values are the best fit for the CMB multipole expansion and the Hot Big Bang prediction. The most complete model that physicists have on matter and its interactions, in other words on all forms of energy we can interact with, is the Standard Model of particles (SM), presented in the next chapter. Unfortunately, this model covers only $\simeq 5\%$ of the energy present in the Universe, which means that we have very little clue about the nature of the remaining 95%. Moreover, even if future models manage to characterize dark matter as the Standard Model does with ordinary matter, we would still lack the explanation of their origin. As of today, there is no established model providing an explanation of the origin of these states of energy, i.e. 100% of the Universe's energy content.

These puzzles lead to the three biggest open questions of cosmology, that we will briefly present now.

1.3.1 Dark Energy

Tackling the Dark Energy problem is like opening Pandora's box: quickly the puzzles cascade and we come across questions as fundamental as the anthropic principle, our place in the Universe, etc. For this reason, we will restrict ourselves to a brief overview of the problem for completeness and redirect curious readers to more complete sources. The following sketch is based on Refs. [51, 52].

The designation of *Dark Energy* is often mixed with the cosmological constant problem and the *vacuum energy*, and this is for good reason, as we aim to clarify this nomenclature. To do so, let us start from the beginning and recast the Einstein equations (1.1). For reasons of his own, Einstein defended the vision of a static universe, hence he famously chose to introduce a non-zero constant Λ as (1.20) in his equations with a value such that the dynamic of the Universe corresponds to his belief.

As we know, more observations made it more and more obvious that the Universe was expanding, therefore Λ was assumed to vanish. This choice was convenient because even if Λ had been non zero, it would have been so small that the easiest thing to do was still not to worry about it. Indeed, the fact that the Universe is large compared to the Planck length

$$r_\Lambda \gg l_{\rm pl} = \sqrt{\frac{G\hbar}{c^3}} \simeq 1.616 \cdot 10^{-35} \text{ m} \tag{1.145}$$

and old compared to the Planck time

$$t_\Lambda \gg t_{\rm pl} = \sqrt{\frac{G\hbar}{c^5}} \simeq 5.391 \cdot 10^{-44} \text{ s} \tag{1.146}$$

implies $\Lambda \ll M_{\rm pl}^2$, as any non-zero value of Λ introduces a length and time scale

$$r_\Lambda = c\, t_\Lambda = \sqrt{\frac{3}{|\Lambda|}}. \tag{1.147}$$

If we use the information about the Universe size and age at our disposal we find the bound

$$|\Lambda| \lesssim 10^{-118} \ M_{\rm pl}^2 \tag{1.148}$$

largely compatible with the assumption $\Lambda \simeq 0$. There are, however, two tiny details that prevent us from getting rid of this issue in that way.

First, today's accelerated expansion, exposed in 1998 [2, 3], is consistent with a positive, non-zero value of Λ, as it sets the bound [53]

$$\rho_\Lambda \equiv \Lambda\, M_{\rm pl}^2 \simeq (2.33 \pm 0.17) \cdot 10^{-121} \ M_{\rm pl}^4. \tag{1.149}$$

This conclusion has been crosschecked by, for instance, the spatial flatness of the Universe explained by the above value, and which cannot be accounted for by baryonic and dark matter alone.

Second, it appears that the SM provides a dark energy candidate in the shape of vacuum energy. It is well known from quantum mechanics that a harmonic oscillator has non-zero vacuum energy as its hamiltonian writes

$$\hat{H} = \int d^3x \sqrt{-g}\, V + \sum_k \omega_k \left(a_k^* a_k + \frac{1}{2} \right), \tag{1.150}$$

where a_k^* (a_k) are the creation (annihilation) operators canonically normalized as $[a_k, a_{k'}^*] = \delta_{kk'}$. In quantum field theory (QFT), the vacuum state is the state with the lowest energy, i.e. the ground state $|0\rangle$ defined by $a_k|0\rangle = 0$. This means that the vacuum is not empty. It has a latent energy, described by the Heisenberg principle $\Delta_E \Delta_t \geqslant \hbar/2$, that allows for quantum fluctuations of a given energy E in a given amount of time t. In the modern, quantum path, formalism of QFT, this phenomenon takes the shape of virtual particles interaction, or loops. By Lorentz invariance, the only consistent energy-momentum tensor (1.9) is

$$T_{\mu\nu} = -\rho_{\rm v}\, g_{\mu\nu} \tag{1.151}$$

with

$$\rho_{\rm v} = V + \frac{1}{2\mathcal{V}} \sum_k \omega_k, \qquad \mathcal{V} = \int d^3x \sqrt{-g}. \tag{1.152}$$

Furthermore, the energy conservation condition (1.13) implies that the vacuum energy density ρ_v is constant. This means that the vacuum energy well described by the SM acts like a cosmological constant in Einstein equations, hence it must be considered as such, i.e. with the properties of Dark Energy: a perfect fluid with equation of state $w = -1$.

The problem is now that this contribution can be quantified from the SM and it can be shown that the vacuum energy receives many contributions much larger than the bound (1.149). As a toy model, we will compute the vacuum energy density (1.152) from some SM state with mass m. The energy ω_k associated to each momentum is given by Eq. (1.47) hence we see that the integral is quadratically divergent. This is called an ultraviolet divergence and one way out is to cutoff the integral at an arbitrary scale $\Lambda \geqslant k \gg m$. Then

$$\rho_v = V + c_0 \Lambda^4 + c_2 \Lambda^2 m^2 + c_4 m^4 + ... \tag{1.153}$$

with calculable dimensionless coefficients c_i. As we will see in the next chapter, we have broken down the general theory to an effective one valid up to scale Λ. We can now calculate the loop contribution to the vacuum of any SM species at a specific scale. For instance, electron loops up to the cutoff $\Lambda = 100$ GeV have a contribution of order $\rho_v \sim 10^{-66} M_{\rm pl}^4$, which is already 55 orders of magnitude bigger than (1.149). Moreover, if one takes the largest scale of the SM, the Planck scale, we found a discrepancy of about 120 orders of magnitude between the SM contribution to the vacuum and the actual measurement!

Normally such a large disagreement spawns many new candidate theories. The problem here is that for the vacuum, nothing can be added by definition and for now there is no alternative theory of quantum fields at all. The problem arises because of the robustness of the prediction of the SM, as the computation is based on a solid theory that already reconciles the requirements of special relativity and quantum mechanics. These 60 to 120 orders of magnitude discrepancy in a quantity as "basic" as empty space represents a serious crisis in modern physics.

In addition, we can graft to this puzzle an anthropic question since one can show that galaxies form only in a region of spacetime where ρ_Λ is comparable to the present matter density ρ_m^0. As we can reasonably postulate, that regions without galaxies do not contain any observers, a batch of arguments driven by Weinberg in 1987 supports that we should inevitably observe $\rho_\Lambda^0 \sim \rho_m^0$. From today's abundances (1.34) we see that he was right, as $\rho_\Lambda^0 \simeq 2.24\rho_m^0$.

We have shown in the first section of this chapter that ρ_m redshifts as a^{-3} and ρ_Λ does not redshift (by definition of the cosmological constant). This means that the epoch where $\rho_\Lambda \sim \rho_m$ is unique in the history of the Universe since in the past we had $\rho_\Lambda \ll \rho_m$ and in the future we will have $\rho_\Lambda \gg \rho_m$. So the only epoch where both energy densities are comparable is the one when there can be an observer to make that observation. Therefore if this coincidence has any explanation it will have to be an anthropic one.

To conclude and summarize, we must distinguish between: (i) the cosmological constant problem, which arises from the need of explaining the (non) zero value of ρ_Λ in the Einstein equations, (ii) the Dark Energy, which is the state of energy with equation of state $p = -\rho$, and (iii) the vacuum energy problem, which is the huge contribution of the quantum field theory to the vacuum. It appears that, as the vacuum energy acts fully like a cosmological constant in the Einstein equations of motion, we can identify it as Dark Energy. Depending on the authors and the models in the literature, the distinction is more or less stressed. Although this is not the most studied problem at the moment, many proposals have been made to solve this problem, but until now none of them was convincing enough, see Ref. [51] for a discussion.

1.3.2 Dark Matter

In the 1970s, observations of spiral galaxies rotation curves by Rubin and Ford [54] show the evidence of a strong difference between dynamical mass and luminous mass. Until then all the mass of the Universe was considered to emit light, which seemed reasonable, considering that gravitational attraction makes matter collapse into stars, this process having been described by astrophysicists. Furthermore the assumption that nearly all mass emits light was observationally confirmed by the solar system in which more than 99% of all mass was found to be in the Sun.

Concerning spiral galaxies, Freeman formulated an empiric law for luminosity [55] stating that it decreases exponentially from the center $I(r) = I_0 \, e^{-r/R_D}$, where R_D is the radial scale length of the disk. If one assumes the same behaviour for the mass, a simple Newtonian analysis can show that the velocity of the stars outside the bulge (that contains almost all the mass) follows a $r^{-1/2}$ law. Indeed, Newton's law $F = ma$ applied to a star gives

$$\frac{GmM}{r^2} = m\frac{v^2}{r}, \quad r \gg R_D, \tag{1.154}$$

which can also be deduced from the virial theorem. However, this prediction does not agree with Rubin and Ford's observation that v becomes approximately constant after reaching a maximal value.

The following sketch does not aim to be exhaustive but to give a qualitative understanding of the problem: the light we receive from the Universe tells us the amount of the baryonic matter abundance in the Universe, Ω_b^0, whereas we can deduce the total abundance of matter Ω_m^0 from an analysis of the galaxies dynamics. It turns out that Ω_m^0 is six times bigger than Ω_b^0. The lack of matter therefore must come from some type of non-visible matter with the abundance

$$\Omega_{DM}^0 = \Omega_m^0 - \Omega_b^0 \simeq 0.26. \tag{1.155}$$

This kind of matter has been named dark matter (DM), see e.g. Ref. [56] for a review. In the last decades, other evidence for DM has been found. The strongest is the value for Ω_m^0 deduced by the analysis of the CMB anisotropies, whereas BBN theory leads to constraints on Ω_b^0. This argument is of a different nature and gives credence to the existence of such kind of energy state.

The fact that DM is dark implies that it does not interact electromagnetically, hence it is electrically neutral. Beyond this constraint, several models are possible, as long as they fit with observations and the results of DM experiments.

DM can be relativistic (hot DM) or non relativistic (cold DM). A famous hot DM candidate is the sterile neutrino [57, 58]. It can be shown that ordinary neutrinos cannot be DM candidates because their masses are too small. The model of hot DM suffers from its prediction of structure formation from large to low scales, which is in disagreement with observations because galaxies are in dynamical equilibrium, whereas large structures such as superclusters are not.

Structure formation might happen from low to large scale, which is in the range of cold dark matter predictions. Cold DM is constituted of massive and non-relativistic particles. One good cold DM candidate is the Weakly Interacting Massive Particle (WIMP) [59], because it was found that the Ω_{DM} value can only be fitted if the cross sections of dark matter particles are similar to those of the weak interactions. This observation is known as the WIMP miracle but the corresponding candidate has not been detected so far.

Also for completeness we have to mention that there is another way out. When facing a discrepancy, physicists have two options: either they change the players of the game, i.e. postulating new particles, new symmetries, new forces, etc., or they can change the rules of the game, i.e. Einstein gravity over Newton gravity. Adding DM to the standard cosmology model is the reaction of the first kind. The other option is to assume that the theory of gravity deviates from Einstein's pre-

diction at large scales. These *modified Newton dynamics*, or MOND, theories thus aim to explain the galaxies' dynamics without the need of introduction new states of energy such as DM, see e.g. Ref. [60].

1.3.3 Baryon asymmetry

In 1928, Paul Dirac derived an equation of motion for relativistic fermionic quantum fields [61]. He found the energy of the state to be (1.47). Normal people would have stopped calculating, refuting the possibility of negative energy states (since $\sqrt{E^2} = \pm E$), but Dirac interpreted those states as antiparticles with positive energy. The underlying image is nowadays referred to as the Dirac Sea: states with negative energy cannot be occupied because they already are, and vacuum fluctuations can create particles with positive energy, leaving a hole in the sea. This hole is seen as an antiparticle. With this model at hand, Dirac predicted the existence of the positron which was discovered by Carl Anderson in 1932 [62]. This is how the concept of antiparticles with the same mass and the same energy distribution as their particle counterparts, but with opposite charge, were introduced to the new theory of quantum fields.

This foundation of particle physics has not been revised ever since, however, we are compelled to note that the theoretical framework does not reflect our everyday life: both obvious and less obvious evidence of a matter/antimatter asymmetry (or baryon asymmetry) has led to the conclusion that there must have been baryogenesis in the early Universe although the standard and inflationary cosmology models are not able to explain this phenomenon. For a review, see e.g. [63]

Characterization

The symmetric part of the baryonic matter (i.e. all fermions and antifermions of the SM) annihilates into photons through electromagnetic interactions such that one does not need to worry about it. The asymmetric part, defined as the difference between the baryon and anti-baryon number density, $n_b - n_{\bar{b}}$, is not an ideal measure of the asymmetry because it redshifts as a^{-3}. Instead, we usually consider its ratio with another quantity that redshift the same way. It can be the number density of photons or the entropy density

$$\eta_\gamma = \frac{n_b - n_{\bar{b}}}{n_\gamma}, \qquad \eta_s = \frac{n_b - n_{\bar{b}}}{s}, \qquad (1.156)$$

where s is given by (1.50). The former is a useful measure because it remains constant with the expansion of the Universe, at least at late times. However at early times and high temperatures, many heavy particles were in thermal equilibrium, which later annihilated to produce more photons but not baryons. In this case, the latter is more convenient to use. Both are related by

$$\eta_\gamma \simeq 7.04\,\eta_s \qquad (1.157)$$

where the conversion factor is valid in the present universe since the epoch when neutrinos went out of equilibrium and positrons annihilated. In this work we will mainly use the entropic version of the asymmetry parameter that we will denote as $\eta_B \equiv \eta_s$.

A third related way to express the asymmetry is in terms of the baryonic abundance Ω_b^0 (1.34) as

$$\eta_\gamma = 2.74 \cdot 10^{-8}\,\Omega_b^0\,h^2 \qquad (1.158)$$

where h is defined such that

$$H_0 = 100\,h \text{ km/s Mpc}. \qquad (1.159)$$

As we are studying the primordial plasma, we will use the Hubble value obtained from the early Universe measurements, so the one given by (1.27). This yields $h \simeq 0.67$.

Evidences for baryon asymmetry

The first evidence for the existence of a baryon asymmetry is provided by everyday's life observation. Obviously there is hardly any antimatter on Earth or inside the Solar System. In cosmic rays the fraction of antimatter is way below that of matter, with about 10^4 more protons than antiprotons and 10^5 more helium than anti-helium atoms. This proves that there is almost no antimatter in our galaxy. Suppose that regions where antimatter dominates did exist in the Universe. These would border to matter-dominated regions, considering that it is very unlikely for antimatter-dominated and matter-dominated regions to be separated by vacuum. At the interfaces between the matter- and the antimatter-dominated regions, annihilation reactions would produce gamma-rays, however, no such rays have been observed to date. Some assumptions suggest that antimatter is concentrated beyond our horizon but this is in contradiction with the large scale homogeneity of the Universe on which the standard model of cosmology is based.

The CMB furnishes the second and strongest proof for the existence of a matter/antimatter asymmetry, wiping away any lingering doubts left by the above conclusions: the multipole expansion of the CMB anisotropy is in outstandingly good agreement with theories involving a baryon asymmetry, see Fig. 1.2 and Sec. 1.2.3. We see in the left panel of Fig. 1.4 that changing the value of the asymmetry parameter modifies the shape of the spectrum plot. This is because the CMB provides information about baryon acoustic oscillations in which baryons and photons form a plasma exhibiting sound waves. The pressure of the photons tends to erase anisotropies, whereas the gravitational attraction of the baryons, moving at speeds much slower than light, makes them tend to collapse to form overdensities. These two effects compete to create acoustic oscillations, which give the microwave background its characteristic peak structure. The peaks correspond, roughly, to resonances in which the photons decouple when a particular mode is at its peak amplitude. Nowadays, the best fit, obtained by the Planck collaboration, is [6]

$$\eta_B = (8.70 \pm 0.11) \cdot 10^{-11} \qquad (95\% \text{ CL}). \qquad (1.160)$$

Another proof for baryon asymmetry is the accuracy of the BBN predictions, see Sec. 1.1.6, as all the light element abundances depend on the baryon to photon ratio, see Fig. 1.4. The observed abundances of all the BBN isotopes today coincide with the value [12]

$$8.2 \cdot 10^{-11} \leqslant \eta_B \leqslant 9.2 \cdot 10^{-11} \qquad (95\% \text{ CL}) \qquad (1.161)$$

compatible with the CMB measurement.

Sakharov's conditions

In 1967, Andrei Sakharov published a paper [66] on the baryon asymmetry in the Universe (BAU). It gives three conditions any dynamical process creating a baryon asymmetry under $\mathcal{CPT}$ symmetry must satisfy.

The first one is quite obvious:

1. The process should violate the baryon number B.

Schematically this can be written with a rate

$$\Gamma(X \rightarrow Y + B) \neq 0, \qquad (1.162)$$

where X and Y are some particle species and B a third one that carries an excess of baryon number. But this is not enough. If the reverse process happens at the same rate, no net baryon number can be produced. Therefore one should require that
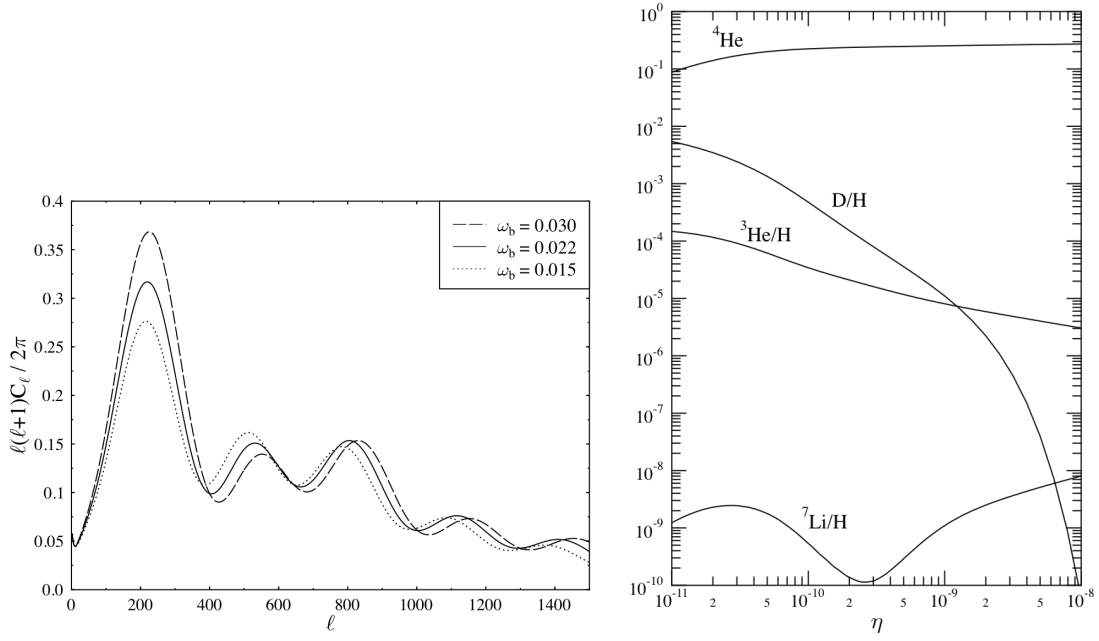
Figure 1.4. Left: The effect on the multipole expansion of a deviation of the baryon-to-photon-ratio from its reference value $\omega_b \equiv \Omega_b^0 h^2 = 0.022$, which corresponds to $\eta_B = 8.56 \cdot 10^{-11}$, taken from [64]. Right: Population of the primordial (lightest) elements as a function of the parameter η_γ, taken from [65]. D stands for deuterium ^{2}H. The aim of this figure is to show how the value of the asymmetry parameter affects theoretical predictions of the CMB multipole expansion and BBN abundances.

2. The process should be out of thermal equilibrium

such that

$$\Gamma(X \to Y + B) \neq \Gamma(Y + B \to X). \tag{1.163}$$

A third (double) condition is required. Indeed, if charge conjugation $\mathcal{C}$ is a symmetry, then

$$\Gamma(X \to Y + B) = \Gamma(\bar{X} \to \bar{Y} + \bar{B}) \tag{1.164}$$

and

$$\frac{dB}{dt} = \Gamma(X \to Y + B) + \Gamma(\bar{X} \to \bar{Y} + \bar{B}) = 0. \tag{1.165}$$

Moreover if charge conjugation $\mathcal{C}$ and parity $\mathcal{P}$ are simultaneously a symmetry, then

$$\begin{aligned} \Gamma_L \equiv \Gamma(X_L \to Y_L + B_L) = \Gamma(\bar{X}_R \to \bar{Y}_R + \bar{B}_R) \equiv \bar{\Gamma}_R \\ \bar{\Gamma}_L = \Gamma_R \end{aligned} \tag{1.166}$$

hence

$$\frac{dB}{dt} = \Gamma_L + \Gamma_R + \bar{\Gamma}_L + \bar{\Gamma}_R = 0 \tag{1.167}$$

Without $\mathcal{CP}$ violation, we can get an asymmetry between left and right-handed particles but no baryon asymmetry. This is why we shall impose that

3. The process should violate $\mathcal{C}/\mathcal{CP}$ symmetries.

These three conditions are called the Sakharov conditions. They are based on the assumption of

$\mathcal{CPT}$ invariance for the fields.

Baryogenesis models

To be successful, any model of baryogenesis must come with a clear manifestation of these three conditions. An out-of-equilibrium condition often comes from a specific out-of-equilibrium decay or from a first order phase transition (electroweak, QCD, Peccei-Quinn, etc.). As for the two other requirements, the first attempts focused on grand unified theory (GUT) with, for instance, out-of-equilibrium extra particles decay in a $SU(5)$ symmetry breaking [67, 68].

Then other models were proposed such as *Leptogenesis*, where the asymmetry is generated in the lepton sector before being transferred to the baryon sector with some mechanism [69–71], or supersymmetry in the Affleck-Dine mechanism where the BAU is produced by coherent motion of scalar fields [72]. Also, there is one model called *spontaneous baryogenesis* that does not need the Sakharov conditions and can hence be described in thermal equilibrium, but it breaks $\mathcal{CPT}$ symmetry. In this model, the classical evolution of a scalar field can cause a baryon asymmetry by generating an effective chemical potential for baryon number [73, 74].

Lastly, let us introduce what our concern will be in this work. During the development of the GUT baryogenesis, it was not known that the SM had a usable source of B violation, see Sec. 2.3.6. Besides, there are processes in the SM that violate the $\mathcal{CP}$ symmetry, see Sec. 2.3.4, so, along with the Higgs mechanism (see Sec. 2.3.3), these two observations meet all three Sakharov conditions, thus another class of models was born dubbed as *electroweak baryogenesis*. They use the chiral nature of the electroweak interaction to produce an excess of baryons during a first order electroweak phase transition (EWPT) [75, 76].

Today it appears that the EWPT is second order, so its transition rate is governed by the expansion rate of the Universe, which at the weak epoch is about 14 orders of magnitude slower than scattering processes, hence the Universe would maintain quasistatic thermal equilibrium. Nevertheless, because the joint effects of the weak sphaleron and helical hypermagnetic fields, a second order EWPT can still provide out-of-thermal equilibrium conditions for baryogenesis to happen, as we will see in Sec. 3.1.3.

On the other hand, as we will see in the next chapter, one needs new sources of $\mathcal{CP}$ violation and hence new physics beyond the SM in order to generate a sizable amount of baryon asymmetry. Even if there is no theorem proving that it is impossible to find some other mechanism that does work within the SM, there are so far no convincing demonstrations, and most practitioners of baryogenesis agree that $\mathcal{CP}$ violation in the SM is too weak. The aim of this thesis is therefore to produce the BAU with as little physics beyond the SM (BSM) as possible.

For more details about the models mentioned in this section, see e.g. Ref. [63, 77].

Chapter 2

Particle physics

The Standard Model is a quantum gauge field theory that classifies all known subatomic particles and describes three of their four fundamental interactions: strong, weak and electromagnetism. In the 20th century, research in nuclear physics after World War II led to the development of particle accelerators which revealed the existence of dozens of particles living in what some scientists call the particle zoo. In a similar fashion to the unification of electricity and magnetism by Maxwell, the first success of the Standard Model in the 1950s was to explain this large diversity of particles as combinations of a few elementary particles. It basically describes all exotic hadrons found in colliders in terms of quarks. Ever since, it has pursued its vocation of unifying all descriptions of matter and of interaction using a small number of parameters. The Standard Model is not a theory of everything, since it neither includes gravity, nor any dark matter candidate. Furthermore it leaves some phenomena such as neutrino oscillations unexplained and is not compatible with the standard model of cosmology.

It is clear that a complete description of the Standard Model would fill more than one book. Therefore we will stick to a short overview of its content, the structure of fundamental interactions and the anomaly equations which will be relevant for the main purpose of this thesis.

2.1 Preliminary: a note on quantum field theory

As soon as we discover the topic of analytical mechanics, and how closely related it is to quantum mechanics, since the Poisson brackets are replaced by commutation relations and variables by operators to obtain the dynamics

$$\frac{d\mathcal{O}}{dt} = \frac{\partial\mathcal{O}}{\partial t} + \{\mathcal{O}, H\} \quad \rightarrow \quad \frac{d\mathcal{O}}{dt} = \frac{\partial\mathcal{O}}{\partial t} + [\mathcal{O}, H], \tag{2.1}$$

known as the Ehrenfest theorem, it is very tempting to think that the action

$$S[q] = \int \mathrm{d}t\, L\,[q(t), \dot{q}(t)] \tag{2.2}$$

is the most general quantity we can think of. In the above relation, we related the Lagrangian L and the Hamiltonian H of the system by

$$L\,[t, q(t), \dot{q}(t)] = (\text{kinetic energy}) - (\text{potential energy}),$$
$$H = \dot{q}\,\frac{\partial L}{\partial \dot{q}} - L. \tag{2.3}$$

By "most general", we mean the object that contains all the information about the dynamics of all the objects we are studying. This is true in classical mechanics, where the action encodes all possible world-lines of the system, and, by picking the one that minimizes the action $\delta_f S = 0$, we get the equation of motion for the object f.

The shift to quantum field theory is made by replacing variables with fields and Lagrangians with Lagrangian densities

$$
\begin{aligned}
q &\rightarrow \phi(x^\mu) \\
L\left[t, q(t), \dot{q}(t)\right] &\rightarrow \mathcal{L}\left[x^\mu, \phi(x^\mu), \partial_\mu \phi(x^\mu)\right]
\end{aligned}
\tag{2.4}
$$

such that the action for QFT reads

$$
S[\phi] = \int \mathrm{d}^4 x \, \mathcal{L}(x).
\tag{2.5}
$$

Note that, although this is mathematically possible, it is rare that L ($\mathcal{L}$) depends explicitly on t (x^μ)[6], so we will generally omit this dependence from now on.

Naively, we would simply have to repeat everything we did for analytical mechanics, but for quantum fields now these replacements have been done. It appears that the aforementioned method is valid for the study of classical field theory only. The quantum description of a propagation involves the path integral formalism, and the only object that contains all the quantum effect of the system, its only true library, is the generating functional

$$
Z[J] = \langle 0| \mathrm{e}^{-iHt} |0\rangle = \int \mathcal{D}\phi \, \mathrm{e}^{iS[\phi]+iJ\phi}
\tag{2.6}
$$

where J is the current associated to the field ϕ. Its name comes from the property of producing the Green's function of the theory when functional derivatives are applied to it:

$$
iG(x - y) = \frac{\delta^2 Z[J]}{\delta J(x) \, \delta J(y)}.
\tag{2.7}
$$

This procedure is known as the LSZ reduction formula (see e.g. Ref [78]). We break down the differences between classical field theory and a full description of a quantum system with some highlights:

- Fields are integration (dummy) variables. In the literature (and in this thesis), the starting point is almost always given by the Lagrangian density, sometimes by the action, but it is crucial to have in mind that all the fields in the operator will at some point be (path) integrated to produce the observable physics.

- A symmetry can leave the action invariant while changing the measure of the path integral $\mathcal{D}\phi$, resulting in a non-conserved current. This effect is called an anomaly (see Sec. 2.3.6) because it is anomalous from the conventional analytical mechanics point of view.

- The generating functional maps the current to a number, which means the true physical input are the currents because they source the wave equations through Green's functions. Indeed, Green's functions G are the solutions of a linear differential operator L

$$
\mathrm{L}(x^\mu) \, G(x^\mu - y^\mu) = \delta^{(4)}(x^\mu - y^\mu).
\tag{2.8}
$$

---

[6]If it does, the energy E is not conserved in the system and $H \neq E$.

The linear differential operator depends on the theory. For instance, for free scalar field it is $L = \partial^2 - m^2$, resulting in the Klein-Gordon equation. Green's functions are used to compute the field's equation of motion in the presence of a source. Indeed, the solution of

$$L(x^\mu)\,\phi(x^\mu) = J(x^\mu) \tag{2.9}$$

is given by the convolution of G with the source

$$\phi(x^\mu) = \int \mathrm{d}^4y \; G(x^\mu - y^\mu) J(y^\mu). \tag{2.10}$$

For the purpose of gauge theory, we can stick to a classical description. As we will see, the quantization of the gauge fields yields to particles that carry the associated interaction. However, in the next section we will only use a classical approach and the subtleties we have outlined will come back into play later on.

2.2 Gauge symmetries

In the beginning of the 20th century, with the birth of electrodynamics and quantum mechanics, came the development of gauge theory, which formalizes how the redundancies of a theory are linked to conserved quantities. Gauge theories make use of group theory, symmetries and topology. In order to avoid losing the physical context, an effort will be made in this chapter to connect the mathematical result with its physical implications. The aim of this section is to give the background information for the Standard Model as well as the main clues about the way it can provide baryon number non-conservation.

2.2.1 Noether's theorem

In 1918, Noether proved the equivalence between conserved quantities and the invariants of physical laws called symmetries [79]. As an example, the invariance of Newton's second principle under spatial translations leads to momentum conservation. In a more modern and anomaly free formulation, a symmetry is defined by the invariance of the action defined as Eq. (2.5), under a given transformation: $\mathcal{L}\,\mathrm{d}^4x \to \mathcal{L}'\,\mathrm{d}^4x'$, where $\mathcal{L}$ is the Lagrangian density[7]. To each symmetry, defined by the transformations of the coordinates and the fields

$$x^\mu \to x'^\mu \simeq x^\mu - \epsilon_i^\mu(x^\mu)\alpha^i, \tag{2.11a}$$

$$\phi_a(x^\mu) \to \phi_a'(x'^\mu) \simeq \phi_a(x^\mu) + \Delta_{ai}(x^\mu)\alpha^i, \tag{2.11b}$$

the ith conserved current can be associated:

$$j_i^\mu = \sum_a \frac{\partial \mathcal{L}}{\partial(\partial_\mu \phi_a)}\Delta_{ai} - \epsilon_i^\mu \mathcal{L}, \tag{2.12a}$$

$$\partial_\mu j_i^\mu = 0, \tag{2.12b}$$

with $\Delta_{ai}\alpha^i = \Delta_a = \phi_a'(x^\mu) - \phi_a(x^\mu)$. The α_i are called Lie parameters. Their nature will become clear in the next section. The spatial integration of the time component yields the conserved charges

$$Q_i = \int j_i^0 \, \mathrm{d}^3x. \tag{2.13}$$

---

[7]To simplify the notation, we will generally omit this designation since it is clear within the context of field theory.

This means we can view j_i^0 as the charge density of the symmetry involved. Indeed, if we consider the $U(1)$ group as an example, we have that Eq. (2.12b) is the covariant formulation of the *continuity equation*

$$\partial_\mu j^\mu = 0 \quad \Leftrightarrow \quad \frac{\partial \rho(t, \boldsymbol{x})}{\partial t} = -\boldsymbol{\nabla} \cdot \boldsymbol{j}(t, \boldsymbol{x}) \quad \Leftrightarrow \quad \frac{dQ(t)}{dt} = -\int_{\partial V} \boldsymbol{\Phi}(t) \cdot d\boldsymbol{S} \qquad (2.14)$$

where $j^\mu \equiv (\rho, \boldsymbol{j})$, which states that the rate of change of a given quantity in a volume V is given by the integrated flux $\boldsymbol{\Phi}$ thought the bounding surface ∂V.

If we now consider the Lorentz symmetry, we can formally derive the energy-momentum tensor, already used in the previous chapter. It can be found by generalizing the above sketch involving Newton's principle and its invariance under spatial translations. Considering spacetime symmetry, the conserved current takes the form:

$$T_\nu^\mu = (j^\mu)_\nu = \frac{\partial \mathcal{L}}{\partial(\partial_\mu \phi_a)}\partial_\nu \phi_a - \delta_\nu^\mu \mathcal{L}, \qquad (2.15)$$

which is the energy-momentum tensor. The four-component conserved charge is then

$$p_\mu = (E, \boldsymbol{p}) = \int T_\mu^0 \, \mathrm{d}^3 x, \qquad (2.16)$$

which is the four-momentum.

A historical example: Electromagnetism

Gauge symmetries are a description of n degrees of freedom with $m > n$ variables leading to redundancies in the mathematics that never change the observable physics. This characteristic appeared in Maxwell's theory of electromagnetism. Since the electric $\boldsymbol{E}$ and magnetic $\boldsymbol{B}$ fields can be written in terms of the potentials V and $\boldsymbol{A}$ as

$$\begin{aligned}
\boldsymbol{E} &= -\boldsymbol{\nabla}V - \partial_t \boldsymbol{A}, \\
\boldsymbol{B} &= \boldsymbol{\nabla} \wedge \boldsymbol{A},
\end{aligned} \qquad (2.17)$$

and, since performing the transformation

$$\begin{aligned}
V &\to V' = V - \partial_t \chi(t, \boldsymbol{x}), \\
\boldsymbol{A} &\to \boldsymbol{A}' = \boldsymbol{A} + \boldsymbol{\nabla}\chi(t, \boldsymbol{x})
\end{aligned} \qquad (2.18)$$

leaves the equations of motion unchanged, the function $\chi(t, \boldsymbol{x})$ is an additional degree of freedom called a gauge function. It is a symmetry that depends on the spacetime coordinates, unlike a global transformation, which remains the same at every point.

In a covariant formulation, $A^\mu = (V, \boldsymbol{A})$, the electric and magnetic fields become

$$E_i = F_{i0}, \qquad (2.19\text{a})$$

$$B_i = \frac{1}{2}\varepsilon_{ijk}F^{jk}, \qquad (2.19\text{b})$$

where ϵ_{ijk} is the Levy-Civita anti-symmetric tensor of rank 3 and where

$$F_{\mu\nu} = \partial_\mu A_\nu - \partial_\nu A_\mu \qquad (2.20)$$

is called the field strength tensor. In this language, Eq. (2.18) reads simply

$$A_\mu(x) \to A'_\mu(x) = A_\mu(x) + \partial_\mu \chi(x). \tag{2.21}$$

The Lagrangian of electromagnetism without interactions is

$$\mathcal{L}_{\text{EM}} = -\frac{1}{4} F_{\mu\nu} F^{\mu\nu}, \tag{2.22}$$

where the overall minus sign ensures that the energy is positive. Note that the Lagrangian is invariant under the gauge transformation (2.21) due to the fact that $F'_{\mu\nu} = F_{\mu\nu}$.

Mathematically, these kinds of symmetries form a group, and symmetry groups can be described in terms of Lie groups. If the symmetry is local, the group is called a gauge group in physics. Groups and Lie groups are whole fields of research in mathematics so we will not go into much detail.

2.2.2 Gauge groups

A group is a set of elements G associated with a composition law under which it is closed, and that obeys three properties: the existence of a unique neutral element, the existence of a unique inverse element for each element of the group and the associativity of multiplication. If multiplication is commutative for every element of the group, the group is called Abelian, otherwise it is called non-Abelian. Lie groups are smooth matrix groups, in other words manifolds which can be viewed in a $\mathbb{R}^{2n^2}$ Euclidean space. They depend on the so-called Lie parameters and are differentiable with respect to them.

The tangent space to a curved manifold of dimension n is a real vector space of dimension n, so that any element $\omega(x)$ of the Lie group near unity can be written as

$$\omega(x) = 1 + iAx + \mathcal{O}(x^2), \tag{2.23}$$

with A belonging to the Lie algebra of the group. It is straightforward to see that a multiplication in the group correspond to an addition in the algebra, and moreover, that the commutator is the composition law of the algebra. When applying the commutator to the vector basis of the Lie algebra $\{T_i\}$, which are called the generators of the group, one will always find an element of the algebra because the commutator is closed. The commutator can hence be written in term of the basis $\{T_i\}$:

$$[T_i, T_j] = if_{ijk}T_k. \tag{2.24}$$

The scalars f_{ijk} are called the structure constants of the group. They encode all the information about the group because they determine the Lie brackets of all elements of the Lie algebra (and thus of the corresponding Lie group).

Compact, i.e. closed and bounded, Lie groups have an interesting property of great importance in gauge theories: in the corresponding (compact) Lie algebra there exists a bilinear form which defines a scalar product in terms of the trace operation. When we choose the vector basis of the algebra to be orthonormal, which is always possible, their normalization under the aforementioned scalar product takes the form

$$\text{Tr}(T_i, T_j) = \frac{1}{2}\delta_{ij}. \tag{2.25}$$

The factor multiplying δ_{ij} is called the *Dynkin index*.

As the historical example of electromagnetism suggests, gauge groups describe interactions. Out of the four fundamental interactions in physics, there are (at least) three that can be described by gauge groups: the electromagnetic, the weak and the strong interaction. Let us ignore gravitation for the moment. Interactions must be able to take place between the constituents of matter in order

to have a physical meaning. In quantum field theory, matter particles (fermions) are excitations of the associated fermionic fields which are spinor fields. Under each symmetry they transform in the fundamental representation of the associated Lie group:

$$\psi(x) \rightarrow \psi'(x) = \omega(x)\psi(x) \quad \omega \in G. \tag{2.26}$$

Any Lagrangian containing derivatives of ψ cannot be invariant under this transformation because of the local character of gauge transformations, which would make derivatives of ψ transform as $\partial_\mu \psi \rightarrow \omega \partial_\mu \psi + \psi \partial_\mu \omega$. It is therefore impossible to find a symmetry without modifying the derivative such that it transforms in the same way as the fundamental representation, i.e. as

$$D_\mu \psi(x) \rightarrow \omega(x) D_\mu \psi(x). \tag{2.27}$$

Such a derivative is called a covariant derivative. In virtue of the transformation (2.21), the covariant derivative is given by $D_\mu = \partial_\mu - iA_\mu$, which is in agreement with (2.27) if one sets $\omega(x) = e^{i\chi(x)}$. Therefore, the group G describing electromagnetism consists of only one parameter ω such that $\omega^\dagger = \omega^{-1}$, which corresponds to the unitary group of dimension one, denoted $U(1)$.

The weak and the strong interactions are described by the $SU(2)$ and the $SU(3)$ gauge groups, respectively, which can be represented by unitary square matrices of dimension 2 and 3, respectively, with unit determinant and which are simply connected[8], compact and non-Abelian. $\mathfrak{su}(N)$ is the Lie algebra of Hermitian $N \times N$ matrices with zero trace. Since $\omega(x) \in SU(N)$ will not transform in (2.27) in the same way as $\omega(x) = e^{i\chi(x)}$, we are forced to reconsider the gauge transformation of the field A_μ belonging to $\mathfrak{su}(N)$ if we want to keep the above definition of the covariant derivative. Requiring (2.27) with the transformation (2.26) and the same covariant derivative for the gauge field leads, after some algebra, to the transformation

$$A_\mu \rightarrow A'_\mu = \omega A_\mu \omega^{-1} + i\omega \partial_\mu \omega^{-1}. \tag{2.28}$$

If $\omega = e^{i\chi(x)} \in U(1)$ one recovers (2.21). This change has an impact on the expression of the field strength. Because we still want the Lagrangian to be invariant under the gauge transformation, we should generalize its definition in order to recover the electromagnetic case when $\omega(x) \in U(1)$. Firstly, because A_μ takes values in the Lie algebra of the group G, it can be written in a basis of the vector space. The analog is true for $F_{\mu\nu}(x)$:

$$A_\mu(x) = \sum_{a=1}^{\dim(G)} T^a A_\mu^a(x), \qquad\qquad F_{\mu\nu}(x) = \sum_{a=1}^{\dim(G)} T^a F_{\mu\nu}^a(x), \tag{2.29}$$

where T^a are the generators of the group and $A_\mu^a(x)$ are the associated coefficients. After a more careful look we remark that the relevant term in the Lagrangian of electromagnetism is $F_{\mu\nu}^a F^{\mu\nu\,a}$ with $a = \dim(G) = 1$. To make things simpler and the notation lighter, we will always write $F_{\mu\nu}F^{\mu\nu}$ because the two formulations are equivalent in this group. This turns not to be the case in a general compact Lie group. Using Eq. (2.29) and the normalization (2.25), the generalization is straightforward

$$\mathcal{L} = -\frac{1}{4} F_{\mu\nu}^a T^a F^{\mu\nu\,b} T^b \delta^{ab} = -\frac{1}{2} \text{Tr}(F_{\mu\nu}F^{\mu\nu}). \tag{2.30}$$

Considering the cyclic property of the trace one should have $F_{\mu\nu} \rightarrow \omega F_{\mu\nu}\omega^{-1}$. This condition and Eq. (2.28) can be satisfied simultaneously by defining

$$F_{\mu\nu} = \partial_\mu A_\nu - \partial_\nu A_\mu - i[A_\mu, A_\nu]. \tag{2.31}$$

---

[8]A space is simply-connected when every loop within this space can be shrunk to a point.

The non-Abelian character of the group is now explicit. It becomes even more obvious when $F_{\mu\nu}$ is written in terms of its components:

$$F^a_{\mu\nu} = \partial_\mu A^a_\nu - \partial_\nu A^a_\mu + f^{abc} A^b_\mu A^c_\nu. \tag{2.32}$$

Now we have the tools to characterize the gauge groups of weak and strong interactions.

$SU(2)$ gauge group

$SU(2)$ is a 3-dimensional compact gauge group, hence having three generators which are hermitian 2×2 matrices. The usual choice of basis for the algebra are traceless matrices τ_a which are proportional to the Pauli matrices

$$\sigma_1 = \begin{pmatrix} 0 & 1 \\ 1 & 0 \end{pmatrix}, \qquad \sigma_2 = \begin{pmatrix} 0 & -i \\ i & 0 \end{pmatrix}, \qquad \sigma_3 = \begin{pmatrix} 1 & 0 \\ 0 & -1 \end{pmatrix}. \tag{2.33}$$

By defining

$$\tau_a = \frac{\sigma_a}{2}, \tag{2.34}$$

we obtain

$$M = M_a \tau_a, \ \forall M \in \mathfrak{su}(2), \ M_a \in \mathbb{R}, \tag{2.35a}$$

$$[\tau_a, \tau_b] = i\epsilon_{abc} \tau_c. \tag{2.35b}$$

$SU(3)$ gauge group

$SU(3)$ is an 8-dimensional compact gauge group, hence having eight generators which are hermitian 3×3 matrices. The usual choice of basis for the algebra is the traceless matrices η_a proportional to the Gell-Mann matrices:

$$\lambda_1 = \begin{pmatrix} 0 & 1 & 0 \\ 1 & 0 & 0 \\ 0 & 0 & 0 \end{pmatrix}, \qquad \lambda_2 = \begin{pmatrix} 0 & -i & 0 \\ i & 0 & 0 \\ 0 & 0 & 0 \end{pmatrix}, \qquad \lambda_3 = \begin{pmatrix} 1 & 0 & 0 \\ 0 & -1 & 0 \\ 0 & 0 & 0 \end{pmatrix},$$

$$\lambda_4 = \begin{pmatrix} 0 & 0 & 1 \\ 0 & 0 & 0 \\ 1 & 0 & 0 \end{pmatrix}, \qquad \lambda_5 = \begin{pmatrix} 0 & 0 & -i \\ 0 & 0 & 0 \\ i & 0 & 0 \end{pmatrix}, \qquad \lambda_6 = \begin{pmatrix} 0 & 0 & 0 \\ 0 & 0 & 1 \\ 0 & 1 & 0 \end{pmatrix}, \tag{2.36}$$

$$\lambda_7 = \begin{pmatrix} 0 & 0 & 0 \\ 0 & 0 & -i \\ 0 & i & 0 \end{pmatrix}, \qquad \lambda_8 = \frac{1}{\sqrt{3}} \begin{pmatrix} 1 & 0 & 0 \\ 0 & 1 & 0 \\ 0 & 0 & -2 \end{pmatrix}.$$

Defining

$$\eta_a = \frac{\lambda_a}{2}, \tag{2.37}$$

we obtain

$$M = M_a \eta_a, \ \forall M \in \mathfrak{su}(3), \ M_a \in \mathbb{R}, \tag{2.38a}$$

$$[\eta_a, \eta_b] = i f_{abc} \eta_c, \tag{2.38b}$$

where f_{abc} is the completely antisymmetric structure constant of $SU(3)$ with the values

$$f_{123} = 1, \qquad f_{147} = f_{246} = f_{257} = f_{345} = f_{376} = \frac{1}{2}, \qquad f_{458} = f_{678} = \frac{\sqrt{3}}{2}. \tag{2.39}$$

2.2.3   Topology of gauge groups

In this section, we will see that non-Abelian gauge groups have a non trivial vacuum structure. We will prepare the theoretical ground for the axion description made in Sec. 2.4, which will provide $\mathcal{CP}$- and B-violating terms required by the Sakharov condition for baryogenesis, see Sec. 1.3.3.

Elementary homotopy

Let X and Y be two topological spaces and $\mathcal{F}$ the set of continuous maps from X to Y. The latter are said homotopic if, for $f, g \in \mathcal{F}$, $f(X)$ can be continuously deformed to $g(X)$ in Y. The idea of homotopy theory is to study and classify all the maps from X to Y according to this homotopy equivalence. A homotopy class is a set containing all the elements which are homotopic among themselves. One element of a homotopy class is called a representative.

As a sandbox example, let us take $\mathbb{R}^2$ and $\mathbb{R}^2 \setminus \{0\}$ and see how loops (paths that begin and end at the same point) can be mapped inside. In the first space, any loops can be continuously deformed to a point whereas in the second only loops that do not contain the hole do have this property. Therefore, in $\mathbb{R}^2$ a loop is homotopic to a point and hence the space is said trivial. By contrast, the loops in $\mathbb{R}^2 \setminus \{0\}$ can be classified according to the number of times they wrap the hole with a winding number $\nu \in \mathbb{Z}$ (the negative sign accounts for the path direction change). Thus they form a homotopic class labelled by π_1 where the simplest representative is the circle S^1 as S^n has definition

$$S^n = \{x \in \mathbb{R}^{n+1} \mid |x|^2 = 1\}. \tag{2.40}$$

To summarize in a more rigorously way we can state that $\pi_1(\mathbb{R}^2 \setminus \{0\}) = \mathbb{Z}$. Of course the same property arises when considering the loop's mapping on S^1: $\pi_1(S^1) = \mathbb{Z}$.

If we consider now $\mathbb{R}^3$ and $\mathbb{R}^3 \setminus \{0\}$ we see that any closed paths can be shrunk to a point in both spaces whereas the homotopic class of closed surfaces π_2 is shrinkable only in $\mathbb{R}^3$. For the other spaces, a classification of the different wrappings with a winding number enters in the description. As we go higher in the dimensions the same scheme repeats itself, allowing us to state, not in the most rigorous way, that

$$\begin{aligned} \pi_k(S^n) &= 0 \text{ for } k < n, \\ \pi_n(S^n) &= \mathbb{Z}, \end{aligned} \tag{2.41}$$

where π_k is the homotopic class of closed dimension-k hypersurfaces. Because one is interested in the result of this discussion and not in the demonstrations, we have skipped the mathematical definitions of most of the concept used (path, loop, contraction, etc.). For the complete story, the reader should refer to e.g. Ref. [80].

SM gauge groups homotopy

In this section, we will be interested in the structure of $U(n)$ and $SU(n)$ Lie groups, or, more precisely, we want to know which kind of simpler groups they are equivalent to.

The case of $SU(2)$ is quite simple to demonstrate. Consider a matrix representation of $SU(2)$. Any element R of this representation can be written as

$$R = \begin{pmatrix} u & -v^* \\ v & u^* \end{pmatrix}, \quad \text{such that} \quad |u|^2 + |v|^2 = 1, \tag{2.42}$$

where $u, v \in \mathbb{C}$. The asterisk denotes the conjugation operation. In terms of the real numbers a, b, c, d satisfying $u = a + ib$ and $v = c + id$, the condition of unit determinant turns out to be $a^2 + b^2 + c^2 + d^2 = 1$, which defines a 3-dimensional sphere of radius 1. This shows that $SU(2)$ is homotopically equivalent to S^3. The same demonstration with identical outcome can be done for

$SU(3)$. In fact, we have

$$\pi_3\left[SU(n)\right] = \mathbb{Z}, \quad \forall n \geqslant 2. \tag{2.43}$$

More generally, an important result of homotopy theory is that

$$\pi_3(G) = \mathbb{Z} \tag{2.44}$$

for any simple (simply-connected, locally compact and non-Abelian without non-trivial connected normal subgroups) compact Lie group G [80]. Therefore we will have to give a closer look to the non-Abelian groups of the SM in the next section and find what the consequence are of their non trivial topology.

Lastly, as a consequence for the gauge group of the electromagnetic interaction, $\pi_k\left[U(1)\right] = 0$ for $k \geqslant 2$. This means that, unless the theory is in 1+1 dimensions, $U(1)$ gauge theory has just the one trivial vacuum.

2.2.4 Degenerate vacua

The result (2.43) implies the existence of a class of bijective maps $g_\nu : SU(n) \rightarrow S^3$ (called a diffeomorphism in homotopy theory) defining an infinite number of wrappings labelled by a winding number $\nu \in \mathbb{Z}$. Thus, the vacuum state of non-Abelian gauge groups is degenerate since there are an infinite number of pure gauge configurations [81].

The instanton

One can go from a vacuum to another by performing a so-called global gauge transformation (by opposition of a local, standard gauge transformation)

$$\Omega|0\rangle_n = |0\rangle_m. \tag{2.45}$$

The instanton is the soliton that connects two gauge equivalent but different vacua characterized by winding number change of 1 :

$$U|0\rangle_n = |0\rangle_{n+1}. \tag{2.46}$$

It corresponds to a tunneling between two neighboring vacua whose transition amplitude can be computed using a Wick rotation $t \rightarrow -i\tau$ in the Euclidean action $S \rightarrow iS_E$, like any quantum tunneling [82]. The Euclidean action of a $SU(n)$ type free field is

$$S_E = \int \frac{1}{2} \operatorname{Tr}(F_{\mu\nu} F^{\mu\nu}) \mathrm{d}^4 x, \tag{2.47}$$

where the replacement $A_0^a \rightarrow -iA_0^a$ must be made in order to have $F_{0i}^a \rightarrow -iF_{0i}^a$ and $F_{0i}^a F^{0i\,a} \rightarrow -F_{0i}^a F^{0i\,a}$. For the action to be finite, the fields must decay sufficiently quickly at large distances. Therefore $\exists L$ such that $F_{\mu\nu}(x) = 0$, $\forall |x| \geqslant L$. This means that A_μ are pure gauges at large distances and thus that, if for $|x| \geqslant L$, $A_\mu(x) = i\omega\partial_\mu\omega^{-1}$ with $\omega \in SU(n)$, then

$$F_{\mu\nu} = \partial_\mu(i\omega\partial_\nu\omega^{-1}) - i(\omega\partial_\mu\omega^{-1})(\omega\partial_\nu\omega^{-1}) - (\mu \leftrightarrow \nu) = 0, \tag{2.48}$$

where the double arrow denotes the repetition of the previous terms with a change of indices. The fact that this happens when $|x| = L$ is crucial, because this condition puts us in the topological space $\{x \in \mathbb{R}^4 \mid |x| = L\}$ which is homotopic to S^3. Thus (2.44) applies: the $SU(n)$ groups have a degenerate structure of vacua, each one being characterized by zero energy in a different topological

class labelled by the winding number, which classifies the map

$$
\begin{aligned}
g \ : \ S^3 &\longrightarrow \mathfrak{su}(n) \\
x &\longmapsto A_\mu(x) = i\omega(x)\partial_\mu\omega^{-1}(x).
\end{aligned}
\tag{2.49}
$$

The instanton action is given by [83]

$$
S_E = \mp \frac{1}{2} \int \mathrm{Tr}(F_{\mu\nu}\tilde{F}^{\mu\nu})d^4x,
\tag{2.50}
$$

where we defined the dual of the field strength as

$$
\tilde{F}_{\mu\nu} \equiv \frac{1}{2}\epsilon_{\mu\nu\rho\sigma}F^{\rho\sigma}.
\tag{2.51}
$$

Hence the action depends on a gauge invariant topological Lorentz scalar, as the two tensors are not contracted with the metric. Moreover, this quantity is topologically closed, which means that its exterior derivative[9] vanishes $\mathrm{d}\,\mathrm{Tr}(F_{\mu\nu}\tilde{F}^{\mu\nu}) = 0$. Therefore, by the Poincaré lemma[10] there exists K^μ such that

$$
\partial_\mu K^\mu = \mathrm{Tr}(F_{\mu\nu}\tilde{F}^{\mu\nu}).
\tag{2.52}
$$

It is straightforward to verify that

$$
K^\mu = \epsilon^{\mu\nu\rho\sigma}\mathrm{Tr}(F_{\nu\rho}A_\sigma + \frac{2}{3}iA_\nu A_\rho A_\sigma).
\tag{2.53}
$$

This quantity is called the Bardeen current or the Chern-Simons (CS) current. We can integrate it to obtain the so-called CS number, an integer defined as [83]

$$
N_{\mathrm{CS}} = \frac{g^2}{16\pi^2} \int d^4x \, F_{\mu\nu}^a \tilde{F}^{\mu\nu\,a} = \frac{g^2}{16\pi^2} \int d^3x \, K^0 \left.\vphantom{\int}\right|_{t=-\infty}^{t=+\infty}
\tag{2.54}
$$

which measures the change of the degree of mapping g (in other words, the change of the winding number of $SU(n)$ over S^3). It is a topological charge in the sense that due to the integral it does not depend on the position in space, nor does it depend on the metric, since K^μ is the contraction of terms proportional to the gauge field with an antisymmetric tensor. As its name suggests, the topological charge is a measure of the topological properties of the space.

In more detailed computations [83], it appears that the sign of N_{CS} depends on the choice to cancel the RHS of (2.50). If we choose $F_{\mu\nu} = \pm\tilde{F}_{\mu\nu}$, we have $N_{\mathrm{CS}} \gtrless 0$ and therefore S_E is always positive. Moreover, since N_{CS} represents the change in the number of vacua, the instanton is strictly speaking only defined for $N_{\mathrm{CS}} = 1$. The value $N_{\mathrm{CS}} = \nu$ corresponds to ν instantons. The reverse change in the topology, with $N_{\mathrm{CS}} = -1$, is called the anti-instanton. Taking all these results into account, the minimal action becomes

$$
S_E = \mp\frac{8\pi^2}{g^2}N_{\mathrm{CS}}.
\tag{2.55}
$$

In the semi-classical situation, the tunneling rate is given by $\Gamma_i \propto e^{-2S_E}$, since it is related to the probability which in turn is proportional to the transition amplitude squared. Therefore in the case of weak interaction, $g^2 = 4\pi\alpha_W$ with $\alpha_W = 1/29$, the rate of tunneling between two

---

[9]The exterior derivative is a differential defined in topology and should not be confused with the ordinary or covariant derivative. Readers interested in this matter are referred to Ref. [80].

[10]If X is a contractible open subset of $\mathbb{R}^n$, then any smooth closed p-form defined on X is exact with $p \in \mathbb{Z}$, $p \leqslant n$ (an exact form is a differential form that is an exterior derivative of another differential form).

neighbours minima is $\Gamma_W \propto e^{-\frac{4\pi}{\alpha_W}} \sim 10^{-160}$, which is so small that it is impossible to occur within the lifetime of the Universe.

As a closing remark we would like to mention that because it is localized in Euclidean time, an instanton has no worldline. It is an object that does not exist in real time (in 3+1 dimensions), it lives at one *instant*, hence the name due to 't Hooft.

The sphaleron

Since tunneling is unlikely, it is necessary to pass through non-vacuum, i.e. finite energy field configurations, in order to change from a vacuum configuration to another one. The potential barrier between adjacent vacua has an energy scale given by a peculiar static solution of the classical gauge fields equations. The solution of the equation of motion at the saddle point of the potential is called the sphaleron [84]. A sphaleron, being static and localized in space, is particle-like, but since it is unstable, we do not want to call it a soliton. Unlike a soliton, a sphaleron does not correspond to a stable particle state in the quantum theory. Finally, let us mention that the term *sphaleron* was coined by Klinkhamer and Manton from the Greek, meaning "ready to fall".

At zero temperatures, the energy is insufficient to allow for a transition other than a tunneling and hence this process is entirely negligible. At high temperatures, the situation is different. The energy barrier E_{sph} represented by the classical sphaleron solution is finite, hence a thermal kick, if strong enough, would suffice to overpass the barrier. The probability associated to this process is proportional to $e^{-E_{\mathrm{sph}}/T}$ and hence it is exponentially suppressed at today's energy scale, making it unobservable. However, in the early Universe the sphaleron comes in thermal equilibrium as eventually $T \gg E_{\mathrm{sph}}$ [11], which changes its nature as it is now referred as the *thermal spaleron*. Taking the $SU(2)$ weak sphaleron as an example, it has been pointed out that its energy barrier is

$$E_{\mathrm{sph,W}} \simeq \frac{4m_W}{\alpha_W} \sim 10^4 \text{ GeV}, \tag{2.56}$$

where m_W is the mass of the $W^\pm$ boson, see Sec. 2.3.3.

At energies above E_{sph}, the sphaleron has so much energy that the system evolves from a neighborhood of one vacuum to another in a classical way, without tunneling. Mathematically, we can consider it taking a random walk in the vacuum, which is characterized by the equations

$$\langle N_{\mathrm{CS}} \rangle = 0, \qquad \langle N_{\mathrm{CS}}^2 \rangle \sim \Gamma_{\mathrm{sph}} t. \tag{2.57}$$

This means that the variance $\mathrm{Var}(x) = \langle x^2 \rangle - \langle x \rangle^2$ which contains information on the diffusion properties of the system, increases with time. Hence the change in the topological charge is diffusive as long as $T \gg E_{\mathrm{sph}}$. The detailed calculation shows that for both weak and strong sphalerons we have $\Gamma_{\mathrm{sph}}/V \propto \alpha^5 T^4$ [85–87]. We will come back to the effects of sphalerons when in thermal equilibrium with the primordial plasma in Sec. 3.1 because it participates in the baryogenesis mechanism presented in this work.

The θ vacuum

The true vacuum of the group cannot be one of these vacua, labeled $|0\rangle_i$, because they are not gauge invariant. Also taking one $|0\rangle_i$ as the vacuum wave function would violate a basic property in field theory, which is that the VEV of the product of several local operators at causally independent points must be reducible to the product of the VEV for each operator. In other words, we must have

$$\langle O_1 O_2 \rangle = \langle O_1 \rangle \langle O_2 \rangle. \tag{2.58}$$

---

[11]Detailed calculations showed that the weak sphaleron is in thermal equilibrium for 130 GeV $\lesssim T \lesssim 10^{12}$ GeV, see Sec. 3.1.2 and references therein.

This property can be traced back to the causality and unitarity of the theory [88].

Hence we shall find a true vacuum of the theory in order to properly compute VEV. The latter is called the θ vacuum and is defined as the superposition of all the possible vacua

$$|\theta\rangle = \sum c_n |0\rangle_n. \tag{2.59}$$

To determine the coefficients c_n, let's apply U to $|\theta\rangle$:

$$U|\theta\rangle = \sum c_n |0\rangle_{n+1} = \sum c_{n-1} |0\rangle_n. \tag{2.60}$$

We want the true vacuum to be invariant under gauge transformation, hence $c_n = e^{i\theta} c_{n-1}$. It follows that $c_n = e^{in\theta}$. So we get

$$|\theta\rangle = \sum_{n=0}^{\infty} e^{in\theta} |0\rangle_n \tag{2.61}$$

and thus

$$U|\theta\rangle = e^{i\theta} |\theta\rangle. \tag{2.62}$$

The transition amplitude (2.6) must therefore be modified to take into account that in general the path of the field does not need to start and end with configuration of the same winding number [89]. In other words, the vacuum can change during the transition amplitude and the path integral really computes

$$\langle\theta|e^{-iHt}|\theta\rangle = \int \mathcal{D}\phi \, e^{iS[\phi]+iJ\phi}. \tag{2.63}$$

In order to isolate the θ vacuum effects on the path integral, we compute the transitions from true vacuum to true vacuum by ν instantons:

$$\langle\theta|\theta\rangle = \sum_{m,n} e^{-im\theta} e^{in\theta} {}_m\langle 0|0\rangle_n = \sum_{\nu} e^{i\nu\theta} \sum_n {}_{n+\nu}\langle 0|0\rangle_\nu. \tag{2.64}$$

Therefore, the transition amplitudes ${}_{n+\nu}\langle 0|0\rangle_\nu$ are given by a path integral in which the space-time integral of $F\tilde{F}$ is fixed by (2.54). The extra factor of $e^{i\nu\theta}$ in (2.64) corresponds to an additional piece of the action

$$e^{iS_{\text{eff}}[\phi]} = e^{iS_{SU(n)}[\phi]+iS_\theta} \tag{2.65}$$

which is $S_\theta = \theta N_{\text{CS}}$ with N_{CS} given by (2.54). Finally, putting everything together we get

$$\langle\theta|\theta\rangle = \sum_{\nu} \int \mathcal{D}\phi \, e^{iS_{\text{eff}}[\phi]+iJ\phi} \, \delta\left(\nu - \frac{g^2}{16\pi^2} \int \mathrm{d}^4x \, F_{\mu\nu}^a \tilde{F}^{\mu\nu\,a}\right). \tag{2.66}$$

We see therefore that the non trivial nature of the $SU(n)$ vacuum leads directly to the potentially $\mathcal{P}$, $\mathcal{T}$ and $\mathcal{CP}$-violating effective Lagrangian

$$\mathcal{L}_{SU(n)}^{\text{eff}} = \mathcal{L}_{SU(n)} + \mathcal{L}_\theta \tag{2.67}$$

where

$$\mathcal{L}_\theta = \frac{g^2}{16\pi^2} \theta F_{\mu\nu}^a \tilde{F}^{\mu\nu\,a}. \tag{2.68}$$

Therefore, and to conclude, the non trivial vacuum structure of the $SU(n)$ gauge groups brings a new parameter in the theory, labeled as θ, with an associated Lagrangian so-called *topological density* Lagrangian. Concerning the SM, we will see in the next section how this affects the model.

2.3   The Standard Model

The Standard Model of particle physics (SM) is a QFT model based on the $SU(3)_c \otimes SU(2)_L \otimes U(1)_Y$ gauge group, where c stands for color, L for left-handed and Y for hypercharge. Its description restraints to the so-called baryonic matter (a misnomer which includes leptons and bosons) abundance of the Universe Ω_b^0 (see Sec. 1.1.2) which accounts for only $\sim 5\%$ of the Universe energy share.

The SM is a model describing three of the four known fundamental forces : the electromagnetic, weak, and strong interactions, in the universe, as well as classifying all known elementary particles. It exhibits a wide range of physics including spontaneous symmetry breaking, anomalies and non-perturbative behavior. The SM is a renormalizable theory (see Sec. 2.3.5) and can also be viewed as an effective field theory[12]. In that regard, the model's content corresponds to an energy scale of $\lesssim 100$ GeV while high-energy colliders, such as LHC, probe much higher energies. As a consequence, in order to describe our contemporary low-energy physics, as well as energy physics at scale $\gtrsim 100$ GeV (such as inflation), physicists use effective field theories which extend the SM with higher dimensional operators, see Eq. (2.82).

Lastly, the SM does not explain the origin of its content, neither the nature of DM nor the neutrino masses. An effective Lagrangian for gravitation can be added, but only at tree-level, hence it can only describe interactions with an empty space energy density (known as the cosmological constant).

All data and values are taken from [12].

2.3.1   Content

Because it is a QFT, from the point of view of the SM its contents are particles. From the spin-statistic theorem, we know that all particles that move in three dimensions have either integer spin or half-integer spin (in units of $\hbar$). In the first case, the wavefunction is symmetric under the permutation of two elements and the associated particles are called bosons. In the other case the wavefunction is anti-symmetric under the permutation of two elements and the associated particles are called fermions with the implication that the amplitude for two identical fermions to occupy the same state must be zero. The fact that two identical fermions cannot occupy the same state is called the *Pauli exclusion principle*. We stress that it does not apply to bosons.

In the SM, bosons are the force carriers and fermions are the elementary bricks of matter. Both their statistics are given by the distribution fonction Eq. (1.43). From the point of view of QFT, all particles ψ are excitations of their corresponding fields which are representations of the (proper-orthochronous) Lorentz group, the group of all Lorentz transformations of Minkowski spacetime. They are labelled by two half-integer numbers (j_-, j_+) which classify the Lie Algebras. The trivial case $(0,0)$ is the case of scalar fields to which the Higgs and the axion belong. The other SM bosons belong to the $(\frac{1}{2}, \frac{1}{2})$ representation and are called vector fields. We will come back to the fermions representation in the section dedicated to them. Lastly, let us mention for completeness that the graviton lies in the $(1,1)$ representation of the group.

Bosonic sector

There are three fundamental forces among the four that have been gauged. To this we shall add the Higgs field responsible of the Higgs mechanism (see Sec. 2.3.3).

---

[12]To be more explicit, we consider in this thesis that the SM consists only of renormalizable dimension 4 operators in the Lagrangian. Initially not included, aspects such as gravity, neutrino masses or heavier states can be added to the SM in an effective approach, mostly as higher dimensional operators.

Strong interaction   The theory of strong interactions is called quantum chromodynamics (QCD). It is based on the $SU(3)$ gauge group, hence has eight force carriers called the gluons described by the eight gauge fields written G_μ^a. They are real massless vectors. There are three conserved charges called colors. Quarks do carry color, hence they are the only matter constituent to couple to the strong interaction. Quarks q enter in the fundamental representation of $SU(3)$ that is a column vector of three different states

$$q = \begin{pmatrix} q_r \\ q_g \\ q_b \end{pmatrix}, \tag{2.69}$$

where the color labels are (conventionally) red, green and blue. This means that from the perspective of the strong interaction, a given red and green quark are as different as an electron and an electron-neutrino from the perspective of the weak interaction, see Eq. (2.73).

At scales $\Lambda \lesssim 1$ GeV, the quarks are confined, because the interaction coupling blows up with decreasing energy (Landau pole, see section 2.3.5). From an effective point of view, there is no quark at low scale, only bound states. Quarks "appear" at high energy. The bound states (hadrons) are colorless.

Electroweak interaction   The weak force couples only to left-handed fermions, as an experiment on decay of the muon [90] showed that a right-handed lepton never decays through weak interaction.

Process	Rate
$\mu_L^- \longrightarrow e_L^- + \bar{\nu}_{eL} + \nu_{\mu L}$	100%
$\mu_R^- \longrightarrow e_R^- + \bar{\nu}_{eR} + \nu_{\mu R}$	0%

The SM is therefore a chiral theory. In other words left and right-handed particles are treated differently, the first difference being that the right-handed neutrinos do not exist in the SM. The weak force associated gauge group is $SU(2)$, hence it has three force carriers written as W_μ^a. They are complex massless vectors. Left-handed fermions are in the fundamental representation of the group, see Eq. (2.73).

In the 1960s, Glashow, Weinberg and Salam discovered a way of combining electromagnetism and the weak interaction into the electroweak interaction [91–93]. The electroweak theory is based on the $SU(2)_L \otimes U(1)_Y$ gauge group, meaning that a new electromagnetism-like gauge group is added to the weak interaction. This interaction has a conserved charge called hypercharge and is denoted as such.

Hypercharge interaction is inoperative at our low-energy scale, but couples to every fermion at scales $\gtrsim 100$ GeV. Like ordinary electromagnetism, each fermion is in a singlet representation of $U(1)_Y$ and carries a specific value of hypercharge Y_ψ. The associated massless vector boson is written Y_μ. This implies at our scale that the electroweak interactions are broken down to ordinary electromagnetism. The process of this breaking down is called the Higgs mechanism, see Sec. 2.3.3.

In order to describe it, we shall add a new boson in the representation $(0,0)$ of the Lorentz group, hence a scalar, whose potential controls the breaking of the electroweak group to the electromagnetism group. This boson is called the Higgs boson. Its associated field is a complex massive scalar $SU(2)_L$ doublet[13], i.e. four real degrees of freedom,

$$\Phi = \begin{pmatrix} \Phi^+ \\ \Phi^0 \end{pmatrix}, \qquad\qquad \Phi^c = i\sigma_2\Phi^* = \begin{pmatrix} \Phi^{0\,\dagger} \\ -\Phi^- \end{pmatrix} \tag{2.70}$$

---

[13]Here we write the Higgs doublet in another representation than the one used in Eq. (1.127) but they are equivalent. At first order, this can be checked by expanding $e^{i\zeta^a\tau^a} \simeq 1 + i\zeta^a\tau^a$ and identifying the four scalar fields (ζ^a, h) with the four real degrees of freedom of (Φ^+, Φ^0).

with weak hypercharge $Y_\Phi = 1/2$. It is self-interacting and couples to every fermion via the Yukawa interaction.

During the Higgs mechanism, the field looses three degrees of freedom that become the longitudinal modes of the massive $W^\pm$ and Z^0 bosons in the unitary gauge (their so-called longitudinal polarization). Only one massive scalar real field remains, the physical Higgs boson h. Through the corresponding Yukawa couplings, all fermions also acquire their mass that way.

The photon, written A_μ, is a linear combination of Y_μ and the diagonal part of $SU(2)_L$ written Z^0_μ, see Eq. (2.90c).

Fermionic sector

The fermions of the SM ψ are classified into quarks and leptons, depending on whether they couple to the strong force or not. This distinction was made by experimentalists in the second half of the 20th century when they discover, on the one hand a wide variety of heavy particles they called hadrons (heavy in Greek) and, on the other hand, much lighter ones they named leptons (light in Greek). Note that some of the hadrons are bosons, and they are called *mesons*, but they are not elementary particles which the SM aims to describe. Moreover, stable hadrons found in the Universe are very few: the proton and the neutron, which are fermions and called *baryons*.

Hence in the SM the matter constituents are, 6 leptons[14] and, if we disregard counting color states, 6 quarks, spin $\frac{1}{2}$ elementary particles. They are classified into 3 generations we can differentiate only by their masses.

$$e^i = (e, \mu, \tau) \qquad \nu^i = (\nu_e, \nu_\mu, \nu_\tau) \qquad u^i = (u, c, t) \qquad d^i = (d, s, b) \tag{2.71}$$

Each fermion ψ has its own antiparticle denoted $\bar{\psi}$. Their antiparticles have same mass, but opposite charge. Depending on the gauge field they couple to, they can carry electric charge Q, color, weak isospin I_3, etc. In particular, it is straightforward to see from (2.33) that the upper component of any $SU(2)_L$ doublet has $I_3 = 1/2$ and the lower one has $I_3 = -1/2$. Moreover, all fermions transform under the hypercharge gauge group and carry a hypercharge Y_ψ. A summary of the classification of SM fermions is shown in table 2.1. We normalize the electric charge in a way that makes the charge of a proton unity. Besides, the particles also carry handedness and mass, but here we focus only on the parameters that enter into their interactions. Moreover, no invariant mass term is allowed by the SM symmetries, so fermions will acquire their mass from the Yukawa interactions and the Higgs mechanism, see sections hereafter. Lastly, since the SM cannot explain the phenomenon of neutrino oscillations, neutrinos are considered massless in the SM. Handedness should be discussed in detail because experiments to date have not been able to prove the existence of right-handed neutrinos.

From the point of view of QFT, all fermions are excitations of spinor fields. The spinor representation is the first non trivial representation of the Lorentz group. It comes in two types: the left-handed spinors ψ_L are part of the $(\frac{1}{2}, 0)$ representation and the right-handed spinors ψ_R are in the $(0, \frac{1}{2})$ representation. $\psi_{L/R}$ fields are called Weyl spinors. The generators of the spinor representation are the Pauli matrices σ_a. Hence the algebras of $\psi_{L/R}$ are $\mathfrak{su}(2)$ and $\psi_{L/R}$ are in the fundamental representation. The basis of left-, and respectively right-handed matrices are given by

$$\sigma^\mu = (I_2, \sigma_a), \qquad\qquad \bar{\sigma}^\mu = (I_2, -\sigma_a). \tag{2.72}$$

Left-handed fermions couple to the weak force and hence form $SU(2)$ doublets

$$Q^i_L = \begin{pmatrix} u^i_L \\ d^i_L \end{pmatrix} \qquad\qquad L^i_L = \begin{pmatrix} e^i_L \\ \nu^i_L \end{pmatrix} \tag{2.73}$$

---

[14]The 3 neutrinos are Weyl fermions, with only the left chirality.

Type	Particle	Handedness	Q	I_3	Y
LEPTON	e, μ, τ	left	-1	-1/2	-1/2
		right	-1	0	-1
	ν_e, ν_μ, ν_τ	left	0	1/2	-1/2
		right	-	-	-
QUARK	u, c, t	left	2/3	1/2	1/6
		right	2/3	0	2/3
	d, s, b	left	-1/3	-1/2	1/6
		right	-1/3	0	-1/3

Table 2.1. Fermion classification in the Standard Model with the values of electric charge Q, weak isospin I_3 and hypercharge Y, related by $Q = I_3 + Y$, Eq. (2.88).

in the fundamental representation of the gauge group. The right-handed ones are singlets, but without right-handed neutrinos ν_R^i as this species is absent from the SM.

Two observations suggest that we build a representation that embeds both right- and left-handed spinor: the Dirac representation. The first is that a parity transformation flips the two half integers $P : (j_-, j_+) \longmapsto (j_+, j_-)$, meaning that one does not take parity into account when only considering ψ_L or ψ_R alone. The second is that the left-handed and the complex conjugate of the right-handed representation are related by a unitary transformation, which means that, for instance, $(\frac{1}{2}, 0)^*$ transforms like $(0, \frac{1}{2})$ under a Lorentz transformation. Defining therefore the Dirac representation as $(\frac{1}{2}, 0) \oplus (0, \frac{1}{2})$ and the Dirac spinor as

$$\psi = \begin{pmatrix} \psi_L \\ \psi_R \end{pmatrix}. \tag{2.74}$$

the Dirac algebra naturally arises from the algebra of Weyl spinors. It is given in terms of the gamma matrices:

$$\gamma^\mu = \begin{pmatrix} 0 & \sigma^\mu \\ \bar{\sigma}^\mu & 0 \end{pmatrix}. \tag{2.75}$$

The fifth gamma matrix, which is not a gamma matrix despite its name, is given by the product of all gamma matrices:

$$\gamma_5 = i\gamma^0\gamma^1\gamma^2\gamma^3 = \begin{pmatrix} -I_2 & 0 \\ 0 & I_2 \end{pmatrix}. \tag{2.76}$$

The subscript 5 is not an index, it is a relic of the old notation in which γ^0 was written as γ^4. That is why we will always use the 5 as a subscript and never move it. The matrix γ_5 is used to deal with chirality (i.e. left- and right-handedness), see Sec. 2.3.6.

2.3.2   Lagrangian

The full Lagrangian of the Standard model is

$$\mathcal{L}_{\text{SM}} = \mathcal{L}_{\text{gauge}} + \mathcal{L}_{\text{fermion}} + \mathcal{L}_{\text{Higgs}} + \mathcal{L}_{\text{Yukawa}} + \mathcal{L}_{\text{graviton}} + \mathcal{L}_{\bar{\theta}} + \mathcal{L}_{\text{corrections}} \tag{2.77}$$

where

$$\mathcal{L}_{\text{gauge}} = \sum_{\text{spin 1 bosons}} -\frac{1}{4} F^a_{\mu\nu} F^{\mu\nu\,a} \tag{2.78a}$$

$$\mathcal{L}_{\text{fermion}} = \sum_{\text{fermions}} i\bar{\psi}\gamma^\mu D_\mu \psi \tag{2.78b}$$

$$\mathcal{L}_{\text{Higgs}} = (D_\mu \Phi)^\dagger D^\mu \Phi + m^2 |\Phi|^2 - \lambda |\Phi|^4 \tag{2.78c}$$

$$\mathcal{L}_{\text{Yukawa}} = Y_{ij} \psi_L^{\dagger i} \Phi \psi_R^j \tag{2.78d}$$

$$\mathcal{L}_{\text{graviton}} = \mathcal{L}_{\text{grav kin}} + \mathcal{L}_{\text{grav int}} \tag{2.78e}$$

$$\mathcal{L}_{\bar{\theta}} = \frac{g^2}{16\pi^2} \bar{\theta} G_{\mu\nu}^a \tilde{G}^{\mu\nu\, a} \tag{2.78f}$$

with

$$\mathcal{L}_{\text{grav kin}} = -\frac{1}{2} \partial_\mu h_{\nu\sigma} \, \partial^\mu h^{\nu\sigma} + \frac{1}{2} \partial_\mu h^\nu_\nu \, \partial^\mu h^\nu_\nu + \partial_\mu h^{\mu\nu} \, \partial_\sigma h^\sigma_\nu + \partial_\mu h^\nu_\nu \, \partial_\sigma h^{\sigma\mu} \tag{2.79a}$$

$$\mathcal{L}_{\text{grav int}} = \sqrt{G} \, h_{\mu\nu} T^{\mu\nu}. \tag{2.79b}$$

The graviton Lagrangian is not officially part of the SM, as is it still at the stage of effective field theory. It should be removed for purists, but it has been put here for completeness. $\mathcal{L}_{\text{corrections}}$ accounts for all counterterms coming from renormalization and so-called ghosts that together make the SM a renormalizable theory (see section 2.3.5). The gauge covariant derivative D_μ is introduced so that the derivatives of the fields transform the same way as the fields themselves under the SM gauge groups. It introduces a coupling between the fermions and the interaction they couple to via the associated gauge field. It writes

$$D_\mu = \partial_\mu - ig' Y_\psi Y_\mu - ig\tau^a W_\mu^a - ig_s \eta^a G_\mu^a \tag{2.80}$$

where the matrices τ^a and η^a have been defined by (2.34) and (2.37) respectively.

In the Yukawa Lagrangian, Y_{ij} is a matrix of the Yukawa couplings y_ψ, where i, j label the generation. For a more accurate Yukawa Lagrangian, see Eq. (2.96). After diagonalization, the mass of every fermion is directly related to its Yukawa coupling as

$$m_\psi = \frac{y_\psi v}{\sqrt{2}}. \tag{2.81}$$

As we will see in Sec. 2.3.4, when the states $\psi^i_{L/R}$ are in the flavor basis, the mass matrix is not diagonal. Making use of the CKM matrix in the quark sector, it is possible to diagonalize it to be in the mass eigenstate, but then $\psi^i_{L/R}$ are in a mixed flavor basis.

In the effective approach, the SM Lagrangian can be extended to operators of higher dimensions and we can see $\mathcal{L}_{\text{SM}}$ as the leading term in the expansion:

$$\mathcal{L}_{\text{SM,full}} = \mathcal{L}_{\text{SM}} + \sum_{n \geqslant 1} \frac{1}{\Lambda^n} \mathcal{O}^{(n+4)}. \tag{2.82}$$

The added terms can then be viewed as corrections to $\mathcal{L}_{\text{SM}}$, relevant for scales of order Λ.

Parameters

The 19 free parameters of the SM are:

- The nine fermion masses (6 quarks and 3 charged leptons) via the Higgs mechanism, see Sec. 2.3.3.

- The $U(1)_Y$, $SU(2)_L$ and $SU(3)_c$ gauge couplings [94].

$$g' = 0.3587 \qquad g = 0.6483 \qquad g_s = 1.1666 \tag{2.83}$$

given at two-loops correction in the $\overline{\text{MS}}$ scheme at the top mass $m_t = 173.35$ GeV, see Sec. 2.3.5.

- The four parameters of the CKM matrix, see Sec. 2.3.4.

- The QCD $SU(3)$ θ vacuum angle, see Sec. 2.2.4 and Eq. (2.68).

- The Higgs vacuum expectation value $v = 246.21971 \pm 0.00006$ GeV [94], see Sec. 2.3.3.

- The Higgs mass $m_h = 125.25$ GeV.

Note that in the SM neutrinos are massless. In the effective theory approach, we can consider a dimension-five mass term for each left-handed neutrino. Hence in this extension, we have to include three neutrino masses and their correspond mixing angles that come in the Pontecorvo-Maki-Nakagawa-Sakata (PMNS) matrix, an analog of the CKM matrix, which accounts for the neutrino oscillations.

Accidental symmetries

If, after imposing the gauge symmetries from interactions and renormalizing the theory, symmetries still remain, these are called accidental symmetries. They are symmetries that we did not impose but that the action exhibits anyway. They are usually valid up to a certain point in the EFT expansion (2.82). We call accidental symmetries of the SM the accidental symmetries at leading order ($\mathcal{L}_{\mathrm{SM}}$ given by (2.77)).

Some accidental symmetries of the SM are

- The product of parity $\mathcal{P} : \boldsymbol{x} \to -\boldsymbol{x}$, times the charge conjugation $\mathcal{C} : \psi \to -\mathcal{C}\bar{\psi}^T$ where $\mathcal{C} = i\gamma_0\gamma_2$, that change handedness of the fermions: $\psi_L \leftrightarrow \psi_R$, times the time reversal $\mathcal{T} : t \to -t$: $\mathcal{CPT}$.

- The global $U(1)_B$ that conserve the baryon number B.

- Three global $U(1)_\ell$ where $\ell = e, \mu, \tau$ that conserve each generation of lepton number.

The first symmetry is discrete and stands that every localized quantum system should be invariant under these three symmetries applied together. We ofter write the two last symmetries as

$$U(1)_B \otimes U(1)_e \otimes U(1)_\nu \otimes U(1)_\tau \qquad \text{or} \qquad U(1)_B \otimes U(1)_L, \tag{2.84}$$

where $U(1)_L = [U(1)_\ell]^3$. Sometimes we also refer to the accidental global $U(1)_{B-L}$ symmetry.

Accidental symmetries have huge implications on a theory. For instance, a Majorana mass term violates the $U(1)_{B-L}$ symmetry by two units. Neutrino masses are therefore protected by this symmetry.

As already stated in Sec. 2.1, accidental symmetries do not necessarily conserve the generating functional $Z[J]$ defined in (2.6) because the measure in the path integral can change even if the action remains untouched. Indeed, the field ϕ is shifted according to (2.11b), hence does $\mathcal{D}\phi$. When this happens, the corresponding current is not conserved $\partial_\mu j^\mu \neq 0$ and the symmetry is said to be *anomalous*. In Sec. 2.3.6 we give an overview of the chiral anomaly in the SM and how it is linked to the accidental global symmetries.

2.3.3   The Higgs mechanism

The Higgs mechanism is a description of the spontaneous symmetry breaking of the electroweak sector into electromagnetism that happens at scale ~ 100 GeV. Spontaneous breaking of symmetry happens when the ground energy of a system (the vacuum) has less symmetry than the system itself. For instance, consider magnetic materials, which are characterized by the presence of magnetic moments. These are due to the movement of the so-called valence electrons in the atoms. When

hot, the direction of the magnetic moments are randomly distributed among microscopic patch of the material. Thus, at macroscopic level the resulting magnetization results to zero by isotropy, hence there is an $O(3)$ symmetry of the system. However, the state of lowest energy (the ground state) of these materials corresponds to all the magnetic moments being aligned in the same direction. In that state, the global symmetry has been broken down to Z_2 and the material is now macroscopically magnetized.

In field theory, it it possible to mobilise the same mathematical tools to describe how global and gauge symmetries can be partially or totally broken. In addition to this aim, the Higgs mechanism also explains how the electroweak bosons and fermions got massive during the process. Consider the electroweak sector of the SM (2.77) given by

$$\mathcal{L}_{\text{EW}} = -\frac{1}{4}W^a_{\mu\nu}W^{\mu\nu\,a} - \frac{1}{4}Y_{\mu\nu}Y^{\mu\nu} + (D_\mu\Phi)^\dagger D^\mu\Phi - V(\Phi) + \mathcal{L}_{\text{Yukawa}}. \tag{2.85}$$

Assume that the Higgs potential has a minimal value for the specific doublet value

$$\langle\Phi\rangle = \frac{1}{\sqrt{2}}\begin{pmatrix} 0 \\ v \end{pmatrix}, \qquad \langle\Phi^c\rangle = \frac{1}{\sqrt{2}}\begin{pmatrix} v \\ 0 \end{pmatrix}. \tag{2.86}$$

This can be possible if the quadratic term in the Higgs potential (2.78c) is negative. With the sign convention we used this means $m > 0$. Then the shape of the potential is the one of a Mexican hat and the neutral component of the scalar doublet acquires a non-zero vacuum expectation value (VEV). The ground state (i.e. the vacuum) is then defined to be

$$\Phi = \langle\Phi\rangle, \qquad W^a_\mu = 0, \qquad Y_\mu = 0. \tag{2.87}$$

The unbroken generators Q of the vacuum symmetry subgroup are Hermitian matrices such that $Q\langle\Phi\rangle = 0$. If one chooses the generator of $U(1)_Y$ to be $Y = 1/2$ on the Higgs, it means that we have $Q = \tau^3 + Y$, where τ^3 was defined in (2.34).

Thus when the Higgs field sits at its minimum, there is an unbroken $U(1)$ gauge group which is different from the original $U(1)_Y$ group and to which electromagnetism is identified. The $U(1)_{\text{EM}}$ subgroup therefore has a single gauge field A_μ which is a linear combination of the τ^3 component of the $SU(2)_L$ gauge field and the hypercharge gauge field. In quantum mechanics, hermitian operators are observables, hence Q corresponds to the electromagnetic charge, τ^3, sometimes written as I_3, denotes the weak isospin and Y is the hypercharge. Due to our choice of the $U(1)_Y$ generator, these three parameters are related by

$$Q = I_3 + Y. \tag{2.88}$$

As a bottom line, the physics when $\Phi = 0$ (the symmetric phase) is drastically different from the one when $\Phi = \langle\Phi\rangle$ (the broken phase). The way that the primordial plasma transitions from one phase to another is described by the changing shape of the Higgs potential that depends on the Universe temperature, and is referred to as the electroweak phase transition (EWPT). Phase transitions can either be first or second order, see Fig. 2.1. In the first case, the transition is abrupt as quantum tunneling is possible. Like liquid water becoming gas, one phase suddenly appears among the other and forms bubbles that, under some conditions, can expand before dominating the Universe. The second case is a continuous crossover, like liquid water becoming solid. Today, experimentation and results are in favor of a second order EWPT. Today, the rate of transition is still under study and will be of great importance for us because the EWPT can provide the out-of-equilibrium situation required by the Sakharov conditions. We will come back to this issue when talking about the baryon asymmetry generation mechanism, see Sec. 3.1.

The symmetric phase is described by the Lagrangian (2.85) whereas the broken phase La-
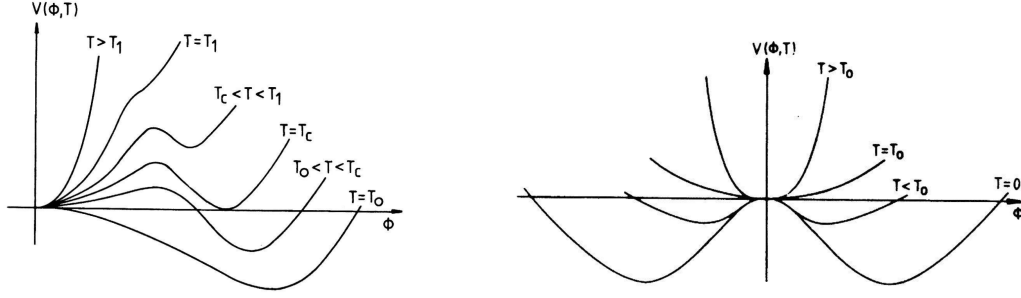
Figure 2.1. Left: A typical first order phase transition with a potential normalized at $\phi = 0$ for all values of T. At $T_1 > T$, the only minimum is at $\phi = 0$ and the symmetry is said to be restored. At $T = T_1$, a local minimum appears as an inflection point and a barrier between both minimum starts to develop as temperature falls. At the critical temperature $T = T_c$ both minima are degenerate. As soon as $T_c > T$, the original minimum becomes metastable and tunneling is possible, which starts the phase transition. The tunneling rate depends on the barrier's height and for some potentials the tunneling becomes efficient later. Finally, when $T = T_o$ the barrier disappears and the original minimum is now a maximum. Right: A typical second order phase transition with a potential normalized at $\phi = 0$ for all values of T. As for first order phase transition, at $T > T_o$ the only minimum is at $\phi = 0$ and the symmetry is said to be restored. At $T = T_o$, the global minimum becomes a local maximum and when T falls the field simply rolls down the potential acquiring a new expectation value different from zero. This transition is said to be soft, as the minimum of $V(\phi)$ continuously changes from the high temperature global minimum to a new position at low temperatures. Figures taken from [95].

grangian can be obtained at leading order by studying the perturbations around the Higgs potential vacuum. In fact, the physical (scalar) Higgs field h is a small linear perturbation of the doublet around the vacuum. As long as $\Phi \neq 0$, any configuration of the field close to the classical vacuum is gauge equivalent to the following configuration, in the unitary gauge,

$$\Phi = \begin{pmatrix} 0 \\ \frac{v+h}{\sqrt{2}} \end{pmatrix}. \tag{2.89}$$

If we now define the fields

$$W_\mu^\pm = \frac{W_\mu^1 \mp i W_\mu^2}{\sqrt{2}} \tag{2.90a}$$

$$Z_\mu^0 = W_\mu^3 \cos\theta_W - Y_\mu \sin\theta_W \tag{2.90b}$$

$$A_\mu^0 = Y_\mu \cos\theta_W + W_\mu^3 \sin\theta_W \tag{2.90c}$$

the EW Lagrangian terms become in the broken phase

$$-\frac{1}{4} W_{\mu\nu}^a W^{\mu\nu\,a} - \frac{1}{4} Y_{\mu\nu} Y^{\mu\nu} = -\frac{1}{2} W_{\mu\nu}^+ W^{-\,\mu\nu} - \frac{1}{4} Z_{\mu\nu} Z^{\mu\nu} - \frac{1}{4} F_{\mu\nu} F^{\mu\nu} + ... \tag{2.91a}$$

$$(D_\mu \Phi)^\dagger D^\mu \Phi = \frac{1}{2} \partial_\mu h \partial^\mu h + m_W^2 W_\mu^+ W^{-\,\mu} + \frac{m_Z^2}{2} Z_\mu^0 Z^{0\,\mu} + ... \tag{2.91b}$$

where we wrote only the quadratic terms with

$$m_W = \frac{gv}{2}, \qquad m_Z = \frac{m_W}{\cos\theta_W}, \qquad \cos\theta_W = \frac{g}{\sqrt{g^2 + g'^2}}, \qquad \sin\theta_W = \frac{g'}{\sqrt{g^2 + g'^2}}. \tag{2.92}$$

We can see that the resulting Lagrangian describes four vector fields, like (2.85), but three of them

are massive. The second equation shows that three of the four Higgs doublet degrees of freedom became the longitudinal components of the $W^\pm$ and Z^0 bosons. We identify the massless vector field with the photon. The full broken phase Lagrangian contains nonlinear terms describing the field interactions that we eluded here.

Note that the number of longitudinal components match the number of broken generators $(\tau^a, Y) \to Q$. This is part of the Goldstone theorem which states that, to each broken generator of a global symmetry corresponds a massless scalar field called a *Goldstone boson*. As we have seen, for a gauge symmetry, the Goldstone boson becomes the longitudinal polarization of the associated vector field. If the symmetry is global but approximate, each broken generator provide a massive boson called a *pseudo Nambu-Goldstone boson*.

The bosons $W^\pm$ and Z^0 have been detected experimentally; their masses are $m_W \simeq 80$ GeV and $m_Z \simeq 91$ GeV. Besides, the weak angle θ_W is measured independently by studying the interaction of photons and the massive bosons with other particles. This is possible because θ_W is determined by the coupling constants g and g'. The experimental value is $\sin^2 \theta_W \simeq 0.23$, hence the equation $m_W = m_Z \cos \theta_W$ is satisfied in nature with good accuracy.

The covariant derivative in (2.85) contained all four EW gauge fields in the symmetric phase, see Eq. (2.80). In the broken phase it becomes

$$D_\mu = \partial_\mu - ieA_\mu \tag{2.93}$$

where

$$e = \frac{gg'}{\sqrt{g^2 + g'^2}} = 0.3139 \tag{2.94}$$

computed according to the values given by (2.83).

The physical Higgs h has a mass $m_h = \sqrt{2\lambda}v$ (that we shall not confuse with the mass parameter m) and a VEV

$$v \equiv \langle h \rangle = \frac{m}{\sqrt{\lambda}} \simeq 246 \text{ GeV}. \tag{2.95}$$

The quartic coupling λ is a free parameter in the SM, and hence, there is no a priori prediction for the Higgs mass. Moreover, the sign of the mass parameter $m^2 = \lambda v^2$ is crucial for the EW symmetry breaking to take place, but is not specified in the SM. There should be a sign difference between the quadratic and the quartic terms; here we put it explicitly in the potential definition. The experimentally measured Higgs mass, $m_h \simeq 125$ GeV, implies that $\lambda \simeq 0.13$ and $m = 88.8$ GeV at the top mass scale[15]. The Higgs boson was predicted in 1964 [96–98] and discovered at CERN in 2012 [99, 100],

2.3.4 Flavor and mass mixing

In the previous section we focused of the gauge part of the EW symmetry breaking. In this one, we will study the consequence on the fermion sector, in particular the Yukawa interactions, and how it leads to flavor mixing in the broken phase. Recall the Yukawa Lagrangian (2.78d)

$$\mathcal{L}_{\text{Yuk}} = (Y_\ell)_{ij} \bar{L}_L^i \Phi e_R^j + (Y_u)_{ij} \bar{Q}_L^i \Phi u_R^j + (Y_d)_{ij} \bar{Q}_L^i \Phi^c d_R^j \tag{2.96}$$

where $\bar{\psi}_L^i \equiv \psi_L^{i\dagger} \gamma^0$ is a left-handed doublet of generation i and ψ_R^j a right-handed singlet of generation j. The matrices $(Y_\psi)_{ij}$ encode the Yukawa coefficients of the three $SU(2)$ families of fermions. The first term stands for leptonic sector, the second for up-type quark and the last for down-type quark, see Eq. (2.71). We could add a term $Y_{ij} \bar{L}_L^i \Phi^c \nu_R^j$ but right-handed neutrinos have not been observed yet.

---

[15]All SM couplings values are given at a specified energy scale as they are running with it, see Sec. 2.3.5.

The Higgs doublet then gets a VEV given by (2.86), hence using the doublet representation (2.73), the Yukawa Lagrangian becomes

$$\mathcal{L}_{\text{Yuk}} = (M_\ell)_{ij} e_L^{i\dagger} e_R^j + (M_u)_{ij} u_L^{i\dagger} u_R^j + (M_d)_{ij} d_L^{i\dagger} d_R^j \tag{2.97}$$

where we defined

$$(M_\psi)_{ij} \equiv \frac{v\,(Y_\psi)_{ij}}{\sqrt{2}} \tag{2.98}$$

as the mass mixing matrix of the family ψ. These three matrices can be diagonalized by the use of the unitary matrices $V_{L,R}^\psi$. Without index notation, it writes

$$M_\psi = V_L^\psi D_\psi (V_R^\psi)^\dagger \tag{2.99}$$

with

$$\begin{aligned}
D_\ell &= \text{diag}(m_e, m_\mu, m_\tau) \\
D_u &= \text{diag}(m_u, m_c, m_t) \\
D_d &= \text{diag}(m_d, m_s, m_b)
\end{aligned} \tag{2.100}$$

With those changes, the Yukawa Lagrangian now writes

$$\mathcal{L}_{\text{Yuk}} = e_L^\dagger V_L^\ell D_\ell (V_R^\ell)^\dagger e_R + u_L^\dagger V_L^u D_u (V_R^u)^\dagger u_R + d_L^\dagger V_L^d D_d (V_R^d)^\dagger d_R. \tag{2.101}$$

This way of writing things is relevant because the propagators are defined in the mass eigenstate of the fermions as they should satisfy the equation $(\partial^2 - m^2)G(x,y) = \delta(x-y)$, see Eq. (2.8). Hence, in order to draw Feynmann diagrams and calculate anything from it, it is needed to put the fields in the mass basis. To do so, we use the accidental symmetries of the SM (2.84) and perform rotations for the fermion fields. For the lepton part this works well, since by $U(3)_L \otimes U(3)_R$ rotating

$$L_L \to V_L^\ell \, L_L = \begin{pmatrix} V_L^\ell e_L \\ V_L^\ell \nu_L \end{pmatrix}, \qquad\qquad e_R \to V_R^\ell \, e_R, \tag{2.102}$$

we can go to a basis where the mass mixing is removed. This is because there is as many fields $(L_L,\, e_R)$ as there are rotating matrices $(V_L^\ell,\, V_R^\ell)$. Once in this basis, there is a residual symmetry $[U(1)_\ell]^3$ that distinguishes the three lepton families. Thus, the take away message is that there is no mixing in the lepton sector and we can always consider the SM in the lepton mass eigenstate.

However, the story is different in the quark sector, because there are 3 fields $(Q_L,\, u_R,\, d_R)$ for 4 unitary matrices $(V_L^u,\, V_L^d,\, V_R^u,\, V_R^d)$. Therefore we cannot simultaneously diagonalize them as there is not enough symmetry to put all quarks in mass eigenstates without mixing their flavors. This is because u_L and d_L must transforms the same way since they belong to the same $SU(2)$ doublet. Therefore there is a $4-3$ residual mixing matrix called the CKM matrix.

We have the choice then between two fields redefinition to make one mass mixing matrix diagonal,

$$Q_L \to V_L^{u/d} \, Q_L = \begin{pmatrix} V_L^{u/d}\, u_L \\ V_L^{u/d}\, d_L \end{pmatrix}, \quad u_R \to V_R^u \, u_R, \quad d_R \to V_R^d \, d_R, \tag{2.103}$$

where $V_L^{u/d}$ stand for the fact that there is the possibility to choose (once for all) between V_L^u or V_L^d as the diagonalizing matrix. If we choose V_L^u and define the Cabibbo-Kobayashi-Maskawa (CKM) matrix as $V_{\text{CKM}} = (V_L^u)^\dagger V_L^d$, which is unitary transformation, we can then perform a residual mass mixing in the quark sector as $\tilde{M}_d = V_{\text{CKM}} D_d V_{\text{CKM}}^\dagger$ and the Yukawa Lagrangian in the mass

eigenstate becomes

$$\mathcal{L}_{\text{Yuk}} = \sum_{i=e,\mu,\tau} m_i e_L^{i\dagger} e_R^i + \sum_{i=u,c,t} m_i u_L^{i\dagger} u_R^i + \sum_{i,j=d,s,b} (\tilde{M}_d)_{ij} d_L^{i\dagger} d_R^j \qquad (2.104)$$

As a consequence, to interpret the SM Lagrangian in term of mass eigenstates, we need to redefine the quark fields as

$$\begin{aligned} u_{L,R}^i &\to u_{L,R}^i, \quad d_R^i \to d_R^i \\ d_L^i &\to (V_{\text{CKM}})_{ij} \ d_L^j \end{aligned} \qquad (2.105)$$

which induces *flavor mixing* [101].

The CKM matrix

The CKM matrix is a 3×3 unitary matrix, $V_{\text{CKM}} \in U(3)$. It has 9 parameters because the unitarity condition $V_{\text{CKM}}^\dagger = V_{\text{CKM}}^{-1}$ removes 9 degrees of freedom to the 9 complex entries. It explicitly writes

$$V_{\text{CKM}} = \begin{pmatrix} V_{ud} & V_{us} & V_{ub} \\ V_{cd} & V_{cs} & V_{cb} \\ V_{td} & V_{ts} & V_{tb} \end{pmatrix} \qquad (2.106)$$

The transition amplitude from i to j is proportional to $|V_{ij}|^2$. There are 5 $U(1)$ global symmetries, namely Q_L, u_R, d_R, L_L, e_R, that allow a shift to remove the phase of the corresponding fields. Those shift angles are unobservables and contribute to the $\mathcal{CP}$ problem as we will see in Sec. 2.4.1. At the end of the day, 4 free parameters remain for the CKM matrix and various representations of them exist. The standard one is

$$V_{\text{CKM}} = \begin{pmatrix} 1 & 0 & 0 \\ 0 & c_{23} & s_{23} \\ 0 & -s_{23} & c_{23} \end{pmatrix} \begin{pmatrix} c_{13} & 0 & s_{13}e^{-i\delta} \\ 0 & 1 & 0 \\ -s_{13}e^{i\delta} & 0 & c_{13} \end{pmatrix} \begin{pmatrix} c_{12} & s_{12} & 0 \\ -s_{12} & c_{12} & 0 \\ 0 & 0 & 1 \end{pmatrix} \qquad (2.107)$$

where $s_{ij} = \sin\theta_{ij}$ and $c_{ij} = \cos\theta_{ij}$. Here we see the three rotations and the remaining phase explicitly.

As shown, the unitary rotation (2.105) makes the mass matrices M_u and M_d diagonal but with the price of flavor mixing. Because the propagators are always in their mass eigenstate, the latter is carried by charged bosons from EW sector in their mass eigenstate: the $W^\pm$ bosons. In other words, when drawing a Feynmann diagram, every vertex involving a $W^\pm$ will have a V_{ij}. This comes from the coupling to $SU(2)$ in the covariant derivative :

$$i\bar{\psi}\gamma^\mu D_\mu \psi \quad \overset{SU(2)\text{ term}}{\to} \quad \frac{g}{2}\psi_L^{\dagger i}\bar{\sigma}^\mu \sigma^a \psi_L^j W_\mu^a \qquad (2.108)$$

where i,j are the flavor indices. Under $SU(2)_L$ the representation (2.73) explicitly writes

$$\mathcal{L}_{SU(2)}^{\text{int}} = \frac{g\bar{\sigma}^\mu}{2} \begin{pmatrix} u_L^{\dagger i} & d_L^{\dagger i} \end{pmatrix} \begin{pmatrix} Y_\mu + W_\mu^3 & W_\mu^1 - iW_\mu^2 \\ W_\mu^1 + iW_\mu^2 & Y_\mu - W_\mu^3 \end{pmatrix} \begin{pmatrix} u_L^j \\ d_L^j \end{pmatrix} \qquad (2.109)$$

where $u_{L/R}^i$ and $d_{L/R}^i$ are both flavor families, see Eq. (2.71). We now go to the broken phase basis using (2.90) and we write schematically $Y_\mu \pm W_\mu^3 = C_1^\pm A_\mu^0 + C_2^\pm Z_\mu^0$ where $C_1^\pm$ and $C_2^\pm$ are constant

depending solely on g and g', see (2.92). Therefore, the interaction (2.109) becomes

$$\mathcal{L}^{\text{int}}_{SU(2)} = \frac{g\bar{\sigma}^{\mu}}{\sqrt{2}} \left[u_L^{\dagger i}(C_1^+ A_\mu^0 + C_2^+ Z_\mu^0)u_L^i + u_L^{\dagger i}W_\mu^+ V_{ij}^{\text{CKM}}d_L^j \right.$$
$$\left. + d_L^{\dagger i}V_{ij}^{\dagger\text{CKM}}W_\mu^- u_L^j + d_L^{\dagger i}(C_1^- A_\mu^0 + C_2^- Z_\mu^0)d_L^i \right]. \tag{2.110}$$

Since $V_{\text{CKM}}^{\dagger}V_{\text{CKM}} = 1$, we see that neutral bosons (γ^0, Z^0) conserve flavor because the CKM matrices cancel out, whereas the $W^{\pm}$ bosons inevitably mix the quarks by converting an up-type to a down-type of quark or vice-versa (but never an up-type to an up-type or a down-type to a down-type quark). This can also been seen with the commutation relation $\left[V_L^{u/d}, \tau^3 \right] = \left[V_L^{u/d}, Q \right] = 0$, because the photon and the Z^0 boson are linear combinations of τ^3 and Q, see Sec. 2.3.3. We say that neutral currents conserve flavor. Note that this vertex only apply to left-handed fermions.

$\mathcal{CP}$ violation in the SM

The δ shift phase parameter is a $\mathcal{CP}$-violating term. There are only two $\mathcal{CP}$-violating parameters in the SM, δ and θ, giving rise to the strong $\mathcal{CP}$ problem, see Sec. 2.4.1. Moreover, only three quark families can provide a non vanishing δ, since in a $U(2)$ group field redefinition reabsorbs all the phases. This can be seen from the Jarlskog invariant, a parameter built from triangles in the complex plane of CKM matrix elements called unitarity triangles, whose areas are all equal to S. In the standard parametrization the parameter writes to [12].

$$J = 2S = c_{12}c_{23}c_{13}^2 s_{12}s_{23}s_{13}\sin\delta = (3.08^{+0.16}_{-0.18}) \cdot 10^{-5}. \tag{2.111}$$

We notice that it involves four V_{ij}, thus a diagram with four $W^{\pm}$ vertices at least is needed to have a $\mathcal{CP}$-violation operator. Moreover, the three quark families are necessary because J is a product from the mixing angle between all the families. When only two families are involved, even with four $W^{\pm}$ vertices, it is always possible to perform a global $U(1)$ quark number rotation to get rid of the phase.

To conclude, there is a $\mathcal{CP}$ violation in the SM but it needs the three families of quarks getting involved. This can only happen in a minimum of two-loop process which is hence highly suppressed. Therefore the SM $\mathcal{CP}$-violation process is not strong enough to produce enough baryon asymmetry with regard to Sakharov conditions (see Sec. 1.3.3) and we will need to add $\mathcal{CP}$-violating terms in a successful theory of baryogenesis, see Secs. 2.4 and 3.2.

2.3.5 Renormalization and β functions

This sketch on renormalization is made to be intuitive and does not enter in the mathematical details. Renormalization has to be understood as the corrections one should apply to every QFT on a first naive Lagrangian that we are still forced to begin with. It is impossible to write a QFT which is already renormalized because each first draft of a theory must then be corrected in a way dictated by the theory itself.

The renormalization process ensures that the parameters of a theory, namely the masses and couplings, are the true physical quantities from measurement. It is done by adding *counterterms* and *ghost* fields to the original bare Lagrangian and leads to the effective redefinition of the couplings, making them *run* according to their β functions, see hereafter.

Since the renormalizability of a theory depends on its number of dimensions, the simplest way to renormalize it is to compute the corrections with dimensional regularization. It means we should first write the theory in $d = 4 - \epsilon$ dimensions and take the limit $\epsilon \to 0$ at the end of the computation. Once the corrected propagator has been computed, there will be constant terms and terms that

depend on ϵ in the result. The way to absorb these terms in the renormalization is left to a choice called *renormalization scheme.* Amongst the infinite schemes at our disposal, two are most-known.

- The Minimal Subtraction scheme (MS) originally used by 't-Hooft where only $1/\epsilon$ is removed and absorbed into the counterterms.

- The bare Minimal Subtraction scheme ($\overline{\text{MS}}$) used nowadays where

$$\frac{1}{\epsilon} - \gamma_E + \log 4\pi \tag{2.112}$$

are removed and absorbed into the counterterms, where

$$\gamma_E = \sum_{k=1}^{\infty} \left[\frac{1}{k} - \log\left(1 + \frac{1}{k}\right)\right] \simeq 0.577\,215\,665 \tag{2.113}$$

is the Euler-Mascheroni constant.

By changing the dimension 4 to $4 - \epsilon$, dimensional regularization introduces a (spurious) scale $\mathcal{Q}$, called the renormalization scale, which physical observables should not depend on.

All schemes should give the same physics. The scheme must be viewed as a renormalization degree of freedom. The same principles as for gauge symmetry apply. A renormalized quantity Γ_R will depend on the used scheme

$$\Gamma_R = Z(R)\Gamma \tag{2.114}$$

without changing the physical information it contains. It is hence possible to pass from one scheme to another with the rule

$$\Gamma_{R'} = Z(R', R)\Gamma_R, \qquad Z(R', R) = \frac{Z(R')}{Z(R)}. \tag{2.115}$$

The factors $Z(R', R)$ respect the composition law, the existence of a neutral element and an inverse; therefore they form a group called the *Renormalization Group.*

Consider now as physical quantity the effective action $\Gamma[\phi_c]$, where ϕ_c is the classical value of the scalar field in the effective potential, that may depend on the interaction couplings g_i, which also includes the mass m, etc. Physically, Γ should not depend on the renormalization scale $\mathcal{Q}$, i.e. $\frac{d\Gamma}{d\mathcal{Q}} = 0$. It is convenient to perform a chain derivative and multiply by $\mathcal{Q}$ to get

$$\mathcal{Q}\frac{d\Gamma}{d\mathcal{Q}} = \left(\mathcal{Q}\frac{\partial}{\partial\mathcal{Q}} + \mathcal{Q}\frac{dg_i}{d\mathcal{Q}}\frac{\partial}{\partial g_i} - \mathcal{Q}\frac{d\phi_c}{d\mathcal{Q}}\frac{\partial}{\partial\phi_c}\right)\Gamma[\phi_c] = 0. \tag{2.116}$$

We define the renormalization group functions as

$$\beta_i = \mathcal{Q}\frac{dg_i}{d\mathcal{Q}} \tag{2.117a}$$

$$\gamma = \frac{\mathcal{Q}}{\phi_c}\frac{d\phi_c}{d\mathcal{Q}} \tag{2.117b}$$

that measure how the couplings change with the energy scale. The first are denoted as the β functions and will be of prime importance in the following. Finally we obtain

$$\left(\mathcal{Q}\frac{\partial}{\partial\mathcal{Q}} + \beta_i\frac{\partial}{\partial g_i} - \gamma\phi_c\frac{\partial}{\partial\phi_c}\right)\Gamma[\phi_c] = 0 \tag{2.118}$$

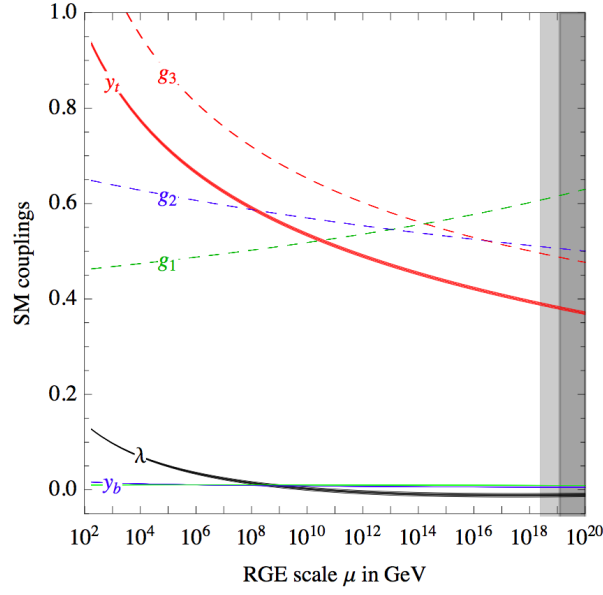called the *Renormalization Group Equation* (RGE).

Figure 2.2. SM renormalization group evolution of the gauge couplings $g_1 = \sqrt{5/3}g'$, $g_2 = g$, $g_3 = g_s$, of the top and bottom Yukawa couplings (y_t, y_b), and of the Higgs quartic coupling λ. Here $\mu \equiv \mathcal{Q}$. All couplings are defined in the $\overline{\text{MS}}$ scheme. Plot taken from [102].

According to the RGE, all the SM couplings change with energy. We show the runnings on Fig. 2.2 of the three gauge couplings

$$g_1 = \sqrt{\frac{5}{3}}\, g', \qquad\qquad g_2 = g, \qquad\qquad g_3 = g_s, \qquad\qquad (2.119)$$

the top/bottom yukawa $y_{t/b}$ as well as the Higgs quartic coupling λ.

The β functions for the gauge couplings are given at 1-loop correction by [78]

$$\beta_1^{(1)} = \frac{g_1^3}{16\pi^2}\left(\frac{20}{9}n_g + \frac{1}{6}\right) \qquad\qquad (2.120a)$$

$$\beta_2^{(1)} = \frac{g_2^3}{16\pi^2}\left(-\frac{22}{3} + \frac{4}{3}n_g + \frac{1}{6}\right) \qquad\qquad (2.120b)$$

$$\beta_3^{(1)} = \frac{g_3^3}{16\pi^2}\left(-11 + \frac{4}{3}n_g\right) \qquad\qquad (2.120c)$$

where $n_g = 3$ is the number of generation.

The β function for the top yukawa is given at 1-loop correction by [103, 104]

$$\beta_{y_t}^{(1)} = \frac{y_t}{16\pi^2}\left(\frac{9}{4}y_t^2 - \frac{17}{40}g_1^2 - \frac{9}{8}g_2^2 - 4g_3^2 + \frac{1}{2}y_\tau^2 + \frac{3}{4}y_b^2\right) \qquad\qquad (2.121)$$

Last, the β function for the Higgs potential parameters are given at 1-loop correction by [105]

$$\beta_{m^2}^{(1)} = \frac{m^2}{16\pi^2}\left(y_\tau^2 + 3y_b^2 - \frac{9}{4}g_2^2 - \frac{3}{4}g_1^2 + 6\lambda + 3y_t^2\right) \qquad\qquad (2.122a)$$

$$\beta_\lambda^{(1)} = \frac{1}{16\pi^2}\left(-y_\tau^4 - 3y_b^4 + \frac{9}{16}g_2^4 + \frac{3}{8}g_1^2 g_2^2 + \frac{3}{16}g_1^4 + 2\lambda y_\tau^2 \right. \qquad\qquad (2.122b)$$

$$+6\lambda y_b^2 - \frac{9}{2}\lambda g_2^2 - \frac{3}{2}\lambda g_1^2 + 12\lambda^2 + 6\lambda y_t^2 - 3y_t^4\bigg).$$

As we can see from Fig. 2.2 and deduce from computation, the Higgs self-coupling becomes negative for a scale $\mathcal{Q}_I \sim 10^{9\text{-}11}$ GeV. This results in a negative potential for values $h \gtrsim \mathcal{Q}_I$. This is called the Higgs instability or vacuum catastrophe problem. Still it has been proven that the fake electroweak vacuum is metastable, and its life time is much larger than the present age of the Universe. Any model and any physics involving the Higgs at such scale may come with a solution to fill the vacuum. It usually requires altering the Higgs UV physics in order to influence the behavior of the beta function at scales $\gtrsim 100$ GeV. This must be done for instance in the Higgs inflation model (see Sec. 1.2.6), where the physical Higgs field plays the role of the inflaton at scales $\sim M_{\text{pl}} \gg \mathcal{Q}_I$. In Chap. 6 we will introduce an inflation and baryogenesis model that has the additional feature to stabilize the Higgs potential.

2.3.6   Anomalies

Symmetries play an important role, if not the most important role, in the SM, either being conserved, being violated or being anomalous. Unlike a gauge symmetry, the group elements ω of a global symmetry are constant, i.e. $\partial_\mu \omega = 0$. It would be wrong to believe that global symmetries are of less interest than the gauge ones because of their comparative apparent simplicity. We have already devoted some sections to gauge groups and began to draw some links with the SM. In Sec. 2.3.2 we have seen that the SM exhibits accidental global symmetries. Here we aim to show how gauge and global symmetries articulate themselves with the matter sector in the SM. For references, see e.g. [88, 106–108].

Global $U(1)$ symmetry

Consider a field ψ charged under a $U(1)$ symmetry with some charge Q. Then, a group element $\omega = e^{i\alpha} \in U(1)$ acts on ψ as $\psi \to e^{iQ\alpha}\psi$. Because $e^{i\alpha+2ni\pi}$ is the same element as ω, it means that

$$e^{iQ\alpha}\psi = e^{iQ(\alpha+2n\pi)}\psi, \quad \forall n \in \mathbb{Z}. \tag{2.123}$$

Therefore the allowed charges under a $U(1)$ symmetry are quantized: $Q \in \mathbb{Z}$. They must be integers. In other words, they are quantum numbers. We can hence use global $U(1)$ symmetry groups to count objetcts. This becomes more obvious if we compute the associated current and charges of a Weyl spinor. As we have seen, they come in two representations of the Lorentz group, $(\frac{1}{2},0)$ and $(0,\frac{1}{2})$, that we label L/R for left-/right-handedness. Hence the theory

$$\mathcal{L} \supset i\psi_L^\dagger \bar{\sigma}^\mu D_\mu \psi_L + i\psi_R^\dagger \sigma^\mu D_\mu \psi_R \tag{2.124}$$

has a $U(1)_L \otimes U(1)_R$ global symmetry where the two $U(1)$ factors rotate the fermions independently: $\psi_L \to e^{i\alpha_L}\psi_L$ and $\psi_R \to e^{i\alpha_R}\psi_R$. The charges (q_L, q_R) of ψ_L and ψ_R under this group are $(1,0)$ and $(0,1)$ respectively. From Noether theorem their associated currents (2.12a) and charges (2.13) write

$$j_L^\mu = \psi_L^\dagger \bar{\sigma}^\mu \psi_L, \qquad j_R^\mu = \psi_R^\dagger \sigma^\mu \psi_R,$$
$$Q_L = \int \psi_L^\dagger \psi_L \, d^3x, \qquad Q_R = \int \psi_R^\dagger \psi_R \, d^3x. \tag{2.125}$$

One recognizes the number operator $a^\dagger a$ in the integrals, therefore $Q_{L/R}$ counts the particle number of the Weyl spinor field in the left/right representation.

Of course, we can equivalently use the Dirac formulation of spinor (2.74) in which $\mathcal{L} \supset i\bar{\psi}\gamma^\mu D_\mu \psi$ and define the same global symmetry $U(1)_V \otimes U(1)_A$ in another basis. Here V stands for vector

and corresponds to $\alpha_L = \alpha_R$ and A for axial where $\alpha_L = -\alpha_R$. The names come from the fact that their associated currents are respectively a vector and a pseudovector, see Eq. (2.127) below.

In the Dirac representation, the symmetries write

$$\psi \to e^{i\alpha}\psi \quad \text{(vector)}, \qquad\qquad \psi \to e^{i\alpha\gamma_5}\psi \quad \text{(axial)}, \qquad\qquad (2.126)$$

and the associated current and charge are

$$\begin{aligned} j_V^\mu = \bar{\psi}\gamma^\mu\psi = j_L^\mu + j_R^\mu, \qquad\qquad & j_A^\mu = \bar{\psi}\gamma^\mu\gamma_5\psi = -j_L^\mu + j_R^\mu, \\ Q_V = Q_L + Q_R, \qquad\qquad & Q_A = -Q_L + Q_R. \end{aligned} \qquad (2.127)$$

In the classical theory, the standard arguments from Noether 's theorem tell us that all these currents are conserved, $\partial_\mu j^\mu = 0$. However, at quantum level, when working the details, it turns out that the vector and axial currents cannot be conserved simultaneously. In other words, the full group $U(1)_L \otimes U(1)_R$ cannot be gauged, as we cannot couple a gauge field to a non-conserved current. Only the diagonal subgroup $U(1)_V$ can be gauged, which is the gauge group for electromagnetism $U(1)_{\text{EM}}$ that we described in previous sections. This is a major result of the SM called the *chiral anomaly*. It was proven by 't Hooft in 1976 [109], after the explanation by Adler-Bell-Jackiw [110, 111] of the π_0 decay problem (that violates chirality) and leads to non-trivial consequences from a cosmology point of view.

The chiral anomaly

There are many ways to prove the anomaly, either by solving the associated triangle diagrams, or by computing the change in the path integral measure, or by looking the shift in the Landau level under the change of coupled gauge fields. In a more mathematical approach, we can also prove that the chiral anomaly is a manifestation of the Atiyah-Singer index theorem [80, 107]. In this section we aim to give an insight of the phenomenon while avoiding the explicit quantum field theory computation.

The most physical argument is to show how left- and right-handed particles are created/destroyed differently when coupled to a background electromagnetic field (where the electric and magnetic fields share a parallel component). This is usually done in 1+1 dimensions for illustrative purposes as this simplification preserves the key concepts of the mechanism while avoiding the degeneracy in the other directions. In other words, the only Laudau level of interest for the demonstration of the 3+1 dimensions solution is the one retained by the 1+1 model.

Consider a matter field coupled to a $U(1)$ gauge field (that we can choose to be electromagnetism):

$$\mathcal{L} = -\frac{1}{4}F_{\mu\nu}F^{\mu\nu} + i\bar{\psi}\slashed{D}\psi. \qquad (2.128)$$

In 1+1 dimensions, all the interactions mediated by the electromagnetic field reduce to the Coulomb potential $V(x) = ex$ where e is the electric charge, since there are no transverse components. In order to avoid IR divergences, we confine the model in a spatial domain of length L such that $eL \ll 1$. Note that as A_0 becomes negligible, we will thereby treat it as zero in what follows.

The other aspect which is different when two spatial dimensions are removed is the topology. In $\mathbb{R}^4$, $U(1)$ is trivial but on a vector space based on $\mathbb{R}^2$ one has a classification of the gauge field A_μ in terms of a winding number because $\pi_1[U(1)] = \mathbb{Z}$, see Sec. 2.2.3. Thus, A_1 must be considered only on the interval $[0, \frac{2\pi}{L}]$, since it is a matter of gauge transformation to go beyond this domain.
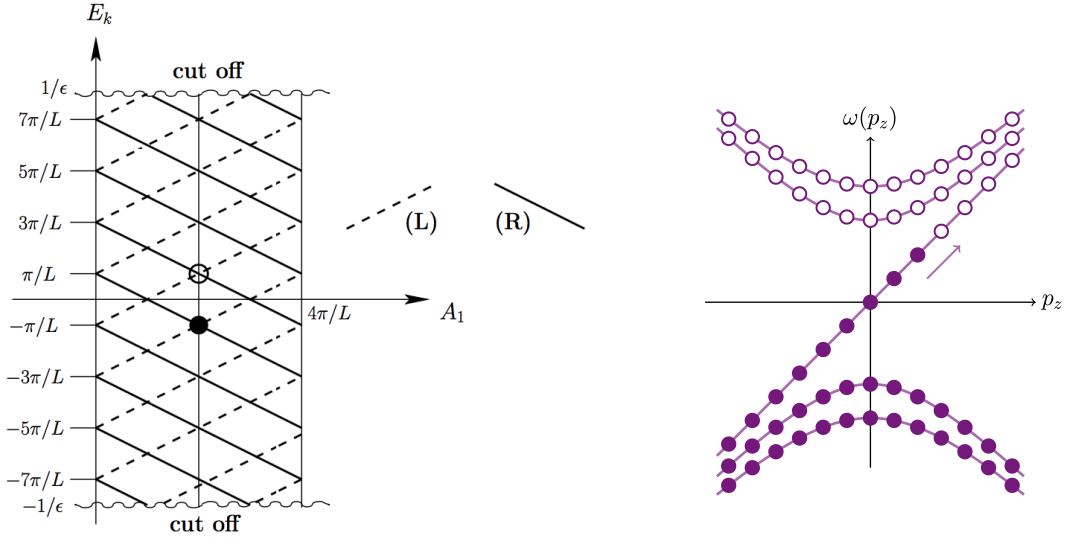
Figure 2.3. Left: Fermion energy levels in function of A_1, taken from [88]. Right: Fermi surface for a fermion in the 3+1 dimensions theory in a uniform magnetic field along the z-direction. The hyperbolic branches of the Landau levels are either fully populated or empty, and the states within these branches simply rearrange under an applied electric field. Only the linear branch changes in the presence of an applied field, effectively reducing to the 1+1 dimensions problem. Taken from [108].

Skipping some details[16], the equation of motion from the above Lagrangian reads

$$i\frac{\partial \psi}{\partial t} - \sigma^3 \left(i\frac{\partial}{\partial x} + A_1 \right) \psi = 0, \tag{2.129}$$

where the correspondence $\gamma^0 = \sigma^2$, $\gamma^1 = i\sigma^1$ for 1+1 dimensional space have been made, and we find that one level of energy E_k is given by

$$\begin{pmatrix} E_k^L \\ E_k^R \end{pmatrix} = \left[\left(k + \frac{1}{2} \right) \frac{2\pi}{L} - A_1 \right] \begin{pmatrix} -\psi_L \\ \psi_R \end{pmatrix}. \tag{2.130}$$

The level of energy shifts in an opposite way for left- and right-handed particles when the value of A_1 changes. If A_1 passes from one configuration to another which is gauge equivalent, a restructuring of the fermion levels take place, see Fig. 2.3. The energy levels of the left-handed particles move upward and right-handed ones downward, or equivalently, the Dirac sea that defines the vacuum simultaneously rises for right-handed particles and falls for left-handed ones. We know that a hole in the Dirac sea is the definition of an antiparticle, because the vacuum is a filled Dirac sea. If we take the true vacuum as our initial state and let A_1 to move from 0 to $\frac{2\pi}{L}$, our final state is composed of a right-handed hole (the sea rises) and a left-handed particle (the sea falls). During this process, the total number of particle Q_V is conserved, but Q_A has been violated because handedness has been flipped: $\Delta Q_A = -2$. Hence, when A_1 changes from $\frac{2\pi n}{L}$ to $\frac{2\pi(n+m)}{L}$ the corresponding change of the axial charge is $\Delta Q_A = -2m$ which implies

$$\dot{Q}_A = -\frac{L}{\pi} \dot{A}_1. \tag{2.131}$$

---

[16]See Ref. [88] for a complete description.

The current corresponding to the latter charge is

$$\partial_\mu j_A^\mu = -\frac{1}{2\pi}\,\epsilon^{\mu\nu}F_{\mu\nu}, \tag{2.132}$$

where $\epsilon^{\mu\nu}$ is the Levi-Civita antisymmetric tensor $\epsilon^{01} = -\epsilon^{10} = 1$. This equality represents the famous axial anomaly in 1+1 dimensions. Although we have derived it by hand-waving arguments, we have preserved the only feature that makes the phenomenon extremely simple and widely known: the crossing of the zero point in the energy scale. The presence of an infinite number of levels and the Dirac sea interpretation constitute the essential elements of the construction. With a finite number of levels there is no place for such an interpretation and there can be no quantum anomaly.

The three-point function of $U(1)$ currents, computed via a loop of fermions, is the classic calculation that revealed the existence of the chiral anomaly. The detail calculation can be found in e.g. Chap 19 of [106], or in Ref. [107]. The triangle anomaly calculation has the virtue of being easily adapted to general symmetry currents, not just $U(1)$.

Indeed, we can repeat the same we did for $U(1)$ as the SM Lagrangian (2.124) is also symmetric under the global $SU(n)_L \otimes SU(n)_R$ group (for $n = 2, 3$). We can then rewrite (2.126) as

$$\psi_L \to \omega_L \psi_L, \quad \omega_L \in SU(n)_L \qquad\qquad \psi_R \to \omega_R \psi_R, \quad \omega_R \in SU(n)_R. \tag{2.133}$$

This implies the following vector and axial currents

$$j_V^{\mu\,a} = \bar{\psi}\gamma^\mu T^a \psi \qquad\qquad j_A^{\mu\,a} = \bar{\psi}\gamma^\mu \gamma_5 T^a \psi \tag{2.134}$$

where T^a are the generator of the $SU(n)$, defined in (2.29). Like the vector $U(1)$ remained a valid anomaly-free symmetry at the quantum level, the same is true with regard of the vector $SU(n)$ currents: they are conserved. The axial currents are anomalous. The conclusion for $SU(n)$ is then per se the same as for $U(1)$, and the chiral anomaly for the $SU(n)$ group is the same, but with the corresponding gauge field instead.

It is found that, for a fermion coupled to a massless spin-1 particle with field strength $F_{\mu\nu}^a$ and coupling g,

$$\partial_\mu j_A^{\mu\,a} = -\frac{g^2}{32\pi^2}\,\mathrm{Tr}\!\left(T^a\,\{T^b, T^c\}\right)\epsilon_{\mu\nu\rho\sigma}F^{\mu\nu\,b}F^{\rho\sigma\,c}\,, \tag{2.135}$$

where T^a are the generators of the algebra, see Sec. 2.2.2.

Alternatively, we can study how a $U(1)$ transformation leads to the measure transformation

$$\int \mathcal{D}\psi \mathcal{D}\bar{\psi} \to \int \mathcal{D}\psi \mathcal{D}\bar{\psi}\,\exp\left(-\frac{ig}{16\pi^2}\int d^4x\,\alpha\,\epsilon_{\mu\nu\rho\sigma}F^{\mu\nu}F^{\rho\sigma}\right). \tag{2.136}$$

The current associated to axial transformations is no longer conserved: instead it obeys (2.135). This method is referred to as the Fujikawa path integral calculation, see e.g. Ref. [107] for the derivation.

In Sec. 2.2.4 we have seen that the RHS of (2.54) is a topological quantity. The same is true for Eqs. (2.141) and therefore (2.143). Using (2.51) and (2.52) we can relate the axial current to the Bardeen current as

$$\partial_\mu j_A^\mu = -\frac{g^2}{8\pi^2}\,\partial_\mu K^\mu. \tag{2.137}$$

Like in the 1+1 dimensions case, these results imply that the axial charge is not conserved anymore, since

$$\dot{Q}_A = \frac{g^2}{8\pi^2}\int \mathrm{d}^3x\,\dot{K}^0, \tag{2.138}$$

the analog to Eq. (2.131), and more importantly, that the change of axial charge is a direct consequence of the change of topology, obeying the selection rule

$$\Delta Q_A = -2\Delta N_{CS} \quad \Rightarrow \quad \Delta Q_L = -\Delta Q_R = \Delta N_{CS}, \tag{2.139}$$

where N_{CS} is the Chern-Simons number defined in Eq. (2.54). Thus, if we perform a global gauge transformation on a gauge-fermion interacting system by the action of an instanton or a sphaleron, the total number of fermions is unchanged but their chirality has been violated, the creation of left (resp. right) handed particles being compensated by the creation of right- (resp. left-) handed anti-particles. We will see that this allows an embedded baryon number violation in the SM which will participate in the mechanism to generate the BAU.

Gauge anomaly

The above statement that gauge fields cannot couple to a non-conserved current is, so to say, a kind of a top-down approach to anomaly. We can rephrase it as such: for a given fermion set, only anomaly-free global symmetries can be gauged.

There is however another approach in which we first gauge any symmetry of interest and, in a second step, we choose the set of fermions charged under this group such that the gauge symmetry is anomaly free. This approach is useful for model building when exotic/dark sectors are introduced to the SM and is often referred to as *gauge anomaly* even though the core idea is that a gauge symmetry cannot be anomalous.

Indeed, while anomalies in global symmetries are physically interesting, anomalies in gauge symmetries kill all physics completely: they render the theory mathematically inconsistent because gauge symmetries refer to redundancies in our description, that are necessary to make sense of the theory. An anomaly in gauge symmetry removes this redundancy. If we wish to build a consistent theory, then we must ensure that all gauge anomalies vanish.

To illustrate this other approach, take for instance a right (left) handed Weyl spinor charged under $U(1)_{\rm EM}$. By computing the associated current divergence, we find that

$$\partial_\mu j_R^\mu = -\partial_\mu j_L^\mu = \frac{1}{2}\,\partial_\mu j_A^\mu, \tag{2.140}$$

hence this theory is anomalous: it must be abandoned or changed such that the anomaly disappears. To do so, we shall add more fermion species in the theory in such a way that their anomaly contributions cancel each other. By adding a left (right) handed Weyl spinor charged under $U(1)_{\rm EM}$ the same way as the initial left-handed one, we ensure that the total current is conserved as in that case we have $\partial_\mu j_V^\mu = \partial_\mu j_R^\mu + \partial_\mu j_L^\mu = 0$.

In both approaches, the result is the same: in order for electromagnetism to be anomaly free, we must couple it to Dirac fermions. A theory with gauge fields which are coupled in the same manner to both left and right-handed fermions is called *vector-like*.

It happens that the SM is a chiral theory because the weak interaction only couples to left-handed particles, thus left and right-handed fermions are coupled differently to gauge fields: it is a chiral theory. Consistency of chiral theories is harder to ensure. Note that chiral gauge theories are necessarily coupled only to massless fermions. This is because a mass term requires both left and right-handed Weyl fermions (see Sec. 2.3.4) and is gauge invariant only if they transform in the same way under the gauge group. In other words, mass terms are only possible for vector-like matter. This is why in the present sketch we have dropped the tree-level mixing from Dirac mass terms, see Eq. (2.150) and Sec. 2.4.1.

ψ	C_ψ^G	C_ψ^W	C_ψ^Y
Q_L	$\frac{N_w}{2}$	$\frac{N_c}{2}$	$N_c N_w Y_{Q_L}^2$
u_R	$-\frac{1}{2}$	0	$-N_c Y_{u_R}^2$
d_R	$-\frac{1}{2}$	0	$-N_c Y_{d_R}^2$
L_L	0	$\frac{1}{2}$	$N_w Y_{L_L}^2$
e_R	0	0	$-Y_{e_R}^2$

Table 2.2.   Coefficients of the anomaly equation (2.141) for each SM gauge group and fermion specie. The multiplicities $N_c = 3$ and $N_w = 2$ take into account the color and weak isospin states of a given family of leptons and quarks. Indeed, the representation (2.73) is considered a singlet under $SU(3)_c$, resulting in a triple contribution to the anomaly. In the same way, the representation (2.69) is considered a singlet under $SU(2)_L$ resulting in a double contribution to the anomaly. The SM hypercharges Y_ψ are given in Table 2.1. The charge conjugates of the displayed fermion species (i.e. their anti-particle state) have the same coefficients with all the signs flipped.

Baryon and lepton number violation

To summarize, in the SM there are 5 global $U(1)$ symmetries, defining 5 classes of fermion species: 2 left quark and lepton $SU(2)_L$ doublets Q_L and L_L, 2 right quark $SU(2)_L$ singlets u_R and d_R and 1 lepton $SU(2)_L$ singlet e_R, see (2.71) and (2.73). Therefore, using Eq. (2.135) the anomaly equation for each of them write [112]

$$\partial_\mu j_\psi^\mu = C_\psi^G \frac{g_s^2}{16\pi^2} G_{\mu\nu}^a \tilde{G}^{\mu\nu\,a} + C_\psi^W \frac{g^2}{16\pi^2} W_{\mu\nu}^a \tilde{W}^{\mu\nu\,a} + C_\psi^Y \frac{g'^2}{16\pi^2} Y_{\mu\nu} \tilde{Y}^{\mu\nu}, \qquad (2.141)$$

where the coefficients C are given for each fermion and gauge group in Table 2.2. Thus, when considering the full SM gauge group, none of the spinors' currents are individually conserved.

A central result that will be extensively used in this thesis is that the baryon and lepton number are not conserved by the SM, which provides the first Sakharov condition for baryogenesis, see Sec. 1.3.3. From previous results the proof is straightforward, simply compute the baryon and lepton current, defined by

$$j_B^\mu = \frac{1}{3} \sum_{i=1}^{N_g} \left(j_{Q_L^i}^\mu + j_{u_R^i}^\mu + j_{d_R^i}^\mu \right), \qquad (2.142a)$$

$$j_L^\mu = \sum_{i=1}^{N_g} \left(j_{L_L^i}^\mu + j_{e_R^i}^\mu \right), \qquad (2.142b)$$

where $N_g = 3$ is the number of generations and the factor $\frac{1}{3}$ accounts for the fact that a baryon consists of three quarks. From the anomaly equations we find

$$\partial_\mu j_B^\mu = \partial_\mu j_L^\mu = \frac{N_g}{2} \left(\frac{g^2}{16\pi^2} W_{\mu\nu}^a \tilde{W}^{\mu\nu\,a} - \frac{g'^2}{16\pi^2} Y_{\mu\nu} \tilde{Y}^{\mu\nu} \right). \qquad (2.143)$$

It is accidental that

$$\partial_\mu j_{B-L}^\mu = 0 \qquad (2.144)$$

but this accident has wide consequences. One of them is that the baryon and lepton number change

by the same amount when varying the RHS:

$$\Delta N_L = \Delta N_B. \tag{2.145}$$

Recall that here N_L is the number of all three lepton generations. Some authors also write the selection rule between the baryon number and *one* lepton species as $3\,\Delta N_L = \Delta N_B$ [17]. We have already seen in Sec. 2.2.4 that the RHS is a topological quantity. This means that the amount of baryon and lepton numbers is a direct consequence of the topology in which the gauge fields live. Since we have also seen that there exists various processes to change from one topology to another (even on the vacuum), the shape of the SM B-violation source starts to appear. This was the first Sakharov condition, see Sec. 1.3.3. In Chap. 3 we will show in more detail how we can generate the BAU from the SM chiral anomaly.

Gauge anomaly cancellation in the SM

Consistency of gauge theory then requires that all 3-point combinations of its gauge group anomalies vanish. For the SM, this translates to the fact that the $SU(N)^3$, $U(1)^3$ and $U(1)SU(N)^2$ anomalies must vanish. We can forget about the Higgs field and associated Yukawa couplings because they do not affect the anomalies.

In the SM with a single generation of fermions, the non-perturbative $SU(2)$ anomaly

$$\pi_4\left[SU(2)\right] = \mathbb{Z}_2, \tag{2.146}$$

where we have defined π_k in Sec. 2.2.3, causes no problem as we will see. The latter equation implies that an $SU(2)$ gauge theory with any odd number of Weyl fermions in the fundamental representation is mathematically inconsistent [113]. To make sense of the theory, Weyl fermions must come in pairs. In other words, they must complete Dirac fermions. Unlike the previously shown anomalies, this one cannot be seen in perturbation theory: it is a non-perturbative anomaly. Since there are four fermions transforming in the doublet representation in the SM with a single generation of fermions, the anomaly is avoided.

Similarly, the $SU(3)^3$ diagram is anomaly free because there are two left-handed and two right-handed quarks. There is also no non-perturbative anomaly as

$$\pi_4\left[SU(n)\right] = 0, \quad \forall n \geqslant 3. \tag{2.147}$$

Finally, all anomalies involving the Abelian factor cancel, see e.g. [107] for a detailed calculation. Therefore, all three gauge currents

$$j_Y^\mu = \sum_\psi Y_\psi \bar\psi \gamma^\mu \psi, \qquad j_W^{\mu\,a} = \sum_{\psi_L} \bar\psi \tau^a \gamma^\mu \psi, \qquad j_G^{\mu\,a} = \sum_{\text{quarks}} \bar\psi \eta^a \gamma^\mu \psi \tag{2.148}$$

have a null divergence. There is a further related criterion arising from a possible gravitational anomaly of a $U(1)$ current, which also vanishes. Hence the Standard Model is arguably the simplest chiral gauge theory that one can write down.

2.4 The Axion

In this section we will first explain the original axion for QCD and how it arose. Then we will give hints on a more general class of axions called axion-like particles (ALP). In the next chapter we will demonstrate how an ALP identified with the inflaton can generate the BAU.

---

[17]With the notation used in this thesis, this equation would be written as $3\,\Delta N_\ell = \Delta N_B$.

2.4.1   The strong $\mathcal{CP}$ problem

In a typical Lagrangian for an interacting fermion

$$\mathcal{L} = -\frac{1}{4}F^a_{\mu\nu}F^{\mu\nu\,a} + i\bar{\psi}\gamma^\mu D_\mu\psi + m\bar{\psi}\psi \tag{2.149}$$

the mass parameter does not necessary need to be real, $m = |m|\mathrm{e}^{i\theta}$ since it is only a mathematical parameter of the theory and not the physical mass. But we can always absorb the $\mathrm{e}^{i\theta}$ term by performing the chiral (or axial) rotation (2.126) $m \to m\mathrm{e}^{-2i\alpha}$. This is called the *spurion* technique and it leads to the relation $2\theta = \alpha$ while the mass parameter becomes real. This is a manifestation of the tree level chiral anomaly

$$\partial_\mu j^\mu_A = 2im\bar{\psi}\gamma_5\psi. \tag{2.150}$$

The same happens for the complete SM mass matrix in the Yukawa sector, see Sec. 2.3.4. The d-quark mass matrix $\tilde{M}_d$ (see Eq. (2.104)) can have a global phase that is possible to cancel by fields redefinition. In general we have

$$\det \tilde{M}_d = \mathrm{e}^{i\phi}. \tag{2.151}$$

As in the above simple model, we can do a chiral rotation to cancel this phase such that $\det \tilde{M}_d = 1$ but then we pay the price of another θ-like contribution (2.68).

Indeed, because of the anomaly, a chiral rotation is equivalent to the introduction in the action of a topological density S_θ given by Eq. (2.68). The $[U(1)_\ell]^3$ rotation freedom in the lepton sector makes it possible to choose a configuration where the $S_\theta^{SU(2)}$ contribution to the SM action vanishes. This is a direct equivalent of the absence of flavor/mass mixing in the lepton sector (in the pure SM) described in Sec. 2.3.4. Conversely, this freedom is not given in the quark sector such that there will always be a topological residue $S_\theta^{SU(3)}$ that survives any rotation. In fact, the standard parametrization of the CKM matrix (2.107) has already assumed that the five-field redefinition has been done, see Sec. 2.3.4. Hence, the physical, observable $\mathcal{CP}$-violating parameter of the effective SM theory contains both contributions, the pure gauge strong vacuum topology and the CKM matrix cleaning [89]

$$\bar{\theta} = \theta + \arg\det\tilde{M}_d. \tag{2.152}$$

We can relate the value of $\bar{\theta}$ with the electric dipole momentum of the neutron

$$d_n \simeq |\bar{\theta}|q_e\frac{m_\pi^2}{m_N^3} \simeq 10^{-16}|\bar{\theta}|q_e \cdot \mathrm{cm}. \tag{2.153}$$

Measurements contraint its value to $d_n < 3 \cdot 10^{-26}$ leading to $|\bar{\theta}| < 10^{-10}$ [114]. The strong $\mathcal{CP}$ problem is, why is the latter value so small? Why do both contributions almost cancel each other? Such a near cancellation is difficult to achieve, given their distinct origin: one from QCD, one from EW.

The $\mathcal{CP}$ problem falls under the scope of a naturalness problem. Since the term (2.68) is allowed by symmetry, a extremely small value of it would need some explanation. Note that if there would be one massless quark (which is in contradiction with measurements), we could make a field redefinition by absorbing the $\bar{\theta}$ angle in the mass term.

2.4.2   The Peccei-Quinn solution

In 1977, Peccei and Quinn showed that if the SM was augmented by a global chiral $U(1)$ symmetry, the dynamics of the theory is such that $\bar{\theta}$ is dynamically set to zero [115, 116].

Let us introduce a global chiral symmetry, $U(1)_{PQ}$, which is spontaneously broken by a scalar field $a(x)$ with zero mass at the tree level: the axion, which is the massless Goldstone boson of this

broken symmetry. Under $U(1)_{PQ}$, the axion has a shift symmetry:

$$a(x) \rightarrow a(x) + \alpha f_a, \tag{2.154}$$

where f_a is the order parameter associated with the breaking. This shift symmetry implies that the axion is a compact field, meaning that the field values live on a circle, which is to say that the value of $a(x)$ is only defined modulo 2π. Thus $a(x) \rightarrow a(x) + 2\pi$ is a redundancy of our theory. This redundancy places strong limitations on the axion Lagrangian. We can only write arbitrary interactions involving $\partial_\mu a$, because this is invariant, and interactions involving 2π-periodic functions like $\cos ka$ (with $k \in \mathbb{Z}$), which can give rise to a mass for the axion. Anyway the strong dynamics of QCD generates a potential for the axion from which the mass can be computed. The existence of a mass for the axion makes it a pseudo Nambu-Goldstone boson and its shift symmetry is approximate.

At last, we can add to the SM Lagrangian an effective axion Lagrangian as

$$\mathcal{L} = \mathcal{L}_{SM} - \frac{1}{2}\partial_\mu a \partial^\mu a + \xi \frac{a}{f_a} \frac{g^2}{16\pi^2} G^a_{\mu\nu} \tilde{G}^{\mu\nu\,a} + \mathcal{L}_{int}\left(\frac{\partial^\mu a}{f_a}; \psi\right) \tag{2.155}$$

where we recall that $G^a_{\mu\nu}$ is the strength tensor of $SU(3)_c$. Here, ξ and $\mathcal{L}_{int}$ are model dependent quantities related to how one assigns $U(1)_{PQ}$ transformations to the fermions in the theory. The second to last term is needed to ensure that the $U(1)_{PQ}$ current has a chiral anomaly

$$\partial_\mu j^\mu_{PQ} = \xi \frac{g^2}{16\pi^2} G^a_{\mu\nu} \tilde{G}^{\mu\nu\,a}. \tag{2.156}$$

To show that the shift symmetry (2.154) implies the Lagrangian (2.155), we use Eq. (2.52) and we perform an integration by parts

$$\frac{a}{f_a} G^a_{\mu\nu} \tilde{G}^{\mu\nu\,a} = \frac{a}{f_a}\partial_\mu K^\mu = -\frac{\partial_\mu a}{f_a} K^\mu + \partial_\mu \left[\frac{a}{f_a} K^\mu\right], \tag{2.157}$$

where we removed the constants for clarity. The last term is a total derivative and these are usually neglected in QFT because fields are square integrable functions, or in a mathematical notation $\psi \in L^2(\mathbb{R})$. It means that fields vanish at infinity and are localized. Here, because of the gauge transformation that change topology, and the change in the path integral measure, it is not the case and the total derivative term brings the instantons (which are in essence global). Leaving this aside, we see that the Lagrangian written is this way has a shift symmetry because of its dependence on $\partial_\mu a$. Of course, the shift must be a constant.

The existence of the $U(1)_{PQ}$ breaking term $aG\tilde{G}$ actually provides a potential for the axion field. Hence it is no longer true that any value of $\langle a \rangle$ is allowed in the vacuum. Including the anomaly contribution, one finds that the VEV of the axion must be [89, 115]

$$\langle a \rangle \equiv \langle \bar{\theta}|a|\bar{\theta}\rangle = -\frac{\bar{\theta}}{\xi} f_a. \tag{2.158}$$

The physical axion is the excitation from this vacuum, hence $a_p = a - \langle a \rangle$. In term of a_p, the effective Lagrangian becomes

$$\mathcal{L} = \mathcal{L}_{SM} - \frac{1}{2}\partial_\mu a_p \partial^\mu a_p + \xi \frac{a_p}{f_a} \frac{g^2}{16\pi^2} G^a_{\mu\nu} \tilde{G}^{\mu\nu\,a} + \mathcal{L}_{int}\left(\frac{\partial^\mu a_p}{f_a}; \psi\right) - \mathcal{L}_{\bar{\theta}}. \tag{2.159}$$

The new Lagrangian does not contain $\mathcal{L}_{\bar{\theta}}$ anymore, since this term is all ready encoded in $\mathcal{L}_{SM}$, see

Eq. (2.77). The presence of the extra $U(1)_{PQ}$ symmetry has removed the CP-violating $\bar{\theta}$ parameter, replacing it by a dynamical field.

2.4.3   Axion-like particles

There are a variety of similar models which introduce a new scalar axion-like field independently of the EW scale, enabling much larger vacuum expectation values, hence very light axions [117–119]. Axion-like particles (ALP) are hypothetical massive pseudoscalar particles that arise from other new symmetries which are spontaneously broken and which appear abundantly in string theory. The most noticeable difference with the original axion from Peccei-Quinn is that for ALP, mass and couplings are independent. Also they are in general not related to QCD, the strong $\mathcal{CP}$ problem or the Peccei-Quinn mechanism. They simply borrow their name from the original and true axion described in the previous section.

In fact, when an approximate $U(1)$ global symmetry is spontaneously broken, the field space is a circle, so the associated pseudo Nambu-Goldstone boson is a periodic scalar field, $a \simeq a + 2\pi$. Therefore it is common for such a periodic scalar field to be referred to as an axion, or ALP, even outside the context of axion solutions of the strong $\mathcal{CP}$ problem.

The terminology around axion is subject to fluctuations. Some people prefer to reserve the word *axion* for the original Peccei-Quinn model and use ALP for the other ones. Other people will use the term *axion* more broadly, and will often say *QCD axion* to refer to the original case, a choice also made in this thesis.

Although the axion has not been detected, axion models have been well studied for over 40 years, giving time for physicists to develop insights into axion effects that might be detected. There are many processes involving the axion we can think of. The most famous one is the Primakov process, which is a decay in the background of charged leptons, and the axion to photons annihilation. Axions are also one of the few remaining plausible candidates for dark matter particles, and might be discovered in some dark matter experiments.

Finally, let us state that in order the generate the BAU we will use an interaction of the form $\phi F\tilde{F}$, see next chapter. In the first models using this mechanism, the inflaton ϕ was identified as an axion. In this thesis we will partially use these results (Chap. 4) but also consider ϕ as a scalar, in order to identify it with the Higgs (Chap. 5), or mix it with the Higgs (Chap. 6).

Part II

Grounds for Baryogenesis

Chapter 3

Electroweak Baryogenesis

Electroweak Baryogenesis is a term that indicates that the baryon asymmetry was generated during a first order electroweak phase transition (EWPT), as the latter provides the necessary out-of-equilibrium condition required by the Sakharov conditions, see Sec. 1.3.3.

As we already explained, a first order transition proceeds with bubble nucleation, where inside the bubbles the Higgs VEV and particle masses are non zero, while they are still vanishing in the exterior symmetric phase. The bubbles expand, to eventually collide, and fill out all the space. In a first order EWPT model, the baryon asymmetry is generated in the vicinity of the bubble wall in motion. This process is much more "violent" than a second order transition, where, even though the sphalerons still go in the direction from equilibrium to out-of-equilibrium, they do so in a continuous way, and uniformly throughout space. This is because the phase transition rate is governed by the expansion rate of the Universe and hence happens in a quasi-static thermal equilibrium. For a review on first order electroweak baryogenesis, see e.g. Refs. [63, 77].

With the recent discovery of the Higgs boson at CERN and its mass measurement, it turns out that the SM EWPT is not even second order, but a crossover, see Sec. 2.3.3. Nevertheless, baryon asymmetry can still happen during a second order EWPT under certain conditions we will provide, as it has been proven that even within the crossover, the difference in the sources and washouts decay rates yield an out-of-equilibrium configuration [120, 121]. To prove this fact requires the resolution of a system of coupled Boltzmann equation, as we will explain in Sec. 3.1.3.

Besides, during a number of years, many studies have investigated the connection between a primordial magnetic field and the BAU, see e.g. Refs. [122–132]. In the meantime there was progress done on the generation of magnetic fields from inflation, see e.g. Refs. [112, 133, 134]. Later, these two ideas were combined in order to generate, from inflation, the magnetic field with the specification required by the baryogenesis model [135]. This idea was further elaborated in a number of papers, see e.g. Refs. [120, 121, 136–139].

In this chapter we will review the necessary conditions for electroweak baryogenesis in a crossover phase transition, that we will use in the models of the following chapters. We will also address the main constraints involved, see Sec. 3.3.

3.1 Primordial magnetic fields and the BAU

The anomaly equation (2.143) provides the necessary ingredients to generate the BAU during the EWPT. In this section we will demonstrate, following [120, 121] (see also [140]), that it leads to an equilibrium value of the baryon asymmetry for $T \simeq 135$ GeV.

This part needs big machinery in plasma physics, namely magnetohydrodynamics, which combines the Navier-Stokes equation from fluid dynamics with the Maxwell equations from electromagnetism. The physics involved used transport equations, and out-of-equilibrium decay modelled by

the Boltzmann equation. We will strive to give as much relevant information as possible for the aim of this thesis, with the fewest possible unnecessary details, as this topic is not central to this work. Furthermore, it is very easy to get lost in the maze of this topic.

3.1.1   Helical fields

A key observation for our baryogenesis model it that the anomalous baryon/lepton current (2.143) depends on the topological density of the hypercharge field. In other words, even if the vacuum structure of $U(1)$ groups is trivial, a B-violating process can be induced from the helicity change of a non-zero helical hypermagnetic field, as we will see in this section. In the next one we will comment on the effect of the $SU(2)_L$ contribution to the anomaly equation.

The relevant equations to describe a (hyper)electromagnetic field in a plasma interaction with charged particles are the magnetohydrodynamics (MHD) equations, which are written in flat space-time as [127, 141, 142]

$$\frac{\partial \boldsymbol{B}}{\partial t} = -\boldsymbol{\nabla} \times \boldsymbol{E}, \tag{3.1a}$$

$$\frac{\partial \boldsymbol{E}}{\partial t} + \boldsymbol{J} = \boldsymbol{\nabla} \times \boldsymbol{B}, \tag{3.1b}$$

$$\boldsymbol{\nabla} \cdot \boldsymbol{B} = 0, \tag{3.1c}$$

$$\boldsymbol{\nabla} \cdot \boldsymbol{E} = \rho, \tag{3.1d}$$

$$\boldsymbol{\nabla} \cdot \boldsymbol{J} = 0, \tag{3.1e}$$

$$\boldsymbol{J} = \sigma(\boldsymbol{E} + \boldsymbol{v} \times \boldsymbol{B}) + \boldsymbol{J}_5, \tag{3.1f}$$

where $\boldsymbol{v}$ is the fluid velocity, and

$$\sigma \simeq \frac{c_\sigma T_{\rm pl}^c}{\alpha \log(\alpha^{-1})}, \qquad c_\sigma \simeq 4.5, \qquad \alpha = \frac{g^2}{4\pi}, \tag{3.2}$$

the conductivity of the thermal plasma [143, 144]. The quantity $T_{\rm pl}^c$ is the typical (comoving) temperature of the plasma, see Eq. (3.66). Furthermore, the current

$$\boldsymbol{J}_5 = \frac{2\alpha}{\pi}\mu_5 \boldsymbol{B} \tag{3.3}$$

is due to the chiral magnetic effect [126, 145, 146] with

$$\mu_5 = \sum_\psi \epsilon_\psi \, N_\psi \, Y_\psi^2 \, \mu_{A,\psi}, \tag{3.4}$$

where ψ runs over all SM species, with multiplicity N_ψ, hypercharge Y_ψ, $\epsilon_\psi = \pm$ for right-/left-handed particles, and $\mu_{A,\psi}$ the chemical potentials. The chiral magnetic effect is the phenomenon whereby a magnetic field induces an electric current in a medium with a charge-weighted chiral asymmetry, and it will have consequences when discussing the constraints on the helicity survival, see Sec. 3.3.3. From this we deduce that $\boldsymbol{J}_5$ vanishes for vector-like fields.

Then, assuming kinetic equilibrium, the chemical potential writes

$$\mu_{A,\psi} = \frac{6Q_{A,\psi}}{N_\psi T^2} \tag{3.5}$$

where $Q_{A,\psi}$ is the axial charge (2.139) for the species ψ. Note that the μ_5-dependent term is only applicable for $\mu_5/T \ll \alpha$, which will always be fulfilled in our case, see [147] and references therein for other regimes.

We will show that the SM B violation is a direct consequence of helicity variation. The helicity is a measure of the linkage, twist, and writhe of a magnetic field, which is defined as

$$\mathcal{H} \equiv \int \boldsymbol{A} \cdot \boldsymbol{B} \, d^3 x. \tag{3.6}$$

When a magnetic field contains helicity, it tends to form large scale structures from small scale ones [148], a phenomenon called the *inverse cascade* and which will be relevant later (Sec. 3.3.3). Since the magnetic vector potential is not gauge invariant, the magnetic helicity is neither gauge invariant in general. It is then useful to use the radiation gauge

$$A_\mu = (0, \boldsymbol{A}), \qquad\qquad \boldsymbol{\nabla} \cdot \boldsymbol{A} = 0. \tag{3.7}$$

The $U(1)$ quantity

$$F_{\mu\nu} \tilde{F}^{\mu\nu} = -4 \, \boldsymbol{E} \cdot \boldsymbol{B}, \tag{3.8}$$

called the *Chern-Simons density*, is the local expression of a change in helicity, as

$$\int \boldsymbol{E} \cdot \boldsymbol{B} \, d^4 x = \frac{1}{2} \int \boldsymbol{A} \cdot \boldsymbol{B} \, d^3 x \, \bigg|_{t=-\infty}^{t=+\infty}. \tag{3.9}$$

This is because, using (2.17) and (3.1a), and the vectorial identity $\boldsymbol{\nabla} \cdot (\boldsymbol{X} \times \boldsymbol{Y}) = \boldsymbol{Y} \cdot (\boldsymbol{\nabla} \times \boldsymbol{X}) - \boldsymbol{X} \cdot (\boldsymbol{\nabla} \times \boldsymbol{Y})$ one has

$$\frac{\partial \boldsymbol{A}}{\partial \tau} \cdot \boldsymbol{B} = -\boldsymbol{E} \cdot \boldsymbol{B}, \qquad\qquad \boldsymbol{A} \cdot \frac{\partial \boldsymbol{B}}{\partial \tau} = -\boldsymbol{E} \cdot \boldsymbol{B} - \boldsymbol{\nabla} \cdot (\boldsymbol{E} \times \boldsymbol{A}), \tag{3.10}$$

and thus

$$\frac{d\mathcal{H}}{dt} = -2 \int \boldsymbol{E} \cdot \boldsymbol{B} \, d^3 x. \tag{3.11}$$

Hence comparing (3.9) with (2.54) and (2.143), we conclude that changes in baryon and lepton numbers can be induced by changes in $U(1)_Y$ hypermagnetic helicity as

$$\Delta N_L = \Delta N_B = -\frac{g'^2}{16\pi^2} \, \Delta \mathcal{H}_Y. \tag{3.12}$$

It is sometimes said, either for simplification or through misuse of language, that the helical fields get *converted* into the BAU at EWPT. This statement refers to the full process presented in this section, and does not mean that baryon and lepton numbers increase on the cost of helical topology. Actually, the last equation states the opposite: baryon/lepton asymmetry and helicity are generated together although with the opposite sign. Therefore without anything more than the chiral anomaly, there is no way to distinguish between a Universe that contains only baryonic matter and a Universe that contains only helical fields. The aim of this section is precisely to give the factors that allowed matter to survive until today.

Note that the electromagnetic $U(1)_{\text{EM}}$ component is absent from the anomaly equation (2.143), as the diagonal parts of $SU(2)_L \otimes U(1)_Y$ cancel out. Indeed, we have seen in Sec. 2.3.6 that vector-like gauge theories, such as $U(1)_{\text{EM}}$, are anomaly-free. Thus, the helicity stored in an ordinary electromagnetic field has no effect whatsoever on the baryon/lepton number.

3.1.2   Sphaleron effect

Combining Eqs. (2.143), (2.54) and (2.57), we can easily see that the EW sphaleron tends to erase the asymmetries stored in the fermions [127] as we can write, schematically

$$\frac{d\eta_\psi}{dt} \propto -\Gamma_{\rm sph}\,\eta_\psi \tag{3.13}$$

which is the Boltzmann equation (1.52) for the particle number asymmetry $\eta_\psi = n_\psi/s$ (analogous to (1.156)), with the number density defined such that $N_\psi = \int n_\psi\, d^3x$.

We have seen in Sec. 2.2.4 that the rate $\Gamma_{\rm sph}$ is negligible at low temperatures. However for temperatures $130 \lesssim T \lesssim 10^{12}$ GeV, EW sphalerons are in thermal equilibrium and lead to the rapid erasure of any baryon/lepton asymmetries in the left sector. Indeed, because sphalerons couple only to left-handed fermions, right-handed ones are preserved from this direct washout. But eventually the asymmetries in right-handed fermions are driven to zero by sphalerons once right- and left-handed particles reach chemical equilibrium via their Yukawa couplings (2.78d).

Due to its small Yukawa coupling, the right-handed electron is the last species to reach chemical equilibrium, at temperatures $\sim 10^5$ GeV. Below this temperature, all the asymmetries are erased. We will see in Sec. 3.3.3, though, that a process called *chiral plasma instability* can potentially convert the asymmetries into hypercharge helicity before they can be erased by sphalerons.

The take-away message is that as long as $T \gtrsim 130$ GeV, the action of the sphaleron in the plasma is to washout any baryon/lepton asymmetry. Thus any asymmetry generated at higher scale can be considered as nonexistent.

Putting the helicity and the sphaleron effects together, Eq. (2.143) yields

$$\Delta N_B = \Delta N_L = N_g \left(\Delta N_{\rm CS} - \frac{g'^2}{16\pi^2}\,\Delta \mathcal{H}_Y \right). \tag{3.14}$$

This is the master equation for baryogenesis. The $B + L$ anomaly, the $U(1)_Y$ helicity and the weak sphaleron are three connected vessels and the challenge of baryogenesis is to understand how they can interact in order to yield a net baryon asymmetry at low-energy scale. In the following sections we will see how the effects of the helicity decay and sphaleron washout balance each other to produce a non-zero η_B (Sec. 3.1.3) while avoiding the transformation of baryon asymmetry back into helicity (Sec. 3.3.3).

3.1.3   Electroweak crossover

In [120, 121] a careful analysis of the transport equations for all SM species during the EWPT has been done, including the effects of gauge fields, in particular strong and weak sphalerons as well as helicity decay. The transport equations can be seen as the generalization of the conservation equation (2.14) where the scalar flux $\boldsymbol{\Phi}$ has been broken down into its convective (how it moves with the fluid flow) and diffusive (how it diffuses into the fluid) components. There is the possibility left to add a source term, absent from (2.14), but of prime interest here. The final baryon asymmetry is determined by the opposition of the helical hypermagnetic field decay and the electroweak sphaleron, both described above.

The study consists of writing the transport equation for each SM species, based on the model of (1.52) and (3.13), including all source terms, Yukawa interaction, sphaleron, electroweak interactions in a regime where all of the SM processes are in chemical equilibrium[18] The system of coupled differential equations then reduce to an equilibrium solution for the baryon asymmetry $\eta_B^{\rm eq}$ whose equation depends on the considered temperature window. As expected, the equilibrium solutions

---

[18]Except for the chiral magnetic effect and electron sign-flip interaction.

take the form of (source)/(washout). For each case, approximations are made, in particular keeping only the dominant reaction rates.

The novelty of this mechanism lies in the introduction of a time-dependent weak mixing angle $\theta_W(t)$, see (2.92), which brings an additional source of the baryon number in the kinetic equation. As the result depends on the subtle balance between the unbroken/broken phase gauge field, a thorough examination of the EWPT is necessary.

If we neglect the thermal effects during the Higgs mechanism, the weak angle, which is the $SO(2)$ parameter that controls the change of basis, see (2.90), makes a discrete change from $\theta_W = 0$ in the symmetric phase to $\theta_W \simeq 28.6°$ in the broken phase. We recall that this process was sketched in Sec. 2.3.3. When the EW symmetry breaking occurs at $T \simeq 160$ GeV, the primordial hypermagnetic field becomes an electromagnetic field. However, the electroweak sphaleron remains in equilibrium until $T \simeq 130$ GeV and threatens to washout the baryon asymmetry. Therefore proper modeling of the epoch $160 \text{ GeV} \gtrsim T \gtrsim 130$ GeV is critical to an accurate prediction of the relic BAU. By making the assumption of zero temperatures, information is lost in the breaking process. We shall then come up with a more complete description of the electroweak crossover than in Sec. 2.3.3.

For finite temperatures, the gauge fields W_μ^a acquire an effective (thermal) mass from their interactions with the plasma, which leads to the screening of the massive fields. In fact, the thermal mass for the transverse modes of W_μ^3, on the diagonal of the mass matrix, initially dominates over the off-diagonal mass from the Higgs VEV which gradually develops during the crossover. On the other hand, no magnetic mass arises for the hypercharge gauge boson or the photon [149–151]. Because of that, the weak angle really smoothly interpolates between the above values during the phase transition, and continues to deviate appreciably from its zero-temperature value $\theta_W \simeq 28.6°$, even at relatively low temperatures somewhat below the EW scale, see Fig. 3.1

In other words, $\theta_W(t)$ is defined as the rotation angle that projects the massless field degree of freedom onto the $U(1)_Y$ field axis. This behavior is confirmed by analytic calculations [150], and numerical lattice simulations [151]. We follow [121, 137] and model it with a smooth step function

$$\cos^2\theta_W = \frac{g^2}{g'^2 + g^2} + \frac{1}{2}\frac{g'^2}{g'^2 + g^2}\left(1 + \tanh\left[\frac{T - T_{\text{step}}}{\Delta T}\right]\right) \tag{3.15}$$

which for $155 \text{ GeV} \lesssim T_{\text{step}} \lesssim 160 \text{ GeV}$ and $5 \text{ GeV} \lesssim \Delta T \lesssim 20 \text{ GeV}$ describes the analytical and lattice results for the temperature dependence reasonably well, see Fig. 3.1.

In the end, this gives rise to a smooth source term for the baryon asymmetry which is controlled by the changing EW angle. Besides, by drawing on analytic and lattice results, the hypermagnetic field is not fully converted into an electromagnetic field even at temperatures as low as $T = 140$ GeV. Therefore, the source term from decaying magnetic helicity remains active, while the washout by EW sphalerons goes out of equilibrium for temperatures $T \simeq 130$ GeV. Consequently, it is possible to generate the observed BAU from a maximally helical magnetic field that was generated prior to the EW crossover. Indeed, including all contributions, the Boltzmann equation for the baryon-to-entropy ratio η_B (1.156) reads

$$\frac{d\eta_B}{dx} = -\frac{111}{34}\gamma_{W\text{sph}}\,\eta_B + \frac{3}{16\pi^2}(g'^2 + g^2)\sin(2\theta_W)\frac{d\theta_W}{dx}\frac{\mathcal{H}_Y}{s}, \tag{3.16}$$

where $x = T/H(T)$, with $H(T)$ being the Hubble rate at temperature T, $\mathcal{H}_Y$ the hypermagnetic helicity that is initially present and s the comoving entropy density of the SM plasma given by (1.50). Furthermore, $\gamma_{W\text{sph}} = 6\Gamma_{W\text{sph}}/T^4$ is the dimensionless transport coefficient for the EW sphaleron which, for temperatures $T < 161$ GeV, is found from lattice simulations to be [152]

$$\gamma_{W\text{sph}} \simeq \exp\left(-147.7 + 107.9\,\frac{T}{130\,\text{GeV}}\right). \tag{3.17}$$

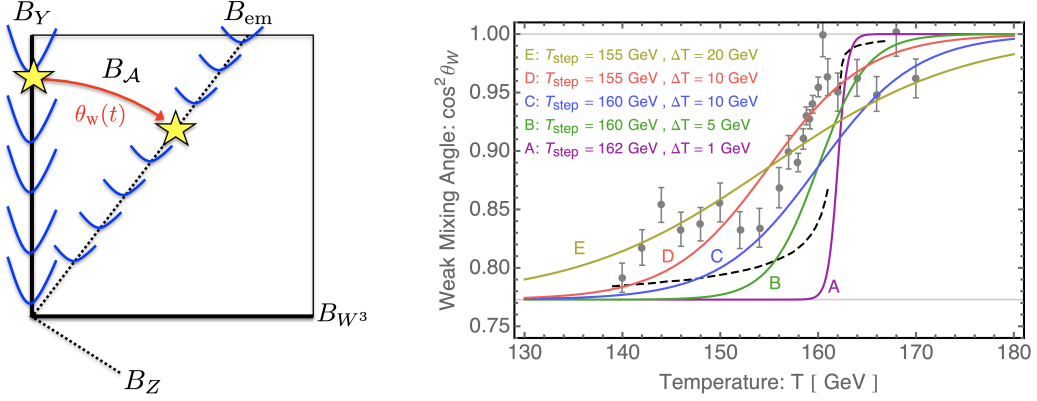**Figure 3.1**. Left: Visualization of the $SO(2)$ change of basis $(W_\mu^3, Y_\mu) \to (Z_\mu, A_\mu)$ that happens at EWPT, see Eq. (2.90). The weak angle $\theta_W(t)$ measures the separation between the massless degree of freedom and the $U(1)_Y$ axis. Right: The same weak angle as a function of temperature during the EWPT. The grey dots are the results from the lattice simulation from [151], whereas the black dashed line displays the one-loop analytical computation from [150]. The plain lines show various possibilities of the smoothed step function (3.15). Both figures are taken from Ref. [121].

The Boltzmann equation (3.16) has been numerically solved in [121] and the baryon-to-entropy ratio η_B was found to become frozen, i.e. $\dot{\eta}_B = 0$, at a temperature $T \simeq 135$ GeV. As expected, this is close to the temperature $T \simeq 130$ GeV at which EW sphalerons freeze out. Setting the RHS of Eq. (3.16) to zero and solving for η_B yields

$$\eta_B \simeq 4 \cdot 10^{-12}\, f_{\theta_W} \frac{\mathcal{H}_Y}{H_E^3} \left(\frac{H_E}{10^{13}\,\text{GeV}} \right)^{\frac{3}{2}} \left(\frac{T_{\text{rh}}}{T_{\text{rh}}^{\text{ins}}} \right), \tag{3.18}$$

where H_E is the Hubble rate at the end of inflation and the (instant) reheating temperature has been defined in (1.97). This result is a main ingredient of this thesis as it directly relates the amount of the final baryon asymmetry of the Universe to the amount of hypermagnetic helicity available at the EWPT.

All the details on the EWPT dynamics are encoded in the parameter f_{θ_W} which is subject to significant uncertainties

$$f_{\theta_W} = -\sin(2\theta_W) \left. \frac{d\theta_W}{d\log T} \right|_{T=135\text{ GeV}} \qquad 5.6 \cdot 10^{-4} \lesssim f_{\theta_W} \lesssim 0.32. \tag{3.19}$$

The bounds on f_{θ_W} are given by varying T_{step} and ΔT in the ranges given below Eq. (3.15).

3.2   Helical magnetic fields generation

Our main interest in this section is to show the simplest way to generate a maximally helical (hyper)magnetic field at the end of inflation in order to source Eq. (3.18). We will follow [112, 135, 136], where an axion inflation model was used together with a $\mathcal{CP}$ even dimension-five coupling, a natural interaction for a pseudoscalar (see Secs. 1.2.2 and 2.4.2) and therefore natural from the EFT point of view. The action is written as

$$S = \int d^4x \left[\sqrt{-g} \left(\frac{1}{2} \partial_\mu \phi \partial^\mu \phi - \frac{1}{4} Y_{\mu\nu} Y^{\mu\nu} - V(\phi) \right) - \frac{\phi}{4 f_\phi} Y_{\mu\nu} \tilde{Y}^{\mu\nu} \right], \tag{3.20}$$

where f_ϕ is the interaction scale in mass dimension. The Higgs is assumed to lie at the minimum of its potential, in other words we are in the symmetric phase, thus the $U(1)$ field is the hypercharge and the fields $\boldsymbol{A}$, $\boldsymbol{E}$, $\boldsymbol{B}$ are, in what follows, the hypercharge version of their electromagnetism counterparts.

3.2.1 Equations of motion and solutions

Varying the action (3.20) with respect to the fields (ϕ, Y_μ) leads to the equation of motion (EoM) for the inflaton and the gauge field.

$$\Box\phi + V'(\phi) + \frac{Y_{\mu\nu}\tilde{Y}^{\mu\nu}}{4f_\phi} = 0, \tag{3.21a}$$

$$\partial_\mu Y^{\mu\nu} + \partial_\mu \frac{\phi\tilde{Y}^{\mu\nu}}{f_\phi} = 0, \tag{3.21b}$$

where $\Box \equiv \partial_\mu\partial^\mu$ is the d'Alembert operator. Using now (1.35), (2.20), (3.8) in the flat FRW metric (1.36), and the radiation gauge (3.7), together with the Gauss-Faraday equation $\partial_\mu\tilde{Y}^{\mu\nu} = 0$, we get

$$\ddot{\phi} + 3H\dot{\phi} + V'(\phi) = \frac{\boldsymbol{E}\cdot\boldsymbol{B}}{a^4 f_\phi}, \tag{3.22a}$$

$$\left(\frac{\partial^2}{\partial\tau^2} - \nabla^2 - \frac{1}{f_\phi}\frac{\partial\phi}{\partial\tau}\,\boldsymbol{\nabla}\times\right)\boldsymbol{A} = 0. \tag{3.22b}$$

During the inflationary period one has, according to (1.35) and (1.38),

$$\frac{\partial\phi}{\partial\tau} = \dot{\phi}a \simeq -\frac{\dot{\phi}}{H\tau}. \tag{3.23}$$

Therefore, defining the instability parameter as

$$\xi = -\frac{\dot{\phi}}{2f_\phi H}, \tag{3.24}$$

the gauge field EoM becomes

$$\left(\frac{\partial^2}{\partial\tau^2} - \nabla^2 - \frac{2\xi}{\tau}\,\boldsymbol{\nabla}\times\right)\boldsymbol{A} = 0. \tag{3.25}$$

Note that if we assume the slow roll regime given by Eqs. (1.73), the instability parameter can be written as

$$\xi \simeq \frac{M_{\text{pl}}^2}{2f_\phi}\frac{V'(\chi)}{V(\chi)} = \frac{M_{\text{pl}}}{f_\phi}\sqrt{\frac{\epsilon}{2}} > 0, \tag{3.26}$$

where in the second step we used Eq. (1.74). The remaining computation assumes that the inflaton is slowly rolling. In Sec. 3.2.3 we will provide the conditions to guarantee this approximation.

We now quantize the gauge field $\boldsymbol{A}$ in momentum space in the helical basis as

$$\boldsymbol{A}(\tau, \boldsymbol{x}) = \sum_{\lambda=\pm}\int\frac{d^3 k}{(2\pi)^3}\left[\boldsymbol{\epsilon}_\lambda(\boldsymbol{k})\,a_\lambda(\boldsymbol{k})\,A_\lambda(\tau, \boldsymbol{k})\,e^{i\boldsymbol{k}\cdot\boldsymbol{x}} + \text{h.c.}\right], \tag{3.27}$$

where λ is the photon polarization and $a_\lambda(\boldsymbol{k})$ $(a_\lambda^\dagger(\boldsymbol{k}))$ are annihilation (creation) operators that

fulfill the canonical commutation relations

$$[a_\lambda(\boldsymbol{k}), a_{\lambda'}^\dagger(\boldsymbol{k}')] = (2\pi)^3 \delta_{\lambda\lambda'} \delta^{(3)}(\boldsymbol{k} - \boldsymbol{k}') . \tag{3.28}$$

The polarization vectors $\boldsymbol{\epsilon}_\lambda(\boldsymbol{k})$ satisfy the conditions

$$\begin{aligned}
\boldsymbol{k} \cdot \boldsymbol{\epsilon}_\lambda(\boldsymbol{k}) &= 0, & \boldsymbol{k} \times \boldsymbol{\epsilon}_\lambda(\boldsymbol{k}) &= -i\lambda k \, \boldsymbol{\epsilon}_\lambda(\boldsymbol{k}), \\
\boldsymbol{\epsilon}_{\lambda'}^*(\boldsymbol{k}) \cdot \boldsymbol{\epsilon}_\lambda(\boldsymbol{k}) &= \delta_{\lambda\lambda'}, & \boldsymbol{\epsilon}_\lambda^*(\boldsymbol{k}) &= \boldsymbol{\epsilon}_\lambda(-\boldsymbol{k}),
\end{aligned} \tag{3.29}$$

where $k \equiv |\boldsymbol{k}|$. Therefore, the equation of motion for the gauge modes (3.25) yields

$$\frac{\partial^2 A_\lambda}{\partial \tau^2} + k\left(k + \lambda \frac{2\xi}{\tau}\right) A_\lambda = 0, \tag{3.30}$$

which is the spherical Coulomb wave equation[19]. Provided that ξ is constant (see Eq. (3.35) and Sec. 3.2.4), its general solution is

$$A_\lambda = \frac{iF_0(\lambda\xi, -k\tau) + G_0(\lambda\xi, -k\tau)}{\sqrt{2k}}, \tag{3.31}$$

where F_0 and G_0 are, respectively, the regular and irregular Coulomb wave functions with index 0 [133, 153].

At early times, the last solution has the asymptotic behavior that corresponds to the Bunch-Davies vacuum of the modes, defined as

$$A_\lambda(\tau, k) = \frac{1}{\sqrt{2k}} \, \mathrm{e}^{-ik\tau} \qquad\qquad (\tau \to -\infty). \tag{3.32}$$

In fact during inflation, where $\epsilon \ll 1$, we obtain, using Eq. (3.24), that $\xi \ll 1$ and therefore $|k\tau| \gg 2\xi$ which implies (3.32). However, the end of inflation happens, by construction, when $\epsilon(\tau_E) \simeq 1$ and so we can have $\xi \gtrsim 1$. Then, only one mode develops both parametric and tachyonic instabilities for $k \simeq k_c$ where

$$k_c = 2\xi a_E H_E, \qquad\qquad a_E = a(\tau_E), \tag{3.33}$$

while the other mode stays close to its vacuum. As in our model $\xi > 0$, and during inflation $\tau < 0$, the mode exhibiting the instability is the one with the $\lambda = +$ polarization. For late times, $k \ll k_c$ (i.e. $|k\tau| \ll 2\xi$), F_0 can be neglected and the growing mode solution can be approximated by [133, 153]

$$A_\lambda \simeq \frac{G_0}{\sqrt{2k}} \simeq \frac{1}{\sqrt{2k}} \left(\frac{k}{2\xi a_E H_E}\right)^{\frac{1}{4}} \exp\left(\pi\xi - 2\sqrt{\frac{2\xi k}{a_E H_E}}\right). \tag{3.34}$$

All modes produced during inflation will get diluted, except the last mode that exits the horizon right before the end of inflation. This mode reenters the horizon at the onset of reheating, and is the source for the BAU. Hence, it is only necessary to consider the mode produced at $\tau \simeq \tau_E$, for which $\epsilon \simeq 1$, and hence, using the last equality in Eq. (3.26), we obtain for ξ the constant value

$$\xi \simeq \frac{M_{\mathrm{pl}}}{\sqrt{2} f_\phi}. \tag{3.35}$$

Let us mention that, even if the first equality in Eq. (3.26) looks model dependent, as it depends

---

[19]In the literature, this equation is sometimes solved using the Whittaker function, as Coulomb wave functions F_0, G_0 can be expressed in terms of Whittaker functions with imaginary arguments: $M_{-i\xi, \frac{1}{2}}(-2ik\tau)$ and $W_{-i\xi, \frac{1}{2}}(-2ik\tau)$.

on the potential and its derivative, in fact it is very model independent because the last relation only relies on the slow roll regime of the inflationary potential, and $\epsilon \simeq 1$ at the end of inflation, see Sec. 3.2.4 for a discussion.

From this approximated value we can see that the parameter ξ can be traded for the value of the parameter f_ϕ such that $\xi \gg 1$ corresponds to $f_\phi \ll M_{\rm pl}$. Moreover, as we see from the explicit solution in Eq. (3.34), there is an exponential magnification for large values of ξ. However, as shown later on in Sec. 3.2.3, for very large values of ξ, the backreaction on the inflation dynamics from magnetic fields cannot be neglected, which would lead to upper bounds on the values of ξ, or correspondingly to lower bounds on the values of f_ϕ.

3.2.2 Plasma macroscopic observables

Assuming homogeneity in momentum space, we recast the definition for the physical helicity of quantum $U(1)$ fields

$$\mathcal{H} \equiv \lim_{V \to \infty} \frac{1}{V} \int_V d^3x \, \frac{\langle \boldsymbol{A} \cdot \boldsymbol{B} \rangle}{a^3}, \tag{3.36}$$

where $\langle \cdot \rangle$ is the expectation value of quantum fields and the integral $V^{-1} \int_V d^3x$ is the spatial average, which is trivial for space independent quantities.

The definition (3.6) was a correct definition for classical fields in Minkowski spacetime, but in an expending Universe it is of prime importance to distinguish between comoving and physical quantities. In this thesis, the main macroscopic plasma quantities, which are the helicity (3.36), the helicity time derivative

$$\mathcal{G} \equiv \frac{1}{2a} \frac{d\mathcal{H}}{d\tau} = - \lim_{V \to \infty} \frac{1}{V} \int_V d^3x \, \frac{\langle \boldsymbol{E} \cdot \boldsymbol{B} \rangle}{a^4}, \tag{3.37}$$

the electric and magnetic energy densities

$$\rho_E \equiv \lim_{V \to \infty} \frac{1}{2V} \int_V d^3x \, \frac{\langle \boldsymbol{E}^2 \rangle}{a^4}, \tag{3.38a}$$

$$\rho_B \equiv \lim_{V \to \infty} \frac{1}{2V} \int_V d^3x \, \frac{\langle \boldsymbol{B}^2 \rangle}{a^4}, \tag{3.38b}$$

and the correlation length of the magnetic field ℓ_B, are all *physical*, i.e they dilute with the Universe expansion[20]. On the contrary, the fields $\boldsymbol{A}$, $\boldsymbol{E}$, $\boldsymbol{B}$, as well as the current $\boldsymbol{J}$ and the conductivity σ are *comoving*, i.e. they scale with the Universe expansion. This allows us simpler computation of vectorial algebra, see Sec. 1.1.3. Note that the definition (3.37) is the analog of (3.11) with the same mentioned changes.

In the helical basis (3.27) these five quantities write as [141]

$$\mathcal{H} = \frac{1}{a^3} \int_0^{k_c} dk \, \frac{k^3}{2\pi^2} \left(|A_+|^2 - |A_-|^2 \right), \tag{3.39a}$$

$$\mathcal{G} = \frac{1}{a^4} \int_0^{k_c} dk \, \frac{k^3}{2\pi^2} \left(|A_+ A'_+| - |A_- A'_-| \right) \tag{3.39b}$$

$$\rho_E = \frac{1}{a^4} \int_0^{k_c} dk \, \frac{k^2}{4\pi^2} \left(|A'_+|^2 + |A'_-|^2 \right), \tag{3.39c}$$

$$\rho_B = \frac{1}{a^4} \int_0^{k_c} dk \, \frac{k^4}{4\pi^2} \left(|A_+|^2 + |A_-|^2 \right), \tag{3.39d}$$

---

[20]They relate to the comoving ones ρ_E^c, ρ_B^c, $\mathcal{H}^c$, and $\mathcal{G}^c$ by the relations $\rho_{B,E}^c = a^4 \rho_{B,E}$, $\mathcal{H}^c = a^3 \mathcal{H}$, $\mathcal{G}^c = a^4 \mathcal{G}$.

$$\ell_B \;=\; \frac{2\pi}{\rho_B\,a^3} \int_0^{k_c} dk\, \frac{k^3}{4\pi^2} \left(|A_+|^2 + |A_-|^2 \right), \tag{3.39e}$$

where we cut off the integrals at the last mode exiting the horizon given by (3.33). We see from the momentum dependence $\propto k^{3\text{-}5}$ of the integrals that only the modes generated during the last e-folds of inflation will significantly contribute to the final macroscopic quantities. In other words, all modes generated formerly $k \ll k_c$ are washed out by the Universe expansion and we can address our efforts on the period $a \simeq a_E$ (or equivalently $\epsilon \simeq 1$).

Since at that time all the modes of one given helicity stay in its BD vacuum, while the other is amplified ($\xi \gtrless 0 \Leftrightarrow A_\pm$ is amplified), we can neglect one mode[21] and set the other one to (3.34) in all the quantities from (3.39), and we find [135, 154]

$$\mathcal{H} \simeq \frac{45}{2^{15}}\, \frac{H_E^3}{\pi^2\xi^4}\, e^{2\pi\xi}, \tag{3.40a}$$

$$\mathcal{G} \simeq \frac{135}{2^{16}}\, \frac{H_E^4}{\pi^2\xi^4}\, e^{2\pi\xi}, \tag{3.40b}$$

$$\rho_E \simeq \frac{63}{2^{16}}\, \frac{H_E^4}{\pi^2\xi^3}\, e^{2\pi\xi}, \tag{3.40c}$$

$$\rho_B \simeq \frac{315}{2^{18}}\, \frac{H_E^4}{\pi^2\xi^5}\, e^{2\pi\xi}, \tag{3.40d}$$

$$\ell_B \simeq \frac{8}{7}\, \frac{\pi\,\xi}{H_E}, \tag{3.40e}$$

where we have used the $\xi \gg 1$ approximation[22]. From these we can extract

$$\rho_E \simeq \frac{4\xi^2}{5}\, \rho_B, \qquad\qquad \rho_{\rm EM} = \rho_E + \rho_B \simeq \rho_B \left(1 + \frac{4\xi^2}{5} \right). \tag{3.41}$$

Hence we see that, except for ℓ_B, all macroscopic quantities grow tremendously with ξ due to the exponential factor. Thus, even for $\mathcal{O}(1)$ values of ξ, enough helicity can be generate at the end of inflation in order to explain the BAU via Eq. (3.18), see Fig. 3.2. The four other quantities will be needed to take care of the constraints and of the Schwinger effect, see next chapter. Moreover, we see explicitly that the scale is given by H_E, i.e. the scale of inflation.

To close this section, we would like to underline that maximally helical fields, $\boldsymbol{E}(\boldsymbol{k})$ and $\boldsymbol{B}(\boldsymbol{k})$, in (Fourier transformed) momentum space are collinear, as using the identities (3.29) one can easily check that both are proportional to $\boldsymbol{\epsilon}_\lambda(\boldsymbol{k})$. Besides, these fields in configuration space are, using the approximation (3.34), (almost) collinear. In fact, one can compute, using our approximated solution for the backreactionless solution, the angle θ measuring the collinearity of the electric and magnetic fields, as

$$\cos\theta \equiv \frac{|\langle \boldsymbol{E} \cdot \boldsymbol{B} \rangle|}{\sqrt{\langle \boldsymbol{E}^2 \rangle \langle \boldsymbol{B}^2 \rangle}} \simeq \frac{|\mathcal{G}|}{2\sqrt{\rho_E \rho_B}}. \tag{3.42}$$

Using Eqs. (3.40) we obtain, for $\xi \gg 1$

$$\cos\theta \simeq \frac{3\sqrt{5}}{7} \simeq 0.958, \tag{3.43}$$

which corresponds to the angle $\theta \simeq 0.0016\pi$. As a result we have proven that the fields $\boldsymbol{E}$ and $\boldsymbol{B}$ are (almost) collinear, a property that will be used when applying the Schwinger effect in Chap. 4.

---

[21]The choice is made such that $\mathcal{H} > 0$.

[22]In fact, we have found that the approximation is valid up to $\mathcal{O}(e^{-8\xi})$ terms, so that it is good enough for $\xi \gtrsim 2$-3.

3.2.3 Slow roll approximation and self-consistency

We can perform the quantum and space average on the EoM (3.22a) and write

$$\ddot{\phi} + 3H\dot{\phi} + V'(\phi) = \frac{\mathcal{G}}{f_\phi} \tag{3.44}$$

where we used (3.37). The LHS did not change as ϕ is a background field.

In the previous sections, we have computed the helical gauge fields generated in the presence of the inflationary background, (eventually) after estimating the backreaction of fermion currents on gauge fields, but we have neglected the backreaction of gauge fields on the inflaton dynamics, i.e. the RHS of ϕ's EoM. We will now compute the actual conditions needed to have negligible backreaction of the generated gauge fields on the inflaton equations of motion, such that we can reliably trust the inflationary predictions, and therefore the actual generation of helical magnetic fields. In other words, we seek the conditions on ξ to guarantee the slow roll regime given by (1.73). Needless to say this condition is mainly a simplifying one, and allows us to work out the inflationary model independently of the generated gauge fields.

Thus, in order to consistently neglect the backreaction on the inflaton, we must simply enforce that, in the inflaton equation of motion (3.44), the RHS term is negligible compared to the potential term, i.e. $|\mathcal{G}/V'| \ll f_\phi$. This condition is independent of the reheating temperature and should hold during the full magnetogenesis process, hence during the last few e-folds of inflation. Due to its exponential growth, putting an upper bound on the quantity $\mathcal{G}$ at the end of inflation ensures that the latter condition is valid during the full inflationary period. Evaluating it then at this time, when $\epsilon = 1$ or, equivalently, $V' \simeq \sqrt{2}V/M_{\rm pl}$, we get

$$\xi\,\mathcal{G}|_{a=a_E} \ll V(\phi_E), \tag{3.45}$$

where we used (3.35). We can express this condition in a different way by combining $\rho_{\rm EM} \simeq \rho_E$ given by (3.40c), together with (3.39b), which yields

$$2\,\rho_{\rm EM} \simeq \xi\,\mathcal{G}. \tag{3.46}$$

Hence, the condition $|\mathcal{G}/V'| \ll f_\phi$, evaluated at the end of inflation, is equivalent to imposing

$$2\,\rho_{\rm EM}|_{a=a_E} \ll V(\phi_E). \tag{3.47}$$

Notice that the condition (3.47) is stronger than the condition for neglecting $\rho_{\rm EM}$ in the Friedmann equation, i.e. $\rho_{\rm EM} \ll 3H_E^2 M_{\rm pl}^2 \simeq V(\phi_E)$, so that the latter does not need to be imposed. On Fig. 3.2, we plot this condition for the results (3.40).

3.2.4 Almost constancy of ξ and model dependance

We have seen that the methods employed to analytically compute the electromagnetic energy density and helicity require an approximate constant behavior of ξ. We aim to demonstrate in this section how this parameter changes during inflation for various models as these results will matter later on in this thesis.

Let us consider the following interaction term in the action between the inflaton ϕ and the CS density

$$S \supset \int d^4x \, F(\phi) \, Y_{\mu\nu}\tilde{Y}^{\mu\nu} \,. \tag{3.48}$$

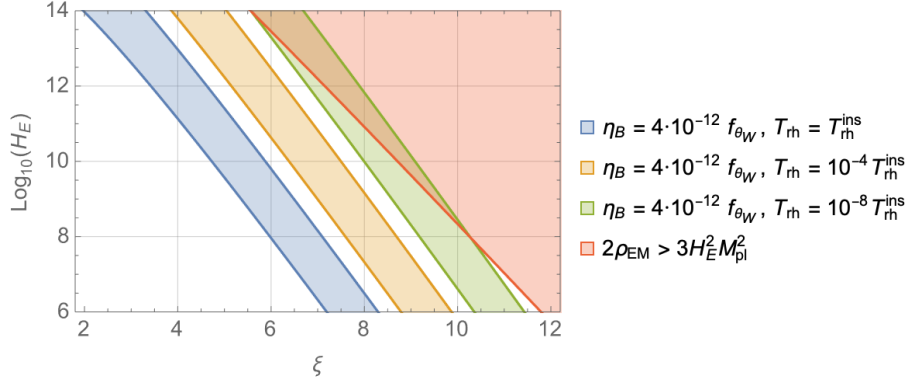If we are in the slow roll regime given by the approximations (1.73), the instability parameter can

Figure 3.2. Baryon asymmetry η_B given by (3.18), and self-consistency condition for the parameter space (ξ, H_E), for various values of the reheating to instant reheating temperature ratio in the case of model given by Eqs. (3.40) (no Schwinger effect). In virtue of condition (3.47), the red region is excluded. The error margin in the value of η_B comes from the significant uncertainty of the parameter f_{θ_W}. We recall that the current bound on the (constant) Hubble parameter is $H_E \lesssim 6 \cdot 10^{13}$ GeV.

be written as

$$\xi = 2F'(\phi) \, \frac{V'(\phi)}{V(\phi)}. \tag{3.49}$$

It is a generalization of Eq. (3.26) where we are taking units with $M_{\rm pl} = 1$. Thus, a constant value of ξ is guaranteed by the condition

$$F'(\phi) \propto \frac{V(\phi)}{V'(\phi)} \tag{3.50}$$

which then depends on the inflaton model. For illustrative purposes, we recast the models presented in Sec. 1.2.5 and we aim to compute under which condition ξ can be constant therein.

Monomial potentials   The potential (1.100) provides $F(\phi) = \phi^2/f_\phi^2$, where the constant f_ϕ has mass dimension. The latter condition can be trivially verified from criterion (3.50).

α attractor models   Criterion (3.50) applied to the potential (1.103) implies

$$F(\phi) = \exp\left(\sqrt{\frac{2}{3\alpha}} \, \phi\right) - \sqrt{\frac{2}{3\alpha}} \, \phi \tag{3.51}$$

This yields for the instability

$$\xi = \frac{8}{3\alpha}. \tag{3.52}$$

Hilltop models   Criterion (3.50), when applied to the potential (1.107) for $\phi < \mu$ implies

$$F(\phi) = \mu^p \, \phi^{2-p}/f_\phi^2. \qquad\qquad (p \neq 2) \tag{3.53a}$$

$$F(\phi) = -\frac{\lambda}{2} \log \phi. \qquad\qquad (p = 2) \tag{3.53b}$$

where λ is a dimensionless parameter. This yields the relations for the instability parameter (3.49)

$$f_\phi^2 \xi = \frac{p(p-2)}{1 - (\phi/\mu)^p} \simeq p(p-2) \qquad\qquad (p \neq 2) \tag{3.54a}$$

$$\mu^2 \xi = \lambda \qquad\qquad (p = 2) \qquad\qquad (3.54b)$$

D-brane models Criterion (3.50) applied to the potential (1.110) implies

$$F(\phi) = \frac{1}{f_\phi^{p+2}} \left(\phi^{p+2} - \frac{p+1}{2}\, \mu^p\, \phi^2 \right) \simeq \frac{\phi^{p+2}}{f_\phi^{p+2}}. \qquad\qquad (3.55)$$

This yields for the instability

$$f_\phi^2\, \xi = p(p+2)\, \frac{\mu^p}{f_\phi^p} \qquad \forall p > 0. \qquad\qquad (3.56)$$

Non minimal couplings We start from the generic action (1.112) in which we include the terms

$$S \supset \int d^4x \left[-\sqrt{-g}\, \frac{1}{4} Y_{\mu\nu} Y^{\mu\nu} - \frac{F(\phi)}{4}\, Y_{\mu\nu} \tilde{Y}^{\mu\nu} \right]. \qquad\qquad (3.57)$$

In the Einstein frame, ϕ becomes a function of the true inflaton field χ, see Eqs. (1.123), then the criterion for a constant ξ (3.50) yields

$$F[\phi(\chi)] \propto \chi^2 + \frac{g^2}{8} \frac{\chi^4}{1 + 6g} \qquad\qquad (p = 1) \qquad\qquad (3.58a)$$

$$F[\phi(\chi)] \propto \exp\left(-\sqrt{\frac{4g}{1 + 6g}}\, \chi \right) \qquad\qquad (p = 2) \qquad\qquad (3.58b)$$

$$F[\phi(\chi)] \propto (c_p - \chi)^{4/(2-p)} \qquad\qquad (p \geqslant 3) \qquad\qquad (3.58c)$$

In term of the field ϕ the latter conditions become

$$F(\phi) \propto \phi \left(\phi + \frac{2}{g} \right) \simeq \phi^2 \qquad\qquad (p = 1) \qquad\qquad (3.59a)$$

$$F(\phi) \propto \phi^2 \qquad\qquad (p \geqslant 2) \qquad\qquad (3.59b)$$

where we recall that we are in the regime $g\phi^p \gg 1$, which means $\chi \to \infty$ for $p = 1, 2$ and $\chi \to c_p$ for $p \geqslant 3$.

To conclude, in the case of a non-minimal coupling $g\phi^p R$, the requirement of a constant ξ put the constraint of a dimension-six interaction term between the inflaton and the gauge field as

$$S \supset - \int d^4x\, \frac{\phi^2}{4f_\phi^2}\, Y_{\mu\nu} \tilde{Y}^{\mu\nu}, \quad \forall p \geqslant 1 \qquad\qquad (3.60)$$

where f_ϕ is a dimensional coupling. The value of the parameter ξ for the different models is then given by

$$f_\phi^2\, \xi \simeq \frac{2p}{1 + 6g}, \qquad (p \geqslant 1). \qquad\qquad (3.61)$$

Discussion

At this stage, several conclusions can be obtained. They all have implications for what we have seen, as well as for the different models we will show in Chaps. 5 and 6.

First, none of the above conditions displayed a linear function $F(\phi) \propto \phi$, which means that the assumption of a constant ξ in the model-independent action, Eq. (3.20), is arguable. Our results show that deep inside the inflation regime, $\epsilon \ll 1$, ξ has indeed an approximate constant behavior

because $\xi \propto \sqrt{\epsilon}$. But, in the absence of a strong friction term[23], the way a field gets out from this regime in any potential is to accelerate more and more, so the exit from the slow roll condition is inevitably done in an abrupt way. We show an illustration for the Starobinsky potential in Fig. 4.4. Hence although ξ has an approximate constant behavior at the early stages of inflation, it grows exponentially at the end, precisely when the gauge field production is dominant.

Although this observation seems to jeopardize the models, we will see in Chap. 4 that the fermion effect on the plasma changes the whole situation, and thus the constant ξ *problem* becomes irrelevant. We will be able to address this issue by means of a numerical solution that can take into account not only the fermion effect, but also a time-dependent instability parameter and the RHS of the inflaton EoM. As a consequence, the corresponding results (3.40) will be replaced by a better description of the system.

On the other hand, if one wishes to keep an analytical description, we can find a way to fix a particular coupling between the inflaton and the CS density; for instance by suggesting a model in which the linear coupling is forbidden in the effective expansion. Indeed, for a naive scalar field inflaton, there is *a priori* no reason why such a term would be missing in favor of a quadratic one. However, in the Higgs inflation model (see Sec. 1.2.6), and identifying the inflaton with the Higgs doublet, this requirement is met as in this theory the linear term is forbidden and the quadratic one is the leading order coupling. Therefore the result (3.60) applies and assuming a constant value of ξ is analytically exact up to some caveats, as we will see in Sec. 5.1.1.

3.3   Constraints

In Sec. 3.2 we have seen a non-perturbative mechanism which generates helical hypermagnetic fields from inflation, hence for scales $H_E \gg 100$ GeV. Earlier, in Sec. 3.1, we have shown under which conditions the hypermagnetic helicity get converted into baryon asymmetry at the EW scale, i.e. $T \sim 100$ GeV. There is thus a gap to bridge between these two distant scales, as we have to make sure that hypermagnetic fields generated during inflation survive until the EWPT.

On the one hand, there are mechanisms (dissipation, chiral plasma instability) that could washout the helicity stored in the gauge sector under some specific conditions. On the other hand, there are observational bounds on a number of associated phenomena (primordial non-Gaussianity, isocurvature perturbations,...) that prevent total freedom in the possible configurations. All of these constraints can further narrow the region of the parameter space where the BAU can really be reproduced by any theory, and will be analyzed in this section. The model dependence on these constraints will be given alongside the different models of baryogenesis in the next chapters. Here we provide their common ground.

3.3.1   Backreactions

Even the backreaction effect is a very generic one, in this thesis we denote by *backreaction* two specific phenomena

1. The backreation of the gauge field on the inflaton field, see Sec. 3.2.3.

2. The backreation of fermions on the gauge fields: in the presence of strong gauge fields, i.e. for $\xi \gg 1$, fermions charged under the gauge group are produced by the backreaction of gauge fields which source the fermion equations of motion. The corresponding currents can then, in turn, backreact on the produced gauge fields and change their (so-called *backreactionless*) solutions given by Eqs. (3.40). This phenomenon is called the *Schwinger effect* and we devote Chap. 4 to its detailed description.

---

[23]The slow roll regime can be ensured, even in a steep potential, if the RHS of the inflaton EoM (3.44) is dominant, thus acting as a strong friction term, see e.g. Ref. [134].

Moreover, the fermions produced by the latter effect are at the origin of another phenomenon, called the *chiral plasma instability*, see Sec. 3.3.3.

3.3.2 Magnetohydrodynamics and Reynolds numbers

The hypercharge gauge fields interact with the thermal plasma of SM particles after reheating and set it into motion. The latter in turn backreacts on the hypercharge gauge fields. This combined system is described by the magnetohydrodynamics (MHD) equations (3.1) where the time dependence shall be replaced by conformal time, i.e. $t \to \tau$, as all quantities in Eqs. (3.1) are from now taken as comoving.

As a result, that we demonstrate hereafter, the physical quantities of interest (amplitudes, energy densities, correlation length and helicity) do not scale adiabatically in such an environment, or equivalently their comoving values are not constant. Therefore there can be a magnetic *diffusion* effect leading to the decay of the helicity. If, on the other hand, the magnetic *induction* is the leading effect, then the helicity can be conserved until the EWPT, and the baryogenesis mechanism can take place. This effect is measured by the magnetic Reynolds number $\mathcal{R}_m$, and we will see that it is enough to require $\mathcal{R}_m > 1$ at reheating for the helicity to be conserved until the EW crossover. Hence, in this section we will study how this constraint affects the region of the parameter space that yields the BAU. In this section we mainly follow Refs. [139, 140, 154–156].

For fluid velocities $|\boldsymbol{v}| \ll 1$, we can neglect the displacement current $\partial_\tau \boldsymbol{E}$ in the Ampère-Maxwell equation (3.1b). This can be seen as follows. If we denote the characteristic electric and magnetic field, and time and length scales of a gauge field configuration with E, B, τ and ℓ, respectively, we can estimate the terms in (3.1b) as $|\partial_\tau \boldsymbol{E}| \sim E/\tau$ and $|\boldsymbol{\nabla} \times \boldsymbol{B}| \sim B/\ell$. Using the estimate $E/B \sim \ell/\tau$, that follows from the Maxwell-Faraday equation (3.1a), we then find $|\partial_\tau \boldsymbol{E}|/|\boldsymbol{\nabla} \times \boldsymbol{B}| \sim (\ell/\tau)^2 \sim |\boldsymbol{v}|^2 \ll 1$.

Combining Eqs. (3.1b), (3.1f), (3.3) and this approximation, we obtain

$$\boldsymbol{E} = \frac{\boldsymbol{\nabla} \times \boldsymbol{B}}{\sigma} - \frac{2\alpha}{\pi} \frac{\mu_5}{\sigma} \boldsymbol{B} - \boldsymbol{v} \times \boldsymbol{B}. \tag{3.62}$$

Together with the Maxwell-Faraday equation (3.1a), this yields the MHD equation for the hypermagnetic field

$$\frac{\partial \boldsymbol{B}}{\partial \tau} = \frac{\boldsymbol{\nabla}^2 \boldsymbol{B}}{\sigma} + \boldsymbol{\nabla} \times (\boldsymbol{v} \times \boldsymbol{B}) + \frac{2\alpha}{\pi} \frac{\mu_5}{\sigma} \boldsymbol{\nabla} \times \boldsymbol{B}. \tag{3.63}$$

This is supplemented by the Navier-Stokes equation for the velocity field of an incompressible fluid interacting with the hypermagnetic field

$$\frac{\partial \boldsymbol{v}}{\partial \tau} = \nu \boldsymbol{\nabla}^2 \boldsymbol{v} - (\boldsymbol{v} \cdot \boldsymbol{\nabla}) \boldsymbol{v} + \frac{(\boldsymbol{\nabla} \times \boldsymbol{B}) \times \boldsymbol{B}}{\rho + p}, \tag{3.64}$$

where ρ and p are respectively the energy and pressure density of the plasma. We use $p = \rho/3$ as the plasma evolves in a radiation dominated universe by definition. The kinematic viscosity

$$\nu \simeq \frac{c_\nu}{\alpha^2 \log(\alpha^{-1}) T_{\mathrm{pl}}^c} \tag{3.65}$$

is used with $c_\nu \approx 0.01$ for temperatures above the EW scale [144]. The typical *comoving* temperature of the plasma is obtained from Eq. (1.99) with $a_E = 1$ as

$$T_{\mathrm{pl}}^c = T_{\mathrm{rh}} \, a_{\mathrm{rh}} \simeq 0.4 \, T_{\mathrm{rh}}^{\mathrm{ins}} \left(\frac{T_{\mathrm{rh}}^{\mathrm{ins}}}{T_{\mathrm{rh}}} \right)^{\frac{1}{3}}. \tag{3.66}$$

Note that the viscous-damping term $\nu\boldsymbol{\nabla}^2\boldsymbol{v}$ is only present in (3.64) if the correlation length of the hypermagnetic field is larger than the mean free path of the particles in the plasma. This will always be fulfilled in our case. See Refs. [155, 156] for the damping term in the opposite regime.

The MHD equations (3.63) and (3.64) determine the coevolution of the hypermagnetic field and the fluid velocity of the thermal plasma. We are in particular interested in the evolution of the hypermagnetic helicity that is generated after inflation. By taking the time derivative of the hypermagnetic helicity defined analogously to Eq. (3.37) and using (3.62), we find

$$a^4\,\mathcal{G} = \lim_{V\to\infty}\frac{1}{V}\int_V d^3x\,\left(\frac{\boldsymbol{B}}{\sigma}\cdot\boldsymbol{\nabla}^2\boldsymbol{A} + \frac{2\alpha}{\pi}\frac{\mu_5}{\sigma}\boldsymbol{B}^2\right). \tag{3.67}$$

Let us for the moment ignore the μ_5-dependent terms in Eqs. (3.63) and (3.67). The hypermagnetic field can change due to magnetic diffusion and induction from the plasma motion, corresponding to the first and second term on the RHS of Eq. (3.63), respectively. Denoting the characteristic strength and correlation length of the magnetic field with B and ℓ_B, respectively, and the typical velocity of the plasma at the length scale ℓ_B with v, we can estimate $|\boldsymbol{\nabla}^2\boldsymbol{B}|/\sigma \sim B/(\ell_B^2\sigma)$ and $|\boldsymbol{\nabla}\times(\boldsymbol{v}\times\boldsymbol{B})| \sim Bv/\ell_B$. The *magnetic Reynolds number* balances these two quantities as

$$\mathcal{R}_m \equiv \sigma\,v\,\ell_B, \tag{3.68}$$

such that $\mathcal{R}_m > 1$ corresponds to the domination of magnetic induction over magnetic diffusion. Lastly, notice that Eq. (3.67) does not depend on the plasma velocity which has dropped out. Induction from the plasma motion therefore does not lead to the decay of the helicity. We then expect that if the magnetic Reynolds number is larger than unity and the dynamics of the hypermagnetic field is dominated by the plasma motion, the helicity is preserved.

We now need to estimate the typical velocity v in order to discuss this in more detail. To this end, we note that the last term on the RHS of Eq. (3.64) acts as a source term that sets the plasma into motion. A steady velocity is obtained by balancing the first and second term with this source term. The general solution should be computed numerically, but for asymptotic cases, when one term clearly dominates over the others in the equation, we can use the *electric Reynolds number* defined by

$$\mathcal{R}_e \equiv \frac{v\,\ell_B}{\nu}. \tag{3.69}$$

If $\mathcal{R}_e > 1$, there is an equipartition between the kinetic energy in the plasma and the magnetic energy. In the opposite case, when $\mathcal{R}_e < 1$, the kinetic energy and velocity are smaller than the magnetic energy.

The hierarchy between both Reynolds numbers is given by the magnetic Prandtl number which balances the viscous over the magnetic diffusion rate defined as

$$\mathcal{P}_m \equiv \frac{\mathcal{R}_m}{\mathcal{R}_e} = \sigma\nu \simeq 150, \tag{3.70}$$

where we used Eqs. (3.2), (3.65), (3.68) and (3.69). Thus the magnetic Reynolds number is much bigger than the electric one and given that, we can compute all quantities in the following two separate cases:

- *Viscous* regime: $\mathcal{R}_e < 1 < \mathcal{R}_m$

- *Turbulent* regime: $1 < \mathcal{R}_e < \mathcal{R}_m$

We omit the other cases, where $\mathcal{R}_m < 1$, since they would rule out the baryogenesis model, hence we are never interested in them.

In summary, the evolution of these two scaling regimes with respect to conformal time τ in a comoving reference frame is

$$\text{For} \quad \mathcal{R}_e < 1: \qquad B \propto \tau^{-\frac{1}{2}}, \qquad \ell_B \propto \tau, \qquad v \sim \frac{\ell_B B^2}{\nu \rho_{\text{pl}}^c} \propto \tau^0, \qquad (3.71\text{a})$$

$$\text{For} \quad \mathcal{R}_e > 1: \qquad B \propto \tau^{-\frac{1}{3}}, \qquad \ell_B \propto \tau^{\frac{2}{3}}, \qquad v \sim \frac{B}{\sqrt{\rho_{\text{pl}}^c}} \propto \tau^{-\frac{1}{3}}, \qquad (3.71\text{b})$$

where here ρ_{pl}^c is the *comoving* plasma energy density. Hence the following relation holds

$$\rho_{\text{pl}}^c = \rho_{\text{rh}}\, a_{\text{rh}}^4 = \left(\frac{a_E}{a_{\text{rh}}} \right)^3 \rho_\phi\, a_{\text{rh}}^4 \simeq 0.4\, \rho_\phi \left(\frac{T_{\text{rh}}^{\text{ins}}}{T_{\text{rh}}} \right)^{\frac{4}{3}}, \qquad (3.72)$$

where we used (1.99), our convention $a_E = 1$, and properties of the inflaton energy density, c.f. Eqs. (1.16) and (1.73): $\rho_\phi \simeq 3M_{\text{pl}}^2 H_E^2 \propto a^{-3}$. Inserting the latter relations for v in (3.68) for both cases and using Eqs (3.2), (3.65), (3.66), (3.72) as well as $B^2 \approx 2\rho_B$, we can estimate the magnetic Reynolds number at reheating as

$$\text{For} \quad \mathcal{R}_e^{\text{rh}} < 1 \quad \Rightarrow \quad \mathcal{R}_m^{\text{rh}} \approx 5.9 \cdot 10^{-6} \frac{\rho_B \ell_B^2}{H_E^2} \left(\frac{H_E}{10^{13}\,\text{GeV}} \right) \left(\frac{T_{\text{rh}}}{T_{\text{rh}}^{\text{ins}}} \right)^{\frac{2}{3}}, \qquad (3.73\text{a})$$

$$\text{For} \quad \mathcal{R}_e^{\text{rh}} > 1 \quad \Rightarrow \quad \mathcal{R}_m^{\text{rh}} \approx 1.1 \cdot 10^{-1} \frac{\sqrt{\rho_B}\ell_B}{H_E} \left(\frac{H_E}{10^{13}\,\text{GeV}} \right)^{\frac{1}{2}} \left(\frac{T_{\text{rh}}}{T_{\text{rh}}^{\text{ins}}} \right)^{\frac{1}{3}}, \qquad (3.73\text{b})$$

which, of course, depend on the electric Reynolds number at reheating $\mathcal{R}_e^{\text{rh}}$. Next, from (3.71), using (3.68) and (3.69), we see that in both regimes both Reynolds numbers grow with time according to the same scaling relations:

$$\text{For} \quad \mathcal{R}_e < 1: \qquad\qquad \mathcal{R}_m \propto \tau, \qquad\qquad \mathcal{R}_e \propto \tau, \qquad (3.74\text{a})$$
$$\text{For} \quad \mathcal{R}_e > 1: \qquad\qquad \mathcal{R}_m \propto \tau^{\frac{1}{3}}, \qquad\qquad \mathcal{R}_e \propto \tau^{\frac{1}{3}}. \qquad (3.74\text{b})$$

Hence, once the requirement $\mathcal{R}_m^{\text{rh}} > 1$ is reached, the magnetic Reynolds number remains greater than one, as long as there is a plasma filling the Universe. The conservation of helicity is due to an inverse cascade in which the helicity is transferred from smaller to larger scales, reflected in the growth of ℓ_B. Therefore, to guarantee the survival of the comoving helicity at the EWPT, it is enough to compute both Reynolds numbers after the end of inflation, at the reheating temperature, i.e. $\mathcal{R}_m^{\text{rh}}$ and $\mathcal{R}_e^{\text{rh}}$, allowing us to ignore the calculation of the plasma evolution at later times.

Now, all we have to know is the regime (viscous or turbulent) that applies at the reheating temperature. This is given by the value of $\mathcal{R}_e$ at that time. Inserting the above expressions for v, Eqs. (3.71a) and (3.71b), in the definition of $\mathcal{R}_e$ Eq. (3.69), and using again Eqs. (3.2), (3.65), (3.66), (3.72), we obtain at reheating

$$\text{For} \quad \mathcal{R}_e^{\text{rh}} < 1 \quad \Rightarrow \quad \mathcal{R}_e^{\text{rh}} \approx 2.5 \cdot 10^{-9} \frac{\rho_B\, \ell_B^2}{H_E^2} \left(\frac{H_E}{10^{13}\,\text{GeV}} \right) \left(\frac{T_{\text{rh}}}{T_{\text{rh}}^{\text{ins}}} \right)^{\frac{2}{3}}, \qquad (3.75\text{a})$$

$$\text{For} \quad \mathcal{R}_e^{\text{rh}} > 1 \quad \Rightarrow \quad \mathcal{R}_e^{\text{rh}} \approx 5.4 \cdot 10^{-5} \frac{\sqrt{\rho_B}\, \ell_B}{H_E} \left(\frac{H_E}{10^{13}\,\text{GeV}} \right)^{\frac{1}{2}} \left(\frac{T_{\text{rh}}}{T_{\text{rh}}^{\text{ins}}} \right)^{\frac{1}{3}}. \qquad (3.75\text{b})$$

To summarize, for a given theory one needs to first compute $\mathcal{R}_e^{\text{rh}}$ to find which regime of $\mathcal{R}_m^{\text{rh}}$ one shall use. Then, hypermagnetic fields generated during inflation will survive at later time thanks to its self-feeding convection if $\mathcal{R}_m^{\text{rh}} > 1$ since this condition implies that $\mathcal{R}_m > 1$ at later times. Note
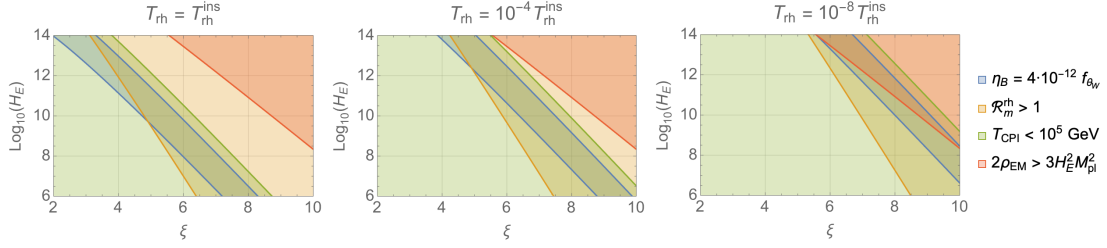
Figure 3.3. Baryon asymmetry (blue), self-consistency condition (red), and summary of the MHD (orange) and CPI (green) constraints in the case of model given by Eqs. (3.40) (no Schwinger effect). The panels displays results for various values of the reheating to instant reheating temperature ratio in the parameter space (ξ, H_E). The red region is excluded and the overlapping regions between blue, orange and green yield a successful BAU at EWPT.

that this mechanism applies, as it stands, to ordinary electromagnetic fields. Indeed, the difference between $U(1)_Y$ and $U(1)_{\rm EM}$ lies in the μ_5 component, that we neglected for the Reynolds number sketches. The effect of the axial current component is studied in the following section.

We display on Fig. 3.3 the allowed region where $\mathcal{R}_m > 1$ in orange for the model given by Eqs. (3.40).

3.3.3   The Chiral Plasma Instability

So far we have ignored the effect of the μ_5-dependent terms in Eqs. (3.63) and (3.67). In Sec. 3.1.1 we have seen that the number density of particles and their antiparticles is generated together with the helicity. Since these asymmetries are related to the helicity via the chiral anomaly, see Eq. (3.12), they can be transformed back into helical gauge fields, resulting in a cancellation of the total helicity, as we will now explain. We remind the reader that in this section all fields, observables and parameters are related to the hypercharge $U(1)_Y$ field.

Let us focus on the right-handed electron since it is the last species to come into chemical equilibrium, at temperatures $\sim 10^5\,\mathrm{GeV}$, and its asymmetry thus survives the longest. If we assume $T \gtrsim 10^5\,\mathrm{GeV}$ and drop the contribution from the Yukawa coupling, the anomaly equation (3.12) gives $\partial_\tau Q_{e_R} \propto -\partial_\tau \mathcal{H}$. From this, we see that if the asymmetry Q_{e_R} is driven to zero, a gauge field configuration with helicity $\mathcal{H} \sim Q_{e_R}/\alpha$ is generated. As before, denoting the characteristic magnetic field of this configuration with B and its characteristic size with ℓ_B, we can roughly estimate its helicity in terms of these quantities using (3.36) as $\mathcal{H} \sim \ell_B B^2$. The energy densities in right-handed electrons and the gauge field configuration are $\sim Q_{e_R}^2/T^2$ and $\sim B^2$, respectively. The gauge field configuration then has lower energy density than the equivalent asymmetry of right-handed electrons for [126]

$$\ell_B \gtrsim \frac{T^2}{\alpha Q_{e_R}}. \tag{3.76}$$

The formation of such an energetically favoured helicity configuration from an asymmetry is called the *chiral plasma instability* (CPI) [126, 157–162]. In Eq. (3.67) for the helicity evolution, it arises from the μ_5-dependent term. The fastest growing mode has a length scale saturating (3.76). Using that $\mu_5 \sim \mu_{e_R} \sim Q_{e_R}/T^2$ in kinetic equilibrium, if only right-handed electrons have an asymmetry, as well as Eqs. (3.67) and (3.76), we can estimate the time scale of the CPI as

$$\tau_{\rm CPI} \propto \frac{\sigma}{\alpha^2 \mu_5^2}\,, \tag{3.77}$$

where we have ignored all numerical prefactors. A more careful analysis of (3.63) and (3.67) in

momentum space shows that (3.77) also applies to the more general situation where several species have asymmetries and gives $\pi^2/2$ as a numerical prefactor [139].

Because $\partial_\tau Q_{e_R} \propto -\partial_\tau \mathcal{H}$, the CPI would convert the asymmetries back into helicity, approximately equal and opposite in sign to the helicity that is already present. This would thus strongly reduce the total helicity. In order to avoid this, we want to ensure that the CPI cannot occur before the electron Yukawa coupling reaches thermal equilibrium and all asymmetries are erased. To this end, we will require the time scale (3.77) for the CPI to be sufficiently long that the Universe has already cooled to temperatures below 10^5 GeV, before it can happen. To determine the parameter μ_5 in Eq. (3.77), let us consider temperatures somewhat above 10^5 GeV where all SM species, except for the right-handed electron, are in chemical equilibrium. Imposing constraints from sphalerons, Yukawa interactions and conserved quantities, the asymmetries and chemical potentials of all SM species can then be expressed in terms of those for the right-handed electron. Using (3.12), we get [139]

$$\mu_5 = -\alpha \frac{2133}{481\pi} \frac{\mathcal{H}}{T^2}. \tag{3.78}$$

On the other hand, at temperatures below 10^5 GeV, the electron Yukawa coupling is in thermal equilibrium and all asymmetries are erased. This gives $\mu_5 = 0$ and the CPI is no longer possible. Relating (3.77) to the temperature of the Universe at that time, and using the last equation, the CPI temperature writes

$$T_{\text{CPI}} \approx \frac{4\,\alpha^2 \mu_5^2}{\pi^2 \sigma H_E} T_{\text{rh}}^{\frac{1}{3}} (T_{\text{rh}}^{\text{ins}})^{\frac{2}{3}} \simeq (4 \cdot 10^{-7} \text{ GeV}) \; \frac{\mathcal{H}^2}{H_E^6} \left(\frac{H_E}{10^{13} \text{ GeV}} \right)^3 \left(\frac{T_{\text{rh}}}{T_{\text{rh}}^{\text{ins}}} \right)^2, \tag{3.79}$$

where in the second equality we used Eqs (1.97), (3.2), (3.66), (3.72), (3.78). Let us emphasize that the derivation of this condition had an approximate nature, and that a numerical MHD simulation taking into account the asymmetries would be required to establish the firmer condition for helicity survival in more detail.

To summarize in other words, the take-away message is that CPI can be avoided if we require that the CPI timescale is long enough to allow all fermionic states to come into chemical equilibrium (so that sphalerons can erase their corresponding asymmetries in particle number densities) before CPI can happen. The last fermion species to enter chemical equilibrium, through its Yukawa coupling with the left-handed electron e_L, is the right-handed electron, e_R, and it happens at the temperature $T \sim 10^5$ GeV. Indeed, when the fermionic states are in chemical equilibrium, their asymmetry is washed out through weak sphalerons and Yukawa couplings. Therefore the constraint $T_{\text{CPI}} \lesssim 10^5$ GeV guarantees that the CPI cannot occur before the smallest Yukawa coupling reaches equilibrium and all particle number density asymmetries are erased, thus preventing the cancellation of the helicity generated at the reheat temperature.

We display on Fig. 3.3 the allowed region where $T_{\text{CPI}} < 10^5$ GeV in green for the model given by Eqs. (3.40).

3.3.4 Primordial non-Gaussianity

Inflation predicts that the statistical distribution of primordial fluctuations is nearly Gaussian. Measuring deviations from a Gaussian distribution, i.e. non-Gaussian correlations in primordial fluctuations, is a powerful test of inflation. While the two-point function for $\delta\phi$ defines the power spectrum, the three-point correlation function encodes departures from Gaussianity [163, 164]. The magnitude of the three-point function is conventionally quantified using the parameters f_{NL}. Non-Gaussian effects from helical gauge fields are maximal when the three modes have comparable wavelength, the so-called equilateral form, which in the backreactionless case where gauge fields are

given by Eq. (3.34) is given by [165, 166]

$$f_{\mathrm{NL}}^{\mathrm{equil}} \simeq 4.7 \cdot 10^{-16} \frac{e^{6\pi\xi_*}}{\xi_*^9}, \tag{3.80}$$

where $\xi_* \equiv \xi(\phi_*)$. Current observational bounds on non-Gaussianity of CMB anisotropies lead to [167]

$$f_{\mathrm{NL}}^{\mathrm{equil}} = -26 \pm 47, \tag{3.81}$$

which translates from Eq. (3.80) into

$$\xi_{\mathrm{CMB}} \lesssim 2.54 \ (95\% \ \mathrm{C.L.}). \tag{3.82}$$

As pointed out in Refs. [165, 166], even if the non-backreaction conditions are satisfied, the coupling (3.48) can generate cosmological fluctuations in the inflation model. The equation for the fluctuation is model dependent, and is found by replacing the background field $\phi(t)$ by Eq. (1.78), see Sec. 1.2.3. Hence we will come back on this topic when discussing specific baryogenesis scenarios, see Chaps. 5 and 6.

For the specific model given by Eqs. (3.40), where ξ is given by (3.26), we can use the scaling relation

$$\frac{\xi}{\xi_*} = \sqrt{\frac{\epsilon(\phi_E)}{\epsilon(\phi_*)}} = \sqrt{\frac{1}{\epsilon(\phi_*)}} \tag{3.83}$$

together with the value (1.91) given by Planck measurement. It yields $\xi \lesssim 38$, a bound already satisfied by other constraints, e.g. condition (3.47).

3.3.5   The baryon isocurvature perturbation

Many models of baryogenesis using (hyper)magnetic fields try to simultaneously explain the origin of the large scale, intergalactic, magnetic fields (IMF) measured today by the Fermi satellite [168–170]. They all face a balance problem when addressing this issue.

While maximally helical fields can indeed generate the BAU without explaining the observed IMF, they would suffer from baryon overproduction should they try to accommodate IMF. In the case of a mixture of helical and non-helical fields, the baryogenesis is less effective so that stronger hypermagnetic fields are needed to explain the present BAU, and hence, in principle, they could meet the lower bound from the IMF observations.

However, it has been recently shown that such models are inconsistent with the baryon isocurvature perturbations, that are constrained by the observations of cosmic microwave background on large scales [171]. In particular, it was pointed out that the baryon isocurvature perturbations, at a scale larger than the neutron diffusion scale at the BBN epoch, is constrained by the deuterium overproduction due to the second-order effect [172]. This translates into an upper bound on the volume average of the baryon isocurvature perturbation, as

$$\overline{\mathcal{S}^2}_{\mathrm{B,BBN}} < 0.016 \quad (2\sigma). \tag{3.84}$$

It was shown that, regardless of their helicity properties, hypermagnetic fields with too large strength and coherence length are not allowed before the EWPT [171]. Still baryogenesis from the hypermagnetic helicity decay can be responsible for the present BAU, but additional magnetogenesis, or an unknown mechanism of the magnetic field amplification after the EWPT, is needed to fit the IMF observations. However the constraints become less severe for more helical hypermagnetic fields. Since in our model the magnetic field produced at the end of inflation is maximally helical,

we should be safe from this constraint. In the following we sketch a demonstration that the bound (3.84) is indeed widely satisfied in the backreactionless model presented in Sec. 3.2.

Baryon isocurvature perturbations can be generated by the presence of strong gauge fields [171]. To be conservative, in this section we will consider the case where the generated gauge fields are as strong as possible. Hence we neglect the Schwinger effect, see Chap. 4, and consider the backreactionless case where the plasma macroscopic quantities are given by Eqs. (3.40). Borrowing the notation from [171], we have the symmetric and antisymmetric combinations, $S(k) = (|A_+(k)|^2 + |A_-(k)|^2)/2$ and $A(k) = (|A_+(k)|^2 - |A_-(k)|^2)/2$. For the case of maximally helical gauge fields one obtains

$$S(k) \simeq A(k) \simeq \frac{|A_+|^2}{2} \simeq \frac{1}{4k_\lambda} \left(\frac{k}{k_\lambda}\right)^{-\frac{1}{2}} \frac{e^{2\pi\xi}}{\xi} \exp\left(-4\sqrt{\frac{k}{k_\lambda}}\right), \tag{3.85}$$

where we are choosing e.g. $A_+(k)$ as the amplified mode, and (3.34) was used together with the definition $k_\lambda = a_E H_E/2\xi \simeq 10^{12}$ GeV, which corresponds to the spectrum peak of A_+. Writing $B^2 \simeq 2\rho_B$ in term of k_λ, and using (3.40d), we obtain a relation for the spectrum given by [171]

$$A(k) \simeq \frac{1024\,\pi^2}{315} \frac{B^2}{k_\lambda^5} \left(\frac{k}{k_\lambda}\right)^{-\frac{1}{2}} \exp\left(-4\sqrt{\frac{k}{k_\lambda}}\right). \tag{3.86}$$

It may be interesting to note that, in this notation, the magnetic field and the helicity are written as

$$B^2 \simeq \frac{1}{4\pi^2} \frac{315}{1024} \frac{e^{2\pi\xi}}{2\xi} k_\lambda^4, \qquad \mathcal{H} \simeq \frac{2}{7} \frac{B^2}{k_\lambda}. \tag{3.87}$$

From this we can estimate the baryon isocurvature perturbation at the BBN as

$$\overline{\mathcal{S}^2}_{\text{B,BBN}} \simeq \frac{7\sqrt{\pi}}{20\sqrt{3}} \left(\frac{k_d}{k_\lambda}\right)^3 \left(\frac{k_\lambda}{k_\lambda^{\text{EWPT}}}\right)^3 + \mathcal{O}\left(\frac{k_d}{k_\lambda}\right)^5, \tag{3.88}$$

where k_d is the comoving neutron diffusion scale at the BBN, $k_d^{-1} \simeq 0.0025$ pc. From the expansion ratio $k_d/k_\lambda \sim 10^{-42}$, we can see that Eq. (3.88) is suppressed provided that $k_\lambda/k_\lambda^{\text{EWPT}}$ is not too big, which we will next demonstrate.

Eq. (3.88) should be evaluated at the time of baryon asymmetry production, at $T_{\text{EWPT}} \simeq 135$ GeV, hence the rescaling for the wave number k_λ. At first glance, this rescaling could appear to be exactly one since k_λ is comoving, but because of the peculiar dynamics of the plasma, described by the MHD equations, comoving quantities do scale with the expansion of the Universe after reheating, as already stated in Sec. 3.3.2.

We shall now study how the comoving coherence length scales until the EWPT. Every plasma quantity (field amplitude, correlation length, wave number) evolves adiabatically from reheating until the eddy turnover temperature $T_t \simeq v T_{\text{rh}}$ where v is the typical bulk velocity of the plasma. For $T < T_t$ the scaling regime depends on the value of the electric Reynolds number at the end of inflation. The velocity of the plasma is

$$\mathcal{R}_e < 1 \quad \Rightarrow \quad v \approx 2.9 \cdot 10^{-10} \frac{\ell_B \rho_B}{H_E^3} \left(\frac{H_E}{10^{13}\,\text{GeV}}\right)^{\frac{3}{2}} \left(\frac{T_{\text{rh}}}{T_{\text{rh}}^{\text{ins}}}\right), \tag{3.89a}$$

$$\mathcal{R}_e > 1 \quad \Rightarrow \quad v \approx 5.3 \cdot 10^{-6} \frac{\sqrt{\rho_B}}{H_E^2} \left(\frac{H_E}{10^{13}\,\text{GeV}}\right) \left(\frac{T_{\text{rh}}}{T_{\text{rh}}^{\text{ins}}}\right)^{\frac{2}{3}}. \tag{3.89b}$$

For $\mathcal{R}_e^{\text{rh}} < 1$, as $\mathcal{R}_e$ grows with time, we eventually reach the point where it becomes one, at

temperature [139]

$$T_1 \equiv T(\mathcal{R}_e = 1) = \mathcal{R}_e^{\mathrm{rh}} \, T_t. \tag{3.90}$$

Once $\mathcal{R}_e > 1$, the scaling regime for comoving quantities becomes (3.71b) until recombination.

In summary, the magnetic energy and correlation length scale adiabatically until the eddy turnover temperature T_t, then they scale according to (3.71a) until $\mathcal{R}_e = 1$, where the regime changes to (3.71b) until recombination. However, we compute the scaling only until $T_{\mathrm{EWPT}} = 135$ GeV, since the comparison with the neutron diffusion scale must be done at the EWPT temperature [171]. This yields a total dilution factor for comoving quantities as

$$\frac{B^{\mathrm{EWPT}}}{B^{\mathrm{rh}}} = \left(\frac{T_{\mathrm{EWPT}}}{T_1}\right)^{\frac{1}{3}} \left(\frac{T_1}{T_t}\right)^{\frac{1}{2}}, \tag{3.91a}$$

$$\frac{\ell_B^{\mathrm{EWPT}}}{\ell_B^{\mathrm{rh}}} = \left(\frac{T_{\mathrm{EWPT}}}{T_1}\right)^{-\frac{2}{3}} \left(\frac{T_1}{T_t}\right)^{-1}. \tag{3.91b}$$

We stress that T_t and T_1 depend on v, which in turn depends on $\ell_B \sim k^{-1}$ and ρ_B. For values of the parameters space yielding the correct BAU, e.g. for $\xi \sim \mathcal{O}(1)$, $H_E \sim 10^{6\text{-}14}$ and $T_{\mathrm{rh}} \sim 1$ - $10^{-8} \, T_{\mathrm{rh}}^{\mathrm{ins}}$, see Fig. 3.2, we find that

$$\frac{B^{\mathrm{EWPT}}}{B^{\mathrm{rh}}} \sim 10^{-6} \text{ - } 10^3, \qquad\qquad \frac{\ell_B^{\mathrm{EWPT}}}{\ell_B^{\mathrm{rh}}} \sim 10^{-4} \text{ - } 10^7. \tag{3.92}$$

Going back to the baryon isocurvature perturbation (3.88), we hence have

$$\left(\frac{k_\lambda}{k_\lambda^{\mathrm{EWPT}}}\right)^3 \propto \left(\frac{T_{\mathrm{rh}}}{T_{\mathrm{rh}}^{\mathrm{ins}}}\right)^{-4}, \qquad \left(\frac{k_\lambda}{k_\lambda^{\mathrm{EWPT}}}\right)^3 \gg 10^{-22}, \tag{3.93}$$

which therefore implies an exceedingly small value for the observable $\overline{\mathcal{S}^2}_{\mathrm{B,BBN}}$. This result also holds for the case where the Schwinger effect is considered, as in this case gauge fields are much weaker than in the backreactionless case studied above, and so their contribution to $\overline{\mathcal{S}^2}_{\mathrm{B,BBN}}$ is expected to be much smaller.

Chapter 4

The Schwinger effect

In the last chapter, we have demonstrated that the inflaton coupling to the Chern-Simons density gives rise to the production of helical hypermagnetic fields, which can then survive until the EWPT and trigger the BAU. However, in the presence of strong gauge fields, light fermions charged under the gauge group are produced by the backreaction of gauge fields that source the fermions EoM [173, 174]. The corresponding currents can then, in turn, backreact on the produced gauge fields. This phenomenon is called the *Schwinger effect* (see e.g. Ref. [175]).

The backreaction of fermion currents on the produced gauge fields acts as a damping force in the explosive production of helical gauge fields, and many of the conclusions from the gauge field production should be revised in the presence of the Schwinger effect[24], in particular those concerning the gauge preheating capabilities and the baryogenesis mechanism, see Sec. 4.4.

In this chapter, we will study the effect of the Schwinger particle production on the helical hypermagnetic fields produced at the end of inflation. In order to consider the backreaction of the produced gauge fields on the inflationary equations of motion, and that of the Schwinger effect on the gauge field production, we will use numerical methods, in particular, the fourth order Runge-Kutta (RK4) algorithm. Our numerical results are validated, as they overlap with some recent semianalytical methods, and the gradient expansion formalism of Refs. [176–179]. Our general finding is that the gauge field production is much less explosive than in the absence of the Schwinger effect, which will jeopardize the conclusions concerning the possibility of gauge preheating, although they leave an open window for baryogenesis.

The content of this chapter was the subject of a publication [180].

4.1 Theoretical grounds

To model the Schwinger effect in a simple way, we take back the action (3.20) in which we include the interaction of fermionic currents

$$S \supset \int d^4x \, \sqrt{-g} \, i \, \bar{\psi} \gamma^\mu D_\mu \psi, \tag{4.1}$$

corresponding to hypercharge Y fermions, with the hypercharge fields encoded in the covariant derivative D_μ, see Eq. (2.80). All gauge field quantities are $U(1)$ hypercharge fields, i.e. $\boldsymbol{A}_Y$, $\boldsymbol{E}_Y$, $\boldsymbol{B}_Y$, etc. To make the notation lighter, we drop the index Y as there will be no ordinary electromagnetic fields in this chapter.

Due to this coupling, massless hypercharged fermions are continuously produced during inflation. They are massless as long as the EW symmetry remains intact and thus contribute to the

---

[24]One possible way out is if there are no light charged fields when gauge fields are produced.

energy density of relativistic radiation as

$$\rho_\psi = \lim_{V \to \infty} \frac{\sigma}{V} \int_V d^3x \, \frac{\langle \boldsymbol{A} \cdot \boldsymbol{E} \rangle}{a^4} = \frac{\sigma}{a^4} \int_{k_{\min}}^{k_c} dk \, \frac{k^2}{2\pi^2} \frac{d}{d\tau} \left(|A_+|^2 + |A_-|^2 \right),$$ (4.2)

where σ is the generalized conductivity, see Eqs. (4.7) and (4.8). In the second step we use the $\boldsymbol{A}$ quantization given by Eq. (3.27).

It has been shown in Ref. [177] that the fermion energy density can easily dominate the radiation energy density at the end of inflation. On the other hand, if the gauge share dominates at least by 80%, the Universe will reheat before the perturbative decay of the inflaton [181], a phenomenon called *gauge preheating*, see Sec. 1.2.4. Thus, in this chapter we will analyze all inflaton, gauge, and fermion energy contributions and compare them to figure out under which conditions gauge preheating and barygenesis can happen.

Notice that, similarly to ρ_E, ρ_B, $\mathcal{H}$ and $\mathcal{G}$, ρ_ψ is a *physical* quantity.

4.1.1   Gauge equation of motion

The system of EoM are exactly the ones from last chapter, i.e. Eqs. (3.22), with the exception of an added current

$$j^\mu = (\rho_c, \boldsymbol{J}) = \sum_\psi ig' Y_\psi \, \bar{\psi} \gamma^\mu \psi$$ (4.3)

such that (3.22b) becomes

$$\left(\frac{\partial^2}{\partial \tau^2} - \nabla^2 - \frac{a \, \dot{\phi}}{f_\phi} \, \boldsymbol{\nabla} \times \right) \boldsymbol{A} = \boldsymbol{J}.$$ (4.4)

We now assume that the Universe does not initially contain any asymmetry of charged particles and that these ones are produced only later in particle-antiparticle pairs. Therefore, we initially set the charge density to zero, $\rho_c = 0$.

The current $\boldsymbol{J}$ is given by the Ohm's law

$$\boldsymbol{J} = \sigma \boldsymbol{E} = -\sigma \frac{\partial \boldsymbol{A}}{\partial \tau}.$$ (4.5)

It implies that when the Schwinger effect is taken into account, Eq. (3.30) becomes

$$A_\lambda'' + \sigma A_\lambda' + k \left(k - \lambda \frac{a \, \dot{\phi}}{f_\phi} \right) A_\lambda = 0.$$ (4.6)

As in this chapter we will have to solve the coupled differential system of the fields (ϕ, A_λ), we kept $\dot{\phi}$ explicitly in the above equation. Of course, it is always possible to define a time-dependent instability parameter with the definition (3.24) but we would lose clarity by hiding the variables in this way. In this chapter we will nevertheless use ξ but only for comparison purposes.

In the case of one Dirac fermion f with mass m_f and charge Q_f under a $U(1)$ group with coupling g, the conductivity can be written as[25] [173]

$$\sigma_f = \frac{|g \, Q_f|^3}{6\pi^2} \frac{a}{H} \, \sqrt{2\rho_B} \, \coth\left(\pi \sqrt{\frac{\rho_B}{\rho_E}} \right) \exp\left(-\frac{\pi m_f^2}{\sqrt{2\rho_E} \, |g \, Q_f|} \right).$$ (4.7)

---

[25]As the conductivity σ relates $\boldsymbol{J}$ and $\boldsymbol{E}$ in (4.5), it is a comoving quantity, i.e. it scales with the Universe expansion. Our definition differs from the one in [177, 178] where the authors used a physical conductivity that we will denote $\hat{\sigma}$ in this chapter, their relation being $\sigma = a \, \hat{\sigma}$.

This conductivity is to be distinguished from the conductivity we defined in Eq. (3.2), as the latter is the conductivity of a thermal plasma after reheating, in a radiation dominated universe, while the above is the conductivity at the end of inflation, before the reheating, produced by fermion pair formation from the magnetic field.

This estimation is valid in the case of collinear electric and magnetic fields, an assumption that we have numerically checked by verifying from Eq. (3.42) that $\cos\theta \simeq 1$. The total conductivity in the plasma is the sum on every SM species involved. Also the electric and magnetic fields are assumed to be slowly varying, as we expect the hypercharge gauge field to reach a stationary configuration, where the tachyonic instability and the induced current balance each other. We have verified from the numerical simulation that this is indeed the case.

The Schwinger effect effectively depends on the masses configuration. For very massive particles it can be avoided while it is maximal for massless ones, see hereafter. Then, when only the first two generations are considered, there is just a factor 3/2 difference with the full SM. We checked that such an $\mathcal{O}(1)$ factor does not make any difference to the final result, since the (hyper)magnetic field production with or without Schwinger effect can vary by orders of magnitude.

In Sec. 3.2 we have shown that the electromagnetic energy density grows tremendously during inflation, which will imply a growth of σ with time. This yields a nontrivial integro-differential system as the damping term grows with the magnetic energy and hence backreacts on the amount of produced electric/magnetic fields. Therefore, we aim to solve this setup of the Schwinger effect numerically.

4.1.2 Conductivity and the Higgs VEV

Concerning the Higgs vacuum expectation value, there are two possibilities during the inflationary period:

i) The first possibility, which we will use in this chapter for the numerical simulations, is that $\langle h \rangle = 0$, and so the electroweak symmetry is unbroken during the inflationary period. In order to ensure unbroken electroweak symmetry, and hence massless SM fermions, which all contribute to the conductivity (4.7), we assume that the SM Higgs field h remains stabilized at the origin in field space by a large mass term throughout the inflationary period. Such a large mass can e.g. be induced by a nonminimal coupling to the Ricci curvature scalar as $\mathcal{L} = \frac{1}{2}\xi h^2 R$ with $\xi > 3/16$ (see e.g. Ref. [26]). Hence, we get

$$\sigma \simeq Z_Y \, \frac{a}{H} \, \sqrt{2\rho_B} \, \coth\left(\pi\sqrt{\frac{\rho_B}{\rho_E}}\right). \tag{4.8}$$

where we have defined

$$Z \equiv \sum_f \frac{|g\,Q_f|^3}{6\pi^2}. \tag{4.9}$$

Thus for the hypercharge group this yields

$$Z_Y = \frac{41\,g'^3}{72\,\pi^2}, \tag{4.10}$$

where $g' \simeq 0.4$ is computed at the characteristic scale $\mu \simeq \left(\langle\boldsymbol{E}\rangle^2 + \langle\boldsymbol{B}\rangle^2\right)^{\frac{1}{4}}$ where the Schwinger effect takes place [178].

ii) The second possibility is that the electroweak symmetry is broken during the inflationary period. In this case after ΔN e-folds of inflation, there is a Gaussian distribution of values of the Higgs field with zero mean and variance $\langle h^2 \rangle = H^2 \Delta N/(4\pi^2)$ with probability $P(h, \Delta N) \propto$

$\exp(-\frac{1}{2}\frac{h^2}{\langle h^2 \rangle})$ dominated by the values $h \lesssim \sqrt{\langle h^2 \rangle}$, see Ref. [26][26]. In this case, the electroweak symmetry is broken and the hypercharge field strength is projected onto the electromagnetic field strength with a coupling to the inflaton given by $f_\phi / \cos^2 \theta_W$, see Eq. (2.90c). Now the conductivity for the hypermagnetic field in Eq. (4.7) should be replaced by a similar expression for the magnetic field, with the replacement $|g'Y| \to |eQ|$. The condition for a fermion f to contribute to the magnetic conductivity $\pi m_f^2 < \sqrt{2\rho_E}\,|eQ_f|$ translates into the condition, for the fermion Yukawa coupling y_f,

$$y_f \lesssim 0.45 \left(\frac{\rho_E}{H^4} \right)^{1/4} \sqrt{|Q_f|}, \tag{4.11}$$

where we used Eqs. (2.81), We have computed all couplings at the characteristic scale $\mu \simeq \left(\langle \boldsymbol{E} \rangle^2 + \langle \boldsymbol{B} \rangle^2 \right)^{\frac{1}{4}}$ where the Schwinger effect takes place. If the three generations of fermions satisfy the above condition then the conductivity for the magnetic field is given by Eq. (4.8) with the replacement $Z_Y \to Z_{\text{EM}}$ where

$$Z_{\text{EM}} = \frac{e^3}{\pi^2}. \tag{4.12}$$

We have checked that, in this case, the results for $f_\phi \lesssim 0.2 M_{\text{pl}}$ are consistent with all three generation fermions contributing to the magnetic conductivity. For $f_\phi \gtrsim 0.2 M_{\text{pl}}$ only the top quark does not contribute. Given that $Z_Y \simeq 0.37\pi^2$ while $Z_{\text{EM}} \simeq 0.36\pi^2$, at the scales where the Schwinger effect takes place, we have found that the results in this second case are qualitatively similar to those for the first case discussed here, see Fig. 4.1. Hence, the results from this chapter are transferable to inflation theories in the broken phase, see Chaps. 5 and 6.

4.1.3   The gauge vacuum

Solving (4.6) is very similar to what we did in Sec. 3.2.1. However, the introduction of non-zero conductivity has implication on the gauge vacuum of the theory, as we will see now.

At very early times, when $|a\dot\phi| \ll k f_\phi$, the modes are in their Bunch-Davies (BD) vacuum given by Eq. (3.32). Initially, we can consider all the modes in the BD vacuum (which would be possible by initializing the numerical simulation such that $a_0 \ll k_0/H_0$). In that case, since $|A_+| = |A_-|$, the fields $\boldsymbol{E}$ and $\boldsymbol{B}$ are plane waves, perpendicular to each other, as $\mathcal{G} = 0$ in (3.42) yields $\cos\theta = 0$. Therefore, there is no Schwinger effect and $\sigma = 0$.

It has recently been shown that in the presence of the conductivity σ, the BD vacuum amplitude of the modes that are still in the vacuum get damped by the ones that left it, Ref. [177]. Indeed, let us consider we are at a time a_* where modes $k > k_*$ are still in the BD vacuum, while modes $k < k_*$ were amplified by both tachyonic and parametric instabilities from Eq. (4.6). Then, the equation of motion for modes such that $|a_*\dot\phi(\tau_*)| \ll k f_\phi$ does not reduce to a plane wave in the presence of a non-zero σ, but instead to $A_\lambda'' + \sigma A_\lambda' + k^2 A_\lambda = 0$, and Eq. (3.32) is not a solution anymore. To derive the generalized BD vacuum, we write the gauge equation of motion (4.6), in cosmic time, as

$$\ddot{A}_\lambda + (\hat\sigma + H)\, \dot{A}_\lambda + \frac{k}{a} \left(\frac{k}{a} - \lambda \frac{\dot\phi}{f_\phi} \right) A_\lambda = 0, \tag{4.13}$$

---

[26]The SM Higgs potential is still unstable at a value of the Higgs field $h = h_I \simeq 10^{11}$ GeV and the condition for $P(h_I, \Delta N) < e^{-3\Delta N}$ (so that it is unlikely to find the Higgs away from its EW vacuum in any of the $e^{3\Delta N}$ causally disconnected regions formed during inflation) implies $H_E < \sqrt{2/3}\,\pi h_I/\Delta N$, a condition that is not fulfilled by any of the models of inflation we have considered. Therefore this possibility would require stabilization of the Higgs potential by some new physics.

where we used the identity (1.40), and perform the transformation $A_\lambda = \sqrt{\Delta}\,\mathcal{A}_\lambda$ with [177]

$$\Delta(t) = \exp\left(-\int_{-\infty}^{t} \hat{\sigma}(t')\,dt'\right). \tag{4.14}$$

We recall that we have defined $\hat{\sigma} = \sigma/a$ as the physical conductivity in footnote 25. The above equation hence becomes

$$\mathcal{A}_\lambda'' + \left[\frac{k}{a}\left(\frac{k}{a} - \lambda\frac{\dot{\phi}}{f_\phi}\right) - \frac{\dot{\hat{\sigma}}}{2} - \frac{\hat{\sigma}^2}{4} - \frac{H\hat{\sigma}}{2}\right] a^2 \mathcal{A}_\lambda = 0, \tag{4.15}$$

where we used the fact that $\dot{\Delta}(t) = -\hat{\sigma}(t)\Delta(t)$. A mode crosses the horizon when the expression in the square brackets vanishes for the first time at least for one polarization, at $k = k_c$. The modes in the vacuum are then characterized by $k \gg k_c$. This yields the momentum of the mode that crosses the horizon at time t, namely the cutoff of the integrals, as

$$k_c = \left|\frac{a\dot{\phi}}{2f_\phi}\right| + \sqrt{\left(\frac{a\dot{\phi}}{2f_\phi}\right)^2 + \frac{a^2}{2}\left[\dot{\hat{\sigma}} + \hat{\sigma}\left(\frac{\hat{\sigma}}{2} + H\right)\right]}. \tag{4.16}$$

Notice that for $\sigma = 0$ we recover Eq. (3.33) with ξ given by (3.24).

Deep inside the horizon, when the first term in square brackets of (4.15) dominates, the solution for $\mathcal{A}_\lambda$ must satisfy the BD condition (3.32). As we have seen, in the presence of finite conductivity, this equation does not fully describe the gauge-field mode function inside the horizon, as the damped BD condition includes an exponential damping factor

$$A_\lambda(\tau, k) = \sqrt{\frac{\Delta(t)}{2k}} e^{-ik\tau} \qquad (\tau \to -\infty). \tag{4.17}$$

The bottom line of this section is that the modes, still in their BD vacuum, see their amplitudes damped because of the effect of the modes that left their vacuum earlier and participate in the equations of motion (3.44) and (4.6). The parameter Δ was first introduced in the context of the gradient expansion formalism in Ref. [177], where it was dynamically solved, while in Ref. [178] it was also considered as a free parameter and validated the corresponding procedure by numerical calculations. In order to compare with results from the gradient expansion formalism in configuration space, we will also both compute Δ numerically and consider it as a free parameter, although our final results will be based upon the dynamical calculation of Δ.

4.2 Analytical estimates

With the introduction of the operator (4.1), the production of the gauge fields and fermions cannot be treated independently. Parallel electric and magnetic fields, created via the tachyonic instability, necessarily lead to chiral fermion production by deforming the fermion energy levels to discrete Landau levels. Populating the lowest Landau level yields the chiral asymmetry, as we have seen in Sec. 2.3.6, while the higher levels are populated through pair-production, the analog to the Schwinger effect [182, 183], hence the actual terminology for this backreaction effect.

In Ref. [173], the induced current was calculated by solving the equations of motion for the fermions in the presence of a gauge field background. Taking into account this backreaction, the authors derived two analytical estimates for the Schwinger effect, the *equilibrium estimate* and the *maximal estimate*, which lie significantly below the results obtained in the absence of fermions, i.e. Eqs. (3.40). Both regimes follow different strategies: in the maximal estimate all quantities are

capped by other relations, that still depend on the parameter ξ, whereas in the equilibrium case the exponential relations from the previous section stay with the counterpart of the substitution (4.18) on ξ.

Besides, in Refs. [176–178], the same computation was done using the *gradient expansion formalism*, a method that describes the time evolution of a set of vacuum expectation values for bilinear hypermagnetic functions in position space. Thus, we will compare our numerical calculations with these three (semi)analytical results that we will first present in more details.

4.2.1   Equilibrium estimate

The Schwinger effect has been proven to roughly be encoded into a redefinition of the ξ parameter, $\xi \to \xi_{\text{eff}}$, as [173]

$$\xi_{\text{eff}} = \xi - \Delta\xi, \qquad \Delta\xi = \frac{Z}{2} \coth\left(\pi \frac{|B|}{|E|}\right) \frac{|E|}{H^2},\qquad (4.18)$$

where Z is given by (4.9) and where we defined

$$|E| \equiv \lim_{V\to\infty} \frac{1}{V} \int_V d^3x \ \sqrt{\langle \boldsymbol{E^2}\rangle} \simeq \sqrt{2\rho_E}, \qquad |B| \equiv \lim_{V\to\infty} \frac{1}{V} \int_V d^3x \ \sqrt{\langle \boldsymbol{B^2}\rangle} \simeq \sqrt{2\rho_B}. \qquad (4.19)$$

Assuming that the energy densities are given by the exponential case (3.40), the correction becomes significant, $\Delta\xi/\xi \gtrsim 0.1$, for $\xi \gtrsim 3.7$, which corresponds to $f_\phi \lesssim 0.2\, M_{\text{pl}}$ in the approximation (3.35). Hence for $\xi \gtrsim 3.7$ the Schwinger effect must be taken into account, and the amplitudes of the gauge fields in equilibrium must satisfy the equation

$$\xi_{\text{eff}} H |E|\, |B| - H(|E|^2 + |B|^2) = \frac{\dot\rho_{\text{EM}}}{2} = 0. \qquad (4.20)$$

In the case of the equilibrium estimate, we take into account the backreaction of the chiral fermions on the gauge fields by just replacing the parameter ξ with the effective one given by (4.18) in the backreactionless solutions (3.40). Using (3.39c), (3.39d) and (4.19), Eq. (4.18) becomes

$$\frac{63\, Z^2}{2^{17}\pi^2} \ \frac{e^{2\pi\xi_{\text{eq}}}}{\xi_{\text{eq}}^3} = (\xi - \xi_{\text{eq}})^2 \ \tanh^2\left(\sqrt{\frac{5}{4}}\, \frac{\pi}{\xi_{\text{eq}}}\right), \qquad (4.21)$$

which is only valid during the last *e*-folds of inflation since we used the backreactionless solutions (3.40) (which are self-consistently found in this approximation). To make explicit which case we are handling, we chose to label the effective parameter as ξ_{eq}. The solution of Eq. (4.21) provides the function $\xi_{\text{eq}} = \xi_{\text{eq}}(\xi)$ and, using (3.24), we can obtain ξ_{eq} as a function of f_ϕ. We show its behavior on Fig. 4.1.

Next, the MHD quantities (3.40) are calculated in the same way as in the case without considering the Schwinger effect, but with the replacement $\xi \to \xi_{\text{eq}}$, hence

$$\mathcal{H}_{\text{eq}} = \mathcal{H}(\xi_{\text{eq}}), \qquad \mathcal{G}_{\text{eq}} = \mathcal{G}(\xi_{\text{eq}}), \qquad \rho_{B/E}^{\text{eq}} = \rho_{B/E}(\xi_{\text{eq}}), \qquad \ell_B^{\text{eq}} = \ell_B(\xi_{\text{eq}}). \qquad (4.22)$$

These equilibrium estimates are shown with a purple line in the plots of Fig. 4.3.

4.2.2   Maximal estimate

In this case we assume the exponential behaviors of the backreactionless solutions (3.40) to be valid until they saturate the maximal value that we will display hereafter. We numerically determine the value of crossing, which happens for $\xi \simeq 4.4$-4.7 depending on each quantity, corresponding to $f_\phi \simeq 0.15\, M_{\text{pl}}$. However, as we just saw, for such value the Schwinger effect can no longer be
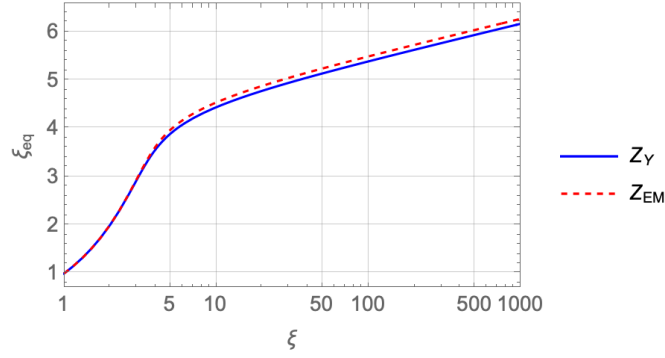
Figure 4.1. In the Schwinger equilibrium estimate, the instability parameter ξ is replaced with an effective one that mimic the fermion backreaction on the gauge fields. We display their relation in the above plot for both hypercharge and electromagnetism groups.

neglected, so there remains in this process a gray area of uncertainty as to the exact transition between the two regimes.

The maximum electric and magnetic energy density can be estimated as the solution of Eq. (4.20). This replacement yields an equation relating the $|E|$ and $|B|$ fields that can be solved analytically. We then choose, as definition of our maximal estimate, the solution $(|E|,|B|)$ of (4.20) that maximizes the product $|E| \cdot |B|$ [27]. We assume $|B| \gtrsim |E|$ such that the hyperbolic cotangent in (4.18) is unity, and then we can write, combining the latter with (4.20),

$$|E|^2 + |B|^2 \simeq \left(\xi - \frac{Z}{2} \frac{|E|}{H^2} \right) |E| \, |B|. \tag{4.23}$$

Under the aforementioned constraint this yields, for $\xi \gg 1$

$$\rho_{\max}^E \simeq \frac{8}{9} \frac{\xi^2 H_E^4}{Z^2}, \tag{4.24a}$$

$$\rho_{\max}^B \simeq \frac{8}{81} \frac{\xi^4 H_E^4}{Z^2}, \tag{4.24b}$$

$$\mathcal{H}_{\max} = \frac{2\mathcal{G}_{\max}}{3H_E} \simeq \frac{32}{81} \frac{\xi^3 H_E^3}{Z^2}. \tag{4.24c}$$

In the numerical calculations, we use the exact (analytical) solutions. In the computation of $\mathcal{G}_{\max}$ we maximized the product by assuming a collinear configuration of $\boldsymbol{E}$ and $\boldsymbol{B}$. We can see that

$$\rho_{\max}^B \simeq \frac{\xi^2}{9} \rho_{\max}^E \tag{4.25}$$

hence for $\xi \gtrsim 3$, our approximation $|B| \gtrsim |E|$ is self-consistent. The maximal estimates for the quantities $\rho_{\max}^E$, $\rho_{\max}^B$, $\mathcal{H}_{\max}$ and $\mathcal{G}_{\max}$ are shown with a pink line in the plots of Fig. 4.3.

Finally, combining (3.39a) and (3.39e), and assuming maximally helical magnetic fields, we get

---

[27]Notice that our definition of maximal estimate departs from that used in Ref. [173], where separate maximal conditions to the configurations for the fields E and B (corresponding to absolute maximal values independently reached by the configurations E and B) are imposed, so that their corresponding partners do not satisfy Eq. (4.20). Conversely, our criterium of maximizing the helicity guarantees that our solution satisfies Eq. (4.20).

for the correlation length (still for large ξ)

$$\ell_B^{\max} = \pi \, \frac{\mathcal{H}_{\max}}{\rho_B^{\max}} \simeq \frac{4\,\pi}{\xi H_E}, \tag{4.26}$$

which does not depend on Z (even for the exact solution).

Note that in the maximal estimate the consistency condition from Sec. 3.2.3 can be reinterpreted as follows. Combining Eqs. (4.24), we obtain, for large ξ,

$$6\,\rho_{\mathrm{EM}}^{\max} \simeq \xi \, |\langle \boldsymbol{E} \cdot \boldsymbol{B} \rangle|_{\max}. \tag{4.27}$$

Hence, in the maximal estimate, imposing the condition $|\mathcal{G}/V'| \ll f_\phi$ is equivalent to requiring

$$6\,\rho_{\mathrm{EM}}^{\max} \ll V(\chi_E), \tag{4.28}$$

which is again stronger than the condition for neglecting the total gauge energy density in the Friedman equation, $\rho_{\mathrm{EM}}^{\max} \ll V(\chi_E)$.

Finally, let us stress that in this case the upper labels "max" on $\rho_{\mathrm{EM}}^{\max}$ and $\ell_B^{\max}$ mean that they are computed from maximal quantities, but do not necessarily mean upper bounds. In fact the estimate for $\ell_B^{\max}$ is a conservative one, as it matches the corresponding backreactionless quantity at a small value, $\xi \simeq 1.4$, so in principle we would expect higher values for $\ell_B^{\max}$, giving rise to bigger Reynolds numbers (see Sec. 3.3.2). Still, we will use the estimate in Eq. (4.26) for our numerical calculations.

4.2.3   Gradient expansion formalism

This method was introduced in Refs. [176–178] and transforms the EoM for the vector field $\boldsymbol{A}$ into EoM for observable quantities, in particular the electric $\boldsymbol{E}$ and magnetic $\boldsymbol{B}$ fields. As the spatial gradients in the EoM do always appear as rot $\boldsymbol{E}$ and rot $\boldsymbol{B}$, the EoM can be written as an infinite series in terms of the bilinears $\mathcal{E}^{(n)} = \langle \boldsymbol{E} \cdot \mathrm{rot}^n \boldsymbol{E} \rangle/a^n$, $\mathcal{G}^{(n)} = \langle \boldsymbol{E} \cdot \mathrm{rot}^n \boldsymbol{B} \rangle/a^n$ and $\mathcal{B}^{(n)} = \langle \boldsymbol{B} \cdot \mathrm{rot}^n \boldsymbol{B} \rangle/a^n$, with $n = 0, 1, \dots$. In this way the coupled system of EoM for the fields $\boldsymbol{E}$ and $\boldsymbol{B}$ transforms into a system of coupled differential equations for the quantities $\mathcal{E}^{(n)}$, $\mathcal{B}^{(n)}$ and $\mathcal{G}^{(n)}$. This system is not block diagonal in the space of the n index so that the system has to be truncated to find solutions.

Moreover, the parameter $\Delta(t)$ in Eq. (4.14), which suppresses the gauge-field amplitude on small scales, depends on the conductivity at all times $t' < t$. So, a precise determination of $\Delta(t)$ would require a complete analytical solution of the infinite-dimensional system of equations. While Δ was dynamically computed in Ref. [177], for the sake of simplicity and generality, it was considered as a free parameter in Ref. [178] and fixed to the values $\Delta = 1$, 10^{-2}, 10^{-4}, 10^{-6}. In our numerical approach we will consider Δ as a function of the conductivity σ, as the initial condition for $\boldsymbol{E}$ and $\boldsymbol{B}$ are plane waves, such that $\boldsymbol{E} \cdot \boldsymbol{B} = 0$ and therefore initially $\sigma = 0$ and so $\Delta = 1$. However, as time is evolving $\boldsymbol{E}$ and $\boldsymbol{B}$ will become collinear, and a nonvanishing conductivity will be developed, as well as the function $\Delta(t) < 1$. In order to compare our numerical results with those from Ref. [178], we also (eventually) will enforce Δ to be a constant in our code. Upon considering a constant value of Δ, our results will agree pretty well with those obtained in the gradient expansion formalism, see Fig. 4.3. In the more realistic cases, where we just compute the value of $\Delta(t)$, we will see that at the beginning $t = t_0$, just very deep inside the inflationary period, $\Delta(t_0) = 1$, while the value of Δ will decrease very fast and at the end of inflation $t = t_E$, $\Delta(t_E) \ll 1$.

4.3 Numerical approach

We find it more convenient to change the variable from the time t to the scale factor a, as the latter is dimensionless. Moreover, by adequate change of variables, we transform all given differential equations to solve into a coupled system of first order differential equations such that

$$\frac{d\boldsymbol{x}}{da} = \boldsymbol{f}(a, \boldsymbol{x}), \tag{4.29}$$

where $\boldsymbol{x}$ is the vector that contains all the variables. Its exact content will be displayed in the sections below for the different cases at hand. To perform each time step Δa, we use the fourth order Runge-Kutta (`RK4`) algorithm:

$$
\begin{aligned}
\boldsymbol{\lambda}_1 &= \boldsymbol{f}(a_i, \boldsymbol{x}_i) \\
\boldsymbol{\lambda}_2 &= \boldsymbol{f}\left(a_i + \tfrac{1}{2}\Delta a, \boldsymbol{x}_i + \tfrac{1}{2}\Delta a\,\boldsymbol{\lambda}_1\right) \\
\boldsymbol{\lambda}_3 &= \boldsymbol{f}\left(a_i + \tfrac{1}{2}\Delta a, \boldsymbol{x}_i + \tfrac{1}{2}\Delta a\,\boldsymbol{\lambda}_2\right) \\
\boldsymbol{\lambda}_4 &= \boldsymbol{f}\left(a_i + \Delta a, \boldsymbol{x}_i + \Delta a\,\boldsymbol{\lambda}_3\right) \\
a_{i+1} &= a_i + \Delta a \\
\boldsymbol{x}_{i+1} &= \boldsymbol{x}_i + \tfrac{1}{6}\Delta a\left(\boldsymbol{\lambda}_1 + 2\boldsymbol{\lambda}_2 + 2\boldsymbol{\lambda}_3 + \boldsymbol{\lambda}_4\right).
\end{aligned}
\tag{4.30}
$$

Runge-Kutta algorithms have the peculiarity to make predictions for the next step by means of the estimated slopes $\boldsymbol{\lambda}_n$. Averaging the four slopes with appropriate weights makes the `RK4` algorithm effective up to an order of convergence of $\mathcal{O}(\Delta a^4)$. Note that $\boldsymbol{x}$ is complex, hence we solve the system (4.29) for both real and imaginary parts, but with their specific initial conditions.

We can see that the above `RK4` algorithm is an explicit scheme such that at each time step we compute the quantities needed to compute the next time step. This can be seen from the last two lines of (4.30) where the LHS are quantities at step $i+1$ obtained from quantities at step i in the RHS. Explicit schemes have the advantages to be cheaper in computation resources, but are less stable than implicit schemes. They also need smaller time steps Δa than implicit schemes.

In (semi)-implicit schemes, the last two lines of (4.30) contain quantities from step $i+1$, i.e. the same time step than the LHS. These schemes have the advantage to be more stable when handling the so-called stiff differential equations and can afford a good convergence with a bigger time step. However, because of this difference, a system of algebraic equations has to be solved at every step. This increases the computational cost considerably. Here, our definition of the conductivity (4.7) assumes slowly varying electric and magnetic fields, hence the conductivity is itself slowly varying so there is no need to use an implicit scheme. We simply have to make sure that we are taking Δa small enough to converge to the solution, which we checked. Therefore for our case the best solution is to use an explicit scheme, hence our choice of the algorithm (4.30).

4.3.1 Gauge sector only

We first start with the numerical solving of the gauge field A_λ only, whereas the inflaton ϕ will be obtained from analytical estimations and injected into the code as external input.

Once we change the time variable to a using (1.41), the gauge field equation of motion (4.6) becomes

$$\frac{\partial^2 A_\lambda}{\partial a^2} + \frac{1}{a}\left(2 + \frac{\sigma}{aH_E}\right)\frac{\partial A_\lambda}{\partial a} + \frac{k}{a^3 H_E}\left(\frac{k}{aH_E} - 2\lambda\xi\right)A_\lambda = 0. \tag{4.31}$$

To match the Schwinger analytical estimate approximation, we assume that the Hubble parameter is constant hence we take its value at the end of inflation H_E. This implies $\mathcal{F} = 0$ in (1.41) because of (1.42).

The Bunch-Davis solutions (4.17) become

$$
\begin{aligned}
A_\lambda(a,k) &= \sqrt{\frac{\Delta(a)}{2k}}\; e^{ik/aH_E} \\
\frac{\partial A_\lambda}{\partial a}(a,k) &= \frac{\sqrt{\Delta(a)}}{a^2 H_E}\left(-i\sqrt{\frac{k}{2}}-\frac{\sigma}{2}\frac{1}{\sqrt{2k}}\right)e^{ik/aH_E}
\end{aligned}
\qquad (a\to 0), \qquad (4.32)
$$

with the analog to (4.14)

$$
\Delta(a) = \exp\left(-\int_{a_0}^{a}\frac{\sigma(a')}{a'^2 H_E}da'\right). \tag{4.33}
$$

The value of H_E sets the scale of all quantities with dimension, hence we will implement the numerical code in units where $H_E = 1$.

Numerical implementation

Writing

$$
x_\lambda(a) = A_\lambda(a), \qquad\qquad y_\lambda(a) = \frac{\partial A_\lambda}{\partial a}(a), \tag{4.34}
$$

Eq. (4.31) becomes, in units of H_E, the following system:

$$
\frac{d}{da}\begin{pmatrix} x_\lambda \\ y_\lambda \end{pmatrix} = \begin{pmatrix} 0 & 1 \\ \frac{k}{a^3}\left(2\lambda\xi-\frac{k}{a}\right) & -\frac{1}{a}\left(\frac{\sigma}{a}+2\right) \end{pmatrix}\begin{pmatrix} x_\lambda \\ y_\lambda \end{pmatrix} \quad\Leftrightarrow\quad \frac{d\boldsymbol{x}}{da} = \boldsymbol{f}(a,\boldsymbol{x}). \tag{4.35}
$$

Note that there is such a system per value of λ, hence there are two of them. Alternatively we can double the array $\boldsymbol{x}$ by defining $\boldsymbol{x} = (x_+, y_+, x_-, y_-)$ and use a 4×4 time stepping matrix. The time iteration is then done using the algorithm (4.30) with time steps Δa distributed on a logarithmic scale

$$
\log a_i - \log a_{i-1} = \log a_{i+1} - \log a_i, \tag{4.36}
$$

so that the discretization is the same for each order of magnitude. This means Δa grows exponentially with a. The advantage of this method is that there is a refinement of the grid for small values of a, at the beginning of inflation[28]. The same is done for the discretization in k.

Indeed, we recall that our quantities of interest (and σ which is needed at each step) are obtained from integrals in the Fourier space, see Eqs. (3.39) and (4.2). These integrals are computed numerically as well, which means we are also discretizing the Fourier space with N_k number of k_i. Thus there are N_k systems (4.35) that are evaluated simultaneously in the code[29]. At each time step, we compute the electric (3.39c) and magnetic (3.39d) energy density as

$$
\rho_E^i = \int_{k_{\min}}^{k_c^i} dk\,\frac{k^2}{4\pi^2}\left(|y_i^+(k)|^2+|y_i^-(k)|^2\right), \tag{4.37a}
$$

$$
\rho_B^i = \frac{1}{a_i^4}\int_{k_{\min}}^{k_c^i} dk\,\frac{k^4}{4\pi^2}\left(|x_i^+(k)|^2+|x_i^-(k)|^2\right), \tag{4.37b}
$$

where the integral over k is done numerically. We nevertheless write here an analytical symbol for the integral in order not to make the notation too heavy. For all the details we refer to App. C, where the numerical code is transcribed.

---

[28] Note that this choice implies that we are using N as the effective time variable, see Eq. (4.57) even if all the code is written in function of a.

[29] To be more specific, there are N_k systems for $\boldsymbol{x}\in\mathbb{C}$ per value of λ, which means $4N_k$ real valued systems

The cutoff k_c^i is obtained from (4.16) as

$$k_c^i = a_i \xi + \sqrt{(a_i \xi)^2 + \frac{a_i^2}{2} \left[\frac{\sigma_i - \sigma_{i-1}}{a_i - a_{i-1}} + \frac{\sigma_i}{a_i} \left(\frac{\sigma_i}{2a_i} + 1 \right) \right]}, \tag{4.38}$$

while $k_{\min}$ is obtained from the initial time of the simulation and the BD penetration factor, see Eq. (4.42). The color matching dashed vertical lines in Fig. 4.2 show the cutoff values k_c^i computed from (4.38). They agree perfectly with the point where the BD vacuum modes become dominant for large k.

Likewise, the helicity (3.39a) and its derivative (3.39b) become

$$\mathcal{H}_i = \frac{1}{a_i^3} \int_{k_{\min}}^{k_c^i} dk \, \frac{k^3}{2\pi^2} \left(|x_i^+(k)|^2 - |x_i^-(k)|^2 \right), \tag{4.39a}$$

$$\mathcal{G}_i = \frac{1}{a_i^2} \int_{k_{\min}}^{k_c^i} dk \, \frac{k^3}{2\pi^2} \left(|x_i^+(k) y_i^+(k)| - |x_i^-(k) y_i^-(k)| \right). \tag{4.39b}$$

If the Schwinger effect is taken into account, we turn on the possibility of having σ computed at each time step a_i of the numerical computation with

$$\sigma_{i+1} = \frac{41 \, g'^3}{72 \, \pi^2} \, a_i \, \sqrt{2\rho_B^i} \, \coth \left(\pi \sqrt{\frac{\rho_B^i}{\rho_E^i}} \right) \tag{4.40}$$

and injected into the calculation of the next step. Otherwise, we keep it zero. Last, the fermion energy density is computed as

$$\rho_\psi^i = \frac{\sigma_i}{a_i^2} \int_{k_{\min}}^{k_c^i} dk \, \frac{k^2}{\pi^2} \sum_{\lambda=\pm} \left[\text{Re}(x_i^\lambda) \text{Re}(y_i^\lambda) + \text{Im}(x_i^\lambda) \text{Im}(y_i^\lambda) \right]. \tag{4.41}$$

Finally, after N_a steps we stop the simulation at $a_{N_a} = a_E$. Quantities at that time are compared to the known analytical results, see Fig. 4.3.

The initial conditions (4.32) are mode-dependent, as it takes longer for modes with bigger wave number to leave the BD vacuum. Therefore, we choose as initial condition for each mode

$$a_{k,0} = \frac{k}{x_{\text{BD}}}, \tag{4.42}$$

where we choose the factor x_{BD} in order to make sure that we initialize the gauge field sufficiently deep inside the Hubble radius. As we can see from Eqs. (3.39), high values of k are dominating the integral hence large modes are negligible compared to small ones. This makes us to choose a lower bound on the k range such that the initial time of the simulation is

$$a_0 = \frac{k_{\min}}{x_{\text{BD}}}. \tag{4.43}$$

In that way, at a_0 we make sure that all the modes are in their respective vacua, which implies $\sigma = 0$ as explained in Sec. 4.1.3. In practice, this means that the modes with $k > x_{\text{BD}} a$ are given by the following relations

$$\text{Re}(x_{\lambda,i}^{\text{BD}}) = \sqrt{\frac{\Delta_i}{2k}} \cos \frac{k}{a_i}, \tag{4.44a}$$

$$\text{Im}(x_{\lambda,i}^{\text{BD}}) = \sqrt{\frac{\Delta_i}{2k}} \sin \frac{k}{a_i}, \tag{4.44b}$$

$$\text{Re}(y_{\lambda,i}^{\text{BD}}) = \frac{1}{a_i^2} \sqrt{\frac{\Delta_i}{2}} \left(\sqrt{k} \sin \frac{k}{a_i} - \frac{\sigma_i}{2\sqrt{k}} \cos \frac{k}{a_i} \right), \tag{4.44c}$$

$$\text{Im}(y_{\lambda,i}^{\text{BD}}) = \frac{1}{a_i^2} \sqrt{\frac{\Delta_i}{2}} \left(-\sqrt{k} \cos \frac{k}{a_i} - \frac{\sigma_i}{2\sqrt{k}} \sin \frac{k}{a_i} \right) \tag{4.44d}$$

while the others are evolving with the RK4 algorithm. Note that the BD solutions do not depend on the helical mode labeled by λ.

We explored the numerical convergence of the solution, both in the number of a_i's, labeled as N_a, and in the number of k_j's, labeled as N_k. Provided that $N_a > 2000$ and $N_k > 200$, the simulations are very stable and the output does not depend on the discretization. For big values of f_ϕ, $f_\phi \gtrsim 0.1\, M_{\text{pl}}$, we can even lower the number of needed time steps.

Besides, we must choose the BD penetration factor x_{BD} such that it produces trustable results. We have done a numerical analysis and conclude that depending on the value of N_a, a range $20 < x_{\text{BD}} < 50$ yields trustable results. We hence choose throughout this work the following values

$$x_{\text{BD}} = 20, \qquad N_a = 500, 1000, 2000, \qquad N_k = 300. \tag{4.45}$$

We display in Fig. 4.2 the spectra of all the observable quantities in order to see how the BD vacuum is dominating the spectra for large k and how the cutoff $k_c(a)$, given by (4.16), efficiently removes that part of the integration. The difference between the BD vacuum and the damped BD vacuum is also clear, as the first goes like k^3 whereas the second goes like $\Delta(a)k^3$ with Δ decreasing with time. Hence the asymptotic behaviors are not superimposed since Δ changes. Finally, we also see explicitly how the growth of ρ_E and ρ_B with the scale factor a is due to the increase in amplitude of the spectrum hump and its shift to larger values of k. For this illustrative purpose we used a constant value of ξ. Here we have fixed $f_\phi = 0.1\, M_{\text{pl}}$, while for other values of this parameter the plots are similar.

Slow roll inflation

Firstly, we use the slow roll approximations (1.73) for ϕ, because the backreactionless solutions (3.40) as well as both Schwinger approximate estimates (Secs. 4.2.1 and 4.2.2) have been obtained in this regime. Also, as we already mentioned in Sec. 4.2.3, the parameter Δ was fixed to constant values in Ref. [178] while ξ, as defined in Eq. (3.24), is often considered as a constant in the slow roll approximation, see Sec. 3.2.1 and Eq. (3.35) in particular. Note that, when assuming that the parameters Δ and ξ are constants, we can treat them as inputs in the code and completely ignore ϕ from our computations.

In Fig. 4.3, we displayed several results already present in the literature that we successfully reproduced with our numerical method. First the backreactionless case, where there is no conductivity, by simply enforcing $\sigma = 0$ (therefore $\Delta = 1$) in the code. The data set is displayed as blue bullets and match the corresponding analytical values given by Eqs. (3.40). Then, in order to reproduce the results from Ref. [178], we considered a non-zero conductivity given by (4.8) while assuming Δ constant during inflation, thus making it a free parameter. In Fig. 4.3, we plot the quantities ρ_B, ρ_E, $\mathcal{H}$ and $\mathcal{G}$ at the end of inflation for chosen values of Δ. We can see that the results agree well with those using the gradient expansion formalism in Ref. [178] and with both Schwinger estimates[30].

---

[30]Regarding ρ_E, the maximal estimate seems violated by our numerical results. But what we call maximal estimate here is not the same as the definition which appears in [173, 178], where $|E|$ and $|B|$ are separately maximized. Instead, we have chosen to maximize the product $|E| \cdot |B|$, which is the relevant quantity for the baryogenesis calculation,
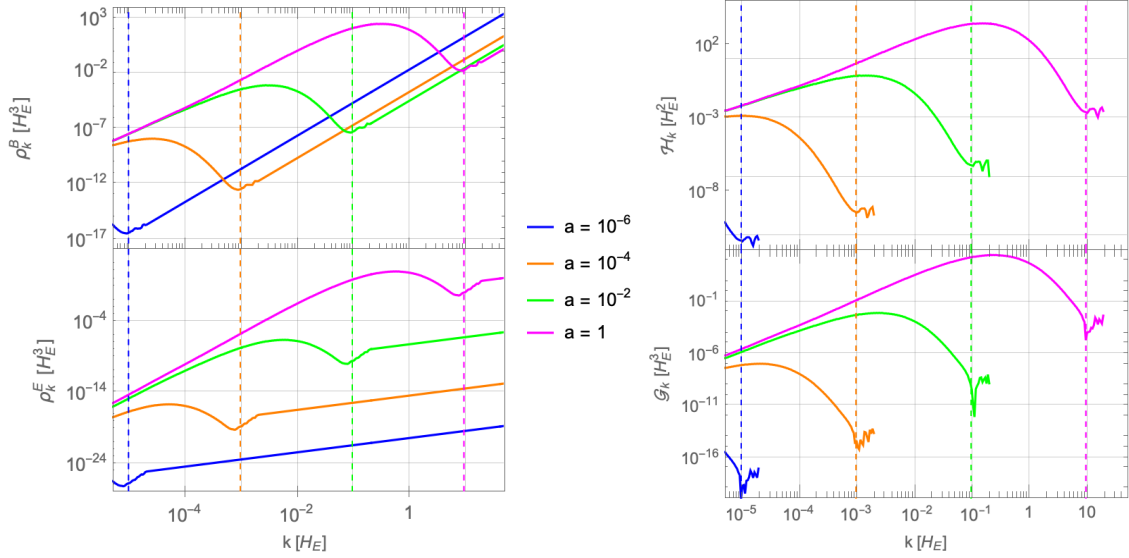
Figure 4.2. Spectra of the magnetic energy (top left), electric energy (bottom left), helicity (top right) and its derivative (bottom right), i.e. the integrands of Eqs. (3.39), for different values of a during inflation simulation. Here we used the variable $\sigma(a)$ and $\Delta(a)$ with constant ξ. The color matching dashed vertical lines show the cutoff values $k_c(a)$ computed from (4.16).

The benefit of the slow roll approximation is that the results look "model independent". However, the trade-off comes with the need of having a constant parameter ξ as the slow roll regime implies an approximately constant $\dot{\phi}$, see Eq. (3.24). Besides, we know that this parameter can also be expressed in terms of the slow roll parameter ϵ, see Eq. (3.26), which is indeed small and constant during inflation but then quickly becomes unity during the last e-folds. We also know that the modes produced during the last e-folds are the ones that contribute the most to the integrals (3.39), as all the modes previously generated get washed out by the Universe expansion, see Sec. 3.2.2.

All these observations lead us to conclude that the most important contribution to the quantities ρ_E, ρ_B, $\mathcal{H}$ and $\mathcal{G}$ is taking place during an epoch when the constant ξ approximation loses its relevance. This is why in a second step we will relax this assumption while maintaining the slow roll description of ϕ. This can only be done by choosing a model for inflation. Hence, in the next section, we will study the same configuration with the numerical code but for the case of the Starobinsky model, see Sec. 1.2.5. Of course in that case the instability parameter will depend on the time variable.

Starobinsky inflation

We have chosen the Starobinsky potential as it provides a realistic model of inflation, and will be a particular case of a more general class of models we will consider to make predictions using the full solution of the system, see Sec. 4.3.3. The purpose of this section will thus be to assess the goodness of the slow roll approximation when computing the full solution to the (ϕ, A_λ) system in the next section.

The Starobinsky potential is given by (1.103) with $\alpha = 1$. Using the slow roll regime (1.73)

---

see Sec. 4.2.2. This explains the apparent contradiction that our data from the numerical simulation provide bigger values for ρ_E than the maximum estimate.
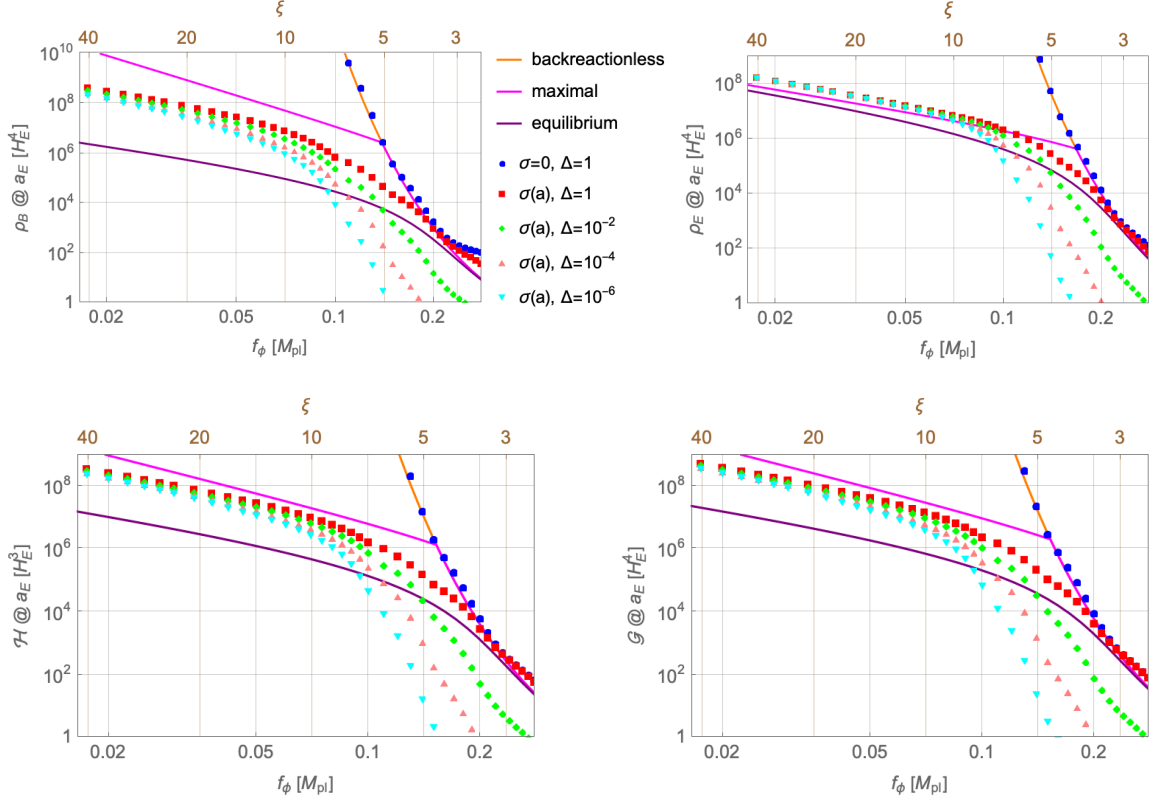
Figure 4.3. Electric ρ_E and magnetic ρ_B energy densities, and the helicity $\mathcal{H}$ and its derivative $\mathcal{G}$, at the end of inflation (i.e. for $\epsilon(a_E) = 1$), in units of H_E, as functions of the coupling f_ϕ assuming Δ constant. We see the plots confirm the result from Fig. 1 of Ref. [178]. Here, we also assumed ξ constant and given by (3.35).

and the change of variables (1.41), the inflaton field $\phi(a)$ is given by

$$\sqrt{\frac{2}{3}} \frac{\phi(a)}{M_{\rm pl}} = -\log\left(\frac{a_E}{a}\right)^{\frac{4}{3}} - \mathcal{W}_{-1}\left[-\beta e^{-\beta}\left(\frac{a_E}{a}\right)^{-\frac{4}{3}}\right] - \beta + \log\beta, \qquad \beta = 1 + \frac{2}{\sqrt{3}} \qquad (4.46)$$

where $\mathcal{W}_n$ is the n-th branch of the Lambert function. We now wish to compute the instability parameter for the Starobinsky potential in the slow roll regime. Hence we use the approximation (3.26) which applied to (1.103) with $\alpha = 1$ provides

$$\xi(a) = \sqrt{\frac{2}{3}} \frac{M_{\rm pl}}{f_\phi} \left[\exp\left(\sqrt{\frac{2}{3}} \frac{\phi(a)}{M_{\rm pl}}\right) - 1\right]^{-1}. \qquad (4.47)$$

This way, we still do not need to simulate the field ϕ in our numerical code while having an approximation for ξ much closer to the numerical solution. We show this in Fig. 4.4 where we plot the different behaviors for the instability parameter ξ, namely the constant slow roll approximation (3.35), the former approximated solution for the Starobinsky model (4.47), and the definition (3.24) where the function ϕ is obtained from the full numerical solution done in the next section. We can see that the Starobinsky estimation is a very good approximation in the sense that for almost the entire duration of inflation it merges with the numerical solution. The two solutions differ only for ϵ close to unity, but the error stays marginal. This way we can check the validity of the full numerical

computation done in the next section. Also, this plot clearly exhibits the problem with the constant ξ approximation, as it is far from both Starobinsky estimation and full solution behaviors. Finally, we verify from the plot that $\xi(a)$ given by (4.47) evaluated at the value a_E such that $\epsilon(a_E) = 1$ (i.e. $a_E = 1$) yields indeed (3.35).
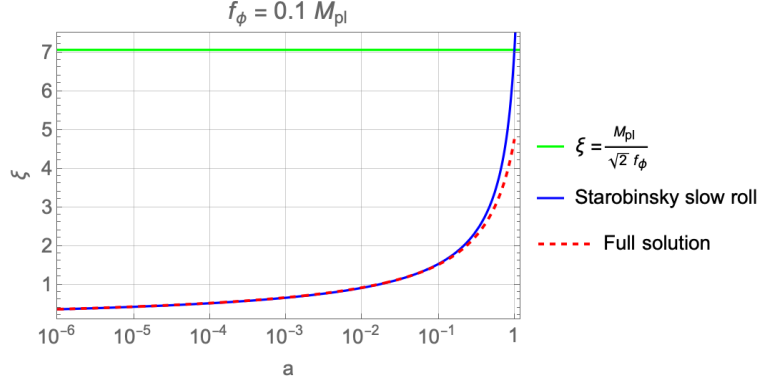
Figure 4.4. Comparison of the instability parameter ξ for the three cases at hand: the constant approximation (3.35) from the slow roll regime (green), the Starobinsky estimation (4.47) also in the slow roll regime (blue) and finally the numerical solution where ξ is obtained from its definition (3.24) and ϕ from the system (4.51) applied to the Starobinsky potential (red, dashed).

In Fig. 4.5, we display in blue results for the Starobinsky model, for various values of ϵ, when σ and Δ vary dynamically. Although the slow roll approximation loses its relevance for values of ϵ closer to 1, we already see a difference with the plots in Fig. 4.3. This is because, no matter the value of the initial time, the function $\Delta(a)$ goes to extremely small values when approaching the end of inflation, thus killing the BD modes that would have been amplified at the very end of inflation and that would have contributed the most to the integrals (3.39), see Fig. 4.6 for a qualitative example. With the assumption of a constant Δ, this suppression is less effective and the tachyonic amplification yields higher energy densities and helicity.

4.3.2 Full solution

In this section, we are not using the slow roll hypothesis for the inflaton equation of motion and consider the full solution to the system given by (3.44) and (4.6) in specific models of inflation. We will first choose the Starobinsky inflationary potential to compare our results with the previous semianalytical results. Then we will use a set of inflationary models that are well known to be in agreement with all cosmological constraints. Finally, we do not assume any peculiar geometry of the Universe.

In the last section we have already disclosed the fact that, for the case of the Starobinsky potential, the full numerical solution and the slow roll approximation are comparable. One could therefore question the need to simulate ϕ alongside the gauge field. However, the main motivation for solving the full system is to obtain results beyond the end of inflation, when the slow roll approach breaks down. So, once our code provides trustable results for the inflation period, we will extend the simulation to a few e-folds after inflation to see how the observable plasma behaves, which will allow us to make a comment on gauge preheating.

Implementation

The first step is to write Eqs. (3.44) and (4.6) in terms of the variable a. Unlike in the previous section, the change of variables must take into account that the Hubble parameter is not constant.

Hence using (1.41) and (1.42), together with the Friedmann equations, c.f. Eqs. (1.11) and (1.12) with $k = 0$, (1.28) and (1.61),

$$H^2 = \frac{\rho}{3M_{\rm pl}^2}, \qquad\qquad \frac{\ddot{a}}{a} = -\frac{3p + \rho}{6M_p^2}, \tag{4.48}$$

we have

$$\mathcal{F} = \frac{1}{H^2 M_{\rm pl}^2} \left(\frac{1}{2}\dot{\phi}^2 + \frac{2}{3}\rho_{\rm EM} + \frac{2}{3}\rho_\psi \right), \tag{4.49}$$

where we used the total energy density and pressure

$$\rho = \frac{1}{2}\dot{\phi}^2 + V + \rho_{\rm EM} + \rho_\psi, \tag{4.50a}$$

$$p = \frac{1}{2}\dot{\phi}^2 - V + \frac{\rho_{\rm EM}}{3} + \frac{\rho_\psi}{3}. \tag{4.50b}$$

Thus, Eqs. (3.44) and (4.6) become

$$\frac{d^2\phi}{da^2} + \frac{4 - \mathcal{F}}{a}\frac{d\phi}{da} + \frac{V'(\phi)}{a^2 H^2} + \frac{\mathcal{G}}{a^2 H^2 f_\phi} = 0 \tag{4.51a}$$

$$\frac{d^2 A_\lambda}{da^2} + \frac{1}{a}\left(2 - \mathcal{F} + \frac{\sigma}{aH} \right)\frac{dA_\lambda}{da} + \frac{k}{a^2 H}\left(\frac{k}{a^2 H} - \frac{\lambda}{f_\phi}\frac{d\phi}{da} \right) A_\lambda = 0, \tag{4.51b}$$

which is the full (ϕ, A_λ) system that takes into account the backreaction of the gauge field on ϕ, the Schwinger effect and the expansion of the Universe.

The Hubble parameter can be computed from the first Friedmann equation, where ρ is given by (4.50a). This way, we can compute the value of H and $\mathcal{F}$ at each time step recursively to feed the equations of motion, like we already did for σ and $\mathcal{G}$. The BD vacuum modes are identical to the previous case, see Eqs. (4.32).

The numerical implementation follows from the previous case. Defining the variables

$$w = \phi, \qquad x = \frac{\partial\phi}{\partial a}, \qquad y_\lambda = A_\lambda, \qquad z_\lambda = \frac{\partial A_\lambda}{\partial a} \tag{4.52}$$

we transform the above coupled system of differential equations (4.51) into the system

$$\frac{dw}{da} = x \tag{4.53a}$$

$$\frac{dx}{da} = -\frac{\mathcal{G}}{a^2 H^2 f_\phi} - \frac{4 - \mathcal{F}}{a}x - \frac{V'(w)}{a^2 H^2} \tag{4.53b}$$

$$\frac{dy_\lambda}{da} = z_\lambda \tag{4.53c}$$

$$\frac{dz_\lambda}{da} = \frac{k}{a^2 H}\left(\frac{\lambda}{f_\phi}x - \frac{k}{a^2 H} \right) y_\lambda - \frac{1}{a}\left(2 - \mathcal{F} + \frac{\sigma}{aH} \right) z_\lambda \tag{4.53d}$$

which is equivalent to writing (4.29) with $\boldsymbol{x} = (w, x, y_+, z_+, y_-, z_-)$. We recall that w, $x \in \mathbb{R}$ and y_λ, $z_\lambda \in \mathbb{C}$. Similarly to the previous calculation in the slow roll regime, we use the RK4 algorithm (4.30) with the values of H, σ, $\mathcal{F}$ and $\mathcal{G}$ computed at each time step and feed back in the next one, see App. C.

Inflaton initial condition could be set to

$$w_0 = \phi_*, \qquad\qquad x_0 = 0. \tag{4.54}$$
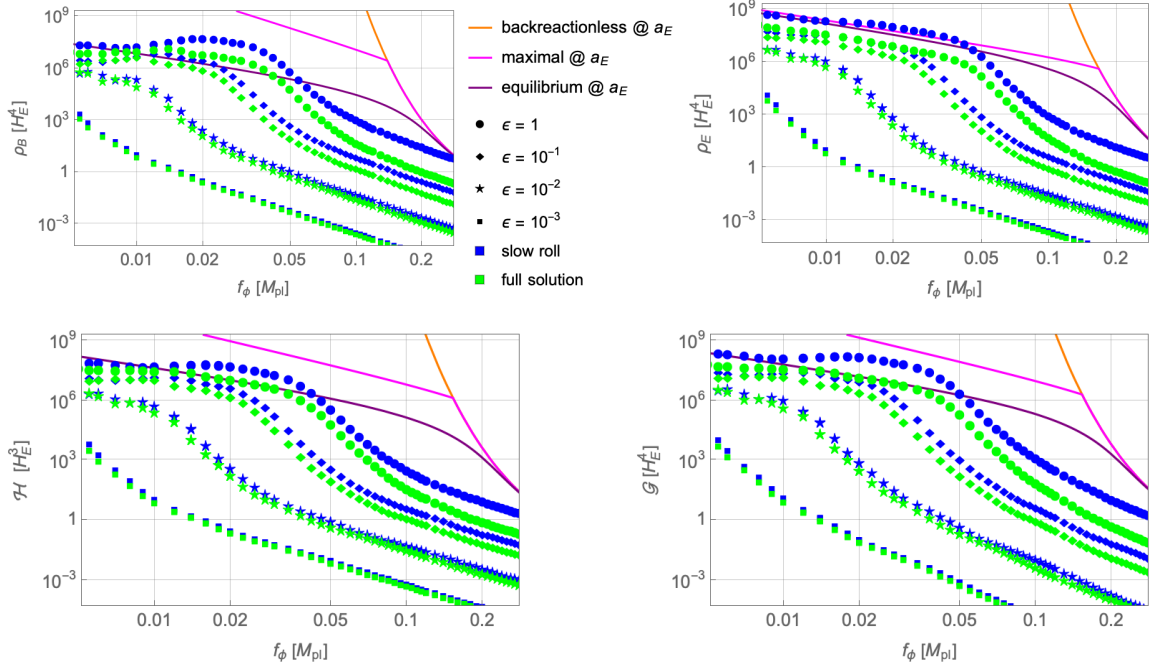
Figure 4.5. Comparison between the slow roll approximation and the full solution for the Starobinsky model. The analytical estimates are given for $\epsilon = 1$. As expected, the slow roll computation diverges from the full solution as inflation is nearing the end, since the slow roll approximation is only valid in the regime $\epsilon \ll 1$. Hence the slow roll computation overshoots the value of all quantities, closer to the value given by the Schwinger equilibrium estimate for $f_\phi \lesssim 0.05\, M_{\mathrm{pl}}$. As expected, we also have compared both analysis, slow roll and full solution, for values of a such that $\epsilon(a) \ll 1$ (in particular $\epsilon = 10^{-1}$, 10^{-2}, 10^{-3}) and found good agreement.

However, the number of e-folds sets the initial time as $a_0 = \mathrm{e}^{-|N_*|} \sim 10^{-26}$, which is too small a number for the numerical implementation. We then proceed as follows. For $a \lesssim k_{\min}/x_{\mathrm{BD}}$, and sufficiently low $k_{\min}$, the gauge field modes stay in their vacuum and the total contribution to $\Delta(a)$ is negligible. Hence we do not need to perform the numerical simulation before that time, as the inflaton is the main player, so we can solve its equation of motion analytically. Instead, we fix the start of the simulation like before, at $a_0 = k_{\min}/x_{\mathrm{BD}}$ and we compute the corresponding number of e-folds N which leads us to the corresponding value of $\phi(N)$. Therefore, the initial condition must be set to w_0 such that

$$\int_{\phi_E}^{w_0} \frac{V(\phi)}{V'(\phi)}\, d\phi = -M_{\mathrm{pl}}^2 \log a_0 \tag{4.55}$$

and, using $\dot{\phi} \simeq -\frac{V'(\phi)}{3H}$ which is valid at the early stages of inflation,

$$x_0 = -\frac{V'(w_0)}{3a_0 H_0^2}. \tag{4.56}$$

As for the gauge field, initial conditions are set in the same way as in the slow roll approximation, i.e. with (4.44).

Results at the end of inflation

In this subsection we will compare our results at the end of inflation, where we are making a full numerical analysis of the EoM, with those obtained using the slow roll approximation for the
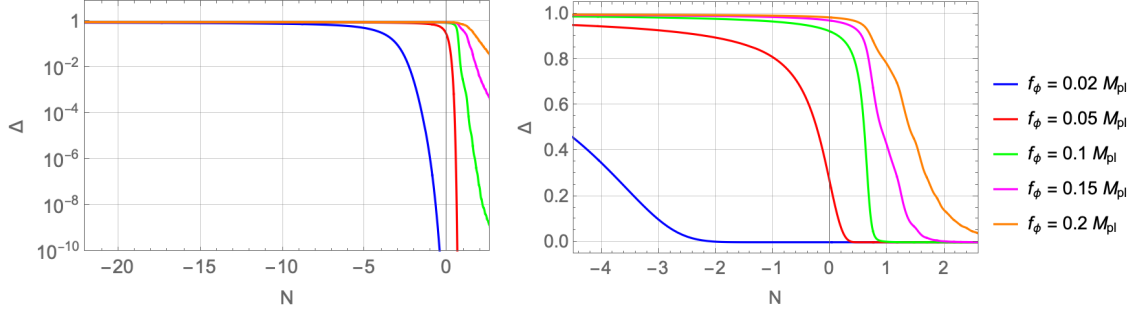
Figure 4.6. Plots of the parameter Δ as a function of the e-fold number (4.57) for the Starobinsky potential when simulating the full system (4.51). We display the results for various value of the coupling f_ϕ for the last third of the inflation period (left) as well as the last e-folds before and after the end of inflation (right). We see that the stronger the coupling $1/f_\phi$ is, the stronger the amplitude suppression from the BD vacuum is, hence greatly reducing the gauge field share at the end of inflation.

inflationary potential. For the sake of comparison we will concentrate on the Starobinsky model given by (1.103) with $\alpha = 1$. In this current framework, we see in Fig. 4.5 that the four studied quantities, namely ρ_B, ρ_E, $\mathcal{H}$ and $\mathcal{G}$, are much closer to the Schwinger equilibrium estimate at the end of inflation.

We present in Fig. 4.5 the values of the physical observables evaluated at various stages of inflation, i.e. various values of the scale factor a, from $\epsilon(a) = 10^{-3}$ to $\epsilon(a) = 1$, as a function of the coupling f_ϕ for the Starobinsky model. We superimpose the analytical results from Secs. 3.2.2, 4.2.1 and 4.2.2, i.e. the backreactionless solution and the Schwinger equilibrium and maximal estimates. From the plots we see that for $f_\phi \lesssim 0.05 \, M_{\rm pl}$ the equilibrium estimate is a good approximation, especially for ρ_E where the predictions of maximal and equilibrium estimates merge. We also verify that $\cos\theta \simeq 1$ hence satisfying the assumption on parallel electric and magnetic fields leading to the conductivity of Eq. (4.7).

In this setup, our numerical code is computing a value of the conductivity σ and Δ for each time step, hence we got the functions $\sigma(a)$ and $\Delta(a)$. The variation and presence of $\Delta(a)$ is not without effects on the final results, see Fig. 4.6. Indeed, the smallest $(k \gg H_E)$ modes are the ones that most contribute to the integrals (3.39). Without the Schwinger effect, these modes are produced last, just at the end of inflation, and only briefly leave the horizon. They therefore should have a significant impact on preheating. When the Schwinger effect prevents their generation, by reducing them by a $\ll 1$ factor, while they are still in the BD vacuum, we can ask ourselves about the effectiveness of gauge preheating. It was shown in previous studies of gauge preheating [181] that its efficiency mainly depends on the electromagnetic energy fraction available at the end of inflation $\rho_{\rm EM}/\rho_{\rm tot}$. To shed light on the last point, we will extend, in the next section, our numerical results beyond the end of inflation when the inflaton is coherently oscillating around its potential minimum. We will do that in a set of particularly interesting phenomenological models that we describe in the next section.

4.3.3 Solution beyond inflation

Now that once we have established a method to numerically compute the quantities ρ_E, ρ_B, ρ_ψ, $\mathcal{H}$ and $\mathcal{G}$, we aim to study the system evolution past $\epsilon = 1$, and the onset of reheating. Indeed, the system (4.51) describes the most general interaction of the zero mode of both hypercharge gauge and inflaton fields. In particular, no assumption was made on the geometry of the Universe, hence there is no specific reason to stop its numerical computation at the end of inflation except perhaps that, with our computational method, we are not considering the contribution to the kinetic inflaton

energy coming from the field spatial gradients. Notice however that as the contribution from the gradients is positive we can still conservatively use our results to exclude the appearance of gauge preheating after inflation. We will also find it convenient to present some numerical results using as the variable the number of e-folds before the end of inflation N, instead of the scale factor a, and related to it by

$$N = -\log \frac{a_E}{a} \tag{4.57}$$

such that $N = 0$ corresponds to the time a_E when $\epsilon(a_E) = 1$ and $N < 0$ to the inflationary period. This last convention introduces a sign difference with the definition (1.63).

We study a benchmark of two classes of inflationary potentials: the α-attractor models (1.103) and the hilltop models (1.107). For each of them we choose the two values of their parameter that bound the range in agreement with the constraints (1.92), namely $\alpha = 1, 100$ and $\mu = 10, 50 \, M_{\rm pl}$, see Eqs. (1.106) and (1.109). We recall that α-attractor model for $\alpha = 1$ is also referred to as the Starobinsky model, which was studied in the last section. We then show the postinflationary energy breakdown for $\alpha = 1, 100$ in Fig. 4.7 and for $\mu = 10, 50 \, M_{\rm pl}$ in Fig. 4.8, for two disctinct values of f_ϕ namely $f_\phi = 0.02, 0.15 \, M_{\rm pl}$.

From the inflaton behavior, we see that as soon as inflation ends, the Universe enters a matter domination era as $\rho_\phi \propto a^{-3}$. For high enough values of f_ϕ, i.e. $f_\phi \gtrsim 0.1 \, M_{\rm pl}$, we reproduce the results shown in Ref. [181], whereas for $f_\phi \lesssim 0.1 \, M_{\rm pl}$ the electric and magnetic fields exhibit a different behavior: the former decay faster than the latter while oscillating. This is due to the fact, already mentioned in Ref. [177], that the energy density for the electric component $\boldsymbol{E} = -\boldsymbol{A}'$ is much more sensitive to the Schwinger effect than the magnetic component $\boldsymbol{B}$, because it directly
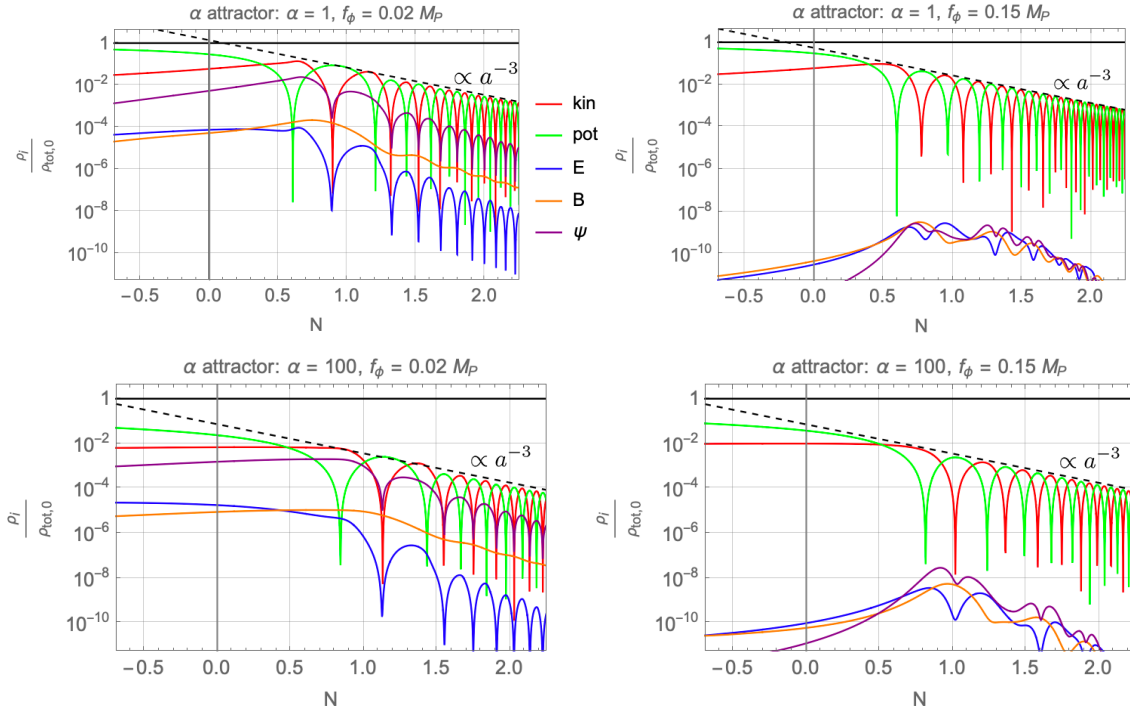
Figure 4.7. Inflaton kinetic and potential energy density, as well as electric, magnetic and fermion energy density ratios to the initial total energy density of the Universe for the α-attractor models with $\alpha = 1$ (upper panels) and $\alpha = 100$ (lower panels). The vertical gray lines display the value a for which $\epsilon(a) = 1$ and the dashed line shows the expected scaling of the dominant sector.
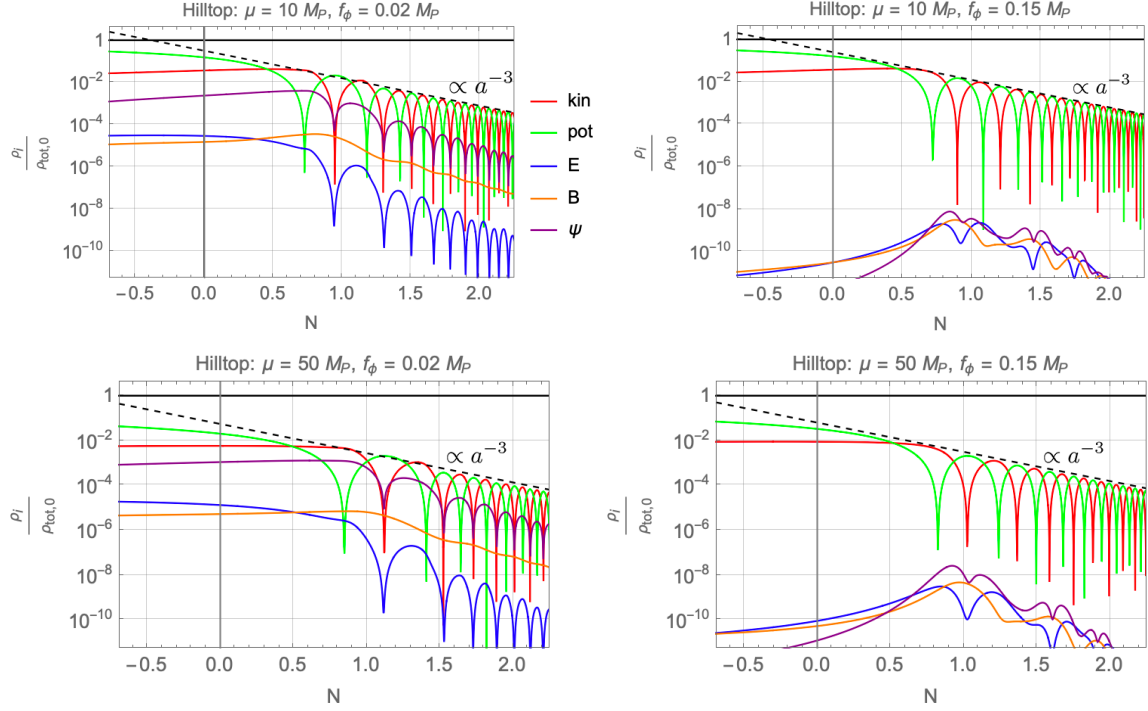
Figure 4.8. Inflaton kinetic and potential energy density, as well as electric, magnetic and fermion energy density ratios to the initial total energy density of the Universe for the hilltop models with $\mu = 10\,M_{\rm pl}$ (upper panels) and $\mu = 50\,M_{\rm pl}$ (lower panels). The vertical gray lines display the value a for which $\epsilon(a) = 1$ and the dashed line shows the expected scaling of the dominant sector.

couples to the conductivity in the gauge field equation of motion (3.30). On the other hand, the magnetic component reflects spatial effects, as it is defined by $\boldsymbol{B} = \boldsymbol{\nabla} \wedge \boldsymbol{A}$. In this work, as already mentioned, we do not consider the inflaton spatial effects, $\boldsymbol{\nabla}\phi$, because this would require one to implement real fermion interactions in a lattice simulation. Hence, for low values of f_ϕ, when the Schwinger effect is strongly affecting the system, the behavior of ρ_B is expected to be subject to changes when the spatial effects are enabled; namely we expect to see a faster decay, like that of ρ_E. As also observed in Ref. [177], the electric field, which is dominant during inflation, becomes subdominant afterwards. Finally, we can see that for low values of f_ϕ the fermion energy density dominates the radiation energy density at the end of inflation as already highlighted in Ref. [177].

4.4   Applications

To conclude this chapter, we will comment on the implications about two related topics: gauge preheating and baryogenesis.

First we will demonstrate that our numerical estimates suggest that the Schwinger effect significantly reduces the share of electromagnetic energy for the considered models and gauge preheating is unlikely to occur. Our results do apply to the above considered class of inflationary models. They show a certain degree of model dependence, so we cannot exclude a qualitatively different result for models of inflation other than the considered ones.

On the other hand, we have seen in Chap. 3 that a successful baryogenesis does depend on a delicate equilibrium between the amount of helicity, magnetic energy density, and magnetic correlation length. Therefore damped fields do not necessarily mean no baryon asymmetry in the late
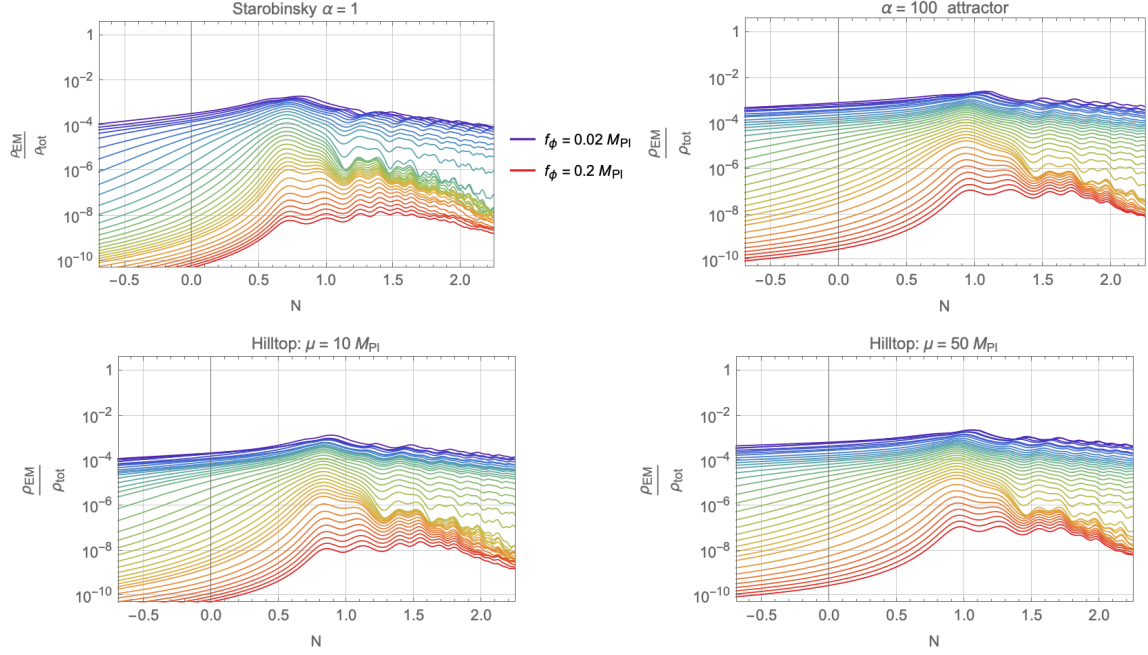
Figure 4.9. Time evolution of the electromagnetic to total energy density fraction, during and after inflation for various values of the coupling f_ϕ. The upper panels correspond to the α-attractor model with $\alpha = 1$ (top left) and $\alpha = 100$ (top right) and the lower panels to the hilltop model with $\mu = 10\,M_{\rm pl}$ (bottom left) and $\mu = 50\,M_{\rm pl}$ (bottom right).

Universe. Actually, as a result of our numerical calculation, we have found there is still a window in the parameter space for baryogenesis to happen.

These two comments should be viewed as hints for future studies that address the production of gauge fields at the end of inflation. Of course, a full lattice simulation of the Schwinger effect involving fermions remains to be done.

4.4.1   Gauge preheating

The authors of Ref. [181] quote a *sufficient criterion* for gauge preheating to happen, namely that at least an 80% fraction of the total energy density of the Universe is electromagnetic energy. In the absence of the Schwinger effect, they found that this criterion is satisfied for values $f_\phi \lesssim 0.1\,M_{\rm pl}$. However, as expected, the Schwinger effect significantly reduces the share of electromagnetic energy, as shown on Fig. 4.9 for the considered models, which displays the ratio $\rho_{\rm EM}/\rho_{\rm total}$ for the four previous considered cases. We can see that the maximum is attained with a value $\sim 10^{-3}$, which precludes any gauge preheating, at least for $f_\phi \gtrsim 0.01\,M_{\rm pl}$. Another conclusion from Ref. [181] is that the spatial effects of the inflaton become relevant for sufficiently low values of f_ϕ and contribute to preheating. Since we are neglecting them in our simplified calculation, any negative statement concerning the possibility of gauge preheating due to the lack of enough electromagnetic energy should be a conservative one.

The final results from our analysis can be summarized in Fig. 4.10, where we plot the maximum value of the electromagnetic to total energy fraction as a function of f_ϕ (preheating efficiency) for the Starobinsky model, the α-attractor model with $\alpha = 100$ and the hilltop models with $\mu/M_{\rm pl} = 10, 50$. For $f_\phi \gtrsim 0.01\,M_{\rm pl}$, we obtain

$$\frac{\rho_{\rm EM}}{\rho_{\rm tot}} \lesssim 0.01, \tag{4.58}$$
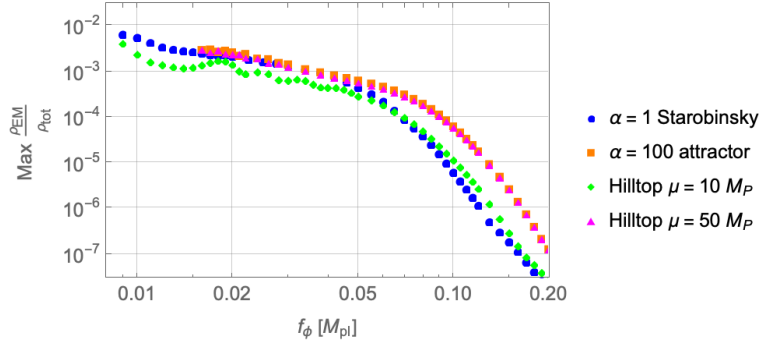
Figure 4.10. Maximum value of the electromagnetic to total energy fraction as a function of f_ϕ for the four considered models: α-attractor models, with $\alpha = 1$, 100, and hilltop models, $\mu = 10$, $50\,M_{\rm pl}$. Gauge preheating seems unlikely to occur.

which seems to prevent gauge preheating as its efficiency is far from the value of ~ 0.8 established in the numerical analysis of Ref. [181].

End of reheating

If gauge preheating does not occur, the inflaton will eventually decay by perturbative processes which depend on the inflaton total decay width Γ_ϕ, see Sec. 1.2.4. Therefore at the time $t_{\rm rh} \sim 1/\Gamma_\phi$, the inflaton has completely decayed and the radiation domination era starts.

Results from last sections have shown that shortly after inflation ends, the Universe is matter dominated, hence using (1.18) and (1.28) we can approximate the Hubble parameter by

$$H \simeq \left(\frac{a_E}{a}\right)^{\frac{3}{2}} H_E, \qquad H \simeq \frac{2}{3t}, \tag{4.59}$$

where $H_E \equiv H(a_E)$, such that

$$a_{\rm rh} \simeq a_E \left(\frac{3H_E}{2\Gamma_\phi}\right)^{\frac{2}{3}} \tag{4.60}$$

is the end value after reheating by inflaton perturbative decays. Of course $a_{\rm rh}$ is a model-dependent quantity, which depends on the value of Γ_ϕ, which in turn, depends on the couplings of the inflaton to the matter.

In particular, the coupling $1/f_\phi$ of the inflaton to the hypercharge CS density provides a channel for the perturbative decay of the inflaton into a pair of hyperphotons A, as $\phi \to AA$. This decay has a width given by [184]

$$\Gamma(\phi \to AA) \simeq \frac{m_\phi^3}{64\pi f_\phi^2}, \tag{4.61}$$

where m_ϕ is the inflaton mass that can be extracted from its potential as

$$m_\phi^2 = \left.\frac{\partial^2 V}{\partial \phi^2}\right|_{\phi=\phi_{\rm min}}. \tag{4.62}$$

For the α-attractor (hilltop quartic) model, we have $\phi_{\rm min,\alpha} = 0$ ($\phi_{\rm min,h} = \mu$) and

$$m_{\phi,\,\alpha}^2 = \frac{4\Lambda_\alpha^4}{3\alpha M_{\rm pl}^2}, \qquad\qquad m_{\phi,\,h}^2 = \frac{32\Lambda_h^4}{\mu^2}. \tag{4.63}$$

In the simplest case where the inflaton is only coupled to the hypercharge gauge bosons through the CS density, the total width is $\Gamma_\phi = \Gamma(\phi \to AA)$. Using the masses found above we see that

$$\Gamma_\phi \simeq 12 \; (3.0) \cdot 10^{-18} \cdot \frac{M_{\mathrm{pl}}^3}{f_\phi^2}, \qquad\qquad \Gamma_\phi \simeq 4.2 \; (21) \cdot 10^{-19} \cdot \frac{M_{\mathrm{pl}}^3}{f_\phi^2} \qquad (4.64)$$

for $\alpha = 1 \; (100)$ in the α-attractor models (left), and for $\mu = 10 \; (50) \, M_{\mathrm{pl}}$ in the hilltop models (right).

The value of the scale factor and the temperature at reheating, a_{rh} and T_{rh}, are given by Eqs (1.99) and (1.97). We recall that

$$\frac{T_{\mathrm{rh}}}{T_{\mathrm{rh}}^{\mathrm{ins}}} \simeq \sqrt{\frac{\Gamma_\phi}{H_E}}. \qquad (4.65)$$

Consequently we can express a_{rh} and T_{rh} as functions of all the involved parameters, namely f_ϕ, and α (μ) for the α-attractor (hilltop quartic) model. In particular, the relevant parameter for baryogenesis is the ratio $T_{\mathrm{rh}}/T_{\mathrm{rh}}^{\mathrm{ins}}$ given by

$$\frac{T_{\mathrm{rh}}}{T_{\mathrm{rh}}^{\mathrm{ins}}} \simeq 1.9 \; (0.8) \cdot 10^{-4} \left(\frac{0.01}{f_\phi/M_{\mathrm{pl}}} \right), \qquad\qquad \frac{T_{\mathrm{rh}}}{T_{\mathrm{rh}}^{\mathrm{ins}}} \simeq 0.4 \; (0.7) \cdot 10^{-4} \left(\frac{0.01}{f_\phi/M_{\mathrm{pl}}} \right), \qquad (4.66)$$

for $\alpha = 1 \; (100)$ in the α-attractor models (left), and for $\mu = 10 \; (50) \, M_{\mathrm{pl}}$ in the hilltop models (right).

In Chap. 3 we have seen that the ratio $T_{\mathrm{rh}}/T_{\mathrm{rh}}^{\mathrm{ins}}$ is a parameter for the baryogenesis model, see Eqs. (3.18), (3.73), (3.79) and Fig. 3.3. Therefore, when a specific model is chosen for the baryogenesis mechanism, the above results will constrain the parameter space by adding a relation that the parameters f_ϕ and the temperature ratio should fulfill, see next section.

In the presence of extra couplings of the inflaton to matter, the predictions for the inflaton decay width, Eqs. (4.64), and the reheating temperature, Eqs. (4.66), will change in a model-dependent way, as well as the model predictions concerning the generation of the baryon asymmetry.

Of course in the hypothetical case where the explosive production of gauge fields should have prevailed over the perturbative inflaton decays, gauge preheating would have taken place over a few e-folds after the end of inflation. As we see from the previous results, this is never the case and gauge preheating is never strong enough to reheat the Universe after the period of cosmological inflation. This result does not preclude that, in the presence of a strong coupling λ of the inflaton with some other field, e.g. a scalar (or a fermion), there could exist an explosive production of that scalar (or fermion), triggering preheating of the Universe after inflation [185].

4.4.2 Baryon asymmetry

Before concluding this chapter, we wish to make a small comment on the baryogenesis issue at the EWPT. In Chap. 3, we presented a baryogenesis mechanism in the slow roll regime that leads to a successful BAU, see Fig. 3.3. Hence it is straightforward, using our numerical analysis in this paper, to make an update of the final results for the BAU for inflation, this time taking into account the Schwinger effect.

Thus, instead of using the backreactionless results Eqs. (3.40), we compute the plasma observables $\mathcal{H}$, $\mathcal{G}$, ρ_E, ρ_B and ℓ_B by numerical means, and we insert them into Eqs. (3.18), (3.73), (3.79) to get the final parameter space. We chose to compute them using the α-attractor model with $\alpha = 1$, namely the Starobinsky potential, as it is the one responsible for Higgs inflation (see Sec. 1.2.6) and it is close to our model shown in Chap. 6. It also provides an accurate value of H_E given by (1.106).

All together, this yields the plot displayed in Fig. 4.11, which is the analog of Fig. 3.3, namely the parameter space that provides a successful BAU. Note that here, ξ has been replaced by f_ϕ, as the former is no longer constant and the latter is the true coupling of the theory. Also, there is no excluded region such as the red one in Fig. 3.3 since our numerical solving is taking into account the backreaction of the gauge field on the inflaton EoM, i.e. the RHS of Eq. (3.44). Lastly, the primordial non-gaussianity and baryon isocurvature perturbations provide no constraints as the Schwinger effect induces a strong damping of all the plasma quantities. Since these constraints were satisfied in the backreactionless case presented in Chap. 3, they also do now.

Therefore, we can conclude that for $f_\phi \gtrsim 0.06\, M_{\rm pl}$ there is no space for the BAU, as the production of gauge fields is too weak. In addition to this we have seen that the reheating temperature is constrained by the model, see Eq. (4.66), as we can see from Fig. 4.11 and the compatibility of the model reheating temperature with the baryogenesis results translates into the baryogenesis region on the parameter f_ϕ

$$f_\phi \lesssim 0.03\, M_{\rm pl}, \tag{4.67}$$

a result valid for the Starobinsky potential. Finally, one other possible take-away of this chapter is that baryogenesis at the EWPT is favored by low reheating temperatures, in the range $10^{-6}\, T_{\rm rh}^{\rm ins} \lesssim T_{\rm rh} \lesssim 10^{-3}\, T_{\rm rh}^{\rm ins}$.
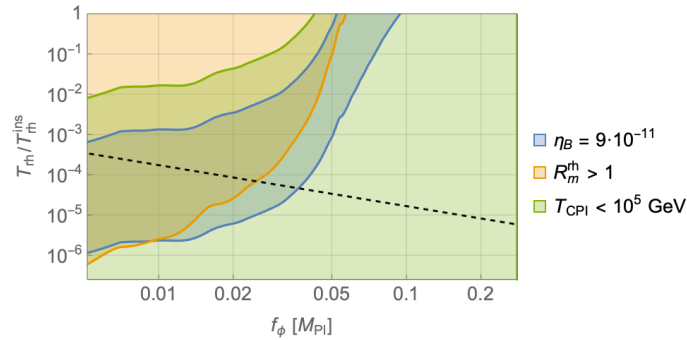
Figure 4.11. The baryogenesis window in the parameter space $(f_\phi, T_{\rm rh}/T_{\rm rh}^{\rm ins})$ for the Starobinsky potential (α-attractor model with $\alpha = 1$). The dashed line corresponds to Eq. (4.66) for $\alpha = 1$.

Part III

Two models

Chapter 5

Higgs Baryogenesis

In this chapter we will study the cosmological implications of the CP-odd dimension-six operator $|\Phi|^2 F\tilde{F}$ which is natural in the Higgs sector from the EFT point of view.

More specifically, we will consider a direct extension of the ordinary Higgs inflation (HI) model (see Sec. 1.2.6) with an arbitrary value of the quartic coupling λ_h. We will be agnostic about the origin on its value and the mechanism stabilizing the Higgs potential as we aim to focus on the helical hypermagnetic fields production from the Higgs non-perturbative decay during inflation, or at least during the last e-folds of inflation. We will therefore mobilize everything we have seen in the previous chapters to take into account all the constraints and give a parameter space for a successful BAU.

Here, there is one key difference with the axion inflation presented in the previous chapters, namely that the Higgs VEV is non zero, hence inflation and the subsequent period until reheating happen in the broken phase. As ordinary electromagnetism gauge fields do not feed the anomaly equation for baryon/lepton number, the baryogenesis scenario will be slightly revisited.

This model was first presented in Ref. [186].

5.1   The model

We include the following term to the HI action given by (1.126)

$$\mathcal{L}_{\mathrm{HI}} \supset -\frac{|\Phi|^2}{2f_h^2}\, Y_{\mu\nu}\tilde{Y}^{\mu\nu} \tag{5.1}$$

where we recall that Φ is the Higgs doublet. A possible UV completion giving rise to this dimension-six CP-odd operator is provided in App. A.2.

The HI model was presented in Sec. 1.2.6. As stated there, the background physical Higgs field h is large during the inflationary stage, hence the EW symmetry is broken. As we have seen in Eq. (1.138), during inflation the Higgs VEV has values $\sim 10^{-2}M_{\mathrm{pl}}$, which implies that the $W^\pm$ and Z^0 bosons are super-heavy, see Eq. (2.91b), and hence much harder to produce in comparison to massless degrees of freedom such a photons. So we can consider the trivial solution $W_\mu^i = 0$. According to Eqs. (2.90) this implies that $W_\mu^\pm = 0$, $Z_\mu = 0$ and also that $Y_\mu = \cos\theta_W A_\mu$ and $W_\mu^3 = \sin\theta_W A_\mu$, meaning we are producing ordinary $U(1)_{\mathrm{EM}}$ magnetic fields. This is also why we do not consider the covariant derivative as (2.93) in the broken phase. Since the physical Higgs h is neutral, its only coupling to electromagnetism is the considered dimension-six operator.

Hence, in the broken phase during inflation, the latter will look like

$$\mathcal{L}_{\mathrm{HI}} \supset -\frac{\cos^2\theta_W}{4}\frac{h^2}{f_h^2}\, F_{\mu\nu}\tilde{F}^{\mu\nu} \tag{5.2}$$

where we used Eq. (2.90c). This term remains untouched by the Weyl transformation that allows us to express the HI action (1.126) in the Einstein frame, yielding the potential (1.131), where χ is the inflaton field with canonical kinetic term. We can relate the Higgs field to it as (1.130), see Secs. 1.2.5 and 1.2.6.

Besides, we want to take into account the Schwinger effect. Hence following Sec. 4.1, we include the interaction of fermionic currents as (4.1). Taking these changes into account, we can redo the derivation presented in Sec. 3.2.1 in order to write the system of EoM for the inflaton and the gauge field as

$$\ddot{\chi} + 3H\dot{\chi} + V'(\chi) = K(\chi)\,\frac{\mathcal{G}}{f_\chi} \tag{5.3a}$$

$$\left(\frac{\partial^2}{\partial\tau^2} - \nabla^2 + 2\xi\,aH\,\boldsymbol{\nabla}\times\right)\boldsymbol{A} = \boldsymbol{J}, \tag{5.3b}$$

analogous to the system (3.22), with

$$K(\chi) \equiv \frac{\mathrm{e}^{\sqrt{\frac{2}{3}}\,\chi}}{6^{3/2}\xi_h^2}, \qquad\qquad f_\chi \equiv \frac{2f_h^2}{\cos^2\theta_W}, \qquad\qquad \xi = -K(\chi)\,\frac{\dot{\chi}}{2Hf_\chi}. \tag{5.4}$$

Notice that if $K(\chi) = 1$, we recover the axion case given by Eqs. (3.22a), (4.4) and (3.24).

We recall that here the main difference is that $\boldsymbol{A}$, $\boldsymbol{J}$, $\boldsymbol{E}$, $\boldsymbol{B}$ and σ are $U(1)_{\mathrm{EM}}$ electromagnetism quantites. As we have seen in Secs. 3.1.1, 3.2.2 and 3.3.2, the helicity, helicity time derivative, energy densities and Reynolds number are computed the same way as for the hypermagnetic field. The only differences are the Z factor in the conductivity, see Sec. 4.1.2 and the fact that $U(1)_{\mathrm{EM}}$ gauge field do not contribute to the anomaly equation (2.143), see more in Sec. 5.3.

We aim to solve the system (5.3) analytically, following the example of Sec. 3.2 but with the Schwinger effect. Thus, we assume the slow roll regime and neglect the RHS of Eq. (5.3a), i.e. we will assume $K(\chi)\mathcal{G} \ll f_\chi V'(\chi)$, a consistency condition that will be checked a posteriori. Then, all the results of Sec. 1.2.6 apply, in particular the value of the inflaton field at the end of inflation, χ_E, given by (1.132) as well as its value N_* e-folds before, χ_* given by (1.133) and the slow roll parameters Eqs. (1.135).

In the next section we will see that we can further simplify this setup, as ξ with the studied coupling barely changes during HI while its main dependence lies in the couplings f_h and λ_h.

5.1.1   Constant ξ approximation

Because the field Φ is an $SU(2)$ doublet, the lowest term in a power expansion is $F(h) \propto h^2$, hence the condition (3.50) is guaranteed. Therefore the coupling (5.2) leads to a constant value of ξ given by (3.61) with $p = 2$, $f_\phi = f_h$ and $g = \xi_h$ given by (1.137). This points to a fundamental difference between axion and Higgs inflation models. Whereas in the axion inflation model, there were no reasons why a linear term would be missing in favor of a quadratic one, the Higgs field provides a natural one. Indeed, a linear term in the function $F(h)$ would explicitly break gauge invariance in the symmetric phase.

In fact, in the slow roll approximation (1.73), the instability parameter for the potential (1.131) is given by, in units where $M_{\mathrm{pl}} = 1$ [31],

$$\xi \simeq \frac{K(\chi)}{f_\chi}\sqrt{\frac{\epsilon}{2}} = \frac{K(\chi)}{f_\chi}\frac{8\sqrt{6}\,\xi_h}{\mathrm{e}^{\sqrt{\frac{2}{3}}\,\chi} - 24\xi_h}. \tag{5.5}$$

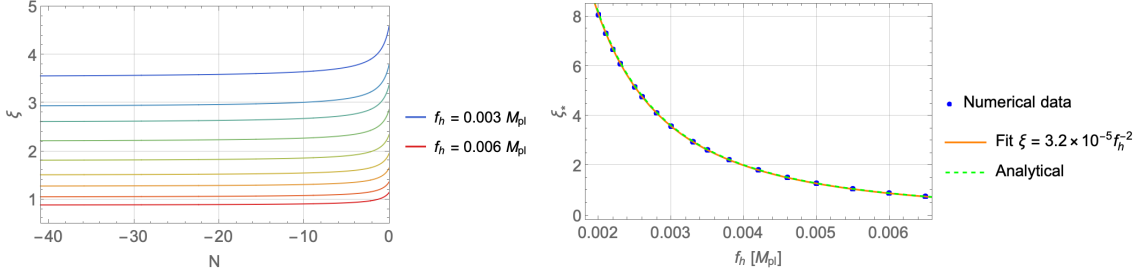[31]We will keep this convention for the rest of the chapter.

Figure 5.1. Left: Plot of the parameters ξ for various values of the coupling f_h. Right: Instability parameter at CMB value ξ_* for various values of f_h from numerical simulations (blue dots) and their numerical fit (orange). Both perfectly overlap with the analytical relation (5.6) in dashed green.

Now, using the definition of $K(\chi)$ and f_χ, we find that ξ is approximately constant provided that $\chi \gtrsim \sqrt{\frac{3}{2}} \log{(24\xi_h)} \simeq \chi_E$, and given by

$$\xi \simeq \frac{4}{3 f_\chi \xi_h} \simeq 3.2 \cdot 10^{-5} \sqrt{\frac{0.1}{\lambda_h}} f_h^{-2} \,, \tag{5.6}$$

which agrees with (3.61). Using the numerical method introduced in Sec. 4.3, we verified the latter by solving the full system (5.3) without making the slow roll approximation and found the behavior displayed on the left panel of Fig. 5.1, where we plot the parameter ξ as a function of the number of e-folds during inflation N for various values of the parameter f_h and $\lambda_h = 0.1$. We see in the figure that ξ stays constant during most of the inflationary period and only increases at the end of inflation. This behavior is in stark contrast to that shown in Fig. 4.4 for $F(\phi) \propto \phi$. The fact that ξ stays almost constant during the inflationary era provides confidence to analytically solve the EoM (3.30), while its small variation provides a window for generating baryogenesis, as we will see later on in this chapter.

To know how much ξ does vary during the N_* e-fold in inflation, we compute, using Eqs. (1.132) and (1.133),

$$\xi(\chi_E) \equiv \xi_E = \frac{4}{3 f_\chi \xi_h} \frac{\beta}{\beta - 1}, \tag{5.7a}$$

$$\xi(\chi_*) \equiv \xi_* = \frac{4}{3 f_\chi \xi_h} \frac{\beta}{\beta - e^{\frac{4N_*}{3} + \beta + W_*}}. \tag{5.7b}$$

Hence

$$\frac{\xi_E}{\xi_*} = \frac{\beta - e^{\frac{4N_*}{3} + \beta + W_*}}{\beta - 1} \simeq 1.84 \,, \tag{5.8}$$

this ratio being insensitive to the value of N_* up the second digit. Notice that it does not contain the self-coupling λ_h, nor f_h.

In conclusion, we see that the instability parameter ξ is flat, regardless of when the simulation begins or on the chosen value of f_h. Only at the very end of the simulation does ξ deviates from its constant value. In fact, if we plot how this constant value changes with the parameter ξ_h, we find a perfect agreement between the numerical calculation and the analytical one (5.6), as we can see in the right panel of Fig. 5.1, where we plot ξ_* as a function of f_h for the different estimates. The case of a constant ξ is suitable for the following scenarios as they both have been studied with this assumption:

- Absence of the Schwinger effect, i.e. $\sigma \simeq 0$. One possibility that can guarantee this result would be a dynamical mechanism such that all fermion Yukawa couplings at the inflation scale are $\mathcal{O}(1)$, so that the criterion (4.11) is not met anymore, and after inflation they relax to the physical values which correspond to fermion masses and mixing angles. A possible mechanism described in App. B appears if flavor is explained by a Froggatt-Nielsen mechanism [187], where the flavon field is coupled to the inflaton and gets a very large VEV of $\sim h$ during inflation, while the flavon VEV relaxes to its low-energy value when $h \simeq v$.

- Presence of the Schwinger effect in the equilibrium estimate. In that case we redefine $\xi \to \xi_{\rm eq}$ with $\sigma \neq 0$ according to Sec. 4.2.1 such that Eq. (5.3b) becomes, in momentum space and helical basis,

$$A_\lambda'' + k\left(k - 2\lambda\xi_{\rm eq}\,aH\right)A_\lambda = 0. \tag{5.9}$$

At the end of this chapter we shall compute the baryogenesis parameter space in both cases accordingly.

5.2   Constraints

5.2.1   Backreactionless consistency condition

In the absence of a backreaction of the gauge field on the inflaton EoM, the inflationary equation (5.3b) with slow roll conditions reduces to $3H\dot\chi \simeq -V'(\chi)$. Thus, in order to consistently neglect the backreaction on the inflaton, we must simply enforce that, in the inflaton EoM, the RHS term is negligible as compared to the kinetic term, i.e.

$$3H\dot\chi \gg K(\chi)\,\frac{\mathcal{G}}{f_\chi}. \tag{5.10}$$

Using the result (3.39b) for $\mathcal{G}$ and the definition of ξ given in Eq. (5.4), this condition becomes

$$\frac{45}{2^{13}}\frac{e^{2\pi\xi}}{\xi^3} \ll \mathcal{P}_\zeta^{-1} \tag{5.11}$$

where the spectrum of primordial perturbations, for around 60 e-folds before the end of inflation (i.e. for $\chi = \chi_*$) is $\mathcal{P}_\zeta^{1/2} = H^2/(2\pi|\dot\chi|) \simeq 4.7 \times 10^{-5}$ [22]. This leads to the upper bound $\xi_* \lesssim 4.74$, for which we can neglect the backreaction of the gauge fields on the inflaton EoM for the value of the inflaton field $\chi = \chi_*$. As we will see in the next section this condition is superseded by the condition of non-Gaussianity effects.

We must however ensure that condition (5.10) is valid throughout the end of inflation. Using the slow roll conditions, and the fact that, for our model, $V'(\chi_E) > V'(\chi_*)$, we found a stronger bound than the former one as Eq. (5.10) can be written as

$$\xi\,\mathcal{G} \ll \frac{V'^2}{6H^2}, \tag{5.12}$$

which leads to $\xi_E \lesssim 6.45$ (i.e. $\xi_* \lesssim 3.48$), at the end of inflation.

Once the non-backreaction condition on the inflaton equation is satisfied, the non-backreaction condition on the Friedmann equation

$$\frac{\langle\mathbf{E}^2 + \mathbf{B}^2\rangle}{2a^4} = \frac{63}{2^{16}}\frac{H^4}{\pi^2\xi^3}e^{2\pi\xi}\left(1 + \frac{5}{4\xi}\right) \ll V \simeq 3H^2 \tag{5.13}$$

holds automatically. In particular the latter condition leads to $\xi_E \lesssim 6.55$ (i.e. $\xi_* \lesssim 3.54$).

5.2.2 Non-gaussianity bounds for HI

As pointed out in Refs. [165, 166], even if the non-backreaction conditions are satisfied, the coupling $h^2 F\tilde{F}$ can generate cosmological fluctuations in the HI model. The perturbations on the inflaton are obtained by replacing $\chi(t,\vec{x}) = \bar{\chi}(t) + \delta\chi(t,\vec{x})$, where $\bar{\chi}(t)$ is the inflationary background and $\delta\chi(t,\vec{x})$ the fluctuation, see Sec. 1.2.3. The equation for the fluctuation is given by

$$\left[\frac{\partial^2}{\partial t^2} + 3H \frac{\partial}{\partial t} - \frac{\nabla^2}{a^2} + V''(\bar{\chi}) - \bar{K}' \frac{\mathcal{G}}{f_\chi} \right] \delta\chi = K(\chi) \frac{\delta\mathcal{G}}{f_\chi} \tag{5.14}$$

where $\bar{K} \equiv K(\bar{\chi})$ and $\delta\mathcal{G} = (\mathbf{E} \cdot \mathbf{B} - \langle \mathbf{E} \cdot \mathbf{B} \rangle)/a^4$.

The function $\bar{K}$ satisfies the condition $\bar{K}' = \sqrt{2/3}\bar{K}$, while for our potential, during the inflationary period, it turns out that $V''(\bar{\chi}) \simeq -\sqrt{2/3}V'(\bar{\chi})$. Then, the last two terms of the LHS of Eq. (5.14) are

$$V'' - \frac{\bar{K}'}{f_\chi}\mathcal{G} \simeq -\sqrt{\frac{2}{3}} \left(V' + \frac{\bar{K}}{f_\chi}\mathcal{G} \right) \simeq -\sqrt{\frac{2}{3}}V' \simeq V'' \tag{5.15}$$

where we have made use of the non-backreaction condition (5.10). In this way the last term in the LHS of Eq. (5.14) can be safely neglected.

The resulting fluctuation equation has been explicitly solved in Ref. [188], provided the backreactionless consistency condition of Sec. 5.2.1 is satisfied, as well as the correlation functions for the curvature perturbations on uniform density hypersurfaces $\zeta(t,\vec{x}) = -H\delta\chi(t,\vec{x})/\dot{\bar{\chi}}$. A good fit for the equilateral configuration of the three-point function yields the fit, valid for values $2 \lesssim \xi \lesssim 3$ [188],

$$f_{\mathrm{NL}}^{\mathrm{equil}} \simeq \frac{1.6 \times 10^{-16}}{\xi^{8.1}} e^{6\pi\xi} \tag{5.16}$$

The current Planck bound on $f_{\mathrm{NL}}^{\mathrm{equil}}$ [167], $f_{\mathrm{NL}}^{\mathrm{equil}} = -26 \pm 47$ yields, at CMB scales, the upper bound $\xi_* \lesssim 2.55$, at 95% CL. A much stronger condition than that leading to the absence of backreaction. Given that in our model the near constancy of ξ leads to the relation (5.8), the non-Gaussianity bound translates in our model into the bound

$$\xi_E \lesssim 4.71. \tag{5.17}$$

As already stated, all the calculations done in the absence of the Schwinger effect apply, in the presence of the Schwinger effect in the equilibrium approximation, to corresponding bounds on the effective parameter, i.e. $\xi_{\mathrm{eff}*} < 2.55$.

5.3 Baryogenesis

During inflation the Higgs background value is non zero, and so the electroweak symmetry is broken, meaning we are producing ordinary $U(1)_{\mathrm{EM}}$ magnetic fields. At reheating, h will drop to its potential minimum at zero because of the sudden dominance of the thermal correction terms, and we will recover the symmetric phase. This is a necessary requirement for a successful baryogenesis as the helical fields participating in the chiral anomaly must belong to the unbroken electroweak sector, see Sec. 2.3.6.

Thus, as the $U(1)_Y$ helical magnetic fields participate in the baryogenesis process, while $U(1)_{\mathrm{EM}}$ helical magnetic fields are produced at the end of inflation, the projection of the latter on the former must be taken into account with a factor

$$\boldsymbol{A}_Y = \cos\theta_W \, \boldsymbol{A}_{\mathrm{EM}}, \qquad \mathcal{H}_Y = \cos^2\theta_W \, \mathcal{H}_{\mathrm{EM}}. \tag{5.18}$$

because of Eq. 2.90c. The Z fields can also project onto $U(1)_Y$ fields but, as stated before, we will ignore this contribution as they were too heavy to be produced.

According to the anomaly equation Eq. (3.14), the sudden hypermagnetic helicity due to the latter projection implies the creation of a $B + L$ asymmetry that is rapidly washed out by the weak sphalerons. So in the end, the scenario is the same as for the hypermagnetic field up a factor $\cos^2 \theta_W$ in the available helicity at EWPT to feed into Eq. (3.18).

For this model we assume instant reheating [50, 138, 189], $T_{\rm rh} \simeq T_{\rm rh}^{\rm ins}$, hence the ratio $T_{\rm rh}/T_{\rm rh}^{\rm ins}$ drops in Eqs. (3.18), (3.73) and (3.79). However, in addition to their dependence on the gauge sector observables, the quantities used in this section vary according to the quartic coupling λ_h as $\xi \propto \lambda_h^{-1/2}$, see Eq. (5.6). Besides, the Hubble ratio at the end of inflation $H_E \simeq \sqrt{V(\chi_E)/3}$ also depends on λ_h as V does.

Hereafter, we will discuss the baryogenesis capabilities the HI model in three cases: the metric formulation of HI, the critical HI model and the Palatini formulation of HI.

5.3.1 Metric Higgs inflation

As we have previously explained we will be agnostic about the mechanism stabilizing the Higgs potential (see Sec. 2.3.5) and then just will consider the self-coupling λ_h as a free parameter. The corresponding plot, for values $10^{-3} \lesssim \lambda_h \lesssim 1$, is shown in Fig. 5.2, for the backreactionless case (left panel) and the Schwinger equilibrium solution (right panel), which shows that condition (3.18) provides a wide window for baryogenesis (in blue). Then we display in orange the region where $\mathcal{R}_m^{\rm rh} > 1$, see Eq. (3.73a), and in green the region where $T_{\rm CPI} \lesssim 10^5$ GeV, see Eq. (3.79). In both plots the red region is excluded because of the CMB non-Gaussianity bound.

We can compute that in this scenario, the BAU is attained for values

$$3.6 \lesssim \xi_E \lesssim 4.1. \tag{5.19}$$

This range is the same for both the backreactionless and the Schwinger equilibrium case by construction of the latter. However, because of the replacement $\xi \to \xi_{\rm eq}$, the relation between ξ and the couplings λ_h and f_h is different in both cases (this is why we showed two panels on Fig. 5.2). These bounds correspond to the values

$$
\begin{aligned}
1.4 \times 10^4 &\lesssim \frac{\rho_E}{H_E^4} \lesssim 1.7 \times 10^5 & \qquad 1.4 \times 10^3 &\lesssim \frac{\rho_B}{H_E^4} \lesssim 1.3 \times 10^4 \\
5.6 \times 10^3 &\lesssim \frac{\mathcal{H}}{H_E^3} \lesssim 6.2 \times 10^4 & \qquad 8.4 \times 10^3 &\lesssim \frac{\mathcal{G}}{H_E^4} \lesssim 9.3 \times 10^4
\end{aligned}
\tag{5.20}
$$

5.3.2 Critical Higgs Inflation

Depending on the values of the Higgs and top quark masses, λ_h could remain positive until the Planck scale, and such that $\lambda_h \ll 1$ and $\beta_{\lambda_h} \ll 1$ (exhibiting a *critical behavior*) without any need of new physics, see Fig. 5.3. In particular this should happen if the top quark mass is $m_t \simeq 171.3$ GeV [102, 190–192], which however exceeds its current value from direct measurements, $m_t = 172.76 \pm 0.30$ [12] by $\sim 3\sigma$. Those models initially proposed in Refs. [193–199] were dubbed critical Higgs inflation (CHI) and in principle would not need any UV completion for the Higgs potential stabilization.

Nevertheless, in view of the actual experimental values of the Higgs and top quark masses, people have been proposing UV completions to change the size of the quartic β function, and such that λ_h, and β_{λ_h}, can attain a critical behavior for the values of the Higgs for which HI takes place, and stay positive all the way down to the electroweak scale [200].
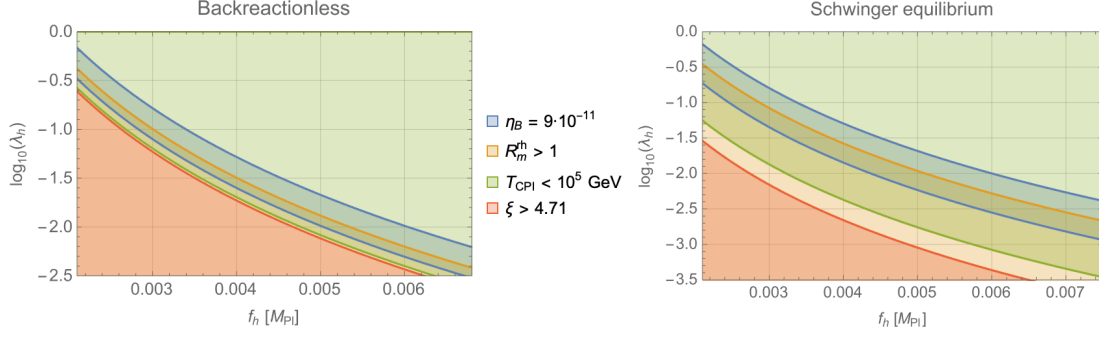
Figure 5.2. The baryogenesis parameter space for the backreactionless (left panel) and Schwinger equilibrium (right panel) cases. The red region is excluded because of CMB non-Gaussianity. We seek the overlapping region between the first three ones. The condition on CPI temperature is no constraint since it overlaps the entire region for η_B. Hence the tradeoff must be made between η_B and the magnetic Reynolds number.
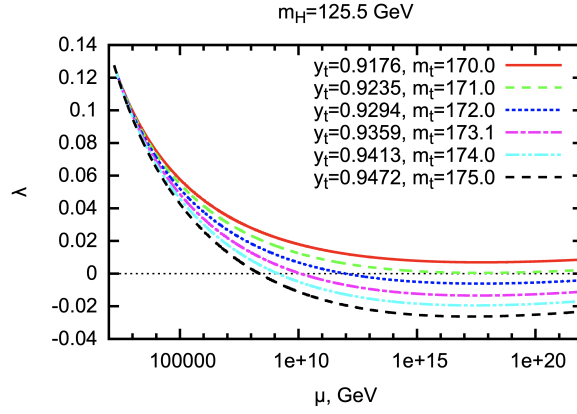

Figure 5.3. Renormalization group running of the Higgs self-coupling for several values of the top quark Yukawa coupling (top pole mass) and fixed 125.5 GeV Higgs boson mass. Figure taken from [192].

In all cases, for critical values of λ_h, CHI has the advantage that the required value of the coupling to the Ricci scalar ξ_h, as given by Eq. (1.137), is considerably reduced with respect to ordinary HI. In particular $\xi_h \lesssim \mathcal{O}(10)$ for $\lambda_h \lesssim 4 \cdot 10^{-8}$. For these reasons, we found it interesting to show a wider parameter window of Fig. 5.2 that covers smaller values of the self-coupling parameter λ_h. We show, in Fig. 5.4, the overlapping region of Fig. 5.2 for $\lambda_h \ll 1$ where all conditions are met to successfully produce the BAU. As in this case, the Higgs self-coupling can be arbitrary small, so we used the exact solutions (1.123b) and (1.125b) instead of their approximations (1.130) and (1.131), with only minor differences.

5.3.3 Palatini formulation

In the Palatini formulation of HI, see Sec. 1.2.6, the inflationary predictions are different than those in the metric one [201]. Hence we are interested here to see if baryogenesis can occur.

From the interaction term (5.2) and the definition (3.48), we can extract

$$F(\chi) = \frac{\cos^2 \theta_W}{4} \frac{h^2(\chi)}{f_h^2} = \frac{\cos^2 \theta_W}{4} \frac{\sinh^2(\sqrt{\xi_h}\chi)}{\xi_h f_h^2}, \tag{5.21}$$
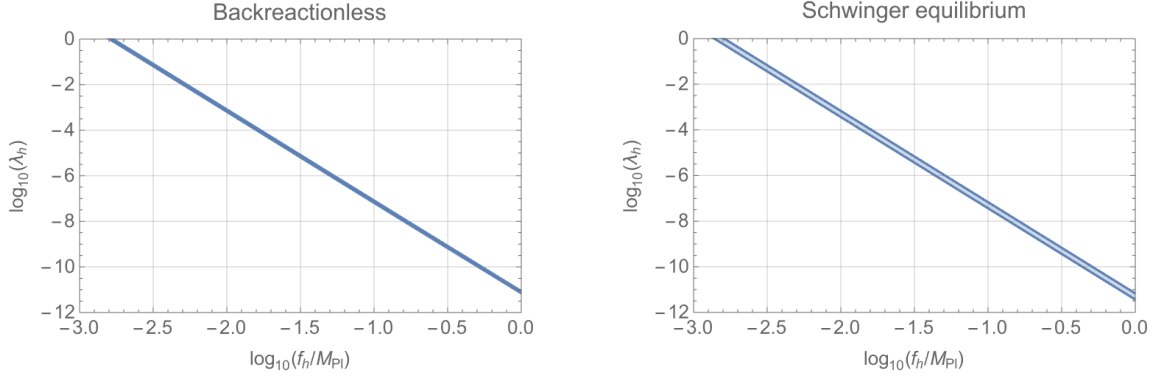
Figure 5.4. Region where the BAU can successfully be achieved, for a wider range of the parameters.

where we used Eq. (1.141a) in the second step. The parameter ξ is given, using Eq. (3.49), by

$$\xi = \frac{4\cos^2\theta_W}{f_h^2}. \tag{5.22}$$

We remind the reader that this result is valid only in the slow roll regime.

Notice the important difference between HI in the metric and the Palatini formalisms:

- In the metric formulation, the parameter ξ is almost constant, just providing the small growth $\xi_E \simeq 1.84\,\xi_*$ at the end of inflation, when the helical magnetic fields are generated relaxing their helicity into the baryon asymmetry at the EWPT. Therefore the non-Gaussianity bound on ξ at the CMB, $\xi_* < 2.55$ translates into the bound $\xi_E < 4.71$ at the end of inflation.

- In the Palatini formulation, the parameter ξ is exactly a constant throughout all the inflationary period, in particular $\xi_E = \xi_*$. Therefore the non-Gaussianity bound at the end of inflation is $\xi_E < 2.55$.

Given the baryogenesis window (5.19) we have found, this result means that while Palatini HI can be a viable candidate to produce cosmological inflation, the magnetic fields produced at the end of Palatini HI do not, however, have enough strength to generate the BAU.

Chapter 6

Combined Higgs – scalar field inflation

In this last chapter, we combine three main ideas we already presented in this thesis to provide a successful history of the Universe. They are the Higgs inflation model (Sec. 1.2.6) to which we will add a new coupling, baryogenesis via chiral (hyper)magnetic fields (Chap. 3), and stabilizing the SM Higgs potential by modifying the RG running of the Higgs quartic coupling (Sec. 2.3.5).

More precisely, motivated by HI we will here propose a model where the SM potential is simply stabilized by a scalar field ϕ coupled to the Higgs, opening up the possibility of direct or indirect detection at present (LHC) and future colliders. Moreover if the stabilizing field has a weak enough self-coupling and is coupled to the Ricci tensor as $\propto g\phi^2 R$, it can trigger cosmological inflation, as the potential becomes flat in the Einstein frame, while the COBE normalization does not impose strong constraints on the g coupling. Besides, in this theory the inflaton can couple to the Chern-Simons component of the SM hypercharge and trigger baryogenesis via the production of helical magnetic fields.

As the model utilizes many existing ideas, the consequence of each idea will be carefully examined to see how they interplay. Lastly, we will provide a successful parameter space for both the inflation model and baryogenesis that also could be probed in the terrestrial experiments like the LHC and electroweak precision constraints. In a devoted section, we will finally study from the point of view of particle physics the phenomenological implications of a light inflaton, one the possible outcomes of our model.

6.1   The model

As stated in the introduction, we will consider, on top of the Higgs field h, a new scalar state ϕ that couples to the Ricci tensor. Similarly to Eq. (1.112) with $p = 2$, we write the action in the Jordan frame as

$$S = \int d^4x \sqrt{-g} \left(-\frac{M_{\text{pl}}^2}{2} R - \frac{g}{2}\phi^2 R + \frac{1}{2}\partial_\mu h \partial^\mu h + \frac{1}{2}\partial_\mu \phi \partial^\mu \phi - U(\phi, h) \right), \qquad (6.1)$$

where $U(\phi, h)$ is the two-field potential, see below.

Notice that in this model we do not need to primarily introduce any $\xi_h |\Phi|^2 R$ term, i.e. the coupling leading to HI, see Eq. (1.126). Although a small value of the parameter ξ_h will be generated anyway by radiative corrections [26], its effects on the inflation mechanism will always be negligible,

even for values of $\xi_h \simeq \mathcal{O}(1)$. So for simplicity we are assuming $\xi_h = 0$. This is a major difference with respect to a previous attempt [202] of stabilizing the EW vacuum.

As we have seen for the non minimal coupling models of inflation in Sec. 1.2.5, because the Ricci term is quadratic in ϕ, $g\phi^2 R$, the beginning of inflation will be controlled by the quartic term $\lambda_\phi \phi^4$, which is the condition that guarantees a flat potential for large values of ϕ. This corresponds to the value $p = 2$ in Eq. (1.113). Therefore, in our model the Higgs field is not the only inflaton, but a component of the inflaton system, as inflation is really driven along a particular path in the two-field space, while its orthogonal direction has a strong curvature around its minimum, where the field system is anchored. We will develop this point in the next subsections.

The potential in the Jordan frame is a function of the two fields ϕ and h, which for Planckian values of the field ϕ can be approximated by the most general renormalizable polynomial satisfying the $\mathbb{Z}_2$ symmetry $\phi \to -\phi$, softly broken by the mixing term ϕh^2, i.e.

$$
\begin{aligned}
U(\phi, h) &= U_{\mathrm{SM}}(h) + \frac{1}{2}m^2\phi^2 + \frac{1}{2}\lambda_{\phi h}\phi^2 h^2 + \frac{1}{4}\lambda_\phi \phi^4 - \frac{1}{2}\mu\phi h^2 \\
U_{\mathrm{SM}}(h) &= -\frac{1}{2}\mu_h^2 h^2 + \frac{1}{4}\lambda_0 h^4.
\end{aligned}
\tag{6.2}
$$

The first four terms of the potential $U(\phi, h)$ are indeed invariant under this symmetry while the last term is a soft breaking that provides a correction in the one-loop β function of the Higgs quartic coupling such that the EW vacuum can be stabilized, see Sec. 6.1.2. Such a coupling was already pursued in Refs. [202, 203] and we will use it to constrain our parameter space.

We close the model presentation with a word on its parameters. Firstly, for large Higgs field configurations we will be neglecting the mass parameter μ_h^2, as compared to the λ_0 term, in $U_{\mathrm{SM}}(h)$. Then, the parameters $\lambda_{\phi h}$ and λ_ϕ should be constrained by the slow roll conditions during inflation to very small values $\lambda_{\phi h}, \lambda_\phi \ll 1$, as we will see in Sec. 6.2. Their smallness is radiatively stable, as can easily be deduced from their one-loop β functions,

$$
\beta_{\lambda_{\phi h}} = \frac{\lambda_{\phi h}}{16\pi^2}\left[12\lambda_0 + 8\lambda_{\phi h} + 6\lambda_\phi - \left(\frac{9}{2}g_2^2 + \frac{9}{10}g_1^2 - 6y_t^2\right)\right]\theta(t - t_0), \tag{6.3a}
$$

$$
\beta_{\lambda_\phi} = \frac{1}{16\pi^2}\left(8\lambda_{\phi h}^2 + 18\lambda_\phi^2\right)\theta(t - t_0), \tag{6.3b}
$$

where $t - t_0 = \log(\mathcal{Q}/m)$, and $\mathcal{Q}$ is the renormalization scale, see Sec. 2.3.5. The choice $\lambda_{\phi h} = 0$ is technically natural at one loop, as can be seen from Eq. (6.3a). For simplicity we will adopt hereafter the value $\lambda_{\phi h} = 0$. Moreover, from the amplitude of density perturbations, we will see that typically $\lambda_\phi \sim 10^{-12}$ (see left panel of Fig. 6.4), a value that is very mildly changed by radiative corrections.

Before studying the inflationary dynamics, our aim is to study the two-fields potential at both high energy $\phi \gg M_{\mathrm{pl}}/\sqrt{g}$ and low-energy $\phi \ll M_{\mathrm{pl}}/\sqrt{g}$ scales to find some analytical approximation that could simplify the inflation description.

6.1.1 Jordan frame

The action (6.1) is defined in the Jordan frame, and it is a valid framework provided that the field ϕ satisfies the condition $\phi \ll M_{\mathrm{pl}}/\sqrt{g}$. In other words, as we have seen in Sec. 1.2.5, no distinction is needed between Einstein and Jordan frames at low-energy scales, when the coupling to the Ricci tensor is subdominant. In this chapter, we hence refer to *Jordan frame* as the region where this is the case and we will see that it encompasses part of the inflationary period, and in particular the end of inflation. The trajectory of fields ϕ and h will proceed along the submanifold given by the minimum of the two-dimensional potential surface, providing a relationship between both fields, as anticipated in the last section.

To find the relationship between both fields ϕ and h, along the potential minimum direction, we will follow a general procedure summarized here. Given a potential $V(x, y)$ of two fields x and y, the contour lines corresponding to constant values of the function $V(x, y) = $ constant, satisfy the relation $dV = 0$, which reads

$$\frac{\partial V}{\partial x} \, dx + \frac{\partial V}{\partial y} \, dy = 0 \quad \Rightarrow F(x, y) \equiv \frac{dy}{dx} = -\frac{\partial V / \partial x}{\partial V / \partial y}, \tag{6.4}$$

where, by definition, the function $F[x, y]$ is the slope along the contour lines at the point (x, y). We wish to find the direction $y = f(x)$ that intersects orthogonally every contour line. The slope of this line is obviously $f'(x)$ and the slope of the orthogonal line is $-1/f'(x)$, so the condition for the orthogonal intersection is

$$F(x, f(x)) = -1/f'(x). \tag{6.5}$$

The idea behind the regions is to divide the potential valley into segments where, approximately, $\phi = ah^n$. The regions are separated according to which term dominates in the potential. Hence, we will find it useful to work with logarithmic variables

$$y = \log \phi, \qquad x = \log h, \tag{6.6}$$

where the ϕ and h fields are considered in some arbitrary mass units, such that the relation between fields translate into straight lines $y = nx + \log a$. Given the shape of our potential we find a unique solution to (6.5) in each region.

The direction $\phi = f(h)$ that intersects orthogonally every contour line in the plane (h, ϕ) is given by the solution to the equation

$$\left. \frac{\partial V / \partial h}{\partial V / \partial \phi} \cdot \frac{h}{\phi} \right|_{\phi = f(h)} = \frac{1}{f'(h)} \tag{6.7}$$

where Eqs. (6.4) and (6.5) have been used.

Therefore, the trajectory in the (ϕ, h) plane is given by relation (6.7), which changes according to the different regions of the potential that we will now introduce. This is validated by the plot of the total potential exhibited in Fig. 6.1. In all cases, the valley acts as an attractor for the fields, as explicitly shown in Ref. [202].

Hereafter, we will first carefully analyze the regions relevant after inflation, where the Einstein and Jordan frames are approximatively equivalent.

Region A

In this region both fields take their maximum allowed values in the (approximated) Jordan frame, and the potential can be approximated by the quartic coupling terms

$$U_{\mathrm{A}} \simeq \frac{1}{4} \lambda_0 h^4 + \frac{1}{4} \lambda_\phi \phi^4 \,. \tag{6.8}$$

The direction along the minimum can be found, after applying Eq. (6.7) to the potential (6.8), with the function $f(h) = (\lambda_0 / \lambda_\phi)^{-1/4} h$, i.e.

$$h = \left(\frac{\lambda_\phi}{\lambda_0} \right)^{\frac{1}{4}} \phi \,. \tag{6.9}$$

We plot in Fig. 6.1 the complete inflationary potential in the Einstein frame (see Sec. 6.1.3) and show the direction from Eq. (6.9) with a solid (green) line as specified in the figure caption.
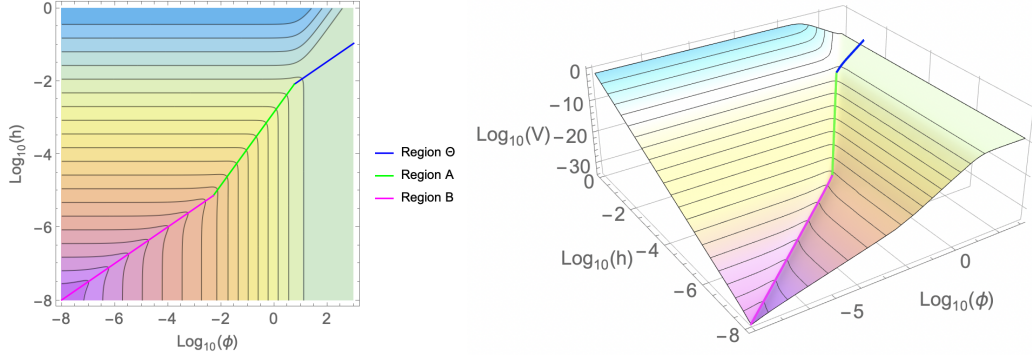
Figure 6.1. Left panel: Contour plot of the potential $V(\phi, h)$ in units where $M_{\mathrm{pl}} = 1$ with Regions Θ, A and B and the corresponding minimum submanifolds. Right panel: 3D plot of the potential with the same color code. We use the following numerical values: $g = 0.01$, $m = 10^{10}$ GeV, $\lambda_0 = 0.23$, $\delta_\lambda = 0.15$, $\lambda_\phi = 10^{-12}$.

Its region of validity is then given by

$$\frac{M_{\mathrm{pl}}}{\sqrt{g}} \gtrsim \phi \gtrsim \frac{2\sqrt{2}m}{\sqrt{\lambda_\phi}} \left(\frac{\delta_\lambda}{\lambda_0}\right)^{\frac{1}{2}}, \qquad\qquad h \gtrsim \frac{2\sqrt{2}m}{(\lambda_\phi \lambda_0)^{\frac{1}{4}}} \left(\frac{\delta_\lambda}{\lambda_0}\right)^{\frac{1}{2}}, \qquad\qquad (6.10)$$

where we have defined the constant δ_λ as

$$\delta_\lambda \equiv \frac{\mu^2}{2m^2}. \qquad\qquad (6.11)$$

Along the minimum direction (6.9) the potential can be written, as a function of ϕ, as

$$U_{\mathrm{A}}(\phi) \simeq \frac{1}{2}\lambda_\phi \phi^4, \qquad\qquad (6.12)$$

which will be used in the next section to describe the end of inflation.

To make contact with HI results, in this region we can also use the Higgs field as the explicit variable using the relation between the fields h and ϕ given by Eq. (6.9). This implies that the Ricci term in Eq. (6.1) can be equivalently written as $-\xi_{\mathrm{A}}/2\, h^2 R$, with $\xi_{\mathrm{A}} = g\sqrt{\lambda_0/\lambda_\phi}$. For typical values of the parameters (e.g. $g \simeq 0.01$, $\lambda_0 \simeq 0.2$, $\lambda_\phi \simeq 10^{-12}$, see Secs. 6.1.2 and 6.2), we get $\xi_{\mathrm{A}} \approx 4 \cdot 10^4$, which is the value required by HI, see Eq. (1.137). Moreover the potential (6.12) can be written, using again (6.9) as

$$U_{\mathrm{A}}(h) \simeq \frac{1}{2}\lambda_0 h^4. \qquad\qquad (6.13)$$

This result shows how, in region A, the results of HI could be interpreted in our model with $g \ll 1$, being perfectly consistent with the unitarity condition $\phi \lesssim \Lambda_\phi$.

Region B

In this region, where

$$\phi \lesssim \frac{2\sqrt{2}m}{\sqrt{\lambda_\phi}} \left(\frac{\delta_\lambda}{\lambda_0}\right)^{\frac{1}{2}}, \qquad\qquad m \lesssim h \lesssim \frac{2\sqrt{2}m}{(\lambda_\phi \lambda_0)^{\frac{1}{4}}} \left(\frac{\delta_\lambda}{\lambda_0}\right)^{\frac{1}{2}} \qquad\qquad (6.14)$$

the potential can be approximated by

$$U_{\mathrm{B}} \simeq -\frac{1}{2}\mu\phi h^2 + \frac{1}{2}m^2\phi^2 + \frac{1}{4}\lambda_0 h^4, \tag{6.15}$$

which, using Eq. (6.7), has its minimum along the direction

$$\phi = f(h) \equiv \left(-\frac{3\mu}{4m^2} + \sqrt{\frac{9\mu^2}{16m^4} + \frac{2\lambda_0}{m^2}}\right)h^2\,. \tag{6.16}$$

Direction (6.16) is shown in the potential plot, Fig. 6.1, with a solid (magenta) line. If we define the coupling λ as

$$\lambda \equiv \lambda_0 - \delta_\lambda\,, \tag{6.17}$$

in the limit $\lambda \ll 1$ we can write the minimum condition as

$$\phi \simeq \sqrt{\frac{\delta_\lambda}{2}}\,\frac{h^2}{m}\,[1 + \mathcal{O}(\lambda)] \tag{6.18}$$

and the potential (6.15) becomes

$$U_{\mathrm{B}} \simeq \frac{1}{4}\lambda h^4 + \mathcal{O}(\lambda^2), \tag{6.19}$$

which shows that the effective quartic coupling in this region is given by λ, instead of λ_0 as written in the original potential (6.2).

Region C

In this region $v < \mathcal{Q} \equiv h < m$, where v is the Higgs vacuum expectation value (VEV) and $\mathcal{Q}$, the renormalization scale, is here identified with the classical value of the Higgs field h. The field ϕ hence decouples and is integrated out as

$$\phi = \frac{\mu}{2m^2}h^2 + \mathcal{O}(h^6) \simeq \sqrt{\frac{\delta_\lambda}{2}}\,\frac{h^2}{m}, \tag{6.20}$$

which yields a potential

$$U_{\mathrm{C}} \simeq \frac{1}{4}\lambda h^4 + \mathcal{O}(h^8). \tag{6.21}$$

Notice that, to leading order, the solution to the equation of motion of ϕ, Eq. (6.20), agrees with the minimum condition in Region B, Eq. (6.18), which guarantees the continuity between both regions. Moreover the stability of the potential in both Regions B and C is provided by the same condition, $\lambda > 0$.

6.1.2   Stability of the potential

In Region C, $h < m$, the inflaton field ϕ is integrated out and the potential, as a function of the Higgs h, is given by Eq. (6.21), so that the parameter λ runs as the quartic coupling in the SM potential, according to the SM β function, $\beta_\lambda^{\mathrm{SM}}$. In Regions B and A, $h > m$, the inflaton ϕ propagates and thus there is an extra contribution to the running of the parameter λ as [202]

$$\beta_\lambda = \beta_\lambda^{\mathrm{SM}} + \frac{1}{2\pi^2}\delta_\lambda(3\lambda + \delta_\lambda)\,\theta(t - t_0), \tag{6.22}$$

where $\theta(x)$ is the Heaviside function, equal to 1 (0) for $x \geq 0$ ($x < 0$), and $t - t_0 = \log(h/m)$. The parameter δ_λ also runs with the renormalization scale as

$$\beta_{\delta_\lambda} = \frac{1}{2\pi^2} \delta_\lambda (3\lambda + 2\delta_\lambda) \, \theta(t - t_0). \tag{6.23}$$

The extra contribution to the running of λ in Eq. (6.22) can solve the Higgs vacuum instability problem provided that:

- The inflaton mass m is smaller than the SM instability scale, $\mathcal{Q}_I \sim 10^{11}$ GeV.

- The value of δ_λ at the scale $\mathcal{Q} = m$, $\delta_\lambda(m)$, is large enough in order to significantly change the value of $\beta_\lambda^{\text{SM}}$.

Of course, smaller values of m (i.e. wider regions where ϕ propagates) allow smaller values of $\delta_\lambda(m)$ to satisfy the second criterion. Conversely, for values of m close to $\mathcal{Q}_I$, the minimum value of $\delta_\lambda(m)$ that solves the instability is a largish one.

Note that should we have, instead, considered in the starting action a linear Ricci term, $g\phi R$, and a quadratic, $m^2\phi^2$ inflationary potential, i.e. $p = 1$ in Eq. (1.112), one could also have achieved the amount of flatness required by the slow roll conditions during the inflationary period, but the size of the amplitude of density perturbations, now controlled by m and no longer by λ_ϕ, would have yielded a value $m > \mathcal{Q}_I$, which is too large to stabilize the EW vacuum.

As we have seen, the condition for the stability of the potential is that the coupling λ defined in Eq. (6.17) is positive definite, $\lambda \geqslant 0$. We have solved at two-loop the RGE's of the theory for the following set of values of the input parameters [204] at the pole top mass $M_t = 172.76$ GeV,

$$
\begin{aligned}
g'(M_t) = 0.358545, \qquad g(M_t) = 0.64765, \qquad g_s(M_t) = 1.1618, \\
\lambda(M_t) = 0.12607, \qquad\qquad\qquad h_t(M_t) = 0.9312.
\end{aligned}
\tag{6.24}
$$

In Fig. 6.2 we show the two-loop running of the parameters λ and λ_0 for two extreme cases, with a light ($m = 1$ TeV, upper panels) and a heavy ($m = 10^{10}$ GeV, lower panels) inflaton. As we can see typical values of δ_λ are smaller for smaller values of m. We have chosen $\delta_\lambda = 0.05$ for $m = 1$ TeV, and $\delta_\lambda = 0.15$ for $m = 10^{10}$ GeV. In both cases the value of $\delta_\lambda(m)$ can be tuned to smaller values, such that the corresponding values of λ at high scales are smaller. On the other hand, larger values of δ_λ are bound by imposing that the theory remains in the perturbative regime up to the high scale. In particular we find for large values of m, $m \simeq \mathcal{Q}_I$, that $\delta_\lambda(m) \lesssim 0.35$, while for m in the TeV region, $\delta_\lambda(m) \lesssim 0.2$. The dashed lines in the left panels are the SM running, shown for comparison. On both left panels, we can see that the condition $0 < \lambda \ll 1$ is satisfied while $\delta_\lambda \gg \lambda$ at $\mathcal{Q} \sim M_{\text{pl}}$.

6.1.3 Einstein frame

For values of the ϕ field such that $\phi > M_{\text{pl}}/\sqrt{g}$, we must redefine the metric and go to the Einstein frame to recover the Einstein-Hilbert action for the Ricci scalar. To do so, we perform a Weyl redefinition of the metric and follow the procedure presented in Sec. 1.2.5 with $p = 2$. We can see from the second (dimension-six effective operator) term in Eq. (1.118) adapted to the current model, i.e. $3\Theta^2 \frac{g^2\phi^2}{M_{\text{pl}}^2}(\partial\phi)^2$, that the cutoff of the theory Λ_ϕ is identified as $\Lambda_\phi \equiv M_{\text{pl}}/g$.

It has been proven in Refs. [44, 46], that there is no tree-level unitarity problem for the amplitude $\mathcal{A}(\phi\phi \to \phi\phi)$ as, in the Einstein frame, see Eq. (6.25), there appears the effective operator $\phi^2(\partial_\mu\phi)^2/\Lambda_\phi^2$ that, upon integration by parts, gives, on-shell, the correction $m^2\phi^4/\Lambda_\phi^2$, and leads to a four-point function that does not grow with the energy, and thus does not violate unitarity. A similar result is obtained in the Jordan frame, where the amplitude $\mathcal{A}(\phi\phi \to \phi\phi)$ grows, in the
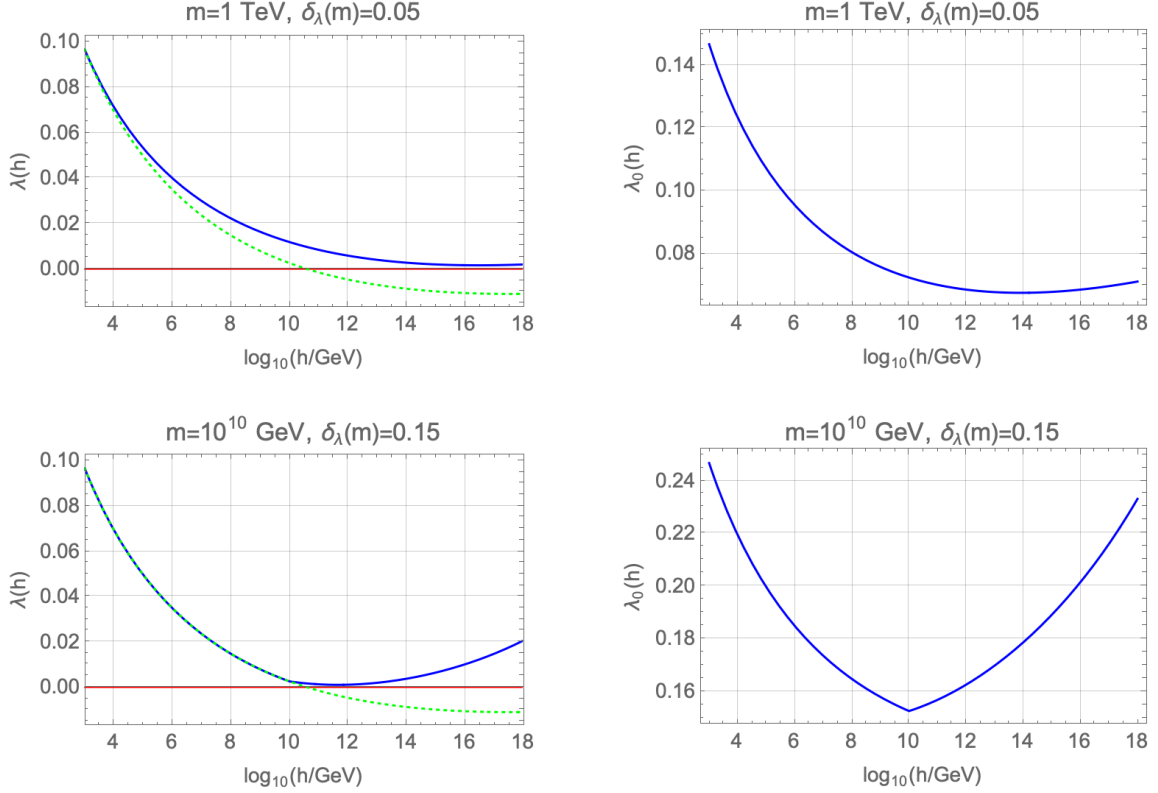
Figure 6.2. In blue, two-loop running of λ (left panels) and λ_0 (right panels) for two cases. Top panels: with $m = 1$ TeV, $\delta_\lambda(m) = 0.05$. Bottom panels: with $m = 10^{10}$ GeV, $\delta_\lambda(m) = 0.15$. The green dashed line is the SM running. In both cases one has $\lambda_0 \simeq \delta_\lambda$ for $\mathcal{Q} \sim M_{\rm pl}$.

s-channel, with the energy, and behaves as s/Λ_ϕ^2. However, considering the cross channels, there is a cancellation, and the four-point amplitude behaves as $(s + t + u)/\Lambda_\phi^2 \propto m^2/\Lambda_\phi^2$. However, the quick conclusion that unitarity is not violated at the scale Λ_ϕ has been challenged in Refs. [45, 46], where it was pointed out that, in the Jordan frame, the above cancellation is very unlikely to appear in loop-induced corrections to the same process $\phi\phi \to \phi\phi$, leading to a cutoff at the value $\sim 4\pi\Lambda_\phi$, where a loop factor has been included. The observation is similar for higher order processes, since e.g. $\phi\phi \to \phi\phi + n\phi$ has a cross section that scales as $\lambda_\phi^2 s^{n/2-1} g^n / M_{\rm pl}^n$, where λ_ϕ is the ϕ quartic coupling. This indicates that the perturbative description breaks down for energies $\sqrt{s} \gtrsim \lambda_\phi^{-2/n} \Lambda_\phi$, which goes to Λ_ϕ for large values of n. Similarly, in the Einstein frame, on top of the nonproblematic effective operator $\phi^2(\partial_\mu\phi)^2$, other higher order operators, e.g. $\phi^2(\partial_\mu\phi)^4$, are expected to be generated by loop effects, and so are expected to trigger violations of unitarity beyond the scale Λ_ϕ. In view of these arguments we will *conservatively* consider in this chapter Λ_ϕ as the scale at which unitarity is violated.

Unlike the generic non minimal coupling model from Sec. 1.2.5, there are here two fields affected by the Weyl transformation so that the (noncanonical) kinetic terms are given by

$$\mathcal{L}_{\rm kin}^E = \frac{\Theta}{2}\left(1 + \frac{6g^2\phi^2}{M_{\rm pl}^2}\,\Theta\right)\partial_\mu\phi\partial^\mu\phi + \frac{\Theta}{2}\partial_\mu h\partial^\mu h \qquad (6.25)$$

leading to the action in the Einstein frame with potential

$$S_E = \int d^4x \, \sqrt{-g} \left(-\frac{M_{\mathrm{pl}}^2}{2} R + \mathcal{L}_{\mathrm{kin}}^{\mathrm{E}} - V(\Theta, h) \right), \qquad V(\phi, h) = \Theta^2(\phi) \, U(\phi, h), \qquad (6.26)$$

where $U(\phi, h)$ is given by Eq. (6.2). The potential region where the values of the field ϕ satisfy the condition $\phi > M_{\mathrm{pl}}/\sqrt{g}$ is denoted as Region Θ and is explored hereafter.

Region Θ

As just stated, Region Θ is characterized by the potential $V(\phi, h)$ in the Einstein frame, i.e. Eq. (6.26) for $g\phi^2 > M_{\mathrm{pl}}^2$, and a straightforward application of Eq. (6.5) shows that, using Eq. (6.7), the direction along the minimum in the two-dimensional potential is given by

$$h^2 = M_{\mathrm{pl}} \left(\frac{\lambda_\phi}{3g\lambda_0} \right)^{\frac{1}{2}} \phi, \qquad (6.27)$$

from where the function $f(h)$ in Eq. (6.7) can easily be read out. Along this direction the potential is

$$V_\Theta(\phi) = \Theta^2(\phi) \, \frac{\lambda_\phi}{4} \, \phi^2 \left(\frac{M_{\mathrm{pl}}^2}{3g} + \phi^2 \right) \simeq \Theta^2(\phi) \, \frac{\lambda_\phi}{4} \, \phi^4, \qquad (6.28)$$

where again the last equality comes from the very definition of the Θ region. Notice that the values of the field ϕ at the beginning of inflation, and in particular its value ϕ_* at horizon crossing of the present Universe, belong to Region Θ.

In Fig. 6.1 we plot the potential in the Einstein frame $V(\phi, h)$ for a chosen set of the parameters values, and we superimpose the lines of minimum submanifolds given by Eqs. (6.27), (6.10) and (6.16), for Regions Θ, A and B, respectively. As we can see they intersect orthogonally, by construction, the contour lines of the potential. In the left panel we plot the contour lines of the potential and in the right panel the three-dimensional plot with the same color codes.

We can try to make contact with HI in Region Θ, as we did in Region A, using the Higgs field h as the explicit variable, by means of the relation between the fields ϕ and h given in Eq. (6.27), which we can write as

$$g\phi^2 = \xi_\Theta \frac{h^4}{M_{\mathrm{pl}}^2}, \qquad \text{with} \quad \xi_\Theta \equiv \frac{3g^2\lambda_0}{\lambda_\phi}. \qquad (6.29)$$

The Ricci coupling can then be written as $-\xi_\Theta h^4 R/M_{\mathrm{pl}}^2$, where $\xi_\Theta \simeq 3 \cdot 10^7$ by using the typical values of the parameters, $g \simeq 0.01$, $\lambda_0 \simeq 0.2$, $\lambda_\phi \simeq 10^{-12}$ (see Secs. 6.1.2 and 6.2). Similarly, using (6.27) we can also write the potential (6.28) as

$$V_\Theta(h) \simeq \left(1 + \xi_\Theta \frac{h^4}{M_{\mathrm{pl}}^4} \right)^{-2} \frac{\lambda_\phi}{4g^2} \, \xi_\Theta^2 \, \frac{h^8}{M_{\mathrm{pl}}^4}. \qquad (6.30)$$

These two expressions show that our model, written in terms of the Higgs field, departs from the conventional HI as it requires an effective dimension-eight operator for the potential which could only appear when the Standard Model is completed by some UV theory, giving rise, after decoupling, to higher dimensional operators.

6.2   Inflation

Inflation takes place only in Regions Θ (for $\sqrt{g}\phi > M_{\mathrm{pl}}$), and A (for $\sqrt{g}\phi < M_{\mathrm{pl}}$), thus we will choose conditions (6.27) and (6.9), respectively, to relate h and ϕ. In this case the kinetic term

(6.25) along the minimum direction can be written in both Regions Θ and A, as

$$\mathcal{L}_{\text{kin}}^{\text{R}} = \frac{\Theta}{2} \left[1 + 6\frac{g^2\phi^2}{M_{\text{pl}}^2}\Theta + \Delta_{\text{R}} \right] \partial_\mu\phi\partial^\mu\phi, \qquad (\text{R} = \Theta, \text{A}) \qquad (6.31)$$

where Δ_{R} corresponds to the (tiny) contribution of the Higgs kinetic term

$$\Delta_{\text{A}} = \left(\frac{\lambda_\phi}{\lambda_0}\right)^{\frac{1}{2}}, \qquad\qquad \Delta_\Theta = \frac{M_{\text{pl}}}{4\phi}\left(\frac{\lambda_\phi}{3g\lambda_0}\right)^{\frac{1}{2}} < \left(\frac{\lambda_\phi}{48\lambda_0}\right)^{\frac{1}{2}} \qquad (6.32)$$

and the last inequality comes from the condition $\sqrt{g}\phi > M_{\text{pl}}$. Putting in numbers we obtain that $\Delta_{\text{A}} \sim 10^{-6}$ and $\Delta_\Theta \lesssim 10^{-7}$, so that Δ_{R} can be safely neglected for numerical calculations in Eq. (6.31).

As for the potential in both inflationary regions, Θ and A, using the previous results we can write it as

$$V_{\text{R}}(\phi) \simeq c_{\text{R}}\, V(\phi), \qquad\qquad V(\phi) = \Theta^2(\phi)\,\frac{1}{4}\,\lambda_\phi\,\phi^4\,, \qquad \begin{matrix} c_\Theta = 1 \\ c_{\text{A}} = 2 \end{matrix} \qquad (6.33)$$

so that, in both regions, they only differ by a global factor. As the slow roll parameters do depend on ratios of the potential and its derivatives, they will not depend on the global factor c_{R} and can thus be given a universal expression. So for the computation of the slow roll parameters we will just remove the global factor c_{R} and use $V(\phi)$ as the inflationary potential.

In the same way as we did in Eqs. (1.121) and (1.122), we can now define the inflaton field χ, c.f. Eq. (1.121) with $p = 2$,

$$\frac{d\chi}{d\phi} \simeq \sqrt{\Theta(\phi)\left(1 + \frac{6g^2\phi^2}{M_{\text{pl}}^2}\,\Theta(\phi)\right)} \equiv f(\phi), \qquad (6.34)$$

which also defines the change of variable $\phi \to \chi$. In the last equality we defined the function $f(\phi)$ which will soon be handy for the slow roll parameters. Solving the above differential equation gives the approximation $\phi(\chi)$ given by Eq. (1.123b) for $\sqrt{g}\phi \gtrsim M_{\text{pl}}$, while for $\sqrt{g}\phi \lesssim M_{\text{pl}}$, we get $\phi \simeq \chi$ as in this limit the Jordan and Einstein frames should coincide.

Although the slow roll parameters must be computed from the inflaton potential $V(\chi)$, we will not need to use this explicit solution to obtain the inflationary parameters. Instead, we can keep ϕ as the explicit variable, since performing the change of variables (6.34) in the slow roll parameters definition allows us to avoid making inevitable approximations stemming from the relationship between the fields ϕ and χ. Hence, we can keep the description of the model in terms of the ϕ field and the potential $V(\phi)$ given in Eq. (6.33). In this framework the slow roll parameters can be written as [205]

$$\epsilon(\phi) = \frac{M_{\text{pl}}^2}{2}\left(\frac{V'(\phi)}{V(\phi)}\right)^2 f^{-2}(\phi), \qquad (6.35\text{a})$$

$$\eta(\phi) = M_{\text{pl}}^2\left[\frac{V''(\phi)}{V(\phi)}f^{-2}(\phi) - \frac{V'(\phi)}{V(\phi)}f'(\phi)f^{-3}(\phi)\right], \qquad (6.35\text{b})$$

$$\xi^2(\phi) = M_{\text{pl}}^4\,\frac{V'(\phi)}{V(\phi)}f^{-4}(\phi) \qquad (6.35\text{c})$$

$$\cdot\left[\frac{V'''(\phi)}{V(\phi)} - 3\frac{V''(\phi)}{V(\phi)}f'(\phi)f^{-1}(\phi) + \frac{V'(\phi)}{V(\phi)}\left(3f'^2(\phi)f^{-2}(\phi) - f''(\phi)f^{-1}(\phi)\right)\right],$$

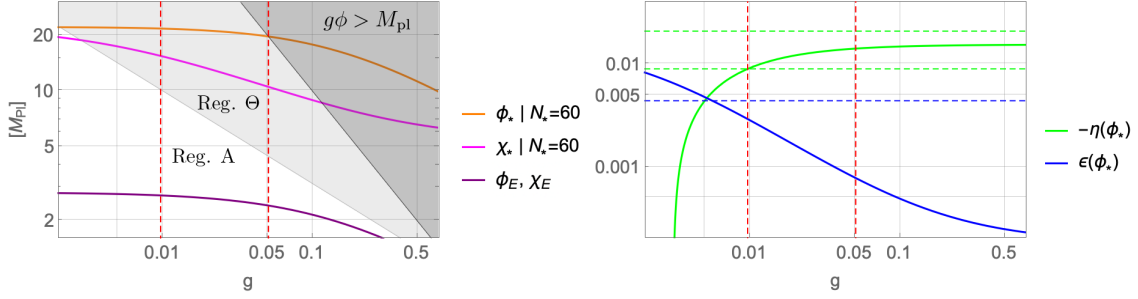**Figure 6.3**. Left panel: ϕ_E, ϕ_* and χ_* in unit of $M_{\rm pl}$, as functions of g. The dark shading region violates the unitarity bound $\phi < M_{\rm pl}/g$. The white area corresponds to Region A and the light shading one to Region Θ. Right panel: slow roll parameters evaluated at the beginning of inflation and their corresponding observational bounds (dashed, matching color). The bound for $\epsilon(\phi_*)$ is an upper bound.

where we dropped the index V from their definition in Eqs. (1.74), (1.75) and (1.76)[32]. Their current observational bounds are given by Eqs. (1.91).

We should evaluate the slow-roll parameters at the field value $\phi_* = \phi(N_*)$ with, recasting Eq. (1.94),

$$N_* = \frac{1}{M_{\rm pl}^2} \int_{\phi_E}^{\phi_*} \frac{V(\phi)}{V'(\phi)} \, f^2(\phi) \, d\phi. \qquad (6.36)$$

Here ϕ_E, the value of ϕ at the end of inflation, is defined by the condition $\epsilon(\phi_E) = 1$ and can be computed analytically. A plot of its dependence on g is shown on the left panel of Fig. 6.3. One can evaluate the integral (6.36) to find

$$N_* = \frac{1}{4} \left[\frac{(1 + 6g)(\phi_*^2 - \phi_E^2)}{2M_{\rm pl}^2} - 3\log \frac{M_{\rm pl}^2 + g\phi_*^2}{M_{\rm pl}^2 + g\phi_E^2} \right] \qquad (6.37)$$

and then solve it for $\phi_* \equiv \phi(N_*)$ [33]. A plot of ϕ_*, for $N_* = 60$, and its dependence on g is shown in the left panel of Fig. 6.3. The dark shading region is excluded as there $\phi_* > \Lambda_\phi \equiv M_{\rm pl}/g$ and so there is a unitarity violation (see however comments in Sec. 6.1.3). This constraint provides an upper bound on the value of the parameter g as $g \lesssim 0.0508$ [34].

We display, in the right panel of Fig. 6.3, the functions $\epsilon(\phi_*)$ and $\eta(\phi_*)$ as functions of g. The observational constraints (1.91) provide a lower bound on the Ricci coupling as $g \gtrsim 0.0096$. When combined with the upper bound from unitarity, the allowed region in the g parameter is given in

---

[32]We stress that the variable ϕ in these definitions must be the inflaton field with a canonical kinetic term, which is not the variable ϕ here but χ.

[33]We can solve Eq. (6.37) for $\phi(N_*)$ recursively, first ignoring the logarithm for the first iteration and then inserting each solution into the next iteration (which this time contains all terms). The sequence converges quickly to the exact solution. After 3–4 iterations the relative error is already $\sim 10^{-3}$ at most.

[34]For $g < 1$ the cutoff Λ_ϕ is trans-Planckian, and from Fig. 6.3 we can see that during inflation $\Delta\phi \simeq 20\,M_{\rm pl}$, which satisfies the so-called Lyth bound [206]. Such behavior induces non-negligible quantum gravity corrections to the potential. However, the terms induced by quantum gravity effects are suppressed, not by factors $\phi^n/M_{\rm pl}^n$, but by factors $V/M_{\rm pl}^4$ and $m^2/M_{\rm pl}^2$, see Sec. 2.4 of Ref. [207]. Hence, as long as the inflationary potential takes sub-Planckian values and $m \ll M_{\rm pl}$ (like in our model), quantum gravity effects are insignificant, regardless of the values of g or Λ_ϕ.

the range[35]

$$0.0096 \lesssim g \lesssim 0.0508. \tag{6.38}$$

Finally we have found that, in the relevant region of the g parameter, the parameter ξ^2 is $|\xi^2| \sim 10^{-4}$, well in agreement with the experimental range in Eq. (1.91).

For the allowed region of the slow roll parameters in Fig. 6.3, the cosmological observables, the scalar spectral index, the spectral index running, and the tensor to scalar ratio given by Eqs. (1.93) fall inside the experimental range given by Eqs. (1.92). In particular, for the allowed range (6.38) in the coupling g the theory predicts that

$$0.96448 \lesssim n_s \lesssim 0.96695 \qquad (0.96783) \tag{6.39a}$$
$$-0.00063 \lesssim n_s' \lesssim -0.00019 \qquad (-0.00005) \tag{6.39b}$$
$$0.0467 \gtrsim r \gtrsim 0.0124 \qquad (0.00296) \tag{6.39c}$$

where the unbracketed RHS bounds come from the unitarity bound, while the bracketed ones come from disregarding the latter in view of the comments in Sec. 6.1.3[36]. As we can see, both predicted ranges (with/without considering the unitarity bound) in (6.39) nicely fit inside the allowed range in Eq. (1.92). These results also agree with those of model $(n,p) = (2,4)$ in the recent work of Ref. [209], where general inflationary models with nonminimal inflaton couplings to gravity have been analyzed.

We now use the constraint on the amplitude of scalar fluctuations to find an analytical relation for the inflaton self-coupling λ_ϕ, since this quantity is obtained from the potential as

$$A_s = \frac{1}{24\pi^2 M_{\rm pl}^4} \frac{V_\Theta(\phi_*)}{\epsilon(\phi_*)}, \tag{6.40}$$

where we are using as inflaton potential V_Θ, as the ϕ_* line in the left panel of Fig. 6.3 is inside the light shading region, where the inflaton potential corresponds to that in Region Θ, Eq. (6.33). We can then compute λ_ϕ as

$$\lambda_\phi = 96\,\pi^2\,g^2\,A_s\,\epsilon(\phi_*)\left(1 + \frac{M_{\rm pl}^2}{g\phi_*^2}\right)^2. \tag{6.41}$$

Using the observed value of A_s from Ref. [22], $A_s^{\rm obs} = 2.2 \cdot 10^{-9}$, as well as the values of $\epsilon(\phi_*)$ and ϕ_* from Fig. 6.3, we plot in the left panel of Fig. 6.4 the parameter λ_ϕ as a function of the Ricci coupling g. Notice that inside the allowed region in Eq. (6.38) we obtain $\lambda_\phi \sim 10^{-12}$ as postulated when presenting the model.

Finally, we can compute the Hubble parameter (1.28) during inflation $H(\phi)$. From the Friedmann equation (1.11) we have that the energy density of the inflaton reads as $\rho(\phi) = 3M_{\rm pl}^2 H^2(\phi)$. Since we are assuming a slow roll evolution (1.73) of the inflaton, we can neglect the kinetic part in the energy density and consider $\rho(\phi) \simeq V_{\rm R}(\phi)$. Therefore in Region A, i.e. around the end of

---

[35]One should worry about the stability, under radiative corrections, of such small values of the g parameter. Contributions to the one-loop β_{ξ_h} function, in the Ricci coupling $(\xi_h/2)\,h^2 R$, from the contribution of the SM fields (top quark, gauge and Higgs bosons), have been computed in Refs. [26, 208] where it is shown that the renormalization from the weak to the high scale of $\xi_{\mathcal{H}}$ is $\lesssim 20\%$. In the case of our coupling $(g/2)\,\phi^2 R$, as ϕ is not directly coupled to the SM fields, the g running between m and the high scales is suppressed by the mixing angle α between the fields ϕ and h (see Sec. 6.5), so that $\beta_g \simeq 2\delta_\lambda(v^2/m^2)\beta_{\xi_h} \ll \beta_{\xi_h}$. In this way the running of the g parameter can be safely neglected.

[36]If we disregard the unitarity bound, see the comments in Sec. 6.1.3, there is no upper bound on g from observational constraints and the cosmological observables for larger values of g asymptotically go to the RHS values in parenthesis.
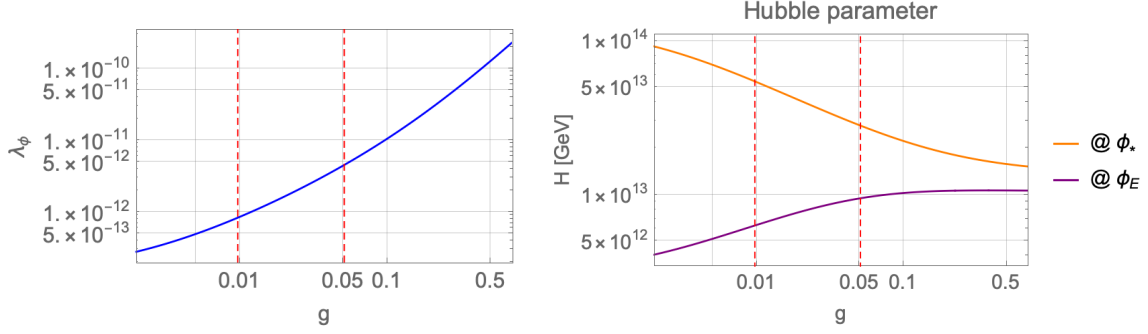
Figure 6.4. Left panel: The inflaton self-coupling λ_ϕ as a function of g. Right panel: The Hubble parameter H at the end of inflation $H(\phi_E)$ and for the number of e-folds N_*, $H(\phi_*)$ as functions of g. In both plots the vertical red lines show the range for g where the slow roll cosmological observables and unitarity constraints are met.

inflation and, in particular, at ϕ_E, $H_E \equiv H(\phi_E)$,

$$H(\phi) = \frac{M_{\rm pl}}{g}\sqrt{\frac{\lambda_\phi}{6}}\left(1 + \frac{M_{\rm pl}^2}{g\phi^2}\right)^{-1}. \tag{6.42}$$

For the value $\phi = \phi_*$, in Region Θ, this further simplifies to

$$H_* \equiv H(\phi_*) = 2^{3/2}\pi M_{\rm pl}\sqrt{\epsilon(\phi_*)A_s^{\rm obs}}. \tag{6.43}$$

We plot in the right panel of Fig. 6.4 the Hubble parameters at the end of inflation, i.e. for $\phi = \phi_E$, H_E, and at the beginning of inflation, for a number of e-folds $N_* = 60$, H_*. As we can see from the right panel of Fig. 6.4, for the lower bound of g, $g \simeq 0.01$, the Hubble parameter changes, between ϕ_E and ϕ_*, by one order of magnitude, from $H_* \simeq 5.5 \cdot 10^{13}$ GeV, to $H_E \simeq 6.4 \cdot 10^{12}$ GeV. On the other hand, for the upper bound of g, $g \simeq 0.05$, the Hubble parameter changes by a little, from $H_* \simeq 2.8 \cdot 10^{13}$ GeV to $H_E \simeq 10^{13}$ GeV. As we can see, the absolute upper bound on the Hubble parameter in our model is $H_* \lesssim 5.5 \cdot 10^{13}$ GeV, or equivalently an inflation scale $V_\Theta^{1/4}(\phi_*) \lesssim 1.5 \cdot 10^{16}$ GeV, in agreement with the observational upper bounds given by Eqs. (1.96). Consequently our model, independently of the value of m, is a high scale inflation model, where the Hubble parameter does depend on the value of g and is maximized for its lower bound.

6.3   Reheating

When studying non minimally coupled models of inflation in Sec. 1.2.5, we have found that the potential (1.125b), i.e. $V[\phi(\chi)]$ from Eq. (6.33), is equivalent to an α-attractor potential with $\alpha = 1 + \frac{1}{6g}$. Thus, the range (6.38) of the present model translates into $4 \lesssim \alpha \lesssim 18$. In Chap. 4 we have studied the baryogenesis and preheating capabilities of an α-attractor potential[37] with $\alpha = 1, 50$, see in particular Figs. 4.10 and 4.11. Our calculations have shown that the results in the cases $\alpha \simeq 4, 18$ are very similar to the case $\alpha = 1$, therefore we can already make some conclusions by retrieving the informations in the previous chapters. The first one is that in our model gauge preheating does not occur and reheating should take place by perturbative decays of the inflaton

---

[37]The computations were done in the symmetric phase while here the Higgs VEV is non zero, but the results are transferable since $Z_Y \simeq Z_{\rm EM}$, see Sec. 4.1.2.

into the SM matter only. The second conclusion concerns the helical hypermagnetic field production and will be addressed in the next section.

In Sec. 4.4.1 we have given some relations, see Eqs (4.66), between the reheating to instant reheating temperature ratio, a quantity entering the baryogenesis parameter space, and the coupling between the inflaton and the CS term f_ϕ. These were based on an inflaton decay to hyperphotons whose rate is given by (4.61). In the present model however, the action (6.2) contains the interaction term $\sqrt{\delta_\lambda/2}\, m\, \chi h^2$ which gives rise to the leading inflaton decay channel $\chi \to hh$, with a decay width given by [210]

$$\Gamma(\chi \to hh) = \frac{\delta_\lambda\, m}{16\pi} \sqrt{1 - \frac{4m_h^2}{m^2}}, \tag{6.44}$$

where $m_h = 125.25$ GeV is the Higgs mass. As the inflaton is stabilizing the EW vacuum (see Sec. 6.1.2), which has an instability around $\mathcal{Q}_I \simeq 10^{11}$ GeV, we can reliably put the upper bound on m as $m \lesssim \mathcal{Q}_I$, and fix e.g. $m \simeq 5 \cdot 10^{10}$ GeV while $\delta_\lambda \lesssim 0.35$ on perturbative grounds (see Sec. 6.1.2). This gives for the decay width $\Gamma(\chi \to hh) \simeq 3.5 \cdot 10^8$ GeV leading, using Eq. (1.97), to a reheating temperature given by $T_{\rm rh} \simeq 1.6 \cdot 10^{13}$ GeV, which corresponds to $T_{\rm rh}/T_{\rm rh}^{\rm ins} \sim 10^{-2}$. On the other hand, the lowest bound on m, fixed by phenomenological considerations (see Sec. 6.5) to $m \simeq 10^3$ GeV, together with $\delta_\lambda \lesssim 0.2$ (see Sec. 6.1.2) provides $\Gamma(\chi \to hh)$ of a few GeV and correspondingly $T_{\rm rh} \simeq 10^9$ GeV, which implies $T_{\rm rh}/T_{\rm rh}^{\rm ins} \sim 10^{-6}$. Hence from now on, we will consider the temperature ratio $T_{\rm rh}/T_{\rm rh}^{\rm ins}$ as a parameter of the model, which as we know is handy for the baryogenesis and constraints calculations. We also stress that this ratio mainly reflects the dependence of coming results on m, as just sketched above.

There are of course other channels that can contribute to Γ_χ such as (4.61) but we have already seen in Sec. 4.4.1 that this one is subleading with respect to the channel $\chi \to hh$ for the relevant values of m and f_ϕ. In particular $\Gamma(\chi \to AA) \simeq 10^{-5}$ GeV for $m = 5 \cdot 10^{10}$ GeV, while $\Gamma(\chi \to AA) \simeq 10^{-28}$ GeV for $m = 10^3$ GeV.

Moreover, there is a mixing angle α between ϕ and h (see Sec. 6.5), which is sizable for $m \sim \mathcal{O}(\text{few})$ TeV, while of course is negligible for $m \gg 1$ TeV, given by $\sin\alpha \simeq \sqrt{2\delta_\lambda}\, v/m$. This mixing opens up the χ decays into the SM channels, with a total decay width into all SM channels given by $\Gamma(\chi \to \text{SM}) = \sin^2\alpha \cdot \Gamma(h \to \text{SM}) \simeq 4\sin^2\alpha$ MeV, in all cases subleading with respect to the decay width $\Gamma(\chi \to hh)$.

Finally, the possibility that the Lagrangian in Eq. (6.2) could induce preheating by the explosive production of scalar fields after inflation was considered in Ref. [185]. In this case, we can identify the scalar fields of Ref. [185] with the Higgs field[38] and this mechanism, if implemented, would be more efficient than the perturbative production that has been considered so far in this section. First of all, as we wanted the inflaton to stabilize the Higgs potential we have imposed the condition on its mass $m < 10^{-7} M_{\rm pl}$. This means that during preheating the inflaton potential term $\frac{1}{4}\lambda_\phi \phi^4$ will dominate the mass term $\frac{1}{2}m^2\phi^2$, as $\lambda_\phi \simeq 10^{-12}$ and $\phi_E \simeq M_{\rm pl}$. In Ref. [185] it was proven that there are no runaway solutions provided that $\delta_\lambda < \lambda_0/4$, and preheating imposes the mild condition $2\delta_\lambda > (100\, m/\phi_E)^2$ which is always satisfied as $100\, m/\phi_E < 10^{-5}$. Still in the rest of the chapter we will be agnostic about the (p)reheating mechanism and will consider the reheating temperature $T_{\rm rh}$ as a free parameter.

---

[38] The relation between the parameters q_3 and q_χ in Ref. [185] and our parameters can be written as

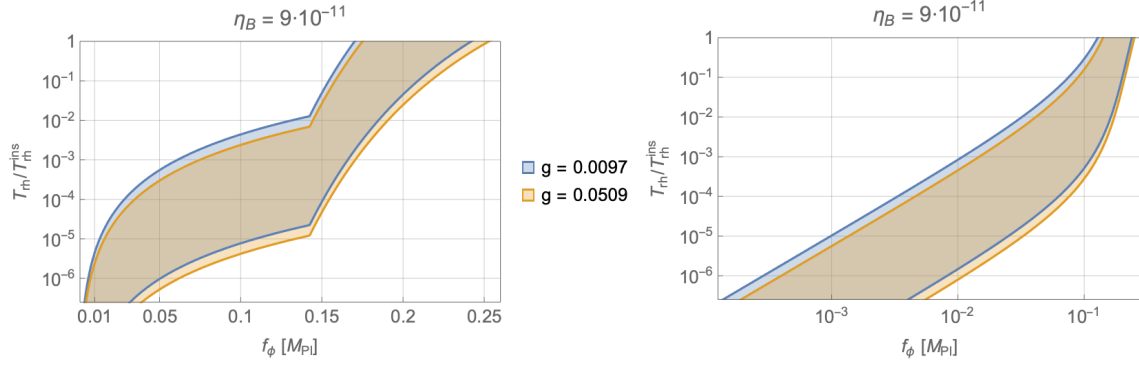$$q_3 = \sqrt{2\delta_\lambda}\frac{\phi_E}{m}, \quad q_\chi = \frac{\lambda_0 \phi_E^2}{m^2}.$$

Figure 6.5. The baryogenesis region. In the shading region the value of η_B satisfies Eq. (3.18). We can see that the dependence on g is tiny. Left panel: Schwinger maximal estimate. Right panel: Schwinger equilibrium estimate.

.

6.4 Baryogenesis

In this section we will consider the generation of fully helical hypermagnetic fields that will be transformed into baryon asymmetry at the EWPT. We need a source of $\mathcal{CP}$ violation and we will assume, similarly to Eq. (3.20), the $\mathcal{CP}$-odd dimension-five operator given by

$$S \supset - \int d^4x \; \frac{\phi}{4f_\phi} F_{\mu\nu} \widetilde{F}^{\mu\nu} \tag{6.45}$$

where by virtue of the minimum condition in Region A, Eq. (6.9), the Higgs background value is non zero (it is anchored to the value of the field ϕ), and so the electroweak symmetry is broken, meaning ordinary $U(1)_{\mathrm{EM}}$ magnetic fields are produced during inflation. At reheating, the Higgs VEV will drop at its potential minimum because of the sudden dominance of the thermal correction terms, and we will recover the symmetric phase. The ordinary magnetic fields are therefore projected according to (5.18) to the hypercharge components where they survive until EWPT if the criteria from the constraints discussed in Sec. 3.3 are met. A UV completion for the above interaction within our model is provided in App. A.1.

We will be concerned by the last e-folds of inflation, corresponding to the inflaton value $\phi \simeq \phi_E$, well inside Region A, with a potential given by Eq. (6.33). This is because we have seen in the previous chapters that the modes that contribute the most to the plasma quantities, Eqs. (3.39), are generated near the end of inflation. This effect is even more pronounced since the instability parameter ξ increases sharply at the end of inflation (see Fig. 4.4), which allows the magnification of modes k after a time τ such that $|k\tau| \sim |2\xi| \sim \sqrt{2\epsilon}/f_\phi$. Therefore, the differential equation (6.34) admits the simple solution $\phi \simeq \chi + \mathcal{O}(g)$ and we can write the EoM for χ as (3.44) with the replacement $\phi \to \chi$.

As an outcome, the results presented in Fig. 4.11 are valid for the present scenario. However, in the following we will develop on this result for the actual model, by having a closer look at the constraints. To do so, we choose for convenience to keep an analytical framework, i.e. we will use the Schwinger equilibrium and maximal estimate (see Secs. 4.2.1 and 4.2.2) for the fermion backreaction, since we have proven in Chap. 4 that the full numerical solution lies in between[39], see

---

[39]Actually, the numerical results are in favor of the Schwinger equilibrium estimate (at least for $f_\phi \lesssim 0.05\,M_{\mathrm{pl}}$) but for completeness we will provide the maximal estimate as well.
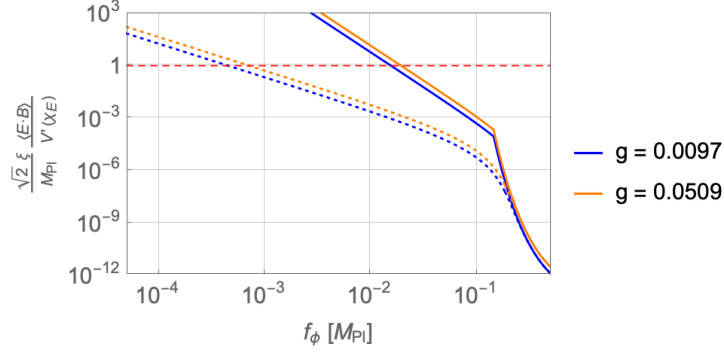
Figure 6.6. Ratio between the potential term and the backreaction term in the inflaton equation of motion, see Sec. 3.2.3, for the range of values of g allowed by inflation. Solid lines are the maximal estimate while dashed lines are the equilibrium estimate, after taking into account the Schwinger effect.

plots on Fig. 4.5. Moreover, we aim to show that the dependence on g of the baryogenesis result is tiny.

Indeed, in Fig. 6.5 we show in the plane $(f_\phi, T_{\rm rh}/T_{\rm rh}^{\rm ins})$, for both bounds on the allowed g range given by Eq. (6.38), and for both Schwinger estimates for the magnetic fields, i.e. maximal (left panel) and equilibrium (right panel) estimates, the region where the value of η_B satisfies Eq. (3.18), taking into account the range in Eq. (3.19) for the quantity f_{θ_W}. As we can see from both panels, together with the range (6.38) on the g parameter where inflationary conditions in Ref. [22] are satisfied, there is an absolute upper bound on the parameter f_ϕ as $f_\phi \lesssim 0.25 \, M_{\rm pl}$ for both Schwinger estimates, corresponding to the reference (instant) reheating temperature where the baryogenesis conditions are met. This result changes a little bit in the case of the numerical result for $\alpha = 1$, where we have $f_\phi \lesssim 0.1 \, M_{\rm pl}$, see Fig. 4.11. Moreover, for the highest reheating temperature we can get from our model of inflation, $T_{\rm rh} \simeq 10^{-2} \, T_{\rm rh}^{\rm ins}$, the bound lowers to $f_\phi \lesssim 0.19 \, (0.17) \, M_{\rm pl}$ for the maximal (equilibrium) Schwinger estimate. For the numerical solution of Fig. 4.11, the bound becomes $f_\phi \lesssim 0.06 \, M_{\rm pl}$. We remind the reader that the value $g = 0.05$ corresponds roughly to $\alpha \simeq 4$.

As we know from Sec. 3.3, there are constraints that can further narrow the region of the parameter space where the BAU can really be reproduced by our theory. Since the dependence on g is tiny, we will from now provide the results for $g = 0.05$ only. We chose this bound as it is the closest to the numerical solving of Sec. 4.4.2. Therefore, the parameter space reduces to $(f_\phi, T_{\rm rh})$.

For the Schwinger estimate to be valid, we must ensure that the self-consistency condition $|\mathcal{G}/V'| \ll f_\phi$ is met, see Sec. 3.2.3, where it was studied for the backreactionless case. Now taking into account the Schwinger effect, the equilibrium estimate is obtained by the replacement $\xi \to \xi_{\rm eq}$ in the expression (3.40b), as described in Sec. 4.2.1. Hence, the consistency condition in the Schwinger equilibrium estimate is given by Eq. (3.47) where $\xi \to \xi_{\rm eq}$, i.e.

$$2 \, \rho_{\rm EM}^{\rm eq} \ll V(\chi_E), \tag{6.46}$$

a stronger condition than the one coming from the Friedman equation $\rho_{\rm EM}^{\rm eq} \ll V(\chi_E)$, but much weaker than Eq. (3.47) where we were ignoring the Schwinger effect, since $\rho_{\rm EM}^{\rm eq} \ll \rho_{\rm EM}$.

On the other hand, for the maximal estimate, a similar reasoning for the consistency condition does apply to this case. Instead, we use the results from the end of Sec. 4.2.2, in particular Eqs. (4.27) and (4.28), where the total energy density is dominated by the energy stored in the magnetic field, $\rho_{\rm EM} \simeq \rho_B$,

We display in Fig. 6.6 the quantity $|\mathcal{G}/(f_\phi V')|$ as a function of f_ϕ for the range allowed on the parameter g by the inflationary observables, using for $\mathcal{G}$ both the maximal and the equilibrium estimates given by Eqs. (4.22) and (4.24c). In conclusion, condition $|\mathcal{G}/V'| \ll f_\phi$ is satisfied for:

$$\begin{aligned} f_\phi &\gtrsim 1.9 \cdot 10^{-2} \, M_{\mathrm{pl}} & \text{(Maximal estimate)}, \\ f_\phi &\gtrsim 7.2 \cdot 10^{-4} \, M_{\mathrm{pl}} & \text{(Equilibrium estimate)}. \end{aligned} \tag{6.47}$$

Moving to the MHD constraints, see Sec. 3.3.2, we conclude from the left panels of Fig. 6.7 that in our scenario $\mathcal{R}_e^{\mathrm{rh}} < 1$, for the range of parameters that provides a successful baryogenesis. We plot the value of $\mathcal{R}_e$ at reheating in solid lines for the two extreme values of the parameter $T_{\mathrm{rh}}/T_{\mathrm{rh}}^{\mathrm{ins}} = 10^{-2}$ (blue color) and 10^{-6} (orange color). Thus, the plasma starts in the viscous regime and the magnetic Reynolds number should be computed using Eq. (3.73a). Plots of $\mathcal{R}_m^{\mathrm{rh}}$, as a function of f_ϕ, are also shown in the left panels of Fig. 6.7 (dashed lines) for the same values of the parameter $T_{\mathrm{rh}}/T_{\mathrm{rh}}^{\mathrm{ins}}$ and the same color codes. We consider the Schwinger maximal (top left panel) and equilibrium (middle left panel) estimates for the gauge fields. As for the bottom panels, they display the numerical results from Sec. 4.4.2. In all cases we exhibit the regions allowed by the baryogenesis constraint, which depend on the corresponding values of the parameter $T_{\mathrm{rh}}/T_{\mathrm{rh}}^{\mathrm{ins}}$, using the same color code than for the different lines (both for $\mathcal{R}_e^{\mathrm{rh}}$ and $\mathcal{R}_m^{\mathrm{rh}}$) in the plot. Then even if $\mathcal{R}_e^{\mathrm{rh}} < 1$, at some later time τ the plasma will eventually fall into the turbulent regime where $\mathcal{R}_e > 1$, with an evolution given by Eq. (3.73b).

As we can see from the dashed lines in the left panel plots of Fig. 6.7 the condition $\mathcal{R}_m^{\mathrm{rh}} > 1$ is not satisfied everywhere in the region allowed by baryogenesis. Therefore, as summarized in Fig. 6.8, the condition for magnetic induction dominance, $\mathcal{R}_m > 1$, constrains the available region from the baryogenesis window. Of course, once the condition $\mathcal{R}_m^{\mathrm{rh}} > 1$ is satisfied (at the reheating temperature), its value increases with time, see Eq. (3.74b), which guarantees that the condition will be fulfilled until the EWPT.

The chiral plasma instability (CPI) constraint, see Sec. 3.3.3, is studied on the right panels of Fig. 6.7. Here we show the plot of T_{CPI} as a function of f_ϕ for both the Schwinger maximal (top panel) and equilibrium (middle panel) estimates, as well as the numerical result from Sec. 4.4.2 (bottom panel) and values of $T_{\mathrm{rh}}/T_{\mathrm{rh}}^{\mathrm{ins}} = 10^{-2}$ (blue color) and 10^{-6} (orange color). In each plot, the region between the vertical bands is that selected by the baryogenesis mechanism for the corresponding value of $T_{\mathrm{rh}}/T_{\mathrm{rh}}^{\mathrm{ins}}$ with the same color code. As we can see from Fig. 6.7, the range of values for T_{CPI} in the corresponding baryogenesis region is

$$10^2 \text{ GeV} \gtrsim T_{\mathrm{CPI}} \gtrsim 10^{-3} \text{ GeV} \tag{6.48}$$

which then prevents the cancellation of any previously generated helicity. So, as we will explicitly exhibit in Fig. 6.8, this constraint is satisfied in all the region provided by the baryogenesis condition.

Before summarizing these result, we finally have to ensure that the primordial non-Gaussianity and the baryon isocurvature perturbation provide no constraint. Recasting Eq. (3.83), which we adapt to the Schwinger estimates, as

$$\frac{\xi_{\mathrm{eq/max}}}{\xi_{\mathrm{CMB}}} = \sqrt{\frac{1}{\epsilon(\chi_*)}} \tag{6.49}$$

where $\xi_{\mathrm{eq/max}} \equiv \xi_{\mathrm{eq/max}}(\chi_E)$ is the value of the effective ξ parameter at the end of inflation in the equilibrium/maximal Schwinger estimate, one can compute corresponding upper bounds on $\xi_{\mathrm{eq/max}}$, at the end of inflation using the value of $\epsilon(\chi_*)$ from our model, see Sec. 6.2 and Fig. 6.3. For the lower value of g allowed by the cosmological observables in our inflation model, $g \simeq 0.01$, one gets
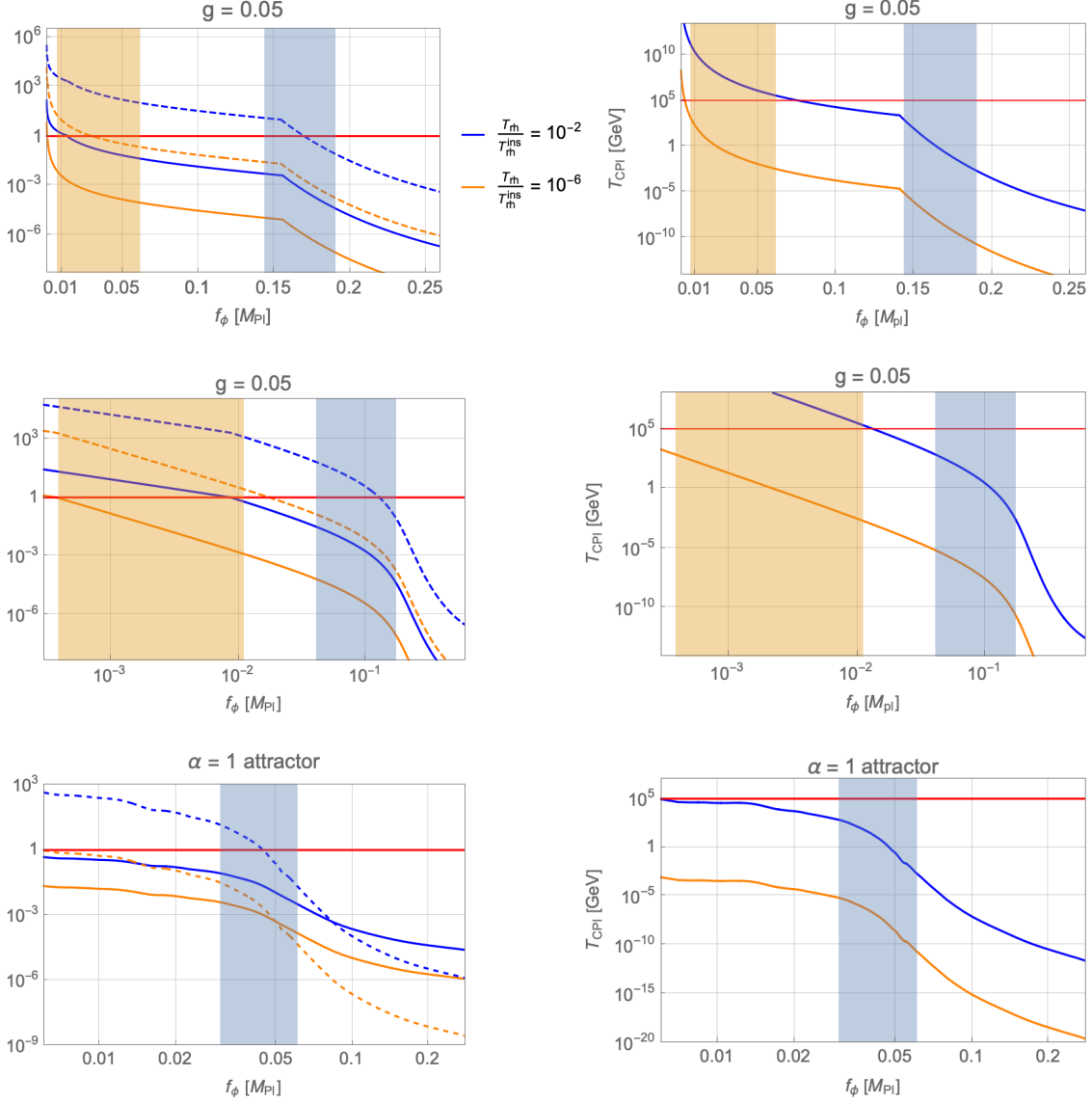
Figure 6.7. Left panels: Plot of the electric (solid lines) and magnetic (dashed lines) Reynolds number at reheating as a function of f_ϕ for different values of $T_{\rm rh}/T_{\rm rh}^{\rm ins} = 10^{-2}$ (blue color) and 10^{-6} (orange color). The ranges of successful baryogenesis for the different values of $T_{\rm rh}/T_{\rm rh}^{\rm ins}$ are displayed here by the vertical bands, whose colors match the corresponding lines color. We see that the production of the helical magnetic fields at reheating always occurs for $\mathcal{R}_e < 1$ but not necessarily for $\mathcal{R}_m > 1$, in the correct baryogenesis region. The latter condition must nevertheless be met for successful baryogenesis, which reduces the parameter window mainly (but not only) for high reheating temperatures. Right panels: Plot of the $T_{\rm CPI}$ temperature. In the baryogenesis regions we always have $T_{\rm CPI} < 10^5$ GeV. Top panels correspond to the Schwinger maximal estimate, middle panels to the equilibrium estimate. In the bottom panels we display, for completeness, the numerical result for the α-attractor potential from Sec. 4.4.2 with $\alpha = 1$. We recall that a value of $g = 0.05$ corresponds to $\alpha \simeq 4$, hence both scenarios are very close.

$\xi_{\rm eq/max} \lesssim 47$ while for the upper bound, $g \simeq 0.05$, one gets $\xi_{\rm eq/max} \lesssim 91$. However those values of $\xi_{\rm eq/max}$ are never reached in our model, as they would correspond to negligibly small values of f_ϕ which are never met. For the case of the equilibrium estimate, this can be seen from the relation between ξ and $\xi_{\rm eq}$ displayed on Fig. 4.1.
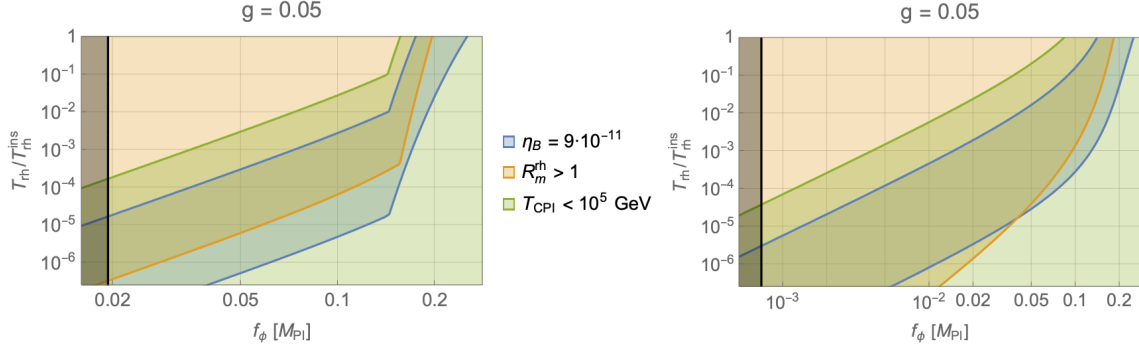
Figure 6.8. Summary of constraints on baryogenesis for $g = 0.05$ (the dependence on g is tiny) in the plane $(f_\phi/M_{\rm pl}, T_{\rm rh}/T_{\rm rh}^{\rm ins})$. The considered constraints are on η_B (blue area), on the magnetic Reynolds number (orange area) and on chiral plasma instability (green area). We are looking for the overlapping region. On the left side of each plot, the black band displays the region where the backreaction of gauge fields on the inflaton can no longer be neglected. Left panel: Schwinger maximal estimate. Right panel: Schwinger equilibrium estimate. The equivalent plot for the numerical result with the α-attractor potential can be found in Fig. 4.11.

In conclusion, in the presence of the Schwinger effect the produced gauge fields are never strong enough to trigger non-Gaussianity in the distribution of the primordial inflaton fluctuations, in good agreement with present observations. In other words, the model prediction in the presence of the fermionic Schwinger currents is $f_{\rm NL}^{\rm equil} \simeq 0$ and so we will not consider this constraint further.

Finally, in Sec. 3.3.5 we have computed the baryon isocurvature perturbation for the plasma quantity in the backreactionless scenario, where they depend exponentially on $2\pi\xi$. We have found that the bound given by (3.84) was largely satisfied. It is thus even more so if the fields are damped by the Schwinger effect, so this constraint does not need to be taken into account any further.

To conclude on baryogenesis, we show on Fig. 6.8 the parameter space of all the aforementioned constraints, where we removed the dependence on g as the results are not sensitive to it, preferring to choose the value $g = 0.05$ in the allowed range from the inflation model.

From both plots we can conclude that the CPI constraint is satisfied in all the regions where the constraint of having enough baryon asymmetry η_B holds. On the other hand the constraint from the magnetic Reynolds number is effective for the case of the Schwinger maximal estimate, by cutting off the larger available values of the parameter f_ϕ for every value of $T_{\rm rh}$. However, for the Schwinger equilibrium estimate the magnetic Reynolds number constraint is effective for the larger values of $T_{\rm rh}/T_{\rm rh}^{\rm ins}$, by cutting off the larger values of the parameter f_ϕ, while for the smaller values of $T_{\rm rh}$, in particular for $T_{\rm rh} \lesssim 5 \cdot 10^{-4}\, T_{\rm rh}^{\rm ins}$, it entirely covers the region satisfied by the constraint on η_B. Finally, given the range $m \in [10^3, 5 \cdot 10^{10}]$ GeV, for the corresponding range on $T_{\rm rh}/T_{\rm rh}^{\rm ins} \in [10^{-2}, 10^{-6}]$, we get the available (approximated) regions, for $g \in [0.01, 0.05]$,

The condition on the nonbackreaction of the gauge fields on the inflaton (see Sec. 3.2.3), displayed by the black bands, becomes a constraint only at low temperature, $T_{\rm rh}/T_{\rm rh}^{\rm ins} \lesssim 2 \cdot 10^{-5}$ ($3 \cdot 10^{-6}$) for the Schwinger maximal (equilibrium) estimate.

$$
\begin{aligned}
f_\phi/M_{\rm pl} &\in [0.14, 0.17] & &\text{for} & T_{\rm rh}/T_{\rm rh}^{\rm ins} &= 10^{-2} \\
f_\phi/M_{\rm pl} &\in [1.9 \cdot 10^{-2}, 2.8 \cdot 10^{-2}] & &\text{for} & T_{\rm rh}/T_{\rm rh}^{\rm ins} &= 10^{-6}
\end{aligned}
\qquad \text{(Maximal estimate)},
$$

$$
\begin{aligned}
f_\phi/M_{\rm pl} &\in [4.1 \cdot 10^{-2}, 0.13] & &\text{for} & T_{\rm rh}/T_{\rm rh}^{\rm ins} &= 10^{-2} \\
f_\phi/M_{\rm pl} &\in [7.2 \cdot 10^{-4}, 1.1 \cdot 10^{-2}] & &\text{for} & T_{\rm rh}/T_{\rm rh}^{\rm ins} &= 10^{-6}
\end{aligned}
\qquad \text{(Equilibrium estimate)}.
$$

These results are to be compared with the numerical case, see Fig. 4.11, which were in favor of the range $0.030 \, M_{\mathrm{pl}} \lesssim f_\phi \lesssim 0.044 \, M_{\mathrm{pl}}$ for $T_{\mathrm{rh}} \simeq 10^{-2} \, T_{\mathrm{rh}}^{\mathrm{ins}}$ while there were no allowed ranges for $T_{\mathrm{rh}} \simeq 10^{-6} \, T_{\mathrm{rh}}^{\mathrm{ins}}$ for the studied values of f_ϕ. However if we accept an extrapolation from the numerical plot, and by comparing with the equilibrium estimates, we can guess that there could be a range for $f_\phi \sim 10^{-3} \, M_{\mathrm{pl}}$, especially since the window for η_B becomes unconstrained for values $f_\phi \lesssim 0.01 \, M_{\mathrm{pl}}$. We leave the confirmation of this intuition for future work.

6.5 Some phenomenological considerations

In some chaotic inflation models, the mass of the inflaton is constrainted to a high value because of the observational constraint on the scalar perturbations amplitude. In our model, though, we have two terms in the inflaton potential: while inflation is controlled by the quartic term, dominant at Planckian scales, the quadratic one controls reheating and low-energy physics. Thus the value of the inflaton mass is decoupled from the inflationary dynamics.

In previous sections, we have considered on the one hand the upper value of the inflaton mass as $m \lesssim \mathcal{Q}_I$, small enough to solve the instability problem of the Higgs potential, and on the other hand we have roughly imposed $m \gtrsim 1$ TeV on phenomenological grounds for the theory to not be excluded by present experimental data. In fact, an inflaton mass at the TeV scale could have implications for low-energy physics. Therefore, in this section we will make some considerations from the point of view of collider physics and the Standard Model in the presence of the inflaton field with the interactions appearing in the Lagrangian (6.2).

6.5.1 The naturalness problem

First of all, our theory has two hierarchically separated scales, the inflaton mass m and the Higgs mass $m_h = 125.25$ GeV, with $m \gg m_h$. As such, the theory should exhibit a hierarchy problem, which in general implies an unnatural fine-tuning of the parameters. In the absence of any symmetry protecting the EW scale from the high-scale UV physics, one has either to accept the fine-tuning (as it is customary done in non supersymmetric extensions of the SM) or to lower the value of the mass m as much as possible. More quantitatively, the coupling in the Lagrangian $\mu\phi|\Phi|^2 = \sqrt{2\delta_\lambda}\, m|\Phi|^2$ generates a contribution to the Higgs mass term μ_h^2 through the one-loop radiative corrections. In the limit $\mu \to 0$ (i.e. $\delta_\lambda \to 0$), there is an enhanced $\mathbb{Z}_2$ symmetry $\phi \to -\phi$ indicating that any value of μ, as small as it can be, is natural in the sense of 't Hooft, since in this limit the symmetry is recovered. Moreover, this coupling induces a correction to the parameter μ_h^2 in the Lagrangian as [211]

$$\Delta\mu_h^2 \simeq -\frac{\delta_\lambda}{8\pi^2}\, m^2 \, \log\frac{m^2}{m_h^2} \, . \tag{6.50}$$

Naturalness would then require $|\Delta\mu_h^2| \lesssim \mu_h^2 = m_h^2/2$, which translates into the bound

$$m \lesssim 1.2 \text{ TeV} \, , \tag{6.51}$$

where we have considered the typical value of the coupling $\delta_\lambda \simeq 0.1$. This leads to the exciting possibility of having an inflaton with an $\mathcal{O}(\text{TeV})$ mass, which does not spoil naturalness, solve the problem of the instability of the EW minimum, and has phenomenological implications for present and future colliders.

6.5.2 The Higgs-inflaton mixing

Near the vacuum, the potential for the Higgs and ϕ fields is given by

$$V(\phi, \Phi) = -\sqrt{2\delta_\lambda}\, m\, \phi|\Phi|^2 + \frac{1}{2}m^2\phi^2 - \mu_h^2|\Phi|^2 + \lambda_0|\Phi|^4 \, . \tag{6.52}$$

The vacuum is defined as the solution to the minimum equations $\partial V/\partial \phi = \partial V/\partial h = 0$, which provides $\langle h \rangle = v = 246$ GeV and $\langle \phi \rangle = v_\phi$, with

$$\mu_h^2 = \lambda v^2, \qquad\qquad v_\phi = \sqrt{\frac{\delta_\lambda}{2}}\,\frac{v^2}{m}, \qquad\qquad (6.53)$$

where the parameters δ_λ and λ were defined in Eqs. (6.11) and (6.17), respectively.

In the presence of the parameter δ_λ, there is a mixing between the Higgs h and ϕ fields given by the squared mass matrix at the minimum

$$\mathcal{M}^2 = \begin{pmatrix} 2(\lambda + \delta_\lambda)v^2 & -\sqrt{2\delta_\lambda}\,mv \\ -\sqrt{2\delta_\lambda}\,mv & m^2 \end{pmatrix}. \qquad\qquad (6.54)$$

This matrix is diagonalized by an orthogonal rotation with angle α [40] as

$$\begin{pmatrix} c_\alpha & s_\alpha \\ -s_\alpha & c_\alpha \end{pmatrix} \mathcal{M}^2 \begin{pmatrix} c_\alpha & -s_\alpha \\ s_\alpha & c_\alpha \end{pmatrix} = \begin{pmatrix} m_{\tilde h}^2 & 0 \\ 0 & m_{\tilde \phi}^2 \end{pmatrix}, \qquad\qquad (6.55)$$

such that the mass eigenstates are

$$\tilde h = c_\alpha\, h + s_\alpha\, \phi, \qquad\qquad \tilde \phi = c_\alpha\, \phi - s_\alpha\, h\,, \qquad\qquad (6.56)$$

and the mass eigenvalues are

$$\frac{m_{\tilde h, \tilde \phi}^2}{m^2} = \frac{1}{2} + (\lambda + \delta_\lambda)\,\frac{v^2}{m^2} \mp \sqrt{\frac{1}{4} - (\lambda - \delta_\lambda)\,\frac{v^2}{m^2} + (\lambda + \delta_\lambda)^2\,\frac{v^4}{m^4}}. \qquad\qquad (6.57)$$

In this way the physical mass eigenstate $\tilde h$ is associated with the Standard Model Higgs, with a mass $m_{\tilde h} = 125.25$ GeV, while $\tilde \phi$ is the physical singlet, and both of them are coupled to the SM fields through the mixing angle α.

Hence this theory predicts then the existence of a scalar $\tilde \phi$ that decays mainly into the channel $\tilde \phi \to \tilde h \tilde h$ with a decay rate

$$\Gamma(\tilde \phi \to \tilde h \tilde h) = \frac{\kappa^2\, m}{32\pi}\sqrt{1 - \frac{4m_{\tilde h}^2}{m_{\tilde \phi}^2}}, \quad \kappa = \sqrt{2\delta_\lambda}\,c_\alpha(1 - 3s_\alpha^2) + 6s_\alpha c_\alpha^2(\lambda + \delta_\lambda)\frac{v}{m}, \qquad\qquad (6.58)$$

which was (possibly) responsible for the reheating in Sec. 1.2.4. Contour lines of $\Gamma(\tilde \phi \to \tilde h \tilde h)$ are exhibited in the upper left panel of Fig. 6.9 in the parameter space (m, δ_λ). As we can see, typically the width of the resonance $\tilde \phi$ is around a few GeV. As was already stated in Sec. 1.2.4, there are also subleading decay channels into SM particles ($X \in$ SM), as $\tilde \phi \to X\bar X$, induced by the mixing with the Higgs, with very suppressed branching fractions

$$\mathcal{B}(\tilde \phi \to X\bar X) = \mathcal{B}(\tilde h \to X\bar X)\cdot s_\alpha^2\,\frac{\Gamma_{\tilde h}}{\Gamma_{\tilde \phi}} \qquad\qquad (6.59)$$

as $\Gamma_{\tilde h} \simeq 4c_\alpha^2$ MeV in the SM, $\Gamma_{\tilde \phi} \simeq \Gamma(\tilde \phi \to \tilde h \tilde h) \simeq$ few GeV, so that $s_\alpha^2 \Gamma_{\tilde h}/\Gamma_{\tilde \phi} \ll 1$.

---

[40] We are using the notation $c_\alpha \equiv \cos\alpha$, $s_\alpha \equiv \sin\alpha$, $t_\alpha \equiv \tan\alpha$.

6.5.3 Electroweak precision constraints

The doublet-singlet mixing can affect the electroweak precision observables (EWPO) through changes in the gauge boson propagators. Explicit expressions for the modified scalar contributions to the W and Z propagators are given in Refs. [212, 213]. In particular the contribution to the S and T oblique parameters from the new physics, $\Delta S \equiv S^{\text{NP}} - S^{\text{SM}}$ and $\Delta T \equiv T^{\text{NP}} - T^{\text{SM}}$, are found to be given by

$$\Delta T \simeq \frac{3}{16\pi} \frac{s_\alpha^2}{s_W^2} \left[\left(\frac{1}{c_W^2} \frac{m_{\tilde{h}}^2}{m_{\tilde{h}}^2 - m_Z^2} \log \frac{m_{\tilde{h}}^2}{m_Z^2} - \frac{m_{\tilde{h}}^2}{m_{\tilde{h}}^2 - m_W^2} \log \frac{m_{\tilde{h}}^2}{m_W^2} \right) - \left(m_{\tilde{h}} \to m_{\tilde{\phi}} \right) \right] \tag{6.60}$$

and

$$\Delta S = \frac{s_\alpha^2}{12\pi} \left[\frac{\hat{m}_{\tilde{h}}^6 - 9\hat{m}_{\tilde{h}}^4 + 3\hat{m}_{\tilde{h}}^2 + 5 + 12\hat{m}_{\tilde{h}}^2 \log(\hat{m}_{\tilde{h}}^2)}{(\hat{m}_{\tilde{h}}^2 - 1)^3} - \left(\hat{m}_{\tilde{h}} \to \hat{m}_{\tilde{\phi}} \right) \right] \tag{6.61}$$

where we are defining masses in units of m_Z, i.e. $\hat{m}_X \equiv m_X/m_Z$.

The model predictions, Eqs. (6.60) and (6.61), must be compared with the experimental values, given by [214]

$$\Delta T = 0.05 \pm 0.06, \qquad \Delta S = 0.0 \pm 0.07 \tag{6.62}$$

and 92% correlation between the S and T parameters. This gives rise to a $\Delta\chi^2(m, \delta_\lambda)$ distribution, which defines the allowed region in the parameter space (m, δ_λ), exhibited in all panels of Fig. 6.9. In particular we display, in orange shading, the region in the parameter space (m, δ_λ) for which $\Delta\chi^2(m, \delta_\lambda) < 5.99$, that corresponds to the bound at 95% C.L. As we can see, for large values of the parameter δ_λ the lower bound on m can be near the TeV scale.

6.5.4 LHC constraints

In this section we will consider several constraints arising from LHC physics where we are led to the exciting possibility to explore the inflaton sector at present and future high energy colliders and, in particular, at the LHC.

The Higgs signal strength

From Eq. (6.56) we see that the coupling of the mass eigenstate $\tilde{h}$ to the SM particles, is suppressed, with respect to the coupling of the SM Higgs h, by the factor c_α. Given that, the signal strength modifier r_i^f for a specific process $i \to \tilde{h} \to f$, is given by

$$r_i^f = \frac{\sigma_i \mathcal{B}^f}{(\sigma_i)_{\text{SM}} \mathcal{B}_{\text{SM}}^f} \simeq c_\alpha^2 \tag{6.63}$$

where σ_i is the production cross section for the initial state into $\tilde{h}$, and $\mathcal{B}^f$ its branching fraction on the final state. For the last equality we have considered that the production cross section is suppressed by c_α^2 while the branching fraction is approximately equal to the SM one. Experimental data from ATLAS [215] and CMS [216] provide the global values

$$r = 1.11^{+0.09}_{-0.08} \quad \text{(ATLAS)}, \qquad r = 1.17 \pm 0.1 \quad \text{(CMS)} \tag{6.64}$$

which are consistent with a value of $r = 1$ (the SM prediction) with $\sim 10\%$ error, thus providing a lower bound on c_α as

$$c_\alpha^2 \gtrsim 0.9. \tag{6.65}$$

For $m \gg v$ the mixing angle is $s_\alpha \simeq \sqrt{2\delta_\lambda}(v/m) \ll 1$ so that the bound (6.65) is easily satisfied. However for TeV values of m the bound (6.65) translates into a lower bound on the value of m.
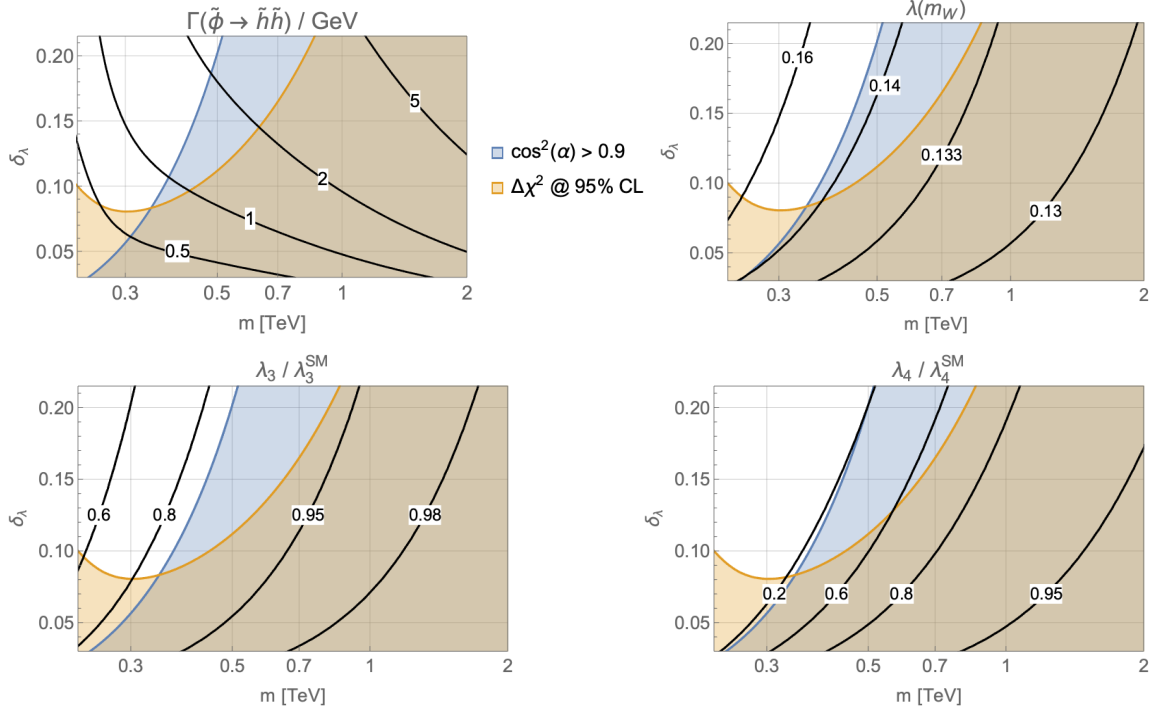
Figure 6.9. Contour lines in the plane $(m/\text{TeV}, \delta_\lambda)$ of the decay rate $\Gamma(\tilde\phi \to \tilde h \tilde h)/\text{GeV}$ (top left panel), the quartic parameter at the weak scale $\lambda(m_W)$ (top right panel) as well as the Higgs trilinear (bottom left panel) and quartic (bottom right panel) couplings normalized to the SM values with the regions of validity defined by the signal strength modifier (6.65) (blue) and the constraints from the electroweak parameters (6.62) (orange) superimposed. One should read the contour lines in black that pass through the overlapping region, and hence satisfy both constraints. As discussed in Sec. 6.1.2, for $m \sim \mathcal{O}(\text{TeV})$, to solve the stability problem and after imposing that the theory remains in the perturbative regime up to the high scale, the parameter δ_λ is constrained to be in the region $0.05 \lesssim \delta_\lambda \lesssim 0.2$.

We shade in blue, in all panels of Fig. 6.9, the region in the parameter space (m, δ_λ), where this constraint is satisfied. In particular we see that, for $\delta_\lambda = 0.1$, the bound (6.65) is satisfied for $m \gtrsim 0.4$ TeV. For $m \simeq 1$ TeV and $\delta_\lambda = 0.1$, the mixing is given by $c_\alpha^2 \simeq 0.988$, which is not excluded by the actual LHC data.

Trilinear and quartic Higgs couplings

As the light state $\tilde h$ is to be identified with the SM Higgs, with mass $m_{\tilde h} = 125.25$ GeV, for any fixed value of the parameter δ_λ the experimental value of the Higgs mass fixes the value of the quartic parameter at the weak scale, $\lambda(m_W)$, at a different value than in the SM case. In the upper right panel of Fig. 6.9 we plot contour lines of $\lambda(m_W)$ in the parameter space (m, δ_λ). As we can see $\lambda(m_W) > \lambda_{\text{SM}}(m_W)$, and only for values of $m \to \infty$ one recovers the SM value.

Moreover, the mixing of the Higgs with the singlet ϕ modifies, in the broken phase, the trilinear λ_3 and quartic λ_4 SM couplings. Recent experiments on di-Higgs searches are putting bounds on these two parameters by looking for possible departures with respect to the SM values $\lambda_3^{\text{SM}} \equiv v\lambda_{\text{SM}}$ and $\lambda_4^{\text{SM}} \equiv \lambda_{\text{SM}}$. In our theory the h-ϕ mixing angle α generates such a departure. After going to the broken phase by means of the shifts $\tilde\phi \to \tilde\phi + \tilde v_\phi$, $\tilde h \to \tilde h + \tilde v$ (where $\tilde v \equiv c_\alpha v + s_\alpha v_\phi$ and

$\tilde{v}_\phi \equiv c_\alpha v_\phi - s_\alpha v$), and integrating out the field $\tilde{\phi}$, which yields the value

$$\tilde{\phi} = c_\alpha \left[\sqrt{\frac{\delta_\lambda}{2}}(1 - 3s_\alpha^2) + 3(\lambda + \delta_\lambda)s_\alpha c_\alpha \frac{v}{m} \right] \frac{\tilde{h}^2}{m} + \cdots , \tag{6.66}$$

one gets the Higgs potential, in the broken phase,

$$V(\tilde{h}) = \frac{1}{2}m_{\tilde{h}}^2 \tilde{h}^2 + \lambda_3 \tilde{h}^3 + \frac{1}{4}\lambda_4 \tilde{h}^4 + \cdots \tag{6.67}$$

where the ellipses are higher order terms, giving rise to powers $\tilde{h}^n$ $(n > 4)$ in the potential, and

$$\begin{aligned}
\lambda_3 &= c_\alpha^3 v \left[\lambda + \delta_\lambda - t_\alpha \sqrt{\frac{\delta_\lambda}{2}} \frac{m}{v} \right], \\
\lambda_4 &= c_\alpha^4 \lambda + c_\alpha^2(-c_\alpha^4 - 4s_\alpha^4 + 4c_\alpha^2 s_\alpha^2 + c_\alpha^2)\delta_\lambda \\
&\quad - 6\sqrt{2\delta_\lambda}\, c_\alpha^3 s_\alpha(c_\alpha^2 - 2s_\alpha^2)(\lambda + \delta_\lambda)\frac{v}{m} - 18s_\alpha^2 c_\alpha^4(\lambda + \delta_\lambda)^2 \frac{v^2}{m^2}.
\end{aligned} \tag{6.68}$$

The model can then, in the future, be excluded or confirmed by experimental data on trilinear (and quartic) Higgs couplings data. Notice that in the limit $m \gg m_h$ the mixing angle behaves as $s_\alpha \simeq \sqrt{2\delta_\lambda}\, v/m$ so that $\lambda_3 \simeq \lambda_3^{SM}$ and $\lambda_4 \simeq \lambda_4^{SM}$ [41], and the decoupling is automatic. We plot in the bottom panels of Fig. 6.9 contour lines of the trilinear and quartic couplings, normalized to the corresponding SM values, as functions of the parameters m and δ_λ. At present, with 89 fb^{-1} of LHC data, the triple Higgs coupling has been constrained by the ATLAS collaboration to be $\lambda_3/\lambda_3^{SM} = 4.0^{+4.3}_{-4.1}$, excluding it outside the interval $[-3.2, 11.9]$ at 95% C.L. [217], while the CMS collaboration finds $\lambda_3/\lambda_3^{SM} = 0.6^{+6.3}_{-1.8}$, excluding it outside the interval $[-3.3, 8.5]$ at 95% C.L. [218]. Theoretical studies based on the HE-LHC at $\sqrt{s} = 27$ TeV and 15 ab^{-1} luminosity foresee exploring the interval range $\lambda_3/\lambda_3^{SM} \in [0.6, 1.46]$ at 68% C.L. [219], while a future 100 TeV hadron collider could achieve the trilinear coupling measurement within better than 5% accuracy [220], thus potentially imposing strong constraints on m from the plots in Fig. 6.9.

Heavy Higgs production

Finally the state $\tilde{\phi}$ can be produced at the LHC by the same mechanisms of Higgs production with a cross section given by

$$\sigma(pp \to \tilde{\phi} + X) = s_\alpha^2\, \sigma(pp \to H + X) \tag{6.69}$$

where H is a heavy SM-like Higgs with a mass equal to m. Using the results of inclusive cross sections for $\sigma(pp \to H)$ for the leading mechanism of gluon-gluon fusion (ggf) [221] we plot, in Fig. 6.10, the cross section $\sigma_{ggf}(pp \to \tilde{\phi})$ as a function of m for two relevant values of the parameter δ_λ for $m \lesssim 1$ TeV and a center of mass energy $\sqrt{s} = 13$ TeV. Given that, as we have explained earlier in this section $\mathcal{B}(\tilde{\phi} \to \tilde{h}\tilde{h}) \simeq 1$, we can compare these cross sections with the SM cross sections for di-Higgs production $\sigma(pp \to hh)$ given by $\sigma_{ggf}^{SM}(hh) \simeq 33.5$ fb [222].

The predicted cross sections in Fig. 6.10 are compared with the present experimental upper bounds at 95% C.L. on the production of a scalar field ($\tilde{\phi}$) which decays into two Higgs bosons, from ATLAS with luminosities 27.5-36.1 fb^{-1} [223] and CMS with luminosity 35.9 fb^{-1} [224], at present LHC center of mass energies $\sqrt{s} = 13$ TeV (see Fig. 6.10). We conclude from here that the present lower bounds on the value of m are

$$m \gtrsim 0.55\ (0.7)\ \text{TeV @ 95% C.L.}, \quad \text{for } \delta_\lambda = 0.05\ (0.15), \tag{6.70}$$

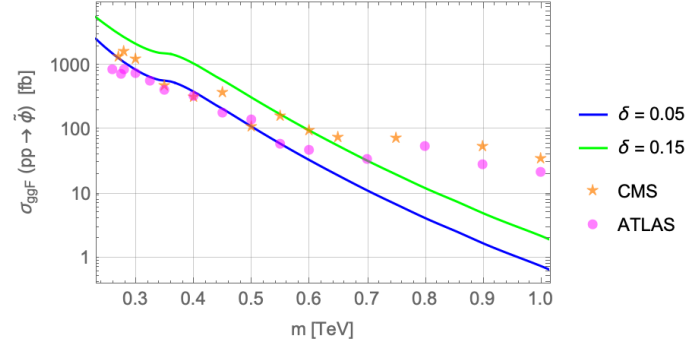[41]Of course, in the limit $m \gg v$, $\lambda \simeq \lambda_{SM}$ as exhibited in the top right panel of Fig. 6.9.

Figure 6.10. Plots of cross section $\sigma(pp \to \tilde{\phi})$ in fb for relevant values of $\delta_\lambda = 0.05, 0.15$. The dots (stars) are the 95% C.L. upper bound from ATLAS [223] (CMS [224]), that bring the approximate constraint $m \gtrsim 0.55$-0.7 TeV, depending on the value of δ_λ.

while in the future much stronger bounds could be achieved.

Conclusion

In this thesis, we have explored how the SM Higgs sector, the inflationary paradigm and a specific baryogenesis mechanism can interplay to provide a successful history of the Universe. In particular, we have studied the implications of an extra coupling, at leading order in the Lagrangian of the Higgs/axion inflation to the Chern-Simons (CS) density, a quantity related to the gauge field topological configuration. Such an interaction generates a (hyper)magnetic field that is maximally helical at the end of inflation. If the helicity survives until the electroweak phase crossover, it can be converted into baryon asymmetry thanks to the chiral anomaly of the SM. Soon after inflation, the Universe reheats and a thermal plasma is generated by the decay of the inflaton into SM particles. Consequently, if the electroweak symmetry was broken because of the model-dependent Higgs dynamics, it is restored until the EWPT by the appearance of thermal masses. Hence in that case the helicity in photons gets transformed into helicity in hypercharge gauge fields. Otherwise, if the physical Higgs has zero VEV during inflation, the produced hypermagnetic fields stay in the symmetric phase until the EWPT at $T \simeq 160$ GeV.

In any case, we must make sure that the helicity survives the various plasma effects between these two epochs. As the Universe is cooling down from the reheating to the EW scale, the helical hypermagnetic fields interact with the thermal plasma which, in turn, backreacts on the gauge fields. This system can be described by the so-called magnetohydrodynamics (MHD) equations, in which the physical quantities of interest (amplitudes, energy densities, correlation length, helicity and its derivative) do not scale adiabatically in such an environment or, in other words, their comoving quantities are not constant. Therefore, there can be a magnetic diffusion effect leading to the decay of the helicity. If, on the other hand, the magnetic induction is the leading effect, then the helicity can be conserved until the EWPT and the baryogenesis mechanism can take place. This effect is measured by the magnetic Reynolds number, and it is a sufficient condition to require it to be bigger than unity, at reheating, for the helicity to be conserved until the EW crossover.

In addition, we also have to prevent the baryon asymmetry generated alongside the helical (hyper)magnetic fields at the end of inflation to get converted back into the gauge sector, as the energy configuration is more favorable there, an effect called the chiral plasma instability (CPI). Thus one must require that all the fermion asymmetry has already been washed out by the EW sphaleron effect when the CPI can happen. The asymmetry in the left-handed fermion sector is rapidly erased, but the right-handed ones are protected from the washout as long as their Yukawa interactions are not in thermal equilibrium. Thus, by requiring that the CPI temperature is lower than $\sim 10^5$ GeV, the temperature at which the Yukawa interaction of the last SM species enters into thermal equilibrium (i.e. the right-handed electron), the CPI is avoided and thus the hypermagnetic helicity survives.

Finally, we have verified that the non-Gausiannity issues, and the bounds on the baryon isocurvature perturbations, are no constraints on our models, as the amount of produced hypermagnetic fields is too low.

The three Sakharov conditions for baryogenesis are met since: *(i)* the chiral anomaly in the SM provides $B + L$ violation through helicity decay (source) and weak sphaleron interaction (washout),

(ii) the interaction term of the type $F(\phi)F_{\mu\nu}\tilde{F}^{\mu\nu}$ is odd under $\mathcal{CP}$ transformation as ϕ is a scalar[42], and, *(iii)* although the EWPT is a crossover, both the $B+L$ source and washout processes become inactive (i.e. they go out of thermal equilibrium) with different rates when the Universe undergoes the phase transition. Therefore, after solving the transport equations system by also taking into account the kinetic equations for all the SM fermion species with their Yukawa interactions, the chiral magnetic effect and a time-dependent weak angle, it is found that a net baryon asymmetry survives at temperature $T \lesssim 130$ GeV [120, 121].

The amount of baryon asymmetry is proportional to the available hypercharge helicity during the crossover. It is therefore essential to quantify it well, as the BAU can easily be under/over estimated when the relevant plasma effects are ignored. It is in this perspective that we considered the Schwinger effect, which is the damping of the gauge fields because of the fermion backreaction. When exiting the vacuum, the gauge modes are strong enough to create particle/antiparticle pairs of light fermions, which contribute to the electrical conductivity of the plasma. The backreaction of fermion currents on the produced gauge fields acts as a damping force on the explosive production of helical gauge fields. The latter significantly reduces the amount of electromagnetic energy and helicity generated at the end of inflation, as the exponential behavior of the backreactionless solutions can be replaced by two polynomial approximations: the *maximal* and *equilibrium estimates*.

This effect was already considered in numerous studies of inflation and/or baryogenesis, where some analytical and numerical estimates were computed, mainly in configuration space. In addition to these estimates that we used in our models, we have studied by means of numerical computations, the effect of the Schwinger particle production on the helical hypermagnetic fields produced at the end of inflation. Unlike the methods just mentioned, our calculation is done in momentum space. The equations of motion are a nontrivial integro-differential system, numerically solved by using a fourth order Runge-Kutta method, with details being displayed in App. C. The computed observables of interest are the electric and magnetic energy density, the helicity, as well as the helicity time derivative. We assumed a homogeneous inflaton with only zero mode, hence we did not treat any spatial effects. We also ensured the convergence of the algorithm and its invariance to the initial conditions.

First of all we have checked that we recover previous results in the slow roll inflation regime, by making the same approximations required by an analytical resolution. In this way, we validate our code, i.e. we verify that our code produces the right results in known cases such as the backreactionless case, where the Schwinger effect is turned off, and the gradient expansion formalism, where the Bunch-Davies parameter Δ was first introduced.

In a second step, still in the slow roll regime, we considered a specific model of inflation, namely the Starobinsky potential, in order to account for the instability parameter as varying function, $\xi(a)$, instead of the constant value imposed by the analytical approximations. That way, we could also implement the effects of the function $\Delta(a)$ obtained from the plasma evolution on the gauge production itself.

We then simulated, in a third step, the full system, where neither the slow roll conditions nor the Universe geometry (e.g. de Sitter) are imposed. In order words, the inflaton equation of motion was computed alongside the gauge one, taking the backreaction of the latter to the former into account, along with the Schwinger effect. We compared our results to the previous setup, and found perfect agreement as long as the slow roll conditions are met. When inflation is near its end, the full solution diverges from the slow roll results and produces, as expected, less energy density and helicity.

As our code is free from any geometrical issues, and only requires a model of inflation, we let the simulations run until the onset of reheating, in order to compute the electromagnetic to total

---

[42]In the case of the axion inflation of Chaps. 3 and 4 , ϕ was a pseudoscalar, the interaction term $\phi F_{\mu\nu}\tilde{F}^{\mu\nu}$ is *even* and $\mathcal{CP}$ is spontaneously broken by the background value $\phi(t)$ which solves the inflaton EoM.

energy density ratio. We choose two well-known classes of models that satisfy the cosmological constraints as illustrative examples: the α-attractor and the hilltop models. Previous studies have quoted a sufficient criterion for gauge preheating to happen, namely that this fraction should be at least $\gtrsim 80\%$ [181]. However, our numerical estimates suggest that the Schwinger effect significantly reduces the share of electromagnetic energy for the considered models, and gauge preheating is unlikely to occur. Moreover, since we are neglecting all spatial effects, any negative statement concerning the possibility of gauge preheating, due to the lack of electromagnetic energy, should be considered as a conservative one. On the other hand, our results do apply to the considered class of inflationary models. They show a certain degree of model dependence, so we cannot exclude a qualitatively different result for models of inflation other than the considered ones. Of course, a full lattice simulation of the Schwinger effect involving fermions remains to be done.

However, because of the considered scales, lattice simulations are defined when the particle number is big, so they can only deal with classical fields. For fermions, the occupation number never exceeds one, hence it is for now not known how to implement the fermion dynamics without strong approximations. Still, an effective treatment of the conductivity, like that in this thesis, is still possible. For instance, a lattice code has been publicly released recently: $\mathcal{C}osmo\mathcal{L}attice$ can simulate the dynamics of interacting scalar field theories with $U(1)$ and $SU(2)$ gauge theories in an expanding FRW background [225, 226]. With an added modulus for axionic dynamics, a future line of research would be to consider the local non-linear production of electromagnetic energy densities and helicity for the CS coupling, along with an implementation of a local effective treatment of the Schwinger effect.

Taking all these constraints into consideration, we have then studied two scenarios where baryogenesis occurs. The first one uses the well known Higgs inflation (HI) model, where the Higgs is non-minimally coupled to gravity, while the second is a modification of it where a new state is added with also a non-minimal coupling to gravity. In both cases, we found a sizable window in the parameter space to achieve the BAU.

In the HI model, by adding a dimension-six $\mathcal{CP}$-violating operator coupling the Higgs Φ to the hypercharge CS density, as $|\Phi|^2 F\tilde{F}$, we have proven there is an explosive production of helical hypermagnetic fields which can produce baryogenesis when the helicity relaxes into the BAU at the electroweak crossover. The parameter ξ responsible for the energy transfer from the inflaton to the gauge fields is almost a constant, due to the particular shape of the inflationary potential and the coupling of the Higgs to the CS density, and we can thus fully rely on analytic approximations to consider the gauge field solutions. We have also proven that the helicity produced at the end of inflation satisfies the required MHD conditions to survive to the EWPT, and produce the observed BAU, for a window of ξ at the CMB scale given by

$$1.96 < \xi_* < 2.23 \qquad \Leftrightarrow \qquad 3.6 < \xi_E < 4.1$$

thus satisfying the bound $\xi_* < 2.55$ on non-Gaussianity.

In the above analysis we have worked out the metric formulation of gravity, and considered two particularly simple cases: *a)* in the absence of Schwinger effect, and; *b)* in the presence of Schwinger effect. We have treated case *a)* by assuming that the SM flavor problem is implemented by means of a Froggatt-Nielsen (FN) mechanism, in the special case where the flavon field is coupled to the inflaton. As a consequence of this coupling, during inflation one can easily impose the condition that all fermions are heavy (say as heavy as the top quark) in such a way that the Schwinger conductivity, which is exponentially suppressed by the fermion mass squared, is negligible and the Schwinger effect turns out to also be negligible. After inflation the flavon field relaxes to its usual minimum, which can describe all fermion masses and mixing angles at the electroweak scale. The

details of the mechanism are described in App. B. As for case $b)$, in the presence of the Schwinger effect, we have taken advantage of the (almost) constancy of the parameter ξ to use the simple Schwinger equilibrium approximation, which simply amounts to a redefinition of the ξ parameter. In all cases we have extended our calculation to the case of critical Higgs inflation and found that for values of the quartic Higgs self-coupling $\lesssim 10^{-10}$, the coupling $1/f_h$ of the Higgs to the CS density $(h^2/f_h^2)F_{\mu\nu}\tilde{F}^{\mu\nu}$ can be $\lesssim M_{\rm pl}^{-1}$ in the weakly coupled region.

We also have considered the Palatini formulation of gravity. In this case the equations for the change from the Jordan to the Einstein frame are analytic, as well as the inflationary potential, and the relation between the inflaton χ and the Higgs field h. As a consequence of the shape of the inflationary potential, it turns out that in this model the parameter ξ is exactly a constant, i.e. $\xi_* = \xi_E$. In this formalism helical gauge fields can still be produced, however the bounds on non-Gaussianity impose that its production is not as explosive as required to trigger electroweak baryogenesis, which is then forbidden in this model. It was already known that the two formalisms of gravity, the metric and the Palatini formulations, were leading to different inflationary predictions. In this work, we have also proven that they behave differently concerning the baryogenesis capabilities of the helical gauge fields produced at the end of inflation.

There are a number of physics problems that are left open and deserve future analysis, some of them being related to the classical problems of HI. One of them is related to the stabilization of the Higgs potential, its relation to the measured value of the top quark mass, and the possibility of getting critical values of the Higgs mass at the inflationary scales. This problem is particularly relevant in the case where the SM flavor problem is solved by a FN mechanism where the flavon field is coupled to the inflaton, in the way we have described in the devoted chapter. This analysis clearly requires a more detailed analysis of the renormalization group running in the presence of the FN mechanism, working at the inflationary scales. Some comments on the effective, $\mathcal{CP}$-violating, operator given by Eq. (5.2) are also in order here. Recall that we get from Eq. (1.138) that $h_E \sim 10^{-2} M_{\rm pl}$ for $\lambda_h \simeq 0.1$, while the value of the scale f_h which provides the BAU, from Fig. 5.4, is such that the expansion parameter $h_E/f_h \gtrsim \mathcal{O}(1)$. For smaller values of λ_h, characteristic of CHI, we obtain similar results. For instance for $\lambda_h = 10^{-8}$, $h_E \simeq 0.6\, M_{\rm pl}$ and the value of f_h which provides the correct value of the BAU, is such that $h_E/f_h \gtrsim O(1)$. As these values are at the limit of validity of the effective theory, the UV completion should be such that higher dimensional operators do not spoil the validity of the results. An example of such UV completion was provided in Ref. [140].

Finally, we have explored the possibility of modifying the HI theory by means of the introduction of an extra scalar field ϕ, with the Ricci coupling $(g/2)\phi^2 R$, and an interaction term $\mu\,\phi h^2$ to solve the stability problem of the electroweak vacuum. Here, the Higgs field is not explicitly coupled to the Ricci scalar and, although such a term is generated by radiative corrections, its effects stay negligible. Both fields, ϕ and h, participate in the dynamics of inflation through the two-field potential $V(\phi, h)$, which has the shape of a valley, along which they are related by simple analytical expressions so that we can express one field in terms of the other. This allows us to define the true inflaton field χ as the one following the valley with a canonical kinetic term, although we kept the description in terms of ϕ for mathematical convenience. A key point is that we have considered a quartic coupling $\lambda_\phi \phi^4$ for the ϕ field, and a squared mass $m^2\phi^2$, such that inflation is driven by the quartic coupling term, while reheating is driven by the mass term. The Lagrangian coupling $\mu\phi h^2$, $\delta_\lambda = \mu^2/2m^2$, triggers a positive contribution to the β function of the Higgs quartic coupling such that, if the mass scale m is in the range $1\,\text{TeV} \lesssim m \lesssim \mathcal{Q}_I$, where $\mathcal{Q}_I \simeq 10^{11}$ GeV is the instability scale of the electroweak potential, the instability problem of the electroweak vacuum can be solved by roughly imposing the mild constraint $\delta_\lambda \lesssim \mathcal{O}(1)$.

We find that the beginning of inflation $\phi(N_*) \equiv \phi_*$ ($N_* = 60$) is mainly driven by the scalar field ϕ, and since the amplitude of density perturbations is fixed by the λ_ϕ quartic coupling (and

not by the Higgs quartic coupling), the main problem of Higgs inflation is easily solved with $g \lesssim 1$. On the other hand, the end of inflation ($N \simeq 0$), where the hypermagnetic helicity will be produced, is equally driven by both the scalar ϕ and the Higgs h quartic terms, so that the role played by the Higgs field is relevant. Both regimes are separated, for $g \simeq 0.01$ (0.05), by a critical value of the field $\phi_c/M_{\rm pl} \simeq 10$ (4), which corresponds to the critical number of e-folds $N_c \simeq 12$ (2). After imposing the Planck and BICEP/Keck conditions on the slow roll parameters, and the unitarity condition $\phi_* \lesssim M_{\rm pl}/g$ (see however Sec. 6.1.3 for a nuance), we obtain the allowed interval on the parameter g, $0.01 \lesssim g \lesssim 0.05$, which translates into the prediction for the cosmological observables in agreement with observations, and with a Hubble parameter almost saturating the Planck upper bound $H_*^{\rm obs} < 6 \cdot 10^{13}$ GeV:

$$0.965 \lesssim n_s \lesssim 0.967, \qquad 0.047 \gtrsim r \gtrsim 0.012, \qquad 5.5 \cdot 10^{13} \text{ GeV} \gtrsim H_* \gtrsim 2.8 \cdot 10^{13} \text{ GeV}$$

By adding a dimension-five coupling between the scalar ϕ and the CS density, we can generate maximally helical magnetic fields during the last e-folds of inflation, and baryogenesis at EWPT as described earlier. This effective $\mathcal{CP}$ breaking operator can be easily obtained from a UV completion with a $\mathcal{CP}$-violating Yukawa coupling of ϕ to a hypercharged vector-like heavy fermion, as it is shown in App. A.1. We chose again to keep an analytical description of the model, so for self-consistency we have to make sure that the gauge field backreaction on the inflaton is negligible. We have found a critical value of the coupling strength of ϕ to gauge bosons in the $\mathcal{CP}$-violating operator, f_ϕ^c, such that this is the case for $f_\phi \gtrsim f_\phi^c$. The field ϕ is thus *weakly* coupled to the gauge fields and the Universe reheating proceeds by the perturbative decay of the inflaton into SM particles (mainly in a couple of Higgs bosons). In particular we find $f_\phi^c/M_{\rm pl} \simeq 0.02$ ($7 \cdot 10^{-4}$) for the Schwinger maximal (equilibrium) estimate.

We have undertaken all constraints from previous chapters and considered both Schwinger analytical estimates, while making comparisons with the numerical results obtained from the Starobinsky potential, a very good approximation to our effective potential in the region where the magnetic fields are generated. The value of the BAU generated at the EW crossover, η_B, depends on the value of the reheating temperature $T_{\rm rh}$, and in particular on its ratio with respect to the reference instant reheat temperature $T_{\rm rh}/T_{\rm rh}^{\rm ins}$ (here $T_{\rm rh}^{\rm ins} \simeq 2 \cdot 10^{15}$ GeV for the range of g allowed by inflation). We have shown that all constraints are satisfied for a large range of the parameters f_ϕ and $T_{\rm rh}$ and are insensitive to the value of the parameter g inside its allowed range from cosmological observables. In summary, one has the ranges

$$\begin{aligned} f_\phi/M_{\rm pl} &\in [0.14, 0.17] & \text{for} \quad T_{\rm rh}/T_{\rm rh}^{\rm ins} &= 10^{-2} \\ f_\phi/M_{\rm pl} &\in [1.9 \cdot 10^{-2}, 2.8 \cdot 10^{-2}] & \text{for} \quad T_{\rm rh}/T_{\rm rh}^{\rm ins} &= 10^{-6} \end{aligned} \qquad \text{(Maximal estimate)}$$

$$\begin{aligned} f_\phi/M_{\rm pl} &\in [4.1 \cdot 10^{-2}, 0.13] & \text{for} \quad T_{\rm rh}/T_{\rm rh}^{\rm ins} &= 10^{-2} \\ f_\phi/M_{\rm pl} &\in [7.2 \cdot 10^{-4}, 1.1 \cdot 10^{-2}] & \text{for} \quad T_{\rm rh}/T_{\rm rh}^{\rm ins} &= 10^{-6} \end{aligned} \qquad \text{(Equilibrium estimate)}$$

The complete available parameter region is summarized in Fig. 6.8. The bounds on the temperature ratio come from the fact that reheating should proceed by perturbative inflaton decays. Then the value of $T_{\rm rh}/T_{\rm rh}^{\rm ins}$ depends on the inflaton decay width Γ_χ. In this model the inflaton mainly decays through the channel $\chi \to hh$, with a width which increases with the value of the inflaton mass m and ranges in the interval $1 \text{ GeV} \lesssim \Gamma_\chi \lesssim 10^9$ GeV, which corresponds to $10^{-6} \lesssim T_{\rm rh}/T_{\rm rh}^{\rm ins} \lesssim 10^{-2}$, for $1 \text{ TeV} \lesssim m \lesssim 5 \cdot 10^{10}$ GeV.

Notice that the fact that the inflaton potential has both quadratic and quartic terms allows us to decouple the mass m from the actual value of the amplitude of density perturbations, which in the absence of a quartic term would fix its value to $m \simeq 10^{12}$ GeV (or smaller only at the price of the introduction of a curvaton scalar), allowing any value $m < \mathcal{Q}_I$ in order to stabilize the electroweak vacuum. This is achieved by the contribution to the Higgs quartic coupling β function, provided by the coupling δ_λ in the Lagrangian term, $\sqrt{2\delta_\lambda}\, m\, \phi\, |\Phi|^2$. We have found, for the parameter δ_λ, the absolute bounds $\delta_\lambda \gtrsim 0.05$ in order to solve the stability problem and $\delta_\lambda \lesssim 0.35$ to not spoil the perturbativity of the theory, although its particular range depends on the actual value of m. Nevertheless, values $m \gg m_h$ create a naturalness/fine-tuning problem, essentially given by the fact that a loop correction to the Higgs squared mass term μ_h^2 appears. It translates into a fine-tuning of the order of $4\pi^2/(\delta_\lambda \rho^2 \log \rho^2)$ where $\rho \equiv m/m_h$. While for $\delta_\lambda \simeq 0.1$ and $m = 10^{10}$ GeV the fine tuning is $\sim 10^{-14}$ (similar to the SM fine-tuning), and for $m = 10$ TeV it is ~ 0.01, there is essentially no fine-tuning for values $m \lesssim 1$ TeV. This leads to the exciting possibility of a light inflaton, which could possibly be detected by direct measurements at LHC and/or future colliders.

The key point here was that the Lagrangian term $\sqrt{2\delta_\lambda}\, m\, \phi\, |\Phi|^2$ creates a ϕ-h mixing, sizeable for low values of the mass m, leading to interesting phenomenology for high energy colliders. In fact all collider phenomenology is triggered by the mixing angle α. The mass eigenstates $(\tilde{\phi}, \tilde{h})$, where in particular $\tilde{h}$ should be identified with the experimentally detected Higgs with a mass equal to 125.25 GeV, are related to the weak eigenstates (ϕ, h) by a rotation with angle α. This implies that $\lambda(m_W)$ is different from $\lambda_{\rm SM}(m_W) \simeq 0.13$, which leads to predictions on the ratios $\lambda_3/\lambda_3^{\rm SM}$ and $\lambda_4/\lambda_4^{\rm SM}$ which could be probed by future experiments, as HE-LHC and/or a 100 TeV collider. The mixing is already bounded by present ATLAS and CMS results on the SM Higgs signal strengths, which provide the bound $m \gtrsim 0.3\ (0.45)$ TeV for $\delta_\lambda = 0.05\ (0.15)$. It also generates a contribution to the oblique electroweak observables, and yields, for e.g. $\delta_\lambda = 0.15$, the lower bound $m \gtrsim 0.5$ TeV. Finally, the mixing is responsible for the inflaton production and decay. In particular $\tilde{\phi} \to \tilde{h}\tilde{h}$, triggered by the coupling δ_λ, is the main decay channel, while other decay channels into the SM particles, via the mixing s_α, are subleading. The inflaton $\tilde{\phi}$ can also be produced mainly by the gluon-gluon fusion mechanism through its Higgs mixing. Present data from ATLAS and CMS translate into lower bounds $m \gtrsim 0.55\ (0.7)$ TeV at 95% C.L. for $\delta_\lambda = 0.05\ (0.15)$.

There are a number of research lines which could be safely explored in the future. First of all, we have considered models of inflation based on the Ricci coupling $\phi^2 R$, and a ϕ dependent potential dominated, for large values of ϕ, by the quartic coupling. These kind of theories, when considered in the Einstein frame, naturally give rise, for large values of ϕ, to flat potentials, appropriate for inflation, without invoking any particular symmetry. It is clear that similar results could also be obtained for theories with a Ricci coupling as $F(\phi)R$, and a Jordan frame potential behaving, for large values of ϕ, as $U(\phi) \simeq F^2(\phi)$. In particular it would be interesting to see what kind of theories would produce enough baryon asymmetry in the presence of a period of preheating, by the nonperturbative production of gauge fields. A recent work [209] has already explored a general class of inflationary potentials, and shown consistency with cosmological observables. In particular, our model, labeled therein by $(n, p) = (2, 4)$, gives results for the cosmological observables, which are in good agreement with this model. These general theories are therefore good candidates to also generate the observed value of the BAU, provided they contain the inflaton coupling to the CS term.

Moreover, at the level of particle physics, the possibility of producing and detecting the inflaton at present or future colliders remains an exciting playground. In particular, future experimental results on the production of heavy scalars coupled to the SM fields, or measurements of the trilinear and quartic Higgs couplings by di-Higgs production, could start cornering the present theory and put stronger bounds on the mass of the inflaton and its mixing with the SM Higgs.

Furthermore, the results from this thesis can be adapted to some other inflationary scenarios

such as R^2 couplings. The reheating mechanism can (and should) also be studied in more detail, as the inflaton decay rate is not a constant, contrary to what is often assumed. Besides, if we manage somehow to have a spatial description of the equations of motion (e.g. by the use of lattice simulations), we could make some predictions in the gravitational waves and primordial black holes sectors. From the inflation model perspective, if the backreaction from the gauge fields on the inflaton is strong enough, it can slow down its rolling regardless of the potential shape [134]. This would enable an inflation model in agreement with the swampland criteria provided that $\rho_\phi > \rho_{\mathrm{EM}}$ during inflation.

Another possibility is to consider an inflaton coupling to a non-Abelian gauge group, such as the CS density of $SU(2)_L$ as $F(\phi)W_{\mu\nu}^a \tilde{W}^{a\,\mu\nu}$, instead of a $U(1)$ coupling, to prevent a wild electromagnetic contribution to the scalar perturbation. This idea is linked to the previous one as it would provide another mechanism to slow down the inflaton despite its potential, this time without the bound $\rho_\phi > \rho_{\mathrm{EM}}$ as here the inflation is driven by electromagnetism. Hence we could have $\rho_{\mathrm{EM}} \gg \rho_\phi$ without spoiling the scalar perturbations.

We close this thesis by mentioning that a study on the effect of a CS coupling with the Ricci scalar, in R^2-Higgs inflation, is in preparation [227]. More specifically the non-minimal couplings in the action written, in the Jordan frame and in units where $M_{\mathrm{pl}} = 1$,

$$S = \int d^4x \sqrt{-g} \left[-\frac{R}{2} \left(1 + \xi_R R + \xi_h |\Phi|^2 \right) + (D_\mu \Phi)^\dagger D^\mu \Phi - U(\Phi) \right] - \frac{R}{4f_R} Y_{\mu\nu} \tilde{Y}^{\mu\nu}$$

induces in the Einstein frame, and in the unitary gauge, a two-field (h, ϕ) inflationary potential similar to the model presented in Chap. 6, as here we include both HI and R^2 non-minimal couplings. Both fields are mixed through their kinetic terms, which induces a system of coupled EoM for both of them and for the gauge field. The latter especially depends on both (h, ϕ) fields time derivatives. Some analytical approximation and/or numerical computation will hence be needed to obtain the BAU produced via this mechanism.

Acknowledgements

Appendix A

UV completions

A.1 Linear CS coupling

$\mathcal{CP}$ violation in our model is driven by the effective dimension-five operator

$$S_{\mathcal{CP}} = -\int d^4x \, \frac{\phi}{4\tilde{f}_\phi} Y_{\mu\nu}\tilde{Y}^{\mu\nu} \tag{A.1}$$

where $Y^{\mu\nu}$ is the hypercharge field strength.

A simple UV completion generating such effective operator can be a massive (with mass M) hypercharged vectorlike fermion ψ with a $\mathcal{CP}$-violating Yukawa coupling to ϕ as

$$\mathcal{L} = -\bar{\psi}_L(M + |\lambda_\psi|e^{i\theta_\lambda}\phi)\psi_R + \text{h.c.} = -|\lambda_\psi|\phi\left[\cos\theta_\lambda\bar{\psi}\psi + \sin\theta_\lambda\bar{\psi}i\gamma_5\psi\right], \tag{A.2}$$

where $\mathcal{CP}$ violation is induced by the angle θ_λ. The $\mathcal{CP}$-even $\phi Y_{\mu\nu}Y^{\mu\nu}$, and $\mathcal{CP}$-odd $\phi Y_{\mu\nu}\tilde{Y}^{\mu\nu}$, couplings are generated by loop diagrams where the fermion ψ propagates in the loop and emits two gauge bosons Y_μ, via the $\cos\theta_\lambda$ and $\sin\theta_\lambda$ couplings in Eq. (A.2), respectively. The corresponding Feynman diagrams are finite and thus one gets $\tilde{f}_\phi \propto M$. For maximal $\mathcal{CP}$ violation, i.e. $\theta_\lambda = \pm\pi/2$, only the coupling $\phi Y_{\mu\nu}\tilde{Y}^{\mu\nu}$ is generated such that

$$M \simeq \frac{|\lambda_\psi|g'^2}{4\pi^2}\tilde{f}_\phi \simeq 8 \cdot 10^{15} \text{ GeV } |\lambda_\psi|\,(\tilde{f}_\phi/M_{\text{pl}})\,. \tag{A.3}$$

Stability of the inflationary potential

The UV completion here proposed could affect the stability of the inflationary potential through radiative corrections in the high energy theory. In fact, the coupling in Eq. (A.2) provides a correction to the β function of the coupling λ_ϕ, similar to the correction to the β function of the Higgs quartic coupling β_λ from the top quark Yukawa coupling. This contribution comes from the box diagram with four ϕ external legs, where the fermion ψ is exchanged, and the resulting contribution to β_{λ_ϕ} is given by

$$\Delta\beta_{\lambda_\phi} = -\frac{2|\lambda_\psi|^4}{16\pi^2}\,\theta(t - t_M), \qquad\qquad t - t_M = \log\left(Q/M\right). \tag{A.4}$$

Notice that the correction given by Eq. (A.4) is negative, as it arises from a fermion loop, which can lead the coupling λ_ϕ to negative values and thus destabilize the whole inflationary scenario, a process similar to the destabilization of the EW vacuum by the loop corrections induced by the top quark. It is then required to prevent such destabilization. A sufficient condition to not destabilize the quartic inflaton coupling, without any tuning of parameters, is to impose $|\lambda_\psi| \lesssim \lambda_\phi^{1/4}$ which

translates, using the typical value, from Fig. 6.4, $\lambda_\phi \simeq 10^{-12}$, into $|\lambda_\psi| \lesssim 10^{-3}$, and so into an upper value of the ψ-mass as

$$M \lesssim 10^{13} \text{ GeV}(\tilde{f}_\phi/M_{\text{pl}}). \tag{A.5}$$

Notice that in the limit $\lambda_\psi \to 0$ the UV Lagrangian has the enhanced $\mathbb{Z}_2$ symmetry, $\phi \to -\phi$, and thus any small value of λ_ψ is natural in the sense of 't Hooft. For instance, values of $\lambda_\psi \sim 10^{-12}$ would lead to values of $M \simeq \mathcal{O}(\text{TeV})$.

Naturalness problem

The UV completion brings a new naturalness problem as there is the hierarchy of masses $M \gg m_h$. In fact, the presence of the vectorlike fermion ψ coupled to the field ϕ through the coupling (A.2), along with the ϕ-h mixing generates the Lagrangian

$$\mathcal{L} = |\lambda_\psi| s_\alpha \, \tilde{h} \, \bar{\psi} i \gamma_5 \psi + |\lambda_\psi| c_\alpha \, \tilde{\phi} \, \bar{\psi} i \gamma_5 \psi \tag{A.6}$$

whose first term provides at one-loop (for scales $\mathcal{Q} \gtrsim M$) a contribution to the mass parameter μ_h^2 as

$$\Delta\mu_h^2 \simeq \frac{1}{4\pi^2} \, s_\alpha^2 \, |\lambda_\psi|^2 \, M^2 \log \frac{M^2}{m_h^2} \tag{A.7}$$

which would require, for large values of M, a fine-tuning. In particular, the naturalness condition $\Delta\mu_h^2 \lesssim m_h^2/2$ implies, for $m \simeq 1$ TeV, the upper bounds on M and $|\lambda_\psi|$ given by

$$M \lesssim (7.6,\, 2.5,\, 0.8) \cdot 10^8 \text{ GeV}, \qquad\qquad |\lambda_\psi| \lesssim (1,\, 3,\, 10) \cdot 10^{-6}\,, \tag{A.8}$$

where the values in parenthesis correspond to $\tilde{f}_\phi/M_{\text{pl}} = (0.1, 0.01, 0.001)$, respectively, and where we have used $\delta_\lambda = 0.15$.

Of course the second term of (A.6) can create a second naturalness problem, as $M \gg m$ by radiative corrections providing a one-loop contribution to $m_{\tilde{\phi}}^2$ as

$$\Delta m_{\tilde{\phi}}^2 \simeq \frac{1}{4\pi^2} \, c_\alpha^2 \, |\lambda_\psi|^2 \, M^2 \log \frac{M^2}{m^2}. \tag{A.9}$$

However, once we have solved the naturalness problem between M and m_h, as $m^2 \gg m_h^2$, the second naturalness problem between M and m is automatically solved as, for all values in Eq. (A.8), it turns out that $\Delta m_{\tilde{\phi}}^2/m^2 \simeq 0.4$.

Cosmological problems

The Lagrangian (A.2) has the (ψ number) discrete $\mathbb{Z}_2$ symmetry $\psi \to -\psi$ making the fermion ψ cosmologically stable, inconsistent with direct Dark Matter detection, and possibly overclosing the Universe. A simple way out is explicitly breaking the $\mathbb{Z}_2$ symmetry. For instance we can identify $\psi \equiv E$ with a heavy vectorlike, $SU(2)$ singlet, lepton $E = (E_L, E_R)^T$, with hypercharge -1, as the SM right-handed leptons e_{R_i}. We can then generate a tiny mixing of e.g. the third generation leptons with E by means of the Yukawa coupling Y_3'

$$\mathcal{L}_E = -M\bar{E}_L E_R - Y_3 \bar{\ell}_{L_3} H \tau_R - Y_3' \bar{\ell}_{L_3} H E_R + h.c. \tag{A.10}$$

The mixing in (A.10) generates a mass matrix as

$$\left(\bar{\tau}_L \ \bar{E}_L\right) \mathcal{M} \begin{pmatrix} \tau_R \\ E_R \end{pmatrix}, \qquad\qquad \mathcal{M} = \begin{pmatrix} m_3 & m_3' \\ 0 & M \end{pmatrix} \tag{A.11}$$

where $m_3 = Y_3 v/\sqrt{2}$ is the τ-lepton mass in the absence of the mixing with the heavy fermion, and $m_3' \equiv Y_3' v/\sqrt{2}$. One can diagonalize the mass matrix $\mathcal{M}$ with left and right unitary transformations, with angles θ_L and θ_R, respectively, as

$$\mathcal{M}_d = U_L^\dagger \mathcal{M} U_R, \qquad\qquad U_{L/R} = \begin{pmatrix} \sin\theta_{L/R} & \cos\theta_{L/R} \\ -\cos\theta_{L/R} & \sin\theta_L \end{pmatrix}. \tag{A.12}$$

In the limit $M \gg m_3, m_3'$ we get

$$\sin\theta_L \simeq \frac{m_3'}{M}\left[1 + \frac{m_3^2}{M^2} + \cdots\right], \qquad \sin\theta_R \simeq \frac{m_3 m_3'}{M^2}\left[1 + \frac{m_3^2 - m_3'^2}{M^2} + \cdots\right]. \tag{A.13}$$

As a consequence of the mixing the mass eigenfunctions are shifted as

$$\tau_R \rightarrow \tau_R + \frac{m_3 m_3'}{M^2} E_R, \qquad\qquad E_R \rightarrow E_R - \frac{m_3 m_3'}{M^2}\tau_R, \tag{A.14a}$$

$$\tau_L \rightarrow \tau_L + \frac{m_3'}{M} E_L, \qquad\qquad E_L \rightarrow E_L - \frac{m_3'}{M}\tau_L, \tag{A.14b}$$

and the mass eigenvalues as

$$m_3 \rightarrow m_\tau = m_3\left[1 - \frac{m_3'^2}{2M^2} + \cdots\right], \qquad M \rightarrow M\left[1 + \frac{m_3'^2}{2M^2} + \cdots\right] \tag{A.15}$$

by which the fermion E decays as $E \rightarrow H\tau$, as well as to leptons and gauge bosons through the mixing with τ_L and τ_R, as $E \rightarrow W\nu_\tau$ or $E \rightarrow \tau Z, \tau\gamma$. These decays prevent the heavy fermion from overclosing the Universe.

A.2 Quadratic CS coupling

In this appendix, we present a possible UV completion which gives rise to the dimension-six operator

$$\mathcal{L} = \frac{1}{2}\frac{|\Phi|^2}{M^2} Y_{\mu\nu}\tilde{Y}^{\mu\nu} \tag{A.16}$$

that we are using to generate the magnetic field after the end of the inflationary period.

A very simple model consists of a complex scalar field S, a singlet under the SM gauge group, which interacts with $Y_{\mu\nu}\tilde{Y}^{\mu\nu}$ via the dimension-five operator

$$\mathcal{L} = \frac{1}{2f_S}\left(e^{i\alpha}S + \text{h.c.}\right)Y_{\mu\nu}\tilde{Y}^{\mu\nu}, \tag{A.17}$$

where α is an arbitrary phase and f_S is a mass scale. After decomposition of the complex field into its real and imaginary parts, $S = r + ia$, this gives rise to the usual axial coupling $(a/f_S)Y_{\mu\nu}\tilde{Y}^{\mu\nu}$ for $\alpha = \pi/2$, but of course the coupling can be much more general.

We will now consider a general renormalizable potential for the field S, with a coupling to the Higgs doublet Φ as

$$V(S, \Phi) = -\mu(e^{i\alpha}S + \text{h.c.})|\Phi|^2 + m_S^2|S|^2 + \lambda_{Sh}|S|^2|\Phi|^2 + \frac{1}{2}\lambda_S^2|S|^4 + V_{\text{SM}}(\Phi), \tag{A.18}$$

where $\mu \geqslant 0$ is a mass parameter, $m_S^2 \geqslant 0$ is the (common) mass-squared of the real and imaginary parts of S, and $\lambda_{Sh} \geqslant 0$, λ_S are real couplings. The global invariance $S \rightarrow e^{i\theta_S}S$, where θ_S is an

arbitrary phase, is explicitly broken by the first term in the potential (A.18) which then prevents the appearance of a massless Goldstone boson if S acquires a VEV once EW symmetry is broken.

For momenta much smaller than m_S, the field S is decoupled from the theory and can be integrated out neglecting its kinetic term and simply using its potential. Minimization of the potential (A.18) yields for

$$S = e^{i\theta}|S| \tag{A.19}$$

the equations determining the minimum

$$
\begin{aligned}
\theta &= -\alpha \\
\mu|\Phi|^2 &= (m_S^2 + \lambda_{Sh}|\Phi|^2 + \lambda_S^2|S|^2)|S| \,.
\end{aligned}
\tag{A.20}
$$

A quick glance at eq. (A.20) shows that for $\mu = 0$ the only solution is $|S| = 0$. For $\mu \neq 0$ and $\lambda_S, m_S \neq 0$ the solution, as can be seen from eq. (A.20), depends on two parameters,

$$\frac{\lambda_S|S|}{m_S} = f(x^2, y^2), \qquad y^2 \equiv \lambda_S \frac{\mu}{m_S}\frac{|\Phi|^2}{m_S^2}, \qquad x^2 \equiv \lambda_{Sh}\frac{|\Phi|^2}{m_S^2}, \tag{A.21}$$

which can be solved analytically. For the validity of the EFT expansion, the parameters x and y should be small. A power series expansion in x and y then gives

$$
\begin{aligned}
|S| &= \mu\frac{|\Phi|^2}{m_S^2}\left[\frac{1}{1+x^2} - \frac{y^4}{(1+x^2)^4} + \frac{3y^8}{(1+x^2)^7} + \cdots\right] \\
&= \mu\frac{|\Phi|^2}{m_S^2}\left[1 - \lambda_{Sh}\frac{|\Phi|^2}{m_S^2} + \mathcal{O}(|\Phi|^4/m_S^4)\right],
\end{aligned}
\tag{A.22}
$$

and the term in eq. (A.17) at the minimum yields

$$
\begin{aligned}
\mathcal{L} &= \frac{\mu}{f_S}\frac{|\Phi|^2}{m_S^2}\left[\frac{1}{1+x^2} - \frac{y^4}{(1+x^2)^4} + \frac{3y^8}{(1+x^2)^7} + \cdots\right]Y_{\mu\nu}\tilde{Y}^{\mu\nu} \\
&= \frac{\mu}{f_S}\frac{|\Phi|^2}{m_S^2}\left[1 - \lambda_{Sh}\frac{|\Phi|^2}{m_S^2} + \mathcal{O}(|\Phi|^4/m_S^4)\right]Y_{\mu\nu}\tilde{Y}^{\mu\nu}\,.
\end{aligned}
\tag{A.23}
$$

Matching the leading term with eq. (A.16) we find

$$M = \sqrt{\frac{f_S}{2\mu}}\,m_S\,. \tag{A.24}$$

Similarly, the potential (A.18) at the minimum is given by

$$
\begin{aligned}
V(\Phi) &= \frac{\mu^2}{m_S^2}|\Phi|^4\left[-\frac{1}{1+x^2} + \frac{y^4}{2(1+x^2)^4} - \frac{y^8}{(1+x^2)^7} + \cdots\right] + V_{\text{SM}}(\Phi) \\
&= \frac{\mu^2}{m_S^2}|\Phi|^4\left[-1 + \lambda_{Sh}\frac{|\Phi|^2}{m_S^2} + \mathcal{O}(|\Phi|^4/m_S^4)\right] + V_{\text{SM}}(\Phi)\,.
\end{aligned}
\tag{A.25}
$$

Consistent with the condition $x^2, y^2 \ll 1$, we will consider field configurations such that

$$\frac{\lambda_{Sh}f_S}{2\mu}|\Phi|^2 \ll M^2, \qquad\qquad \frac{\lambda_S^2 f_S^3}{8\mu}|\Phi|^4 \ll M^6\,, \tag{A.26}$$

where we have used eq. (A.24). We are interested in field values up to $|\Phi| \sim M$. The conditions can then be fulfilled for example for $\lambda_{Sh} \ll 1$ and $\mu \approx f_S \ll M$. This ensures that higher-

dimensional operators in eq. (A.23) of the form $|\Phi|^{2n}Y_{\mu\nu}\tilde{Y}^{\mu\nu}$ for $n \geqslant 2$ and corrections to $V_{\rm SM}(\Phi)$ in eq. (A.25) are greatly suppressed. Moreover, as $m_S \simeq M \gg \mathcal{Q}_I \simeq 10^{-11}$ GeV (see values of $M \equiv f_h \gtrsim 10^{-3}\, M_{\rm Pl}$ in Chap. 5) the coupling of the singlet S with the SM Higgs does not change the instability properties of the SM Higgs vacuum.

Finally, note that a simple way of generating a term like that in eq. (A.17) is through the introduction of a massive hypercharged vector-like (Dirac) fermion χ with Yukawa coupling to S [228] $\lambda = |\lambda|e^{i\theta_\lambda}$, where θ_λ is an arbitrary phase, as was done in App. A.1. The corresponding term reads

$$\mathcal{L} = \lambda\,\bar{\chi}_L S \chi_R + \text{h.c.} = |\lambda||S|\left[\cos(\theta_\lambda - \alpha)\bar{\chi}\chi + \sin(\theta_\lambda - \alpha)\bar{\chi}i\gamma_5\chi\right], \tag{A.27}$$

where the EOMs (A.20) for the field S have been used in the second step. For the phase values $\theta_\lambda = \alpha \pm \pi/2$, eq. (A.27) yields

$$\mathcal{L} = \pm|\lambda||S|\bar{\chi}i\gamma_5\chi\,. \tag{A.28}$$

Through one-loop diagrams where a loop of χ-fermions is exchanged and emits two photons, this gives rise to the interaction in eq. (A.17) evaluated in the minimum in Eq. (A.20)[43].

---

[43]For arbitrary values of the phase θ_λ, the coefficient of the term $\bar{\chi}\chi$ in eq. (A.27) does not vanish, and the corresponding interaction would also give rise to the Lagrangian term $|S|Y_{\mu\nu}Y^{\mu\nu}$.

Appendix B

Froggatt-Nielsen mechanism in de Sitter space

The Froggatt-Nielsen (FN) mechanism [187] is one of the simplest and most elegant solutions to the problem of flavor for the SM fermions. The hierarchy of masses and mixing angles for quarks and leptons can be explained by a global, generation dependent, $U(1)$ symmetry under which the fermions are charged. This symmetry is spontaneously broken by the radial part of scalar field $S \equiv \sigma e^{i\theta}$, the "flavon field", which is charged under the $U(1)$ (with charge conventionally normalized to -1) and which has a VEV, $\langle\sigma\rangle = v_\sigma$. The breaking is communicated to the fermion sector at different orders in the parameter $\lambda(\langle\sigma\rangle) = \langle\sigma\rangle/M_\star$, where $M_\star$ is the scale of flavor dynamics, which depend on the charges of the SM fermions q_i, u_i^c, d_i^c, ℓ_i, e_i^c involved in Yukawa couplings.

If we denote the $U(1)$ charge of the fermion f by $[f]$, the Yukawa coupling matrices are given by

$$Y_u^{ij} \sim \lambda^{[q_i]+[u_j^c]}, \qquad Y_d^{ij} \sim \lambda^{[q_i]+[d_j^c]}, \qquad Y_\ell^{ij} \sim \lambda^{[\ell_i]+[e_j^c]} \tag{B.1}$$

When the field σ is at its minimum, and provided that $\lambda(v_\sigma) \simeq 0.2$, of the order of the Cabibbo angle, one can choose the $U(1)$ charges such that the SM fermion mass spectrum and mixing angles are correctly described. A simple example is provided by (see e.g. Ref. [229] for a pedagogical introduction): $[q_{3,2,1}] = [u_{3,2,1}^c] = (0,2,4)$, $d_{3,2,1}^c = (2,2,3)$, $[\ell_{3,2,1}] = (2,2,3)$, $[e_{3,2,1}^c] = (0,2,4)$. However the details of the model are not important for our argument here.

We will introduce a coupling between the flavon and the inflaton (Higgs fields) as $|S|^2|H|^2$, and assume that the flavon field has a potential given, in the Jordan frame, by

$$U(\sigma) = \lambda_1 \left(|S|^2 - v_\sigma^2 - \lambda_2|H|^2\right)^2 \tag{B.2}$$

which corresponds, in the Einstein frame, to the potential

$$V(\sigma) = \frac{\lambda_1 \left(\sigma^2 - v_\sigma^2 - \frac{1}{2}\lambda_2 h^2\right)^2}{\left(1 + \frac{\xi_h h^2}{M_p^2}\right)^2} \tag{B.3}$$

where $v_\sigma \gg v$, so that at electroweak scales ($h \sim v$) the vacuum expectation value $\langle\sigma\rangle \simeq v_\sigma$, which spontaneously breaks the flavor symmetry[44].

At the electroweak phase transition, when the field σ is at its minimum v_σ, and provided that the flavor scale be $M_* \simeq 5v_\sigma$, it is possible to solve the flavor problem for fermion masses. Moreover,

---

[44] After the global $U(1)$ symmetry breaking a (massless) Goldstone boson will remain in the spectrum. To avoid phenomenological problems it is usually assumed that there is a small explicit soft breaking of the $U(1)$ symmetry giving a mass to the (pseudo) Goldstone boson. These model details are also orthogonal to our argument here.

there is an extra quartic coupling for the Higgs field from the potential (B.2) which is negligible, compared to the SM one, provided that $\lambda_1 \lambda_2^2 \ll \lambda_h$, where λ_h is the SM Higgs quartic coupling evaluated at the electroweak scale. This condition can be widely satisfied e.g. for typical values of the couplings

$$\lambda_1 = \lambda_2 = 0.1 \tag{B.4}$$

However during the de Sitter phase, things can be pretty much different. We will study the possibility that at the end of inflation $\lambda(\langle \sigma \rangle) \simeq 1$. In fact, at the end of inflation $h_E \simeq 10^{-2} M_p$ and one can safely neglect v_σ^2 as compared to $\frac{1}{2} \lambda_2 h_E^2$, so that $\langle \sigma \rangle \simeq \sqrt{\lambda_2/2}\, h_E$, which dictates the flavor scale M_* by imposing the condition $\lambda(\langle \sigma \rangle) \simeq 1$ as

$$M_* \simeq \sqrt{\frac{\lambda_2}{2}}\, h_E\,, \tag{B.5}$$

which yields, e.g. for the values of the couplings in (B.4), $v_\sigma \simeq 10^{15}$ GeV.

Moreover, the condition for the de Sitter fluctuations to be suppressed, so that the field σ stays anchored to its minimum $V(\langle \sigma \rangle) = 0$, during inflation $V''(\langle \sigma \rangle) > \frac{9}{4} H_E^2$ [26], translates into the condition

$$\frac{8\lambda_1 \langle \sigma \rangle^2}{\left(1 + \frac{\xi_h h_E^2}{M_p^2}\right)^2} > \frac{9}{4} H_E^2 \tag{B.6}$$

which, using the value of h_E above and $H_E \simeq 2 \cdot 10^{13}$ GeV, yields the condition $\sqrt{\lambda_1 \lambda_2} \gtrsim 10^{-3}$, which is satisfied for the choice in Eq. (B.4).

What are the implications of the above scenario for the conductivity in the Schwinger effect? As we have seen the conductivity from a Dirac fermion f, of electric charge Q_f and Yukawa coupling Y_f, is exponentially suppressed as $\sim e^{-A_f}$ where

$$A_f = \frac{\pi Y_f^2 h^2}{2|e Q_f||E|} \tag{B.7}$$

and for $A_f \gg 1$ it does not contribute to the Schwinger effect. Now, considering, at the end of HI, $Y_f \sim 1$ and $h_E \simeq 10^{-2} M_{\rm pl}$, the condition for the fermion f to not create any conductivity, $A_f \gg 1$, self-consistently translates into an upper bound on the generated electric field $|E|$ in the absence of Schwinger effect, as

$$\frac{|E|}{H_E^2} \ll \frac{10^7}{|Q_f|} \tag{B.8}$$

The strongest bound is then provided by the leptons, for which $|Q_\ell| = 1$ so that a (conservative) safe bound for all charged SM fermions to not contribute to the Schwinger effect is $E \lesssim 10^6 H_E^2$. If we use the analytic expression for zero conductivity, $\rho_E = 63/(2^{16} \pi^2 \xi^3) e^{2\pi\xi} H_E^4$, we get the corresponding upper bound $\xi \lesssim 6.7$, which translates into the lower bound on the parameter f_h, as $f_h \gtrsim 0.0022 M_{\rm pl}$.

Appendix C

Numerical code

On the following pages we display the numerical code we have written on *Wolfram Mathematica* in order to simulate the fermion backreaction on the gauge plasma during and just after inflation, see Chap. 4. In particular, we present the code for the α-attractor model that simulate the joint evolution of the inflaton and the gauge beyond inflation to see the preheating possibilities of the model. It is run in units of $H(a_0)$ where a_0 set the initialization time. The code for the hilltop model is identical to the exception of the potential, ϕ_E some other functions declarations.

The displayed code is divided into three parts. First we specify which model is simulate by means of the potential and we also define the slow roll parameter functions. We then compute ϕ_E, ϕ_* and Λ_α. In a second part we declare the linear system (4.51) and the initialization function for the inflaton and the gauge field (the BD vacuum) given by (4.44). Next, until the function `Monitor`, we declare every variables used, in particular the ones we want to export for plots. These are array that will be filled at each measurement function happening in the `While` time iteration loop that follows. The latter consists of first the time stepping for the inflaton and every mode of both helicity for the gauge field, then the computation of the plasma integrals and their storage. Once the loop breaks, the data is saved on the computed memory for plots and later use.

All of this is embedded in a `For` loop over the parameter f_ϕ and it can also be for the parameter α, here set to 1, or another one depending on the wanted analysis. Last, note that we have voluntarily omit the code sections corresponding to importing and plotting the datas, are these are already shown in Chap. 4 figures.

Inflation potential

```
In[ ]:= V := Λ^4 Mpleff^4 (1 - Exp[-√(2/(3 α)) √(φ^2)/Mpleff])^2;

ε := Mpleff^2/2 (D[V, φ]/V)^2;

η := Mpleff^2 D[V, {φ, 2}]/V;

φE := √(3 α/2) Log[1 + 2/(√3 √α)] Mpleff;

int := 1/Mpleff^2 Integrate[V/D[V, φ], φ];


NφE[a_] := (φ → φE /. α → a)[[2]];
Nint[a_] := int /. α → a;
NintφE[a_] := int /. φ → φE /. α → a;
Nφast[a_] := FindRoot[Nint[a] - NintφE[a] ⩵ 60, {φ, 5}][[1, 2]];

Asobs = 1.88 × 10^-9 Exp[2 × 0.078];

selfcoup[a_] := Quiet@FindRoot[
    (1/(24 π^2) V/εfun[Nφast[a], a] /. φ → Nφast[a] /. α → a) ⩵ Asobs, {Λ, 1}][[1, 2]];


Vfun[x_, a_] := V /. {α → a, φ → x};
dVfun[x_, a_] := D[V, φ] /. {α → a, φ → x};
εfun[phi_, a_] := ε /. φ → phi /. α → a;
ηfun[phi_, a_] := η /. φ → phi /. α → a;


aendfun[λ_] := aE (3 √(3 alpha) HE/(λ selfcoup[alpha]^2))^(2/3);
```

Function to solve

```
In[◦]:= inflaton[a_, {w_, x_}, EB_, fφ_, H_, F_] := {x, EB/(a^2 H^2 fφ) - (4 - F)/a x - dVfun[w, alpha]/(a^2 H^2)};

initialphi[a0_, af_, a_] :=
   Quiet@ FindRoot[Nint[a] - NintφE[a] == Log[af/a0], {φ, 5}][[1, 2]];


modes[a_, {x1_, y1_, x2_, y2_}, k_, ξ_, σ_, H_, F_] := {y1,
   k/(a^3 H) (2 ξ - k/(a H)) x1 - 1/a (σ/(a H) + 2 - F) y1, y2, - k/(a^3 H) (2 ξ + k/(a H)) x2 - 1/a (σ/(a H) + 2 - F) y2};

initializationRe[a_, ax_, k_, Δ_, σ_, H_] :=
   {Sqrt[Δ/(2 k)] Cos[k/a - k/ax], - 1/(ax^2 H) Sqrt[Δ/2] (Sqrt[k] Sin[k/a - k/ax] - σ/(2 Sqrt[k]) Cos[k/a - k/ax]),

    Sqrt[Δ/(2 k)] Cos[k/a - k/ax], - 1/(ax^2 H) Sqrt[Δ/2] (Sqrt[k] Sin[k/a - k/ax] - σ/(2 Sqrt[k]) Cos[k/a - k/ax])};

initializationIm[a_, ax_, k_, Δ_, σ_, H_] :=
   {Sqrt[Δ/(2 k)] Sin[k/a - k/ax], - 1/(ax^2 H) Sqrt[Δ/2] (- Sqrt[k] Cos[k/a - k/ax] - σ/(2 Sqrt[k]) Sin[k/a - k/ax]),

    Sqrt[Δ/(2 k)] Sin[k/a - k/ax], - 1/(ax^2 H) Sqrt[Δ/2] (- Sqrt[k] Cos[k/a - k/ax] - σ/(2 Sqrt[k]) Sin[k/a - k/ax])};
```

Code

```
fφarray = {0.02, 0.05, 0.1, 0.15, 0.2};
alpha = 1;

na = 2000.;
naMD = 2000.;
saveevery = 5;
af = 50.;

SetSystemOptions["CheckMachineUnderflow" → False];
For[j = 1, j ≤ Length@fφarray, j++,

  fφ = fφarray[[j]];

  a0 = 10^-30;
  nk = 300;
  BDfac = 20;
```

```
kc = 0;
kmin = BDfac a0;
ξ = ────── ;
     √2 fφ
kmax = ξ af;


σ = 0;
Mpleff = 1;
Λ = selfcoup[alpha];
phi0 := initialphi[a0, 1, alpha];
          dVfun[phi0, alpha]
dphi0 := - ─────────────────── ;
                  3 a0
phi = {phi0, dphi0};

          1      ┌─────────────
H := ───────── \│ Vfun[phi0, alpha]
        Mpleff   \│ ───────────────── ;
                          3


(*WE SET THE SIMULATION IN UNITS OF H*)
Mpleff = H⁻¹;
phi = Mpleff {phi〚1〛, phi〚2〛 Mpleff²};
H = 1;
F = 0;
phidot = a0 H phi〚2〛;
                         ┌                         Log@kmax - Log@kmin ┐
kdis = Exp@Range│Log@kmin, Log@kmax, ─────────────────── │;
                └                                  nk - 1              ┘


          ┌                  ┌     k            ┐             ┐
xire = Table│initializationRe│a0, ─────, k, 1, 0, H│, {k, kdis}│;
          └                  └    BDfac           ┘             ┘
          ┌                  ┌     k            ┐             ┐
xiim = Table│initializationIm│a0, ─────, k, 1, 0, H│, {k, kdis}│;
          └                  └    BDfac           ┘             ┘


          ┌         ┌                  Log@1 - Log@a0 ┐
time = Join│Exp@Range│Log@a0, Log@1, ────────────────│,
          └         └                     na - 1      ┘

       ┌      ┌       af - 1 ┐    ┐
   Delete│Range│1, af, ────── │, 1│, {af + 1}│;
       └      └        naMD   ┘    ┘


sigma = {σ};
ρE = {0};
ρB = {0};
ρψ = {0};
hel = {0};
EBi = 0;
EB = {EBi};
cosθ = {0};
inDelta = 0;
Δ = 1;
Delta = {Δ};
```

```
Hubble = {H};
Ffactor = {F};


ξ = - a0 phi[[2]] / (2 Mpleff fϕ) ;

xi = {ξ};

inflatonϕ = { { phi[[1]] / Mpleff , phidot / Mpleff² } };

cutoff = {0};
Stime = {a0};
Ekin = {};
Epot = {};
Boolkmax = True;
BoolE = True;
ai = a0;
i = 1;


Monitor[
 While[ai ≤ af,
    h = time[[i + 1]] - ai;

    (* INFALTON *)
    l1 = inflaton[ai, phi, EBi, Mpleff fϕ, H, F];
    l2 = inflaton[ai + h/2, phi + h/2 l1, EBi, Mpleff fϕ, H, F];
    l3 = inflaton[ai + h/2, phi + h/2 l2, EBi, Mpleff fϕ, H, F];
    l4 = inflaton[ai + h, phi + h l3, EBi, Mpleff fϕ, H, F];
    phi = phi + h/6 (l1 + 2 l2 + 2 l3 + l4);
    phidot = ai H phi[[2]];
    ξ = - ai phi[[2]] / (2 Mpleff fϕ) ;

    (* GAUGE FIELD *)
    spectrum = Transpose@ParallelTable[

        ax = kdis[[n]] / BDfac ;

        If[ai < ax,
          xire[[n]] = initializationRe[ai, ax, kdis[[n]], Δ, σ, H];
          xiim[[n]] = initializationIm[ai, ax, kdis[[n]], Δ, σ, H];
          ,

          (* REAL PART *)
          l1 = modes[ai, xire[[n]], kdis[[n]], ξ, σ, H, F];
```

```mathematica
    l2 = modes[ai + h/2, xire[[n]] + h/2 l1, kdis[[n]], ξ, σ, H, F];

    l3 = modes[ai + h/2, xire[[n]] + h/2 l2, kdis[[n]], ξ, σ, H, F];

    l4 = modes[ai + h, xire[[n]] + h l3, kdis[[n]], ξ, σ, H, F];

    xire[[n]] = xire[[n]] + h/6 (l1 + 2 l2 + 2 l3 + l4);


    (* IMAGINARY PART *)
    l1 = modes[ai, xiim[[n]], kdis[[n]], ξ, σ, H, F];

    l2 = modes[ai + h/2, xiim[[n]] + h/2 l1, kdis[[n]], ξ, σ, H, F];

    l3 = modes[ai + h/2, xiim[[n]] + h/2 l2, kdis[[n]], ξ, σ, H, F];

    l4 = modes[ai + h, xiim[[n]] + h l3, kdis[[n]], ξ, σ, H, F];

    xiim[[n]] = xiim[[n]] + h/6 (l1 + 2 l2 + 2 l3 + l4);

   ];

  {H² kdis[[n]]²/(4 π²) (xire[[n, 2]]² + xiim[[n, 2]]² + xire[[n, 4]]² + xiim[[n, 4]]²),

   1/ai⁴ kdis[[n]]⁴/(4 π²) (xire[[n, 1]]² + xiim[[n, 1]]² + xire[[n, 3]]² + xiim[[n, 3]]²),

   1/ai³ kdis[[n]]³/(2 π²) (xire[[n, 1]]² + xiim[[n, 1]]² - xire[[n, 3]]² - xiim[[n, 3]]²),

   - H/ai² kdis[[n]]³/(2 π²) (√((xire[[n, 1]]² + xiim[[n, 1]]²) (xire[[n, 2]]² + xiim[[n, 2]]²)) -
       √((xire[[n, 3]]² + xiim[[n, 3]]²) (xire[[n, 4]]² + xiim[[n, 4]]²))),

   H/ai² kdis[[n]]²/π² (Abs@(xire[[n, 1]] × xire[[n, 2]] + xiim[[n, 1]] × xiim[[n, 2]]) +
      Abs@(xire[[n, 3]] × xire[[n, 4]] + xiim[[n, 3]] × xiim[[n, 4]])),
   kdis[[n]] (xire[[n, 1]]² + xiim[[n, 1]]² + xire[[n, 3]]² + xiim[[n, 3]]²),
   xire[[n]], xiim[[n]]},

  {n, nk}];


If[i > 2,
 If[Boolkmax,
   kc = Abs@ (ai phidot)/(2 Mpleff fφ) +
      √(Max[0, ((ai phidot)/(2 Mpleff fφ))² + ai²/2 ((H σ - oldH oldσ)/(ai - time[[i - 1]]) + σ/ai (σ/(2 ai) + H))])];
  ];;,
```

```
 kc = 0;
];


oldσ = σ;
If[kmin ≥ kc,
 intQuantity = {0, 0, 0, 0, 0};
 σ = 0;,
 intQuantity = ParallelTable[NIntegrate[
     Interpolation[
       Transpose[{kdis, spectrum〚i〛}]
      ][k], {k, kmin, kc}
   ], {i, 5}];
 σ = ai (41 × 0.42³)/(72 π²) √(2 intQuantity〚2〛) Coth[π √(intQuantity〚2〛/intQuantity〚1〛)];
];


EBi = intQuantity〚4〛;
oldH = H;
H = Mpleff⁻¹ √((1/3) (phidot²/2 + Vfun[phi〚1〛, alpha] +

        intQuantity〚1〛 + intQuantity〚2〛 + oldσ intQuantity〚5〛));

σ = σ/H;
F = Mpleff⁻² H⁻²
    (phidot²/2 + (2/3) (intQuantity〚1〛 + intQuantity〚2〛 + oldσ intQuantity〚5〛));

inDelta = inDelta + (h/2) (σ/(H time〚i + 1〛²) + oldσ/(oldH ai²)) ;

Δ = Exp[-inDelta];


If[Mod[i, saveevery] == 0,

 If[kmin ≥ kc,
  cang = 0;,
  cang = Abs@ EBi/(2 √(intQuantity〚1〛 × intQuantity〚2〛)) ;
 ];


 AppendTo[Stime, ai];
 AppendTo[xi, ξ];
```

```
    AppendTo[inflatonϕ, { phi[[1]] , phidot  }];
                          ───────  ───────
                          Mpleff   Mpleff²

    AppendTo[cutoff, kc];
    AppendTo[Hubble, H];
    AppendTo[Ffactor, F];
    AppendTo[sigma, σ];
    AppendTo[Delta, Δ];
    AppendTo[ρE, intQuantity[[1]]];
    AppendTo[ρB, intQuantity[[2]]];
    AppendTo[hel, intQuantity[[3]]];
    AppendTo[ρψ, σ intQuantity[[5]]];
    AppendTo[EB, EBi];
    AppendTo[cosθ, cang];

    AppendTo[Ekin, 1  phidot² ];
                   ─  ───────
                   2  Mpleff⁴

    AppendTo[Epot, Vfun[phi[[1]], alpha] ];
                   ─────────────────────
                          Mpleff⁴

    ];

    If[εfun[phi[[1]], alpha] > 1 && BoolE,
      iE = i;
      aE = ai;
      HE = H;
      BoolE = False;
      ];

    i++;
    ai = time[[i]];
    xire = spectrum[[-2]];
    xiim = spectrum[[-1]];
   ];
  , {fϕ, i}];
 time = Stime;

 {time, inflatonϕ, Hubble, Ffactor,
   xi, ρB, ρE, ρψ, hel, EB, sigma, cosθ, Delta, cutoff} >>>
  "Documents/Preheating/Datas/preheating-alpha1-8f4-thesis-data1.dat";
];
```

Bibliography

[1] A. Einstein, *Die Feldgleichungen der Gravitation, Sitzungsberichte der Preussischen Akademie der Wissenschaften zu Berlin* (1915) 844–847.

[2] S. Perlmutter, G. Aldering, M. D. Valle, S. Deustua, R. S. Ellis, S. Fabbro et al., *Discovery of a supernova explosion at half the age of the Universe, Nature* **391** (1998) 51–54.

[3] P. M. Garnavich, R. P. Kirshner, P. Challis, J. Tonry, R. L. Gilliland, R. C. Smith et al., *Constraints on cosmological models from Hubble Space Telescope observations of high-z supernovae, The Astrophysical Journal* **493** (feb, 1998) L53–L57.

[4] E. Hubble, *A relation between distance and radial velocity among extra-galactic nebulae, Proceedings of the National Academy of Sciences* **15** (1929) 168–173.

[5] A. G. Riess et al., *A Comprehensive Measurement of the Local Value of the Hubble Constant with 1 km s^{-1} Mpc^{-1} Uncertainty from the Hubble Space Telescope and the SH0ES Team, Astrophys. J. Lett.* **934** (2022) L7, [`2112.04510`].

[6] Planck collaboration, N. Aghanim et al., *Planck 2018 results. VI. Cosmological parameters, Astron. Astrophys.* **641** (2020) A6, [`1807.06209`].

[7] E. Di Valentino, O. Mena, S. Pan, L. Visinelli, W. Yang, A. Melchiorri et al., *In the realm of the Hubble tension—a review of solutions, Class. Quant. Grav.* **38** (2021) 153001, [`2103.01183`].

[8] WMAP collaboration, D. N. Spergel et al., *Wilkinson Microwave Anisotropy Probe (WMAP) three year results: implications for cosmology, Astrophys. J. Suppl.* **170** (2007) 377, [`astro-ph/0603449`].

[9] A. A. Penzias and R. W. Wilson, *A Measurement of excess antenna temperature at 4080-Mc/s, Astrophys. J.* **142** (1965) 419–421.

[10] H. Kurki-Suonio, *Cosmology I lecture notes, 4: Thermal history of the Early Universe*, 2022 (Accessed: `http://www.courses.physics.helsinki.fi/teor/cosmology/Cosm4.pdf`).

[11] D. Samtleben, S. Staggs and B. Winstein, *The Cosmic microwave background for pedestrians: A Review for particle and nuclear physicists, Ann. Rev. Nucl. Part. Sci.* **57** (2007) 245–283, [`0803.0834`].

[12] P. D. Group, R. L. Workman, V. D. Burkert, V. Crede, E. Klempt, U. Thoma et al., *Review of Particle Physics, Progress of Theoretical and Experimental Physics* **2022** (08, 2022) .

[13] W. Rindler, *Visual Horizons in World Models, Monthly Notices of the Royal Astronomical Society* **116** (12, 1956) 662–677.

[14] R. H. Dicke, *Gravitation and the Universe : Jayne Lectures for 1969.* Philadelphia: American Philosophical Society, 1970.

[15] A. H. Guth, *The Inflationary Universe: a possible solution to the horizon and flatness problems, Phys. Rev. D* **23** (1981) .

[16] A. Linde, *A new inflationary universe scenario: A possible solution of the horizon, flatness, homogeneity, isotropy and primordial monopole problems, Phys. Lett. B* **108** (1982) 389.

[17] A. Albrecht and P. Steinhardt, *Cosmology for Grand Unified Theories with radiatively induced symmetry breaking*, Phys. Rev. Lett. **48** (1982) 1220.

[18] D. Baumann, *Inflation*, in *Theoretical Advanced Study Institute in Elementary Particle Physics: Physics of the Large and the Small*, pp. 523–686, 2011. `0907.5424`. DOI.

[19] D. Langlois, *Lectures on inflation and cosmological perturbations*, *Lect. Notes Phys.* **800** (2010) 1–57, [`1001.5259`].

[20] B. A. Bassett, S. Tsujikawa and D. Wands, *Inflation dynamics and reheating*, *Rev. Mod. Phys.* **78** (2006) 537–589, [`astro-ph/0507632`].

[21] L. Sriramkumar, *An introduction to inflation and cosmological perturbation theory*, `0904.4584`.

[22] PLANCK collaboration, Y. Akrami et al., *Planck 2018 results. X. Constraints on inflation*, *Astron. Astrophys.* **641** (2020) A10, [`1807.06211`].

[23] BICEP/KECK collaboration, P. A. R. Ade et al., *Improved Constraints on Primordial Gravitational Waves using Planck, WMAP, and BICEP/Keck Observations through the 2018 Observing Season*, *Phys. Rev. Lett.* **127** (2021) 151301, [`2110.00483`].

[24] D. J. Chung, E. W. Kolb and A. Riotto, *Production of massive particles during reheating*, *Phys. Rev. D* **60** (1999) 063504, [`hep-ph/9809453`].

[25] G. F. Giudice, E. W. Kolb and A. Riotto, *Largest temperature of the radiation era and its cosmological implications*, *Phys. Rev. D* **64** (2001) 023508, [`hep-ph/0005123`].

[26] J. R. Espinosa, G. F. Giudice, E. Morgante, A. Riotto, L. Senatore, A. Strumia et al., *The cosmological Higgstory of the vacuum instability*, *JHEP* **09** (2015) 174, [`1505.04825`].

[27] A. Linde, *Chaotic inflation*, *Physics Letters B* **129** (1983) 177–181.

[28] R. Kallosh, A. Linde and D. Roest, *Superconformal Inflationary α-Attractors*, *JHEP* **11** (2013) 198, [`1311.0472`].

[29] L. Boubekeur and D. H. Lyth, *Hilltop inflation*, *JCAP* **07** (2005) 010, [`hep-ph/0502047`].

[30] G. R. Dvali, Q. Shafi and S. Solganik, *D-brane inflation*, in *4th European Meeting From the Planck Scale to the Electroweak Scale*, 5, 2001. `hep-th/0105203`.

[31] J. Garcia-Bellido, R. Rabadan and F. Zamora, *Inflationary scenarios from branes at angles*, *JHEP* **01** (2002) 036, [`hep-th/0112147`].

[32] C. P. Burgess, M. Majumdar, D. Nolte, F. Quevedo, G. Rajesh and R.-J. Zhang, *The Inflationary brane anti-brane universe*, *JHEP* **07** (2001) 047, [`hep-th/0105204`].

[33] A. Starobinsky, *A new type of isotropic cosmological models without singularity*, *Physics Letters B* **91** (1980) 99–102.

[34] A. Vilenkin, *Classical and quantum cosmology of the starobinsky inflationary model*, *Phys. Rev. D* **32** (Nov, 1985) 2511–2521.

[35] M. B. Mijic, M. S. Morris and W.-M. Suen, *The R**2 Cosmology: Inflation Without a Phase Transition*, *Phys. Rev. D* **34** (1986) 2934.

[36] A. De Felice and S. Tsujikawa, *f(R) theories*, *Living Rev. Rel.* **13** (2010) 3, [`1002.4928`].

[37] F. L. Bezrukov and M. Shaposhnikov, *The Standard Model Higgs boson as the inflaton*, *Phys. Lett. B* **659** (2008) 703–706, [`0710.3755`].

[38] F. L. Bezrukov, A. Magnin and M. Shaposhnikov, *Standard Model Higgs boson mass from inflation*, *Phys. Lett. B* **675** (2009) 88–92, [`0812.4950`].

[39] F. Bezrukov, A. Magnin, M. Shaposhnikov and S. Sibiryakov, *Higgs inflation: consistency and generalisations*, *JHEP* **01** (2011) 016, [`1008.5157`].

[40] J. Rubio, *Higgs inflation*, *Front. Astron. Space Sci.* **5** (2019) 50, [`1807.02376`].

[41] T. Han and S. Willenbrock, *Scale of quantum gravity*, *Phys. Lett. B* **616** (2005) 215–220, [`hep-ph/0404182`].

[42] C. P. Burgess, H. M. Lee and M. Trott, *Power-counting and the Validity of the Classical Approximation During Inflation*, *JHEP* **09** (2009) 103, [`0902.4465`].

[43] J. L. F. Barbon and J. R. Espinosa, *On the Naturalness of Higgs Inflation*, *Phys. Rev. D* **79** (2009) 081302, [`0903.0355`].

[44] R. N. Lerner and J. McDonald, *Higgs Inflation and Naturalness*, *JCAP* **04** (2010) 015, [`0912.5463`].

[45] C. P. Burgess, H. M. Lee and M. Trott, *Comment on Higgs Inflation and Naturalness*, *JHEP* **07** (2010) 007, [`1002.2730`].

[46] M. P. Hertzberg, *On Inflation with Non-minimal Coupling*, *JHEP* **11** (2010) 023, [`1002.2995`].

[47] I. Antoniadis, A. Guillen and K. Tamvakis, *Ultraviolet behaviour of Higgs inflation models*, *JHEP* **08** (2021) 018, [`2106.09390`].

[48] A. Ito, W. Khater and S. Rasanen, *Tree-level unitarity in Higgs inflation in the metric and Palatini formulation*, `2111.05621`.

[49] G. K. Karananas, M. Shaposhnikov and S. Zell, *Field redefinitions, perturbative unitarity and Higgs inflation*, *JHEP* **06** (2022) 132, [`2203.09534`].

[50] J. Rubio and E. S. Tomberg, *Preheating in Palatini Higgs inflation*, *JCAP* **04** (2019) 021, [`1902.10148`].

[51] R. Bousso, *TASI Lectures on the Cosmological Constant*, *Gen. Rel. Grav.* **40** (2008) 607–637, [`0708.4231`].

[52] C. P. Burgess, *The Cosmological Constant Problem: Why it's hard to get Dark Energy from Micro-physics*, in *100e Ecole d'Ete de Physique: Post-Planck Cosmology*, pp. 149–197, 2015. `1309.4133`. DOI.

[53] SDSS collaboration, M. Tegmark et al., *Cosmological Constraints from the SDSS Luminous Red Galaxies*, *Phys. Rev. D* **74** (2006) 123507, [`astro-ph/0608632`].

[54] V. C. Rubin and W. K. Ford, Jr., *Rotation of the Andromeda Nebula from a Spectroscopic Survey of Emission Regions*, *Astrophys. J.* **159** (1970) 379–403.

[55] K. C. Freeman, *On the disks of spiral and SO Galaxies*, *Astrophys. J.* **160** (1970) 811.

[56] J. L. Feng, *Dark Matter Candidates from Particle Physics and Methods of Detection*, *Ann. Rev. Astron. Astrophys.* **48** (2010) 495–545, [`1003.0904`].

[57] S. Dodelson and L. M. Widrow, *Sterile-neutrinos as dark matter*, *Phys. Rev. Lett.* **72** (1994) 17–20, [`hep-ph/9303287`].

[58] T. Asaka and M. Shaposhnikov, *The νMSM, dark matter and baryon asymmetry of the universe*, *Phys. Lett. B* **620** (2005) 17–26, [`hep-ph/0505013`].

[59] R. J. Scherrer and M. S. Turner, *On the relic, cosmic abundance of stable, weakly interacting massive particles*, *Phys. Rev. D* **33** (Mar, 1986) 1585–1589.

[60] B. Famaey and S. McGaugh, *Modified Newtonian Dynamics (MOND): Observational Phenomenology and Relativistic Extensions*, *Living Rev. Rel.* **15** (2012) 10, [`1112.3960`].

[61] P. Dirac, *The quantum theory of the electron*, *Proc. R. Soc. Lond.* **A 117** (1928) 610–624.

[62] C. D. Anderson, *The apparent existence of easily deflectable positives*, *Science* **76** (1932) 238–239.

[63] J. M. Cline, *Baryogenesis*, in *Les Houches Summer School - Session 86: Particle Physics and Cosmology: The Fabric of Spacetime*, 9, 2006. `hep-ph/0609145`.

[64] H. Kurki-Suonio, *Cosmology I lecture notes, 9: Cosmic Microwave Background Anisotropy*, 2022 (Accessed: `http://www.courses.physics.helsinki.fi/teor/cosmology/Cosm9.pdf`).

[65] H. Kurki-Suonio, *Cosmology I lecture notes, 5: Big Bang Nucleosynthesis*, 2022 (Accessed: http://www.courses.physics.helsinki.fi/teor/cosmology/Cosm5.pdf).

[66] A. D. Sakharov, *Violation of $\mathcal{CP}$ Invariance, $\mathcal{C}$ asymmetry, and baryon asymmetry of the universe*, *Pisma Zh. Eksp. Teor. Fiz.* **5** (1967) 32–35.

[67] M. Yoshimura, *Unified Gauge Theories and the Baryon Number of the Universe*, *Phys. Rev. Lett.* **41** (1978) 281–284.

[68] D. V. Nanopoulos and S. Weinberg, *Mechanisms for Cosmological Baryon Production*, *Phys. Rev. D* **20** (1979) 2484.

[69] M. Fukugita and T. Yanagida, *Baryogenesis Without Grand Unification*, *Phys. Lett. B* **174** (1986) 45–47.

[70] W. Buchmuller, P. Di Bari and M. Plumacher, *Leptogenesis for pedestrians*, *Annals Phys.* **315** (2005) 305–351, [hep-ph/0401240].

[71] S. Davidson, E. Nardi and Y. Nir, *Leptogenesis*, *Phys. Rept.* **466** (2008) 105–177, [0802.2962].

[72] I. Affleck and M. Dine, *A New Mechanism for Baryogenesis*, *Nucl. Phys. B* **249** (1985) 361–380.

[73] A. G. Cohen and D. B. Kaplan, *Spontaneous Baryogenesis*, *Nucl. Phys. B* **308** (1988) 913–928.

[74] A. G. Cohen, D. B. Kaplan and A. E. Nelson, *Spontaneous baryogenesis at the weak phase transition*, *Phys. Lett. B* **263** (1991) 86–92.

[75] A. G. Cohen, D. B. Kaplan and A. E. Nelson, *WEAK SCALE BARYOGENESIS*, *Phys. Lett. B* **245** (1990) 561–564.

[76] A. G. Cohen, D. B. Kaplan and A. E. Nelson, *Progress in electroweak baryogenesis*, *Ann. Rev. Nucl. Part. Sci.* **43** (1993) 27–70, [hep-ph/9302210].

[77] M. Dine and A. Kusenko, *The Origin of the matter - antimatter asymmetry*, *Rev. Mod. Phys.* **76** (2003) 1, [hep-ph/0303065].

[78] M. Srednicki, *Quantum Field Theory*. Cambridge University Press, 2007.

[79] E. Noether, *Invariante Variationsprobleme*, *Nachrichten von der Gesellschaft der Wissenschaften zu Göttingen, Mathematisch-Physikalische Klasse* **1918** (1918) 235–257.

[80] M. Nakahara, *Geometry, topology and physics*. Institute of Physics Publishing, second ed., 2003.

[81] R. Jackiw and C. Rebbi, *Vacuum Periodicity in a Yang-Mills Quantum Theory*, *Phys. Rev. Lett.* **37** (Jul, 1976) 172–175.

[82] V. Novikov, M. Shifman, A. Vainshtein and V. Zakharov, *ABC of Instantons*, April, 1994.

[83] V. A. Rubakov, *Classical theory of gauge fields*. Princeton University Press, Princeton, New Jersey, 5, 2002.

[84] F. R. Klinkhamer and N. S. Manton, *A Saddle Point Solution in the Weinberg-Salam Theory*, *Phys. Rev. D* **30** (1984) 2212.

[85] P. B. Arnold, D. Son and L. G. Yaffe, *The Hot baryon violation rate is $\mathcal{O}(\alpha_W^5 T^4)$*, *Phys. Rev. D* **55** (1997) 6264–6273, [hep-ph/9609481].

[86] G. F. Giudice and M. E. Shaposhnikov, *Strong sphalerons and electroweak baryogenesis*, *Phys. Lett. B* **326** (1994) 118–124, [hep-ph/9311367].

[87] G. D. Moore, C.-r. Hu and B. Muller, *Chern-Simons number diffusion with hard thermal loops*, *Phys. Rev. D* **58** (1998) 045001, [hep-ph/9710436].

[88] M. Shifman, *Advanced Topics in Quantum Field Theory: A Lecture Course*. Cambridge University Press, 2012, 10.1017/CBO9781139013352.

[89] R. D. Peccei, *The Strong CP Problem*, *Adv. Ser. Direct. High Energy Phys.* **3** (1989) 503–551.

[90] L. L. R. Garwin and M. Weinrich, *Observation of the failure of conservation of parity and charge conjugation in meson decays: the magnetic moment of the free muon*, Phys. Rev. **105** (1957) .

[91] S. L. Glashow, *Partial-symmetries of weak interactions*, *Nuclear Physics* **22** (1961) 579–588.

[92] S. Weinberg, *A model of leptons*, *Phys. Rev. Lett.* **19** (Nov, 1967) 1264–1266.

[93] A. Salam, *Weak and Electromagnetic Interactions*, *Conf. Proc. C* **680519** (1968) 367–377.

[94] D. Buttazzo, G. Degrassi, P. P. Giardino, G. F. Giudice, F. Sala, A. Salvio et al., *Investigating the near-criticality of the Higgs boson*, JHEP **12** (2013) 089, [1307.3536].

[95] M. Quiros, *Field theory at finite temperature and phase transitions*, Helv. Phys. Acta **67** (1994) 451–583.

[96] P. Higgs, *Broken symmetries, massless particles and gauge fields*, *Physics Letters* **12** (1964) 132–133.

[97] F. Englert and R. Brout, *Broken Symmetry and the Mass of Gauge Vector Mesons*, *Phys. Rev. Lett.* **13** (1964) 321–323.

[98] G. S. Guralnik, C. R. Hagen and T. W. B. Kibble, *Global Conservation Laws and Massless Particles*, *Phys. Rev. Lett.* **13** (1964) 585–587.

[99] G. Aad, T. Abajyan, B. Abbott, J. Abdallah, S. Abdel Khalek, A. Abdelalim et al., *Observation of a new particle in the search for the Standard Model Higgs boson with the ATLAS detector at the LHC*, *Physics Letters B* **716** (2012) 1–29.

[100] S. Chatrchyan, V. Khachatryan, A. Sirunyan, A. Tumasyan, W. Adam, E. Aguilo et al., *Observation of a new boson at a mass of 125 GeV with the CMS experiment at the LHC*, *Physics Letters B* **716** (2012) 30–61.

[101] T. Mannel, *Effective Field Theories in Flavour Physics*. Springer-Verlag Berlin Heidelberg, 2004, https://doi.org/10.1007/b62268105722793.

[102] G. Degrassi, S. Di Vita, J. Elias-Miro, J. R. Espinosa, G. F. Giudice, G. Isidori et al., *Higgs mass and vacuum stability in the Standard Model at NNLO*, *JHEP* **08** (2012) 098, [1205.6497].

[103] K. G. Chetyrkin and M. F. Zoller, *Three-loop β-functions for top-Yukawa and the Higgs self-interaction in the Standard Model*, JHEP **06** (2012) 033, [1205.2892].

[104] A. V. Bednyakov, A. F. Pikelner and V. N. Velizhanin, *Yukawa coupling beta-functions in the Standard Model at three loops*, *Physics Letters* **B722** (2013) 336–340, [1212.6829].

[105] K. G. Chetyrkin and M. F. Zoller, *β-function for the Higgs self-interaction in the Standard Model at three-loop level*, JHEP **04** (2013) 091, [1303.2890].

[106] M. E. Peskin and D. V. Schroeder, *An Introduction to quantum field theory.* Addison-Wesley, 1995.

[107] D. Tong, *Gauge Theory*, 2018 (Accessed: https://www.damtp.cam.ac.uk/user/tong/gaugetheory/gt.pdf).

[108] M. Reece, *TASI Lectures: (No) Global Symmetries to Axion Physics*, 2304.08512.

[109] G. 't Hooft, *Symmetry Breaking Through Bell-Jackiw Anomalies*, *Phys. Rev. Lett.* **37** (1976) 8–11.

[110] S. L. Adler, *Axial-vector vertex in spinor electrodynamics*, *Phys. Rev.* **177** (Jan, 1969) 2426–2438.

[111] J. S. Bell and R. Jackiw, *A PCAC puzzle: $\pi_0 \to \gamma\gamma$ in the σ-model*, *Il Nuovo Cimento A (1965-1970)* **60** (1969) 47–61.

[112] A. J. Long, E. Sabancilar and T. Vachaspati, *Leptogenesis and Primordial Magnetic Fields*, *JCAP* **02** (2014) 036, [1309.2315].

[113] E. Witten, *An su(2) anomaly*, *Physics Letters B* **117** (1982) 324–328.

[114] D. J. E. Marsh, *Axions and ALPs: a very short introduction*, 1712.03018.

[115] R. D. Peccei and H. R. Quinn, *CP Conservation in the Presence of Pseudoparticles*, *Phys. Rev. Lett.* **38** (1977) 1440–1443.

[116] R. D. Peccei, *The Strong CP Problem and Axions*, *Lect.Notes Phys.* **741** (2008) 3–17, [`hep-ph/0607268`].

[117] M. Millea, L. Knox and B. Fields, *New Bounds for Axions and Axion-Like Particles with keV-GeV Masses*, *Physics Review* **D92** (2015) 023010, [`1501.04097`].

[118] H. Georgi, D. B. Kaplan and L. Randall, *Manifesting the invisible axion at low energies*, *Physics Letters* **169B** (March, 1986) 73–78.

[119] E. Armengaud et al., *Physics potential of the International Axion Observatory (IAXO)*, `1904.09155`.

[120] K. Kamada and A. J. Long, *Baryogenesis from decaying magnetic helicity*, *Phys. Rev. D* **94** (2016) 063501, [`1606.08891`].

[121] K. Kamada and A. J. Long, *Evolution of the Baryon Asymmetry through the Electroweak Crossover in the Presence of a Helical Magnetic Field*, *Phys. Rev. D* **94** (2016) 123509, [`1610.03074`].

[122] M. Shaposhnikov, *Baryon asymmetry of the universe in standard electroweak theory*, *Nuclear Physics B* **287** (1987) 757–775.

[123] G. R. Farrar and M. E. Shaposhnikov, *Baryon asymmetry of the universe in the minimal Standard Model*, *Phys. Rev. Lett.* **70** (1993) 2833–2836, [`hep-ph/9305274`].

[124] G. R. Farrar and M. E. Shaposhnikov, *Baryon asymmetry of the universe in the standard electroweak theory*, *Phys. Rev. D* **50** (1994) 774, [`hep-ph/9305275`].

[125] V. A. Rubakov and M. E. Shaposhnikov, *Electroweak baryon number nonconservation in the early universe and in high-energy collisions*, *Usp. Fiz. Nauk* **166** (1996) 493–537, [`hep-ph/9603208`].

[126] M. Joyce and M. E. Shaposhnikov, *Primordial magnetic fields, right-handed electrons, and the Abelian anomaly*, *Phys. Rev. Lett.* **79** (1997) 1193–1196, [`astro-ph/9703005`].

[127] M. Giovannini and M. E. Shaposhnikov, *Primordial hypermagnetic fields and triangle anomaly*, *Phys. Rev. D* **57** (1998) 2186–2206, [`hep-ph/9710234`].

[128] M. Laine and M. E. Shaposhnikov, *A Remark on sphaleron erasure of baryon asymmetry*, *Phys. Rev. D* **61** (2000) 117302, [`hep-ph/9911473`].

[129] Y. Burnier, M. Laine and M. Shaposhnikov, *Baryon and lepton number violation rates across the electroweak crossover*, *JCAP* **02** (2006) 007, [`hep-ph/0511246`].

[130] K. Bamba, *Baryon asymmetry from hypermagnetic helicity in dilaton hypercharge electromagnetism*, *Phys. Rev. D* **74** (2006) 123504, [`hep-ph/0611152`].

[131] K. Bamba, C. Q. Geng and S. H. Ho, *Hypermagnetic Baryogenesis*, *Phys. Lett. B* **664** (2008) 154–156, [`0712.1523`].

[132] T. Fujita and K. Kamada, *Large-scale magnetic fields can explain the baryon asymmetry of the Universe*, *Phys. Rev. D* **93** (2016) 083520, [`1602.02109`].

[133] M. M. Anber and L. Sorbo, *N-flationary magnetic fields*, *JCAP* **10** (2006) 018, [`astro-ph/0606534`].

[134] M. M. Anber and L. Sorbo, *Naturally inflating on steep potentials through electromagnetic dissipation*, *Phys. Rev. D* **81** (2010) 043534, [`0908.4089`].

[135] M. M. Anber and E. Sabancilar, *Hypermagnetic Fields and Baryon Asymmetry from Pseudoscalar Inflation*, *Phys. Rev. D* **92** (2015) 101501, [`1507.00744`].

[136] Y. Cado and E. Sabancilar, *Asymmetric Dark Matter and Baryogenesis from Pseudoscalar Inflation*, *JCAP* **04** (2017) 047, [`1611.02293`].

[137] D. Jiménez, K. Kamada, K. Schmitz and X.-J. Xu, *Baryon asymmetry and gravitational waves from pseudoscalar inflation*, *JCAP* **12** (2017) 011, [`1707.07943`].

[138] E. I. Sfakianakis and J. van de Vis, *Preheating after Higgs Inflation: Self-Resonance and Gauge boson production*, *Phys. Rev. D* **99** (2019) 083519, [`1810.01304`].

[139] V. Domcke, B. von Harling, E. Morgante and K. Mukaida, *Baryogenesis from axion inflation*, *JCAP* **10** (2019) 032, [`1905.13318`].

[140] Y. Cado, B. von Harling, E. Massó and M. Quirós, *Baryogenesis via gauge field production from a relaxing Higgs*, *JCAP* **07** (2021) 049, [`2102.13650`].

[141] R. Durrer and A. Neronov, *Cosmological Magnetic Fields: Their Generation, Evolution and Observation*, *Astron. Astrophys. Rev.* **21** (2013) 62, [`1303.7121`].

[142] T. Vachaspati, *Progress on cosmological magnetic fields*, *Rept. Prog. Phys.* **84** (2021) 074901, [`2010.10525`].

[143] G. Baym and H. Heiselberg, *The Electrical conductivity in the early universe*, *Phys. Rev. D* **56** (1997) 5254–5259, [`astro-ph/9704214`].

[144] P. B. Arnold, G. D. Moore and L. G. Yaffe, *Transport coefficients in high temperature gauge theories. 1. Leading log results*, *JHEP* **11** (2000) 001, [`hep-ph/0010177`].

[145] D. T. Son and A. R. Zhitnitsky, *Quantum anomalies in dense matter*, *Phys. Rev. D* **70** (2004) 074018, [`hep-ph/0405216`].

[146] K. Fukushima, D. E. Kharzeev and H. J. Warringa, *The Chiral Magnetic Effect*, *Phys. Rev. D* **78** (2008) 074033, [`0808.3382`].

[147] D. G. Figueroa and M. Shaposhnikov, *Anomalous non-conservation of fermion/chiral number in Abelian gauge theories at finite temperature*, *JHEP* **04** (2018) 026, [`1707.09967`].

[148] U. Frisch, A. Pouquet, J. LÉOrat and A. Mazure, *Possibility of an inverse cascade of magnetic helicity in magnetohydrodynamic turbulence*, *Journal of Fluid Mechanics* **68** (1975) 769–778.

[149] E. S. Fradkin, *Method of Green's functions in quantum field theory and quantum statistics*, *Trud. Fiz. Inst. Akad. Nauk SSSR (Fiz. Inst. Lebedev)* **29** (1965) 7–138.

[150] K. Kajantie, M. Laine, K. Rummukainen and M. E. Shaposhnikov, *A Nonperturbative analysis of the finite T phase transition in SU(2) x U(1) electroweak theory*, *Nucl. Phys. B* **493** (1997) 413–438, [`hep-lat/9612006`].

[151] M. D'Onofrio and K. Rummukainen, *Standard model cross-over on the lattice*, *Phys. Rev. D* **93** (2016) 025003, [`1508.07161`].

[152] M. D'Onofrio, K. Rummukainen and A. Tranberg, *Sphaleron Rate in the Minimal Standard Model*, *Phys. Rev. Lett.* **113** (2014) 141602, [`1404.3565`].

[153] M. Abramowitz and I. A. Stegun, *Handbook of Mathematical Functions: With Formulas, Graphs, and Mathematical Tables.* Dover Publications, 1965.

[154] Y. Cado and M. Quirós, *Baryogenesis from combined Higgs – scalar field inflation*, *Phys. Rev. D* **106** (2022) 055018, [`2201.06422`].

[155] R. Banerjee, *Evolution of primordial magnetic fields in the early universe*, *PhD Thesis, Ludwig-Maximilians-Universität München, Germany* (2002) .

[156] R. Banerjee and K. Jedamzik, *The Evolution of cosmic magnetic fields: From the very early universe, to recombination, to the present*, *Phys. Rev. D* **70** (2004) 123003, [`astro-ph/0410032`].

[157] A. Boyarsky, J. Frohlich and O. Ruchayskiy, *Self-consistent evolution of magnetic fields and chiral asymmetry in the early Universe*, *Phys. Rev. Lett.* **108** (2012) 031301, [`1109.3350`].

[158] Y. Akamatsu and N. Yamamoto, *Chiral Plasma Instabilities*, *Phys. Rev. Lett.* **111** (2013) 052002, [`1302.2125`].

[159] Y. Hirono, D. Kharzeev and Y. Yin, *Self-similar inverse cascade of magnetic helicity driven by the chiral anomaly*, *Phys. Rev. D* **92** (2015) 125031, [`1509.07790`].

[160] N. Yamamoto, *Scaling laws in chiral hydrodynamic turbulence*, *Phys. Rev. D* **93** (2016) 125016, [1603.08864].

[161] I. Rogachevskii, O. Ruchayskiy, A. Boyarsky, J. Fröhlich, N. Kleeorin, A. Brandenburg et al., *Laminar and turbulent dynamos in chiral magnetohydrodynamics-I: Theory*, *Astrophys. J.* **846** (2017) 153, [1705.00378].

[162] K. Kamada, *Return of grand unified theory baryogenesis: Source of helical hypermagnetic fields for the baryon asymmetry of the universe*, *Phys. Rev. D* **97** (2018) 103506, [1802.03055].

[163] E. Komatsu, *The pursuit of non-gaussian fluctuations in the cosmic microwave background*. PhD thesis, Tohoku U., 2001. astro-ph/0206039.

[164] WMAP collaboration, E. Komatsu et al., *Seven-Year Wilkinson Microwave Anisotropy Probe (WMAP) Observations: Cosmological Interpretation*, *Astrophys. J. Suppl.* **192** (2011) 18, [1001.4538].

[165] N. Barnaby and M. Peloso, *Large Nongaussianity in Axion Inflation*, *Phys. Rev. Lett.* **106** (2011) 181301, [1011.1500].

[166] N. Barnaby, E. Pajer and M. Peloso, *Gauge Field Production in Axion Inflation: Consequences for Monodromy, non-Gaussianity in the CMB, and Gravitational Waves at Interferometers*, *Phys. Rev. D* **85** (2012) 023525, [1110.3327].

[167] PLANCK collaboration, Y. Akrami et al., *Planck 2018 results. IX. Constraints on primordial non-Gaussianity*, *Astron. Astrophys.* **641** (2020) A9, [1905.05697].

[168] A. Neronov and I. Vovk, *Evidence for strong extragalactic magnetic fields from Fermi observations of TeV blazars*, *Science* **328** (2010) 73–75, [1006.3504].

[169] F. Tavecchio, G. Ghisellini, L. Foschini, G. Bonnoli, G. Ghirlanda and P. Coppi, *The intergalactic magnetic field constrained by Fermi/LAT observations of the TeV blazar 1ES 0229+200*, *Mon. Not. Roy. Astron. Soc.* **406** (2010) L70–L74, [1004.1329].

[170] S. Ando and A. Kusenko, *Evidence for Gamma-Ray Halos Around Active Galactic Nuclei and the First Measurement of Intergalactic Magnetic Fields*, *Astrophys. J. Lett.* **722** (2010) L39, [1005.1924].

[171] K. Kamada, F. Uchida and J. Yokoyama, *Baryon isocurvature constraints on the primordial hypermagnetic fields*, *JCAP* **04** (2021) 034, [2012.14435].

[172] K. Inomata, M. Kawasaki, A. Kusenko and L. Yang, *Big Bang Nucleosynthesis Constraint on Baryonic Isocurvature Perturbations*, *JCAP* **12** (2018) 003, [1806.00123].

[173] V. Domcke and K. Mukaida, *Gauge Field and Fermion Production during Axion Inflation*, *JCAP* **11** (2018) 020, [1806.08769].

[174] H. Kitamoto and M. Yamada, *Semiclassical analysis of axion-assisted and axion-driven pair production*, *JHEP* **06** (2022) 103, [2109.14782].

[175] T. D. Cohen and D. A. McGady, *The Schwinger mechanism revisited*, *Phys. Rev. D* **78** (2008) 036008, [0807.1117].

[176] O. O. Sobol, E. V. Gorbar and S. I. Vilchinskii, *Backreaction of electromagnetic fields and the Schwinger effect in pseudoscalar inflation magnetogenesis*, *Phys. Rev. D* **100** (2019) 063523, [1907.10443].

[177] E. V. Gorbar, K. Schmitz, O. O. Sobol and S. I. Vilchinskii, *Gauge-field production during axion inflation in the gradient expansion formalism*, *Phys. Rev. D* **104** (2021) 123504, [2109.01651].

[178] E. V. Gorbar, K. Schmitz, O. O. Sobol and S. I. Vilchinskii, *Hypermagnetogenesis from axion inflation: model-independent estimates*, 2111.04712.

[179] T. Fujita, J. Kume, K. Mukaida and Y. Tada, *Effective treatment of U(1) gauge field and charged particles in axion inflation*, 2204.01180.

[180] Y. Cado and M. Quirós, *Numerical study of the Schwinger effect in axion inflation*, *Phys. Rev. D* **106** (2022) 123527, [`2208.10977`].

[181] J. R. C. Cuissa and D. G. Figueroa, *Lattice formulation of axion inflation. Application to preheating*, *JCAP* **06** (2019) 002, [`1812.03132`].

[182] W. Heisenberg and H. Euler, *Consequences of Dirac Theory of the Positron*, *Zeitschrift für Physik* **98** (1936) 714–732.

[183] J. Schwinger, *On gauge invariance and vacuum polarization*, *Phys. Rev.* **82** (Jun, 1951) 664–679.

[184] P. Adshead, J. T. Giblin, T. R. Scully and E. I. Sfakianakis, *Gauge-preheating and the end of axion inflation*, *JCAP* **12** (2015) 034, [`1502.06506`].

[185] C. Cosme, D. G. Figueroa and N. Loayza, *Gravitational wave production from preheating with trilinear interactions*, `2206.14721`.

[186] Y. Cado and M. Quirós, *Baryogenesis from Higgs Inflation*, accepted for publication in Phys. Rev. D (3, 2023) , [`2303.12932`].

[187] C. D. Froggatt and H. B. Nielsen, *Hierarchy of Quark Masses, Cabibbo Angles and CP Violation*, *Nucl. Phys. B* **147** (1979) 277–298.

[188] N. Barnaby, R. Namba and M. Peloso, *Phenomenology of a Pseudo-Scalar Inflaton: Naturally Large Nongaussianity*, *JCAP* **04** (2011) 009, [`1102.4333`].

[189] F. Dux, A. Florio, J. Klarić, A. Shkerin and I. Timiryasov, *Preheating in Palatini Higgs inflation on the lattice*, *JCAP* **09** (2022) 015, [`2203.13286`].

[190] S. Alekhin, A. Djouadi and S. Moch, *The top quark and Higgs boson masses and the stability of the electroweak vacuum*, *Phys. Lett. B* **716** (2012) 214–219, [`1207.0980`].

[191] D. Buttazzo, G. Degrassi, P. P. Giardino, G. F. Giudice, F. Sala, A. Salvio et al., *Investigating the near-criticality of the Higgs boson*, *JHEP* **12** (2013) 089, [`1307.3536`].

[192] F. Bezrukov, J. Rubio and M. Shaposhnikov, *Living beyond the edge: Higgs inflation and vacuum metastability*, *Phys. Rev. D* **92** (2015) 083512, [`1412.3811`].

[193] F. Bezrukov and M. Shaposhnikov, *Higgs inflation at the critical point*, *Phys. Lett. B* **734** (2014) 249–254, [`1403.6078`].

[194] Y. Hamada, H. Kawai, K.-y. Oda and S. C. Park, *Higgs Inflation is Still Alive after the Results from BICEP2*, *Phys. Rev. Lett.* **112** (2014) 241301, [`1403.5043`].

[195] Y. Hamada, H. Kawai, K.-y. Oda and S. C. Park, *Higgs inflation from Standard Model criticality*, *Phys. Rev. D* **91** (2015) 053008, [`1408.4864`].

[196] J. M. Ezquiaga, J. Garcia-Bellido and E. Ruiz Morales, *Primordial Black Hole production in Critical Higgs Inflation*, *Phys. Lett. B* **776** (2018) 345–349, [`1705.04861`].

[197] A. Salvio, *Initial Conditions for Critical Higgs Inflation*, *Phys. Lett. B* **780** (2018) 111–117, [`1712.04477`].

[198] I. Masina, *Ruling out Critical Higgs Inflation?*, *Phys. Rev. D* **98** (2018) 043536, [`1805.02160`].

[199] M. Drees and Y. Xu, *Overshooting, Critical Higgs Inflation and Second Order Gravitational Wave Signatures*, *Eur. Phys. J. C* **81** (2021) 182, [`1905.13581`].

[200] A. Salvio, *Critical Higgs inflation in a Viable Motivated Model*, *Phys. Rev. D* **99** (2019) 015037, [`1810.00792`].

[201] F. Bauer and D. A. Demir, *Inflation with Non-Minimal Coupling: Metric versus Palatini Formulations*, *Phys. Lett. B* **665** (2008) 222–226, [`0803.2664`].

[202] J. L. F. Barbon, J. A. Casas, J. Elias-Miro and J. R. Espinosa, *Higgs Inflation as a Mirage*, *JHEP* **09** (2015) 027, [`1501.02231`].

[203] G. F. Giudice and H. M. Lee, *Unitarizing Higgs Inflation*, *Phys. Lett. B* **694** (2011) 294–300, [1010.1417].

[204] J. Khoury and T. Steingasser, *Gauge hierarchy from electroweak vacuum metastability*, 2108.09315.

[205] A. De Simone, M. P. Hertzberg and F. Wilczek, *Running Inflation in the Standard Model*, *Phys. Lett. B* **678** (2009) 1–8, [0812.4946].

[206] D. H. Lyth, *What would we learn by detecting a gravitational wave signal in the cosmic microwave background anisotropy?*, *Phys. Rev. Lett.* **78** (1997) 1861–1863, [hep-ph/9606387].

[207] A. D. Linde, *Particle physics and inflationary cosmology*, hep-th/0503203.

[208] M. Herranen, T. Markkanen, S. Nurmi and A. Rajantie, *Spacetime curvature and the Higgs stability during inflation*, *Phys. Rev. Lett.* **113** (2014) 211102, [1407.3141].

[209] T. Kodama and T. Takahashi, *Relaxing inflation models with non-minimal coupling: A general study*, 2112.05283.

[210] L. Kofman, A. D. Linde and A. A. Starobinsky, *Reheating after inflation*, *Phys. Rev. Lett.* **73** (1994) 3195–3198, [hep-th/9405187].

[211] A. de Gouvea, D. Hernandez and T. M. P. Tait, *Criteria for Natural Hierarchies*, *Phys. Rev. D* **89** (2014) 115005, [1402.2658].

[212] S. Profumo, M. J. Ramsey-Musolf and G. Shaughnessy, *Singlet Higgs phenomenology and the electroweak phase transition*, *JHEP* **08** (2007) 010, [0705.2425].

[213] V. Barger, P. Langacker, M. McCaskey, M. J. Ramsey-Musolf and G. Shaughnessy, *LHC Phenomenology of an Extended Standard Model with a Real Scalar Singlet*, *Phys. Rev. D* **77** (2008) 035005, [0706.4311].

[214] PARTICLE DATA GROUP collaboration, P. Zyla et al., *Review of Particle Physics*, *PTEP* **2020** (2020) 083C01.

[215] ATLAS collaboration, G. Aad et al., *Combined measurements of Higgs boson production and decay using up to 80 fb^{-1} of proton-proton collision data at $\sqrt{s} = 13$ TeV collected with the ATLAS experiment*, *Phys. Rev. D* **101** (2020) 012002, [1909.02845].

[216] CMS collaboration, A. M. Sirunyan et al., *Combined measurements of Higgs boson couplings in proton–proton collisions at $\sqrt{s} = 13$ TeV*, *Eur. Phys. J. C* **79** (2019) 421, [1809.10733].

[217] ATLAS collaboration, *Constraint of the Higgs boson self-coupling from Higgs boson differential production and decay measurements*, tech. rep., CERN, Geneva, Mar, 2019.

[218] CMS collaboration, A. M. Sirunyan et al., *Search for nonresonant Higgs boson pair production in final states with two bottom quarks and two photons in proton-proton collisions at $\sqrt{s} = 13$ TeV*, *JHEP* **03** (2021) 257, [2011.12373].

[219] S. Homiller and P. Meade, *Measurement of the Triple Higgs Coupling at a HE-LHC*, *JHEP* **03** (2019) 055, [1811.02572].

[220] D. Gonçalves, T. Han, F. Kling, T. Plehn and M. Takeuchi, *Higgs boson pair production at future hadron colliders: From kinematics to dynamics*, *Phys. Rev. D* **97** (2018) 113004, [1802.04319].

[221] LHC HIGGS CROSS SECTION WORKING GROUP collaboration, S. Dittmaier et al., *Handbook of LHC Higgs Cross Sections: 1. Inclusive Observables*, 1101.0593.

[222] LHC HIGGS CROSS SECTION WORKING GROUP collaboration, D. de Florian et al., *Handbook of LHC Higgs Cross Sections: 4. Deciphering the Nature of the Higgs Sector*, 1610.07922.

[223] ATLAS collaboration, G. Aad et al., *Combination of searches for Higgs boson pairs in pp collisions at $\sqrt{s} =$13 TeV with the ATLAS detector*, *Phys. Lett. B* **800** (2020) 135103, [1906.02025].

[224] CMS collaboration, A. M. Sirunyan et al., *Combination of searches for Higgs boson pair production in proton-proton collisions at $\sqrt{s} = 13$ TeV*, *Phys. Rev. Lett.* **122** (2019) 121803, [1811.09689].

[225] D. G. Figueroa, A. Florio, F. Torrenti and W. Valkenburg, *CosmoLattice*, 2102.01031.

[226] D. G. Figueroa, A. Florio, F. Torrenti and W. Valkenburg, *The art of simulating the early Universe – Part I*, *JCAP* **04** (2021) 035, [2006.15122].

[227] Y. Cado, C. Englert, T. Modak and M. Quirós, *in preparation*.

[228] M. Carena, M. Quirós and Y. Zhang, *Dark CP violation and gauged lepton or baryon number for electroweak baryogenesis*, *Phys. Rev. D* **101** (2020) 055014, [1908.04818].

[229] K. S. Babu, *TASI Lectures on Flavor Physics*, in *Theoretical Advanced Study Institute in Elementary Particle Physics: The Dawn of the LHC Era*, pp. 49–123, 2010. 0910.2948. DOI.